NUI MAYNOOTH
Ollscoil na hÉireann Má Nuad

Title: An Analysis of Hydrological Model Uncertainty at the Local Stage of a Climate Change Impact Assessment in the Suir Catchment

Nuala Murphy

Thesis submitted in fulfilment of the requirements of the Master of Literature Degree,
Faculty of Social Sciences
Department of Geography
National University of Ireland, Maynooth

September 2010

Head of Department: Professor Mark Boyle
Supervisor: Doctor Conor Murphy

I dedicate this thesis to my mother Jan and to the loving memory of my father Michael, who encouraged me in lifelong learning long before it was fashionable and without whose quiet support over the years this thesis would not have been written.

Acknowledgements

I could not have completed this thesis without the support and encouragement of many people. First and foremost I wish to extend my deepest appreciation to my parents, Jan and Michael. They have been a source of great encouragement to all their family especially in the field of learning. As children, we were taken on regular outings to the local mountains and countryside and instilled with a deep interest in and curiosity about the world around us. Indeed, my interest in all things environmental and geographical began during those great summer picnics in the Cooley Mountains. I'm lucky that those picnics took place during the 1970s, one of the driest decades of the twentieth century. Although my father Michael is no longer with us, I still hear his wise words of guidance.

I also wish to thank my brothers and sisters, Liam, Michéal, Peter, Gráinne, Janet, Anthony, Eamonn and Rónan. They were very encouraging of me returning to university and have been a constant source of advice (and some good-natured teasing!). Special mention goes to my brother Rónan, budding Danté scholar, who thoughtfully copy-edited chapter drafts. I also wish to thank my nieces and nephews. Whenever I felt overwhelmed by life's demands, they helped me put it all into perspective.

My friend Alice Blumlein deserves special mention for her continuing words of support, her great outlook and her wonderful cooking skills. I wish to thank her for allowing me to be taster for so many delicious meals. Dr. Georgina Larkin was always at the end of the phone whenever I need to chat about the research process. As one of my oldest friends she provided timely advice, especially during our film outings.

Dr. Ro Charlton, my friend and second supervisor, encouraged me to persevere when the going was tough at the start of the project. Our Sunday runs were very enjoyable and informative as was the obligatory cup of coffee afterwards. Mary Weld, Gay Murphy, Mick Bolger and Jim Keenen in the Geography Department were always ready to help out with a smile. Professor Mark Boyle, Professor John Sweeney and the staff of the Geography Department were also very supportive.

Special thanks are also due to my flat mate Henry Langton. He was always a calming influence and we enjoyed many episodes of Frasier together. My fellow runners in the Lucan Harrier Athletics Club have been a great source of encouragement (both for my running and my masters!) and through the club I have been introduced to the joys of running, surely one of the most effective ways of keeping the mind clear, the body fit and the weight under control. Special thanks to Clodagh Ashe for her words of encouragement during our runs together.

All my fellow research students in ICARUS and in the Geography Department have provided encouragement and great humour on our shared research path. I thank them all. I shared an office with Jackie, Colin, Claire, Nichola, Sylvia and Julia and thank them for the shared laughter and practical advice. Special mention must go to Colin Holman for providing access to Autosim and to Jackie McGloughlin and her husband John who patiently explained document formatting to me. It was always great meeting up with Mary Kelly, Fionnuala Ni Mhorda and Adrienne Hobbs for coffee and a chat. Together we put the world to rights many times over!

The Irish Research Council for Science, Engineering and Technology do great work by funding so many budding scholars in their PhD and masters studies. Without their funding of this project I would not have experienced such a great learning adventure.

Lastly, but by no means least, I extend my sincere thanks to my supervisor, Dr. Conor Murphy, for his patience, his advice and his prompt reading and constructive comments on each chapter draft.

Abstract

This thesis presents an analysis of uncertainty at the local stage of a climate impact assessment. Impact model structural uncertainty and uncertainty due to equifinality of parameter sets are evaluated, in addition to uncertainty due to GCMs and emissions scenarios. The Suir catchment is employed as a case study area to analyse the changes in catchment hydrology and in future flood magnitude and frequency relationships due to climate change. Two lumped conceptual rainfall-runoff models of different degrees of complexity are forced with the output of three GCMs and two emissions scenarios (A2 and B2) downscaled to synoptic station level by empirical statistical downscaling (Fealy and Sweeney, 2007). In the analysis of changes to catchment hydrology for the 2050s and the 2080s, GCM uncertainty is the greatest source of uncertainty. However, by the 2080s, uncertainty due to equifinality of parameter sets and model structure is also a significant source of uncertainty, with increases in streamflow being most extreme in February. Furthermore, results suggest that flood magnitude and frequency relationships will intensify under climate change. A robust finding is the notable agreement in new return period values in the 2080s with both models suggesting that the 10, 25 and 50 year flood events simulated in the control period will become 3.2, 5.4 and 9 year flood events. However, the magnitudes of the flood events differ for each model. These results suggest that model structural uncertainty is a significant source of uncertainty and should be taken into account by employing a suite of hydrological models at the local stage of climate change impact analyses that inform anticipatory flood adaptation decisions or policy frameworks.

Abbreviations

AMS	Annual Maximum Series
AOGCM	Atmosphere/Ocean Global Circulation Model
AR4	IPCC Fourth Assessment Report
CORINE	Co-ordinate of Information on the Environment
CCCM	Canadian Centre for Climate Modelling
CSIRO	Commonwealth Scientific and Industrial Research Organisation
ESRI	Environmental Systems Research Institute
GHG	Greenhouse Gas
GCM	Global Circulation Model
GSI	Geological Survey of Ireland
GLUE	Generalised Likelihood Uncertainty Estimation
HBV	Hydrologiska Byråns Vattenbalansavdelning
HBV-Light	See above
HYSIM	Hydrologic Simulation Model
IPCC	Intergovernmental Panel on Climate Change
IL	Interflow Lower Horizon
IU	Interflow Upper Horizon
MAE	Mean Actual Error
NAOI	North Atlantic Oscillation Index
NS	Nash-Sutcliffe Criterion of Efficiency
OPW	Office of Public Works
OSI	Ordinance Survey Ireland
PBIAS	Percent Bias

PDIFF	Peak Difference
PE	Potential Evaporation
POT	Peaks Over Threshold
PSDI	Pore Size Distribution Index
QMED	median of annual maximum flood series
RCM	Regional Climate Model
RMSE	Root Mean Square Error
R^2	Coefficient of Determination
SERBD	South Eastern River Basin District
SRES	Special Report on Emissions Scenarios
TAR	IPCC Third Assessment Report
UNEP	United Nations Environment Programme
USDA	United States Department of Agriculture

Table of Contents

List of Figures

xiv

List of Tables

Chapter 1 – Introduction

1.1   Introduction

The climate of planet Earth is changing.   Numerous scientific studies indicate that the increase in greenhouse gases emitted by human society since the Industrial Revolution is the main cause of this global warming.   Indeed, the vast majority of climate scientists now accept that anthropogenic emissions are the cause of climate change.   Evidence is already mounting that the planet is warming at an alarming rate.   In The IPCC Fourth Assessment Report (AR4) it states that "warming of the climate system is unequivocal, as is now evident from observations of increases in global average air and ocean temperatures, widespread melting of snow and ice, and rising global average sea level" (IPCC 2007, p.5). However, the effects will be quite diverse and location specific (Dessai and Hulme, 2007).

One method of translating changes in global climate into local impacts is a climate change impact assessment, whereby future socio-economic storylines are translated into global emissions scenarios of greenhouse gases, downscaled to regional level and finally inputted to local impact models (Wilby, 2005). This has been a favoured technique of much research on the hydrological impacts of climate change (e.g., Minville *et al.*, 2008; Murphy and Charlton, 2008; Wilby, 2005; Wilby and Harris, 2006).   Uncertainty flows through impact assessments leading to the so-called "cascade of uncertainty" (Jones, 2000).   However, there are also important flows of uncertainty *within* each stage of an impact assessment. This thesis seeks analyse the flow of uncertainty within the local level stage of such an assessment. Specifically, uncertainty due to model structural error and equifinality of parameter sets will be analysed. Wilby *et al.* (2009, p.1206) note that "Environmental models play an integral part in many climate risk assessments…However, uncertainty in responses due to the impact model structure and/or parameters is very seldom specified let alone reported: much more attention is typically given to the influence of different climate models or downscaling methods on the outcome". The Suir catchment is employed as a case study area to evaluate if uncertainty can be analysed in a meaningful way that will aid in developing more useful adaptation decisions. This case study will examine how the incidence of flood magnitude and frequency may vary in the Suir catchment due to climate

change. The catchment was chosen because of the high quality of the streamflow data from the gauging station at Clonmel (given an A1 (high quality) rating in the forthcoming Office of Public Works Flood Studies Update report). Clonmel is also a flood-prone town, with recent large flood events creating national headlines.

Beven (2000) and Koutsoyiannis (2010) suggest that uncertainty be seen as an intrinsic part of all natural systems (and their representations) and that this should be acknowledged and included in a modelling study. Accordingly, several recent Irish studies into the impacts of climate change on water resources have analysed uncertainty flowing through each stage of an assessment using two well-known hydrological models (HYSIM and HBV-Light) (Charlton *et al.,* 2006; Murphy and Charlton, 2008, Semmler *et al.,* 2006: Steele-Dunne *et al.,* 2008; Wang *et al.,* 2005). Uncertainty due to GCMs, emissions scenarios and equifinality of parameter sets was analysed in these studies. However, only one impact model was employed in each of the above studies thereby preventing a comprehensive analysis of model structural uncertainty. This thesis seeks to fill the gap with an analysis of model structural uncertainty using the aforementioned two models, while also analysing uncertainty due to GCMs, emissions scenarios and equifinality of parameter sets. Specifically, the project will analyse changing flood magnitude/frequency relationships within the Suir catchment in a climate change context. It is important to state at the outset the assumptions in such a project, i.e. that land use remains constant and that soils and their hydrological behaviour remain the same under changing circumstances (e.g. Wilby, 2005). Furthermore, it is assumed that the uncertainties are not so large when the hydrological models are used for extrapolation purposes (i.e., outside their calibration ranges) as to render the extrapolation results meaningless (Bergström *et al.,* 2000).

1.2   Project Objectives

The objectives of the project are threefold:

- ▪ To calibrate and validate two conceptual rainfall-runoff models for use in the climate impact assessment and to analyse the uncertainty derived from their application.

- To assess the likely impacts of anthropogenic climate change on the hydrology of the Suir catchment by forcing two rainfall-runoff models with downscaled data from a range of GCMs and two greenhouse gas emissions scenarios.
- To analyse the uncertainty in future changes to catchment hydrology and flood magnitude/frequency relationships within the Suir catchment originating from the use of different GCMs, emissions scenarios and impacts models.
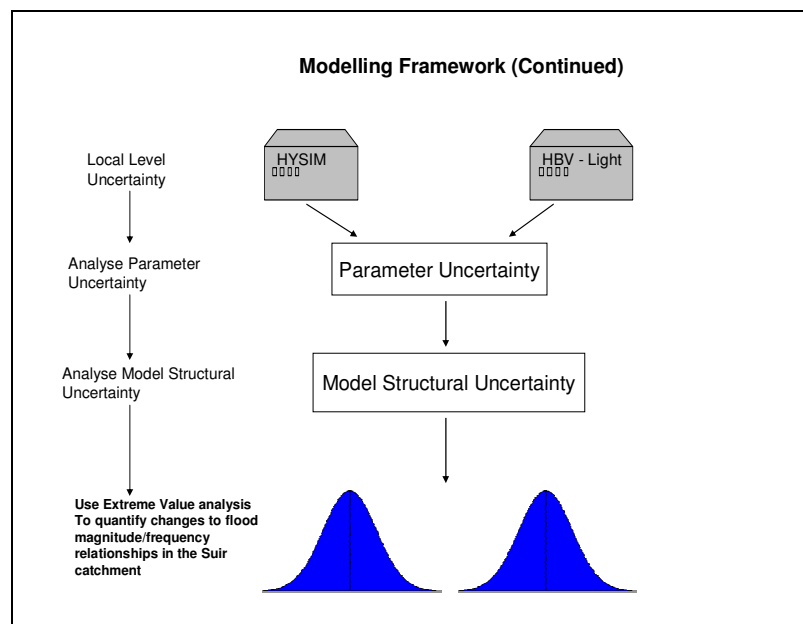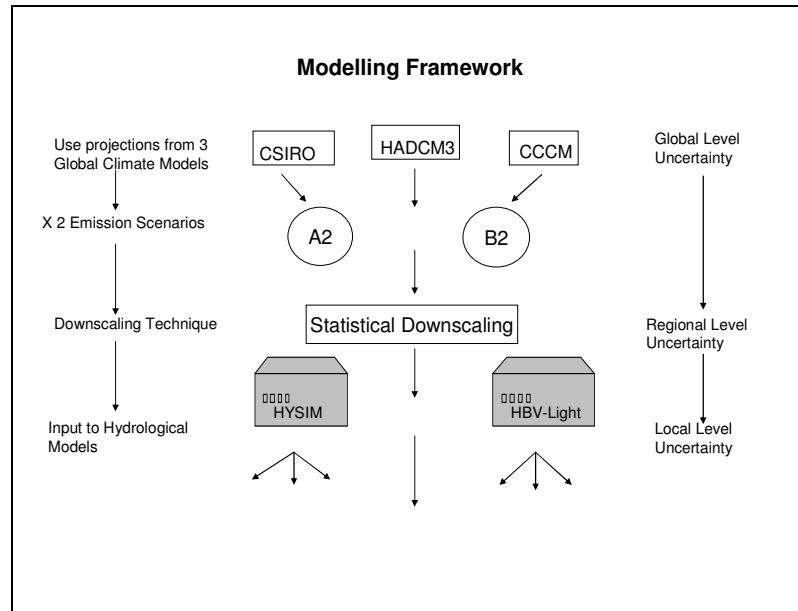
Figure 1.1 Modelling framework employed in the project

3

Figure 1.1 represents the modelling framework adopted in the project. It is important to note that this approach to uncertainty analysis can only measure a portion of the uncertainty embodied within the study context, methodology and the parameter space within each of the hydrological models (see Figure 1.2). It does it purport to present a "global" uncertainty analysis. Another set of models would no doubt deliver a different result, as would the techniques and methodology employed by a different modeller! Indeed, much more uncertainty is omitted from the framework structure than embodied within it. Uncertainty is a multi-dimensional concept that can ultimately be viewed as a function of human consciousness.
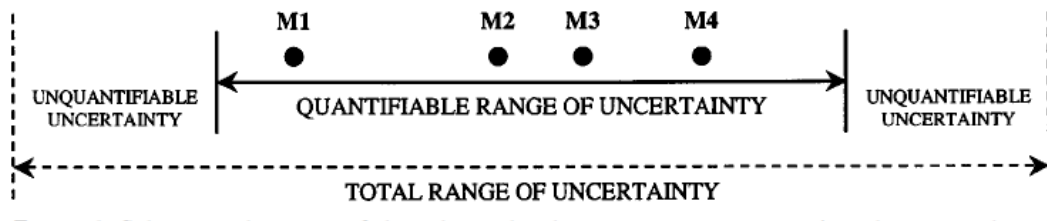
Figure 1.2 Schematic depiction of the relationship between scenarios, a projected range and total uncertainty. M1 to M4 represent scenarios produced by four models. The projected range consists of a quantifiable range of uncertainty that encompasses the scenarios. This lies within a total range of uncertainty that cannot be fully quantified. (Jones, 2000)

1.3 Why use Uncertainty Analysis?

Pappenberger and Beven (2006) present seven reasons why uncertainty analysis is not a standard practice in environmental modelling and then explain why each one of them is untenable. These reasons are:

- Uncertainty analysis is not necessary given physically realistic models.
- Uncertainty analysis is not useful in adding to process understanding.
- Uncertainty (probability) distributions cannot be understood by policy makers and the public.
- Uncertainty analysis cannot be incorporated into the decision-making process.
- Uncertainty analysis is too subjective.
- Uncertainty analysis is too difficult to perform.

- Uncertainty does not really matter in making the final decision.

Beven (2009) and this author assert that uncertainty analysis is critical when carrying out an environmental modelling exercise. Chapter 2 reviews the literature regarding each stage of a climate impact assessment. The focus of Chapter 3 is on a description of the physical characteristics of the Suir catchment and the methodology for generating the future downscaled climatic data (Fealy and Sweeney, 2007). Chapters 4 and 5 describe the structures of HYSIM and HBV-Light and outline the methodologies employed for parameterising both models. The calibration and validation of the models is then described in Chapter 6. Changes to the hydrological regime of the Suir catchment and to flood magnitude and frequency relationships under climate change scenarios will be the focus of Chapter 7 and Chapter 8. Finally, Chapter 9 will outline conclusions drawn and suggestions for further research.

Chapter 2 – Literature Review

2.1   Introduction

This chapter explores the literature regarding climate change impact assessments with a particular focus on uncertainty. The body of literature regarding climate change and local impacts is vast and growing. Uncertainties arising within impact assessments will be presented, namely: uncertainties at the global scale; scenario uncertainty; global climate model (GCM) uncertainty and uncertainty regarding the global climate sensitivity. Regional scale uncertainties arising from the use of different downscaling techniques (dynamical downscaling and empirical statistical downscaling) will then be outlined. The final section of the chapter will detail uncertainties at the local scale, due to model structural uncertainty and equifinality of parameter sets.

2.2   Global Climate Change

2.2.1   Evidence for Global Climate Change

During the nineteenth and twentieth centuries, western societies became dependent on burning fossil fuels as the industrial revolution and the resulting technology and energy developments gathered pace.   The resulting levels of carbon dioxide (CO_2) in the atmosphere have risen dramatically from pre-industrial times, with a present amount of approximately 385 parts per million (ppm) in sharp contrast to pre-industrial levels of 270ppm (IPCC, 2007). This exceeds by far the natural range of CO_2 in the atmosphere over the past 650,000 years (IPCC, 2007). If other greenhouse gases (e.g. methane) are included in this statistic, the resulting concentrations are nearer 425 parts per million by volume (Fealy and Sweeney, 2008).

There now appears to be an overwhelming correlation between climate change and an increase in atmospheric greenhouse gas (GHG) concentrations. In the Fourth Assessment Report (AR4) the IPCC state "warming of the climate system is unequivocal, as is now evident from observations of increases in global average air and ocean temperatures, widespread melting of snow and ice, and rising global average sea level" (IPCC 2007, p.5). During the twentieth century the mean global annual temperature increased on average by

0.07^{o}C per decade, however during the last 50 years of the twentieth century, the decadal temperature increase has accelerated from 0.07^{o}C per decade to approximately 0.13^{o}C per decade (IPCC, 2007). Eleven of the twelve hottest years since temperature records began in 1850 have occurred since 1995 (IPCC, 2007). If greenhouse gas emissions continue unabated, a doubling of atmospheric concentrations of CO_2 is likely by 2100. Throughout the globe the evidence for climate change is mounting through decreases in the artic sea ice, decreases in northern hemisphere snow cover, retreat of mountain glaciers and increases in the strength of tropical cyclones.

2.3   The Role of Uncertainty in the formulation of Climate Projections

While the changes to the earth's average temperature are not unprecedented, contemporary human society has altered the structure of the atmosphere in a way that is unique in earth's history. Humans have also modified the landscape to an unprecedented scale during the nineteenth and twentieth centuries, and the human population is growing exponentially, doubling in size in the past 50 years. Pittock and Jones (2000) note that the impacts of the resulting changes to natural and anthropogenic systems will be extremely complex, with many forces acting collectively.

2.3.1   Towards a Typology of Uncertainty

Predicting the affects of climate change is a complex exercise fraught with uncertainty. Moss and Schneider (2000, p.35) state that "the term 'uncertainty' can range in implication from a lack of absolute sureness to such vagueness as to preclude anything more than informed guesses or speculation….some categories of uncertainty are amenable to quantification, while other kinds cannot be sensibly expressed in terms of probabilities". Walker *et al.* (2003, p.8) define uncertainty as "…any departure from the unachievable ideal of complete determinism". Indeed, uncertainty propagates and intensifies through all the stages of climate change prediction from projections of future socio-economic development paths through the regional stage to local climate change impacts leading to a cascade of uncertainty or uncertainty explosion (Schneider, 1983; Jones, 2000a; Wilby, 2005) (see Figure 2.1). While there is no universal typology of uncertainty, for practical reasons researchers have attempted to distinguish between different dimensions of uncertainty in order to understand it better (Winkler, 1996). Uncertainty results from 'incomplete' knowledge and 'unknowable' knowledge (Hulme and Carter, 1999;

Oberkampf *et al.,* 2002). Incomplete knowledge, otherwise known as epistemic uncertainty (type B) stems from lack of knowledge of different factors that influence events. Examples of epistemic uncertainty are incomplete knowledge about ice and cloud albedo feedbacks. This type of uncertainty is potentially reducible and quantifiable as understanding of the different factors influencing the global climate system advances and computing power increases.
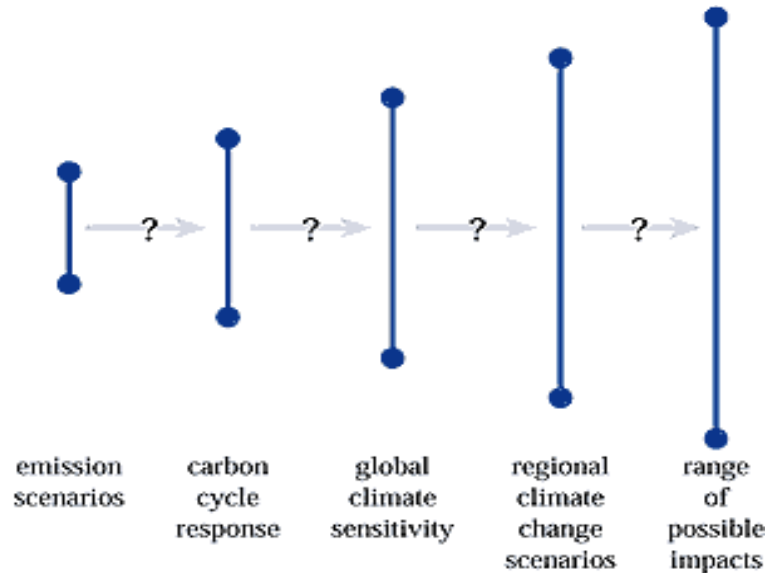
Figure 2.1 The cascade of uncertainty. Modified after Jones (2000) and "cascading pyramid of uncertainties in Schneider (1983)

Aleatory uncertainty (type A) or 'unknowable' knowledge stems from the chaotic, stochastic nature of the global climate system and from the uncertain future pathways of humanity which are the biggest influence on emissions scenarios. The chaotic nature of the global climate system means that a small change in any part of the system can have a large impact (Lorenz, 1993). Such unpredictability is irreducible. Even the best global circulation models will never eliminate this inherent unpredictability. Mitchell and Hulme (1999, p.57) note that "it is commonly inferred from the differences between climate models on regional scales that the models are deficient, but climate system unpredictability is such that …the differences are due to an unresolved combination of climate system unpredictability and model deficiencies".

Dessai and Hulme (2003) have defined another category of uncertainty: human "reflexive" uncertainty. By critically reflecting on information regarding climate change and its impacts, humans will surely act on the problem. They may consider how climate change will affect their livelihoods and those of future generations, and choose new actions and behaviours to reflect this. This can render any probabilities attached to emissions scenarios invalid. Dessai and Hume (2003, p.14) add that "the fact that humans are part of the system being researched in the case of the climate change problem therefore makes the uncertainty irreducible in the context of prediction: it makes all probabilities 'provisional'". Both aleatory and human reflexive uncertainties make up 'deep' uncertainty. Deep uncertainty cannot be adequately quantified, and pervades climate impact assessments from projections of future concentrations of GHGs to local impact assessments (Dessai and Hulme, 2007). Nonetheless, humans have always made adaptation decisions based on imperfect (uncertain) analysis. Furthermore, the possibility of being wrong in making adaptation decisions is not an excuse for inaction (Webster, 2003). Indeed, the presence of uncertainty highlights the need for flexible adaptation decisions which can be updated in light of new information (Hallegatte, 2009; Wilby and Dessai, 2010).

2.4 Uncertainties at the Global Scale

2.4.1 Emission Scenario Uncertainty

In order to account for uncertainty in the future development of human society, the IPCC have developed a range of scenarios in the Special Report on Emissions Scenarios (SRES) (Nakicenovic *et al.*, 2000). The SRES comprises 40 scenarios grouped into four different storylines. Each storyline details a distinctive development pathway to be taken by humanity which encompasses uncertainty due to differences in technological development and demographic and socio-economic change (see Appendix 1). The different developmental pathways were assigned different emissions scenarios which were translated into atmospheric concentrations of greenhouse gases and aerosols.

Six marker scenarios (A1FI, A1B, A1T, A2, B1, B2) were defined and climate modellers employed these as input to drive their GCMs and develop a range of climate scenarios (Arnell *et al.,* 2004.). As with all future scenarios, uncertainty increases the further into the future one projects (Figure 2.1). No likelihoods have been attached to the different

storylines as they are considered equally valid. The SRES do not take account of all possible futures, for example they do not include specific "disaster" scenarios (e.g., a possible melting of the Greenland Ice Sheet and the subsequent effect of rising sea levels). Neither do the SRES storylines take account of possible climate mitigation policies which may be enacted by the international community.
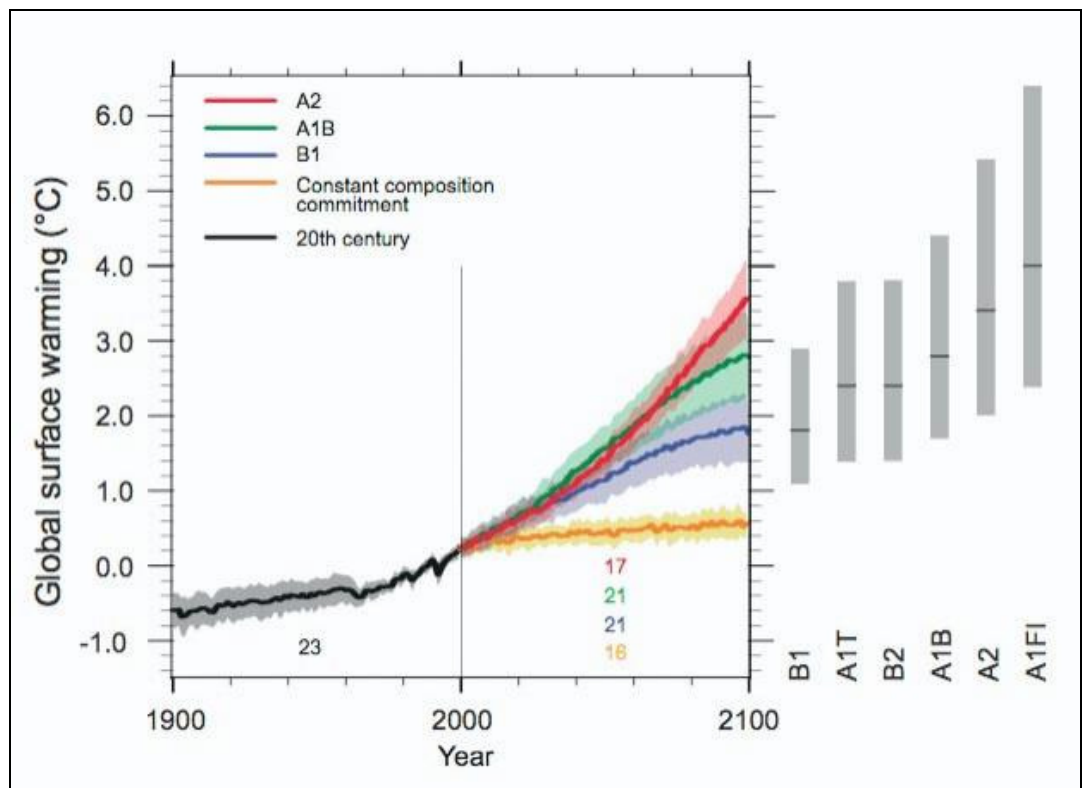
Figure 2.2 Globally averaged surface temperature change by 2100 depending on emission scenario (IPCC, 2007)

The SRES are one of a number of different global scenarios developed to take account of future uncertainties in population, technological and economic change. Other scenarios include the ones detailed in the UNEP Global Environmental Outlook report (2002). Nonetheless the SRES have been the ones most extensively employed as the basis for calculating future greenhouse gas emissions. Arnell *et al.* (2004) recommend the use of a wider range of socio-economic scenarios than those provided in the SRES in order to better estimate the range of possible future climate impacts. They also note that land cover trends, while being consistent with the SRES storylines, are inconsistent with current global developments in land use (Arnell *et al.,* 2004). The EU ENSEMBLES project has recently

developed the E1 scenario, which is the first to incorporate an aggressive mitigation policy. Under this scenario, CO_2 levels peak at 535ppm in 2045 before stabilising at 440 ppm during the 22nd century (Lowe *et al.,* 2009).

Several studies on the effects of climate change on water resources and catchment hydrology have assessed the role of emission scenario uncertainty using the A2 and B2 scenarios (with different GCMs). Wilby (2005) found uncertainty due to emissions scenarios to be comparable to uncertainty due to the choice of calibration period in a simple conceptual rainfall-runoff model. Minville *et al.* (2008) assessed seasonal changes to catchment hydrology and noted that emission scenario uncertainty was less significant than GCM uncertainty, particularly in the 2080s. Wilby and Harris (2006) observed that emission scenario uncertainty was the least significant of the sources of uncertainty analysed (GCM, downscaling method, hydrological model structure and parameters, emission scenario) and GCM uncertainty the most significant.

2.4.2 GCM Uncertainty

The most powerful global circulation models are the coupled atmosphere/ocean models (AOGCMs). These models are extremely complex with many parameters. Additionally, the parameters within each model are unique and reflect the climatological conditions of their region of origin. When different external conditions are used to model the global climate system (e.g. anthropogenic emissions of greenhouse gases, volcanic eruptions, and variations in solar radiation) it is open to question how much uncertainty is due to the inherent unpredictability of the global climate system and how much is due to the different parameter values and model structures of the GCMs. Tebaldi and Knutti (2007, p.2056) observe that "…simplifications, assumptions and choices of parameterisations have to be made when constructing a model, as they inevitably lead to errors in the model and the forecasts it produces". Furthermore, even if a model structure was perfect, uncertainty would remain because of the inherent unpredictability of both human society and climate (Mitchell and Hulme, 1999).

Until recently, the practice of forcing a single GCM by a single emissions scenario led to a suppression of a large amount of uncertainty, which Hulme and Carter (1999) call a "dangerous practice". Current practice involves simulating a given scenario in an ensemble

11

of GCMs, which leads to a more comprehensive representation of uncertainty. The performance of an individual model is often weighted based on its skill at simulating observed climate. However, the ensemble projections are conditional on the scenario(s) and GCMs employed (Hall, 2007). Furthermore, the issue of equifinality (that many parameter sets and model structures simulate observed climate equally well) has been little explored within GCMs to date (Dessai *et al.,* 2009). All the AOGCMs employed in the multi-model ensemble for the IPCC AR4 included parameters for ocean, atmosphere, sea-ice and land (Tebaldi and Knutti, 2007). However, as these models become more sophisticated to include components such as atmosphere chemistry and embedded RCMs it may become increasingly difficult to arrive at a standard interpretation of the ensemble results (Tebaldi and Knutti, 2007). Computing power has also compromised the degree of complexity of GCMs. Nonetheless, the uncertainty space within the models may well increase in tandem with increasing computing power (Dessai *et al*., 2009). Uncertainty due to the choice of GCMs has been shown to be the most significant source of uncertainty in several studies on the effects of climate change on catchment hydrology and extreme fluvial events (e.g., Bergström *et al.,* 2000; Minville *et al.,* 2008; Prudhomme *et al.,* 2003; Wang *et al.,* 2006: Wilby and Harris, 2006).

2.4.3   Global Climate Sensitivity

The standard metric employed in estimating the response of the global climate system to increased concentration of greenhouse gases is the equilibrium climate sensitivity (ΔT), i.e. the increase in global mean surface temperature that results from a doubling of atmospheric CO_2 concentrations over pre-industrial levels (IPCC AR4, p.629). The uncertainty range for the global climate sensitivity has changed little in the last decades. In the IPCC Third Assessment Report (TAR) the global climate sensitivity was estimated to range from 1.5$^{\mathrm{o}}$C - 4.5$^{\mathrm{o}}$C (IPCC, 2001). In estimating the global climate sensitivity using a 53-member model ensemble, Murphy *et al.* (2004) obtained a probability density function (PDF) with a 5% to 95% probability range of 2.4 -5.4$^{\mathrm{o}}$C. In the IPCC AR4 it states "the global climate sensitivity…is *likely* to be in the range of 2$^{\mathrm{o}}$C to 4.5$^{\mathrm{o}}$C with a best estimate of about 3$^{\mathrm{o}}$C, and is *very unlikely* to be less than 1.5$^{\mathrm{o}}$C. Values substantially higher than 4.5$^{\mathrm{o}}$C cannot be excluded, but agreement of models with observations is not as good for those values" (IPCC AR4, p.12; italics mine) (see Figure 2.3). Roe and Baker (2007) emphasise that the climate sensitivity range is unlikely to change much in the next IPCC report due to the non-

linearity of feedbacks of individual climate processes. Indeed, the scientific community are not sure about how uncertain is the response of the climate to radiative forcing (Hall, 2007). The increase in temperature is the most obvious result of anthropogenic climate change, however there are also likely to be changes in precipitation levels over a regional and local basis. These are much more difficult to estimate as precipitation is not normally distributed and is much more variable spatially and temporally than temperature. In the IPCC AR4 it is noted that "for the same emissions scenario, different GCMs produce different geographical patterns of change, particularly with respect to precipitation, which is the most important driver for freshwater resources" (IPCC AR4, p.180).
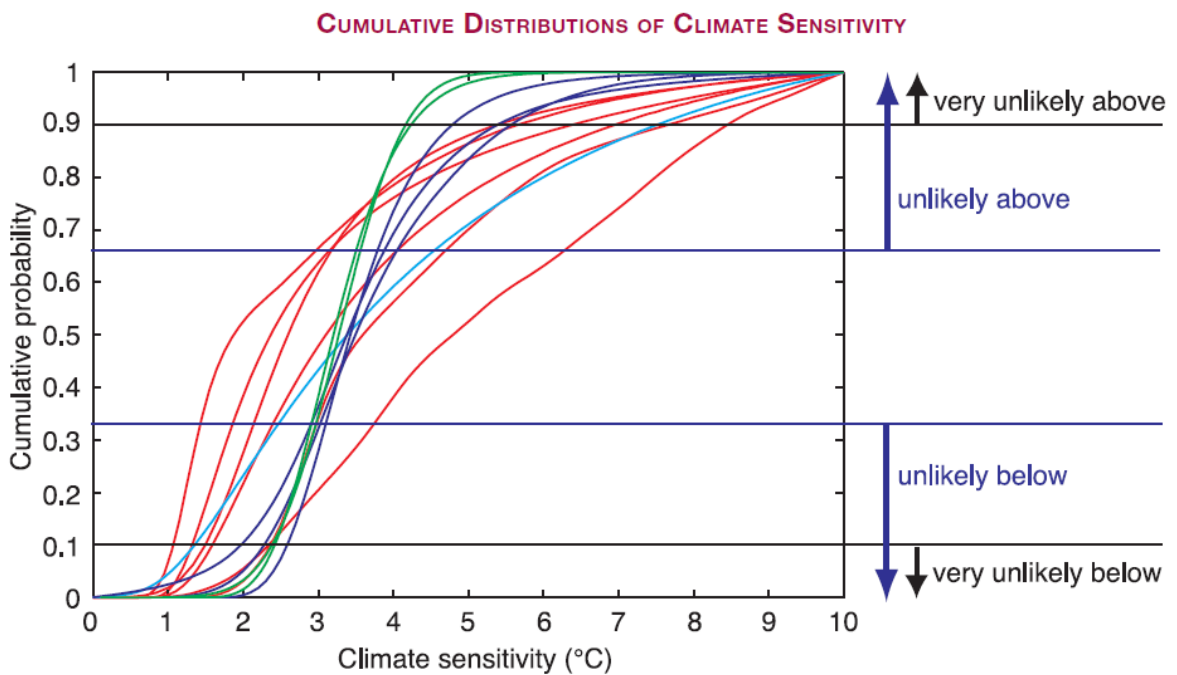
Figure 2.3 Cumulative distributions of global climate sensitivity (IPCC, 2007)

2.5   Regional Level Uncertainties

Uncertainties at the regional level hinge on the choice of downscaling method. GCM output is generally too coarse (typically $150 - 300km^2$) to be of use in regional or local level assessment and therefore some sort of downscaling is required. In recent years two methods of downscaling have come to the fore: dynamical downscaling and statistical downscaling.

2.5.1 Dynamical Downscaling

Recent increases in computational power have led to the increasing use of dynamical downscaling and Regional Climate Models (RCMs) are being more extensively employed RCMs use the information embedded within their parent GCM to derive smaller-scale regional information. They generally have a resolution of 20km to 60km and a domain area of 106km to 107km (UNFCCC, 2010). The advantages of RCMs are that they produce data at a much higher resolution than their parent GCM which takes account of local and regional topography. However, RCMs use a lot of computational resources and require considerable expertise in climate modelling. Moreover, all forms of downscaling propagate the uncertainties contained within their parent GCM as well as adding intrinsic uncertainties of their own. Fowler and Ekström (2009) employed 13 RCMs from the EU PRUDENCE ensemble to assess changes to seasonal precipitation extremes in 9 UK catchments for the 2070 to 2100 period using the A2 scenario. Extremes were well simulated for the winter but poorly simulated for the summer. Dessai *et al.* (2009) highlight the dangers of confusing higher precision (spatial or temporal resolution) with greater accuracy, when in fact there are irreducible uncertainties not amenable to quantification due to the chaotic, unpredictable nature of the global climate system.

2.5.2 Empirical Statistical Downscaling

Another viable method of increasing the resolution of GCMs for use in regional and local analysis is empirical statistical downscaling. Statistical downscaling derives statistical relationships between observed high resolution mesoscale variables e.g., geopotential heights, humidity and vorticity, (typically local level) and lower resolution (GCM) variables. One of the most important assumptions in statistical downscaling is that these relationships will remain stationary in a changing climate (Hewitson and Crane, 2006). Another assumption is that the predictor variables employed in the downscaling are adequately simulated by GCMs (Fealy and Sweeney, 2007; 2008). One advantage of this method is that it uses considerably less computing power than RCMs, and has comparative ease of application (Hewitson and Crane, 2006).

There are many methods of statistical downscaling, including multiple regression techniques and weather generators. The Statistical Downscaling Model (SDSM) was developed by Wilby *et al.* (2002). This model includes both stochastic weather generator

techniques and multiple regression methods. While both RCMs and empirical statistical downscaling use different predictor and predictands, and operate on different spatial domains, it is difficult to compare methods directly. However, the Statistical and Regional Dynamical Downscaling of Extremes for European regions (STARDEX) project has attempted a comparison of both downscaling techniques. One of the focuses of the project was in formulating mean climate projections for the present century. Generally, the models performed better downscaling temperature than precipitation and capturing means rather than extremes (STARDEX, 2006).

2.6 Downscaling of Extreme Values

As this project is concerned with exploring uncertainty in the changing magnitude and frequency of flooding within the Suir catchment due to climate change, it is pertinent to include a brief discussion of the success or otherwise of the simulation of extreme precipitation in both dynamical and statistical downscaling. Fowler *et al*. (2007) note that it this is a difficult exercise, since there are many methods for evaluating extreme values (e.g. 5th and 95th percentiles, or rare events such as the 1 in 50 year rainstorm). One of the conclusions of the STARDEX project was that the models performed better downscaling temperature than precipitation and capturing means rather than extremes (STARDEX, 2006). Moreover, extreme precipitation events vary greatly in magnitude from catchment to catchment. Haylock *et al.* (2006) compared six dynamical and two statistical downscaling models based on their ability to simulate seven seasonal indices of heavy precipitation events at the station scale in the UK. Generally winter showed the highest downscaling skill and summer the lowest. Additionally, precipitation occurrence was better simulated than precipitation intensity. Inter-model differences between future simulations were shown to be as significant as differences between future scenarios for a single model (Haylock *et al.*, 2006). Kyselỳ (2002) notes that extremes produced by all downscaling methods would be too moderate compared with observed data, possibly due to the assumption of linearity in most of the methods.

Although the main focus in Fealy and Sweeney (2008) was also in generating scenarios representing the projected mean climate state for the present century, a significant increasing trend was detected in 5-day rainfall totals in 8 midland and eastern synoptic stations. However, they add that while confidence in the precipitation indices should be

considered low, they are still in agreement with changes in precipitation suggested by the driving GCMs (Fealy and Sweeney, 2008).

2.7   Uncertainties at the Local Level

Much uncertainty accumulates before the local stage of a climate impact assessment. However, local impact models present additional uncertainty. In this section, the literature review focuses on two sources of uncertainty: model structural uncertainty and uncertainty due to equifinality of parameter sets. A methodology for taking account of uncertainty due to equifinality of parameters will also be discussed. Although uncertainty is also associated with input data, it will not be evaluated in this thesis.

2.7.1   Model Structural Uncertainty

Model parsimony, sometimes called Ocham's razor, is the concept that a model should only be as complex as is necessary to simulate observations precisely enough to be useful (Beven, 2000). This idea was outlined in Nash and Sutcliffe (1970) who emphasised that complexity should be added to a model only as long as it increases accuracy and efficiency. As understanding of different catchment processes has become more sophisticated, there is a tendency to build models of increasing complexity to reflect this (Perrin *et al.*, 2001).

However, increasing complexity does not necessarily improve model performance. Studies which have researched this issue include Francini and Pacciani (1991) who compared seven different conceptual rainfall-runoff models and concluded that there was little to distinguish between the models output despite structural differences. Chiew *et al.* (1993) compared six rainfall-runoff modelling approaches and concluded that a complex conceptual model (MODHYROLOG) gave the best simulation of daily high and low flows. However, a simple conceptual model (SFB) gave satisfactory results when simulating monthly and annual yields in wetter catchments.   Jakeman and Hornberger (1993) using only precipitation, air temperature and stream flow as inputs found that a two component linear model with four parameters was the optimal model for simulating flow in 7 catchments with a temperate climate regime. They also noted that the information content in a runoff record alone is too small to conclude that the concepts within the conceptual rainfall-runoff model are 'true' for that catchment even if a good simulation of observed flow is obtained (Jakeman and Hornberger, 1993).

16

Perrin *et al.* (2001) suggested that equifinality of model structures should be investigated to evaluate if different models provide equally good results when simulating observed catchment flow. Perrin *et al.* (2001) in an inter-comparison study of 19 lumped rainfall-runoff models (including HBV) found that 3 to 5 parameters produced satisfactory results in simulating a time-series of daily data. They further argued that even though model parsimony is an important issue or models may become over-parameterised, there are also limits to model simplicity. In their study, Perrin *et al.* (2001) tested the models on 429 catchments in France, the United States, Australia, the Ivory Coast and Brazil in order to evaluate the models' versatility. One of the limitations of the modelling framework employed in this project is that it tests the models on only one catchment so model versatility is not evaluated. One of the conclusions in Georgakakos *et al.* (2004) is that multi-model ensembles should be used to account for uncertainty at the local level of a climate impact analysis. Butts *et al.* (2004), support this finding. Moreover, in their study of model structural uncertainty sensitivity of streamflow to variations in model structure was as large as parameter and measurement uncertainty. A framework for dealing with uncertainty due to model structural error is presented in Refsgaard *et al.* (2006), which involves the use of multiple conceptual models and tests the tenability of each model within a prescribed framework.

2.7.2   Model Structural Uncertainties in Climate Change Studies

It is one thing to test models on catchments not undergoing dynamic change (e.g., land use or climate change), quite another to use rainfall-runoff models in a climate change simulation. Cameron *et al.* (2000) evaluated changes to flood frequency using a continuous simulation methodology with one model (TOPMODEL). The scenarios employed generated little uncertainty, however, the distribution of T year floods changed. Cameron *et al.* (2000) concluded that hydrological model structural uncertainty needs to be accounted for in estimating impacts of climate change. Prudhomme *et al.* (2003) studied the uncertainty of climate change impacts on the flood regime of small UK catchments using 25,000 climate scenarios randomly generated and one hydrological model (PDM). They found that while the magnitude of flood peaks could increase under the climate scenarios, the median value of changes was within the 95% confidence intervals associated with present climate. Wilby and Harris (2006) assessed the different sources of uncertainty in a climate impact assessment of future low-flow in the River Thames using six different

GCMs, two emissions scenarios and two hydrological models (CATCHMOD and REGMOD). Q95 simulated in both models was comparable to observed flow for the calibration period (1961 – 1990), although low flows were more conservatively modelled in the more complex model (CATCHMOD) than for REGMOD. This was believed to be due to the soil moisture accounting routine in CATCHMOD which was unseen in REGMOD (Wilby and Harris, 2006). Højberg and Refsgaard (2005) studied 3 groundwater models of different complexity and concluded that climate change uncertainties would be underestimated if model structural uncertainty was not explicitly taken into account. Ludwig *et al.* (2009) evaluated 3 hydrological models of different complexity (a spatially distributed model – PROMET; a semi-distributed model operating on relative homogenous hydrological units – HYDROTEL; a lumped bucket-type conceptual model – HSAMI) modelling future discharge in the Ammer basin in Southern Bavaria from 2071 - 2100. HSAMI modelled future runoff far below plausible values, while the other two models behaved within a comparable range. One of the conclusions was that simple conceptual models are inadequate for assessing climate change impacts and that an ensemble of impact models should be employed for an improved understanding of local impact model complexity (Ludwig *et al.,* 2009).

2.7.3   Irish Hydrological Impact Studies

In Ireland, several studies have also focussed on the effects of climate change on catchment hydrology and extreme fluvial events (Charlton *et al.,* 2006; Murphy and Charlton, 2008; Semmler *et al.,* 2006; Steele-Dunne *et al.,* 2008; Wang *et al.,* 2006). Murphy and Charlton (2008) assessed changes to the hydrological regime and extreme flows due to climate change in 10 Irish catchments using HYSIM. By the 2050s the current $T50$ flood may become a 7.2 year event and by the 2080s it could be reduced to a 4.5 year event using both A2 and B2 scenarios and HADCM3 GCM. Steele-Dunne *et al.* (2008) evaluated changes to the hydrology of the same Irish catchments from 2021 to 2060 using HBV-Light to model the output from the RCA3 regional climate model driven by the ECHAM 5 GCM and the A1B emission scenario. The risk of extremely high winter flows was projected to almost double in the Suir catchment for the future time period. All the above studies employed only one hydrological model: HYSIM in the former two papers and HBV in the latter. Both models proved plausible representations of Irish catchments. However, as only one hydrological model was used in each study, model structural uncertainty was not

adequately accounted for. Nonetheless, in several studies cited in the paragraph above, model structural uncertainty is an important source of uncertainty at the local stage of a climate impact assessment. If such an assessment is employed to inform adaptation decisions or policy, then an ensemble of hydrological models should be employed at the local stage to better characterise ranges of change in catchment hydrology and extreme events due to climate change (e.g., Butts *et al.,* 2004; Georgakakos *et al.,* 2004; Højberg and Refsgaard, 2005; Ludwig *et al.,* 2009; Refsgaard *et al.,* 2006).

2.7.4 Equifinality of Parameter Sets and Model Structures

Equifinality is the concept that many parameter sets and models give equally good results in simulating observed flow (e.g., Beven and Binley, 1992; Beven, 1993; Beven and Freer, 2001). This can be due to model structural complexity, model structural error, model over-parameterisation, input data error, non-linearity of model structure, parameter interactions and the complexity of the system being modelled. In practice, it can be difficult to differentiate between these different sources of uncertainty (Butts *et. al.,* 2004). Beven (2000, p.21) lists two implications of the above:

- Parameter values determined by calibration are valid only inside the model structure used.

- The optimal parameter set may be a dubious concept in hydrological modelling, where it has been demonstrated that many parameter combinations and models give acceptable simulations of the response of a catchment.

While accepting the concept of equifinality and incorporating it into model calibration and validation implies that some means of quantifying uncertainty must be included at these stages, it can be argued that equifinality is a more realistic way of approaching a hydrological modelling exercise. Recent studies which have found many models giving good fits to observed data include Blasone *et al.* (2008); Cameron *et al.* (2000); Christiaens and Feyen (2002); Højberg and Refsgaard (2005); Murphy (2006); Wilby (2005) and Wilby and Harris (2006). Equifinality of model structure was studied by Perrin *et al.,* 2000. Conversely, the assumption that a given model structure or parameter set represents the "true" version of a catchment response is ill-founded. It is accepted that hydrological

models, no matter how sophisticated, will never fully represent the complex and heterogeneous reality of a river catchment. Indeed, environmental systems are so complex that many different interpretations of that system may be plausible (Beven, 2002).

It can also be argued that model results should be given as a range rather than a single result (Steele-Dunne *et al.,* 2008; Uhlenbrook *et al.,* 1999). The use of just one model structure and one optimal parameter set suppresses much uncertainty. This may lead to dubious results and even maladaptive policies being implemented if the modelling exercise is used as a basis for informing policy decisions. Beven (2000, p.240) notes that "…the choice of just a single model is equivalent to assigning a positive prior likelihood to parameter sets sampled for that model…and zero to all other models". This project attempts to analyse uncertainty of model structure and uncertainty of parameters and to evaluate which provides the greatest source of uncertainty within the modelling framework.

2.7.5   Parameter Definition, Identifiability and Non-Uniqueness
Historically the problem with identifying a global optimal parameter combination was described as an issue of parameter identifiability or non-uniqueness (Beven, 2009). A well-identified parameter is one in which the objective function value decreases away from an optimal value, and has a distinct peak (Uhlenbrook *et al.* 1999). The issue of parameter identifiability (and non-uniqueness) is particularly relevant if the modeller comes from a standpoint of there being a single optimal parameter set within the response surface. However, if equifinality of models and parameter sets is accepted then the scatter graphs show that many parameter values may be behavioural. Moreover, Beven (2000) highlights the fact that scatter graphs of individual parameters are a crude projection of the parameter response surface and cannot show the complex interactions between parameters. A less-than-optimal value of one parameter may be compensated for by other parameters. What is important in taking equifinality into account is not so much the individual parameter values, but the parameter values within behavioural *sets* (Beven, 2000; 2002). Indeed, Beven (2005) argues that parameter non-uniqueness and non-identifiability are intrinsic to the modelling process.

Traditional sensitivity analyses highlight individual sensitive parameters (as opposed to insensitive parameters where various parameter values do not influence the model output).

However, such analyses cannot take account of parameter interactions within the response surface. Uhlenbrook *et al.* (1999) distinguish between insensitive parameters and uncertain ones. Model output does not vary when the values of an insensitive parameter are changed. Conversely, model output may be sensitive to the changing values of an uncertain parameter, but these changes can be compensated for by other parameters in the set. .Beven and Binley (1992) devised a methodology for model calibration and validation which takes account of parameter uncertainty: the GLUE methodology. The advantage of the GLUE methodology is that by randomly sampling parameter sets, these interactions are implicitly captured and behavioural parameter sets can be evaluated by a chosen likelihood measure (Beven, 2009).

2.7.6   The GLUE Methodology

Generalised Likelihood Uncertainty Estimation (GLUE) is a strategy for model calibration and uncertainty estimation based on the theory that there is no optimal model structure or parameter set.   Rather, there are many parameter sets and models which give good simulations of observed data (Beven and Binley, 1992). Variants of the GLUE methodology include Dynamic Identifiability Analysis (Wagener *et al.*, 2003). In GLUE random parameter sets are generated from a prior distribution of parameter values using Monte Carlo sampling. The modelled output from each of these parameter sets is then compared quantitatively to the calibration data using a likelihood measure. Obviously, this methodology depends on a number of subjective decisions. Beven (2000, p.235) identifies the decisions which must be made before GLUE can be implemented.

- A decision about the model or models to be included in the analysis
- A decision about the feasible range for each parameter value
- A decision about the sampling strategy for the parameter sets
- A decision about an appropriate likelihood measure

While these decisions are undoubtedly subjective (in common with similar decisions made in any modelling exercise) and therefore qualitative rather than strictly quantitative, the explicit nature of the decisions and the fact that they can be critiqued ensures that there is some quality control in the methodology (Beven, 2000).

2.8 Conclusion

This chapter has explored the literature regarding uncertainties in each stage of a climate change impact assessment. In several studies, GCM uncertainty was the most significant source of uncertainty, while uncertainty due to emissions scenarios was less significant. There are also sources of uncertainty at the local stage of climate change impact assessments: namely model structural uncertainty and equifinality of parameter sets. The GLUE methodology was introduced as an effective method of analysing such uncertainty. In order to represent model structural uncertainty more comprehensively, it is suggested that a suite of impact models be included in further Irish studies that employ the climate change impact assessment methodology to inform adaptation decisions or policy. This follows the practice of using an ensemble of GCMs to better represent the uncertainties at the global stage of such an assessment.

Chapters 7 and 8 will focus on changes to catchment hydrology and flood magnitude and frequency resulting from project streamflow changes. The next chapter (Chapter 3) will focus on a description of the Suir Catchment and outline the methodology employed to generate the future climate data used in this project.

Chapter 3: Characteristics of the Suir Catchment and Description of the Future Climatic Data

3.1   Introduction

The Suir catchment has been chosen as the case study catchment for this project.   The main characteristics of the catchment will be described under bedrock geology; catchment soils; land use and catchment aquifer potential. These characteristics are especially relevant to the parameterisation of HYSIM. Some causes of climate variability within Ireland will then be examined, followed by a summary of recent trends in Irish climate. The following section of the chapter will provide a brief description the methodology for generating the downscaled future climatic data used in this project and will outline projected changes to temperature and precipitation for the 2050s and the 2080s (Fealy and Sweeney, 2007; 2008).   In the concluding section there will be a more detailed analysis of the future climate scenarios generated for the Kilkenny synoptic station, which is closest to the Suir catchment and from where the future data employed in this project originates.
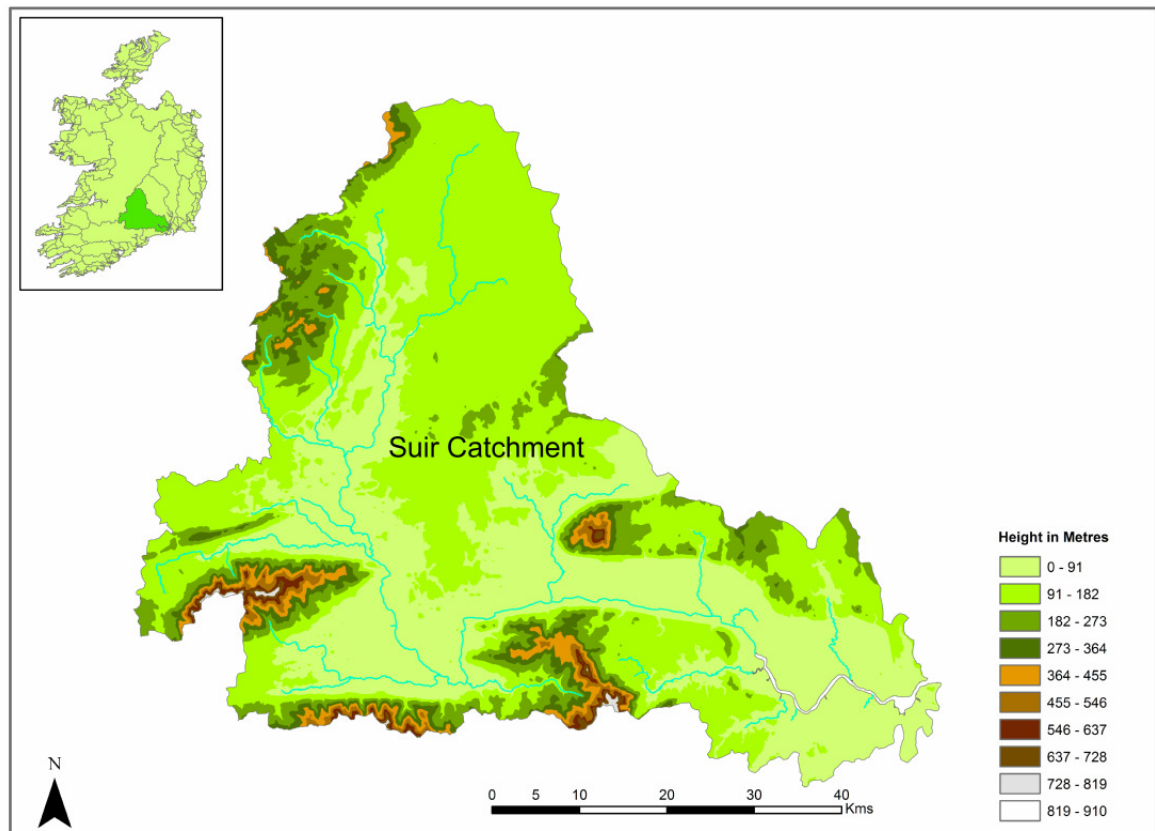
Figure 3.1 The Suir catchment

3.2   The Suir Catchment

The Suir catchment is the largest in the South Eastern River Basin District (SERBD), with a total catchment area of 2143 km^2 to the gauging station in Clonmel (see Figure 3.1). Six Irish counties make up the catchment including Waterford, Tipperary, Laois, Kilkenny, Cork and Limerick. The Comeragh and Knockmealdown mountain ranges form part of the southern boundary of the catchment and the Galtee mountain range lies to the southwest of the catchment.   The topography of the Suir catchment is rolling lowland with a mountainous fringe in southern areas. It has an annual average precipitation of 1110 mms and estimated annual losses of 483 mm, giving total effective rainfall of 627 mms. The mean annual flow in the river at Clonmel from the period 1940 – 2005 has been 45.28 m^3/sec and annual average runoff from 1961 to 2000 is 702.19 mms. The catchment elevation ranges from sea level to 910 metres, with a mean elevation of 129 metres approximately. Most of the land is worked agriculturally and land use in the catchment is dominated by pasture, which accounts for approximately 70% of the total land area. Coniferous forest accounts for 7% of the catchment area. Arable land and peat bogs which account for a further 5% approximately of the total land area of the catchment.

3.2.1   Bedrock Geology of the Suir Catchment

The bedrock geology of the Suir catchment is complex but is comprised mainly of Palaeozoic sedimentary rocks from the Carboniferous Period (354 – 298 million years ago) (see Figure 3.2). Indeed, the bedrock geology of the Suir catchment reflects that of Ireland as rocks from the Carboniferous period (354 – 298 million years ago) are the most abundant of any found on the island. The main formations in the catchment include Old Red Sandstone, conglomerate and siltstone from the Devonian Period (410 – 354 million years ago) which underlies 24% of the catchment and forms the main material in the mountain ranges which lie within the catchment boundary. A further 33% of the catchment is underlain by a marine shelf facies formation of limestone and calcareous shale from the Carboniferous Period. Courceyan limestone from the early Carboniferous Period underlies a further 17% of the catchment area. The bedrock of the Suir catchment gives rise to many regionally and locally important aquifers.
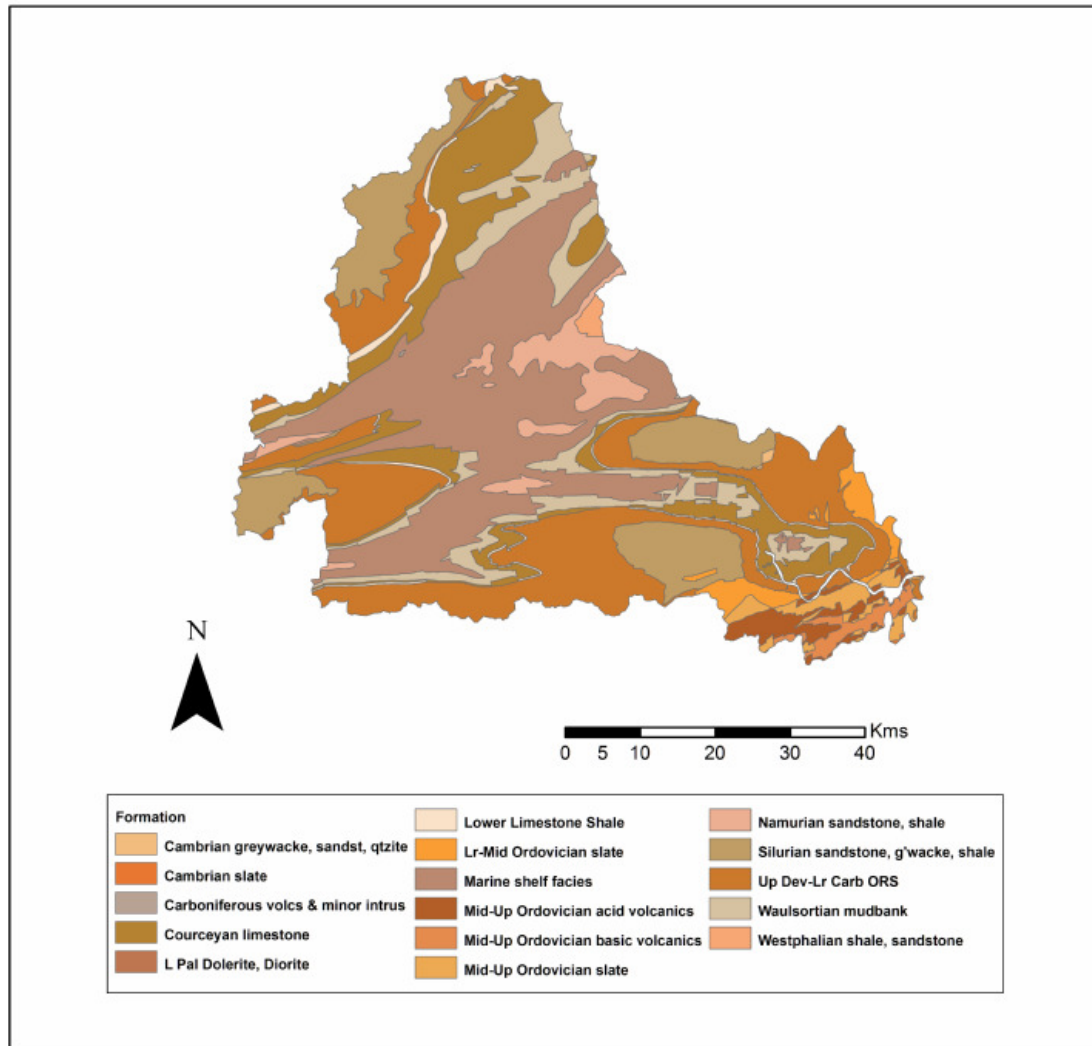
Figure 3.2 Bedrock map of the Suir Catchment

3.2.2   Soils of the Suir Catchment

The Suir catchment is characterised by well drained soils. The most extensive soil types in the catchment are minimal grey brown podzolics, brown podzolics, gleys and acid brown earths (see Figure 3.3).   These soils are part of the Great Soil Groups of Ireland and together account for 79% of all soils in the catchment (Gardiner and Radford, 1980). Many of these soils are subject to the process of podzolisation. During this process the soils are first subject to leeching (whereby solid constituents are carried down through the soil layers). As soon as conditions are suitably acidic, iron and aluminium are removed in solution.

The calcareous parent material which usually forms grey brown podzolics prevents the effects of extensive leeching from these soils. This in turn restricts the podzolisation process and the principal materials moved from the A to the B horizon are clay particles. The B horizon is heavier in texture than the A horizons due to the presence of so many clay particles. Grey brown podzolics make good farming soils, with the heavier textured soils more suitable for pasture production (Gardiner and Radford, 1980).
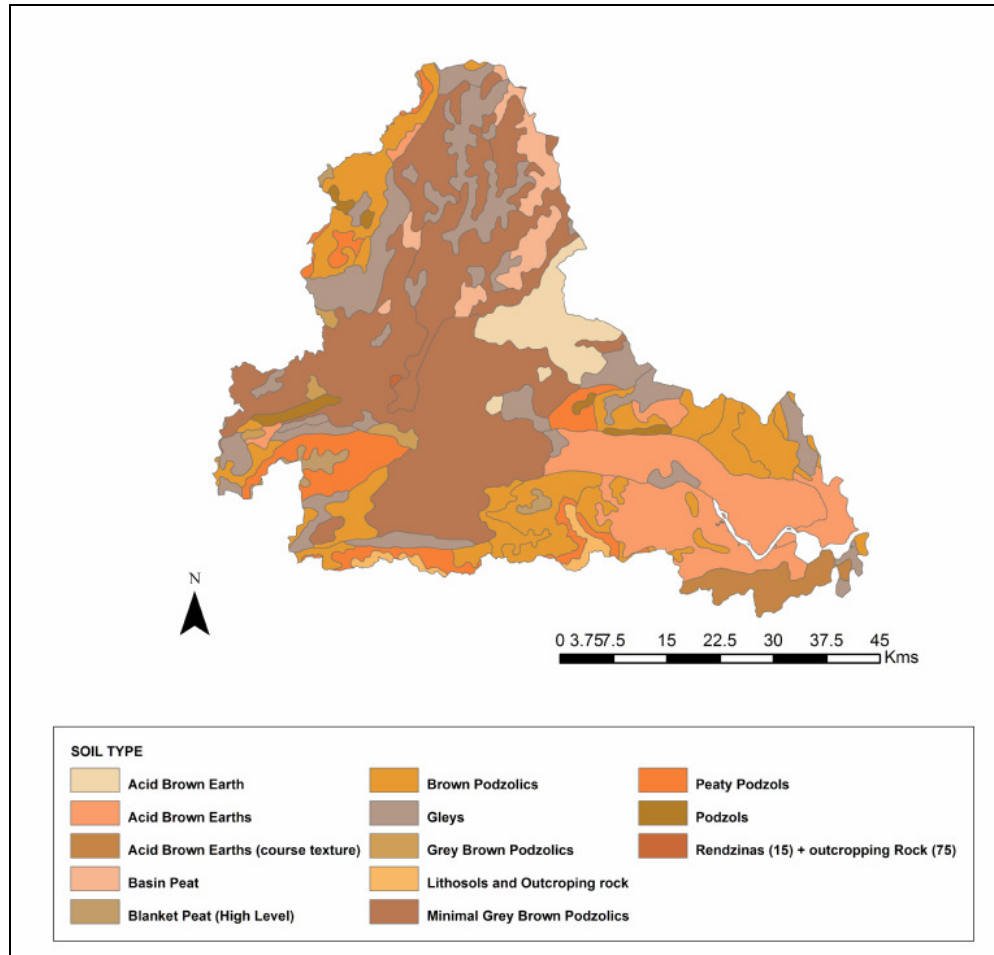
Figure 3.3 Principle soil types in the Suir catchment

The soil profile of brown podzolics consists of an A1 horizon with a mixture of organic and mineral matter. Accumulations of aluminium, iron and sometimes humus are present in the B horizon and unlike podzols, there is no iron pan present. Brown podzolics are good soils for use as pasture and for crop cultivation (Gardiner and Radford, 1980). Gleys develop in permanent or intermittent soil saturation. This may be due to a high water table, or a perched water table due to the impermeable nature of the soil itself. Runoff from slopes

26

can also be a causative factor. The poor physical condition of most gleys makes them unsuitable for cultivation or pasture.

Acid brown earths form well drained, mineral soils with a profile that is uniform and does not consist of distinct horizons. They are not as susceptible to leeching as podzols or brown podzolics. The acidic nature of these soils is due to the lime-deficient parent material. Brown earths are medium textured and because of their high mineral content and good drainage they are extensively cultivated (Gardiner and Radford, 1980). Subsoils within the catchment are formed from glacial tills, sands and gravel. The well drained nature of the soils in the Suir catchment together with highly permeable subsoils means that the Suir is a baseflow dominated river, which is particularly sensitive to soil moisture reductions that may occur as a consequence of climate change. The nature of the soils also has a big influence on land use within the catchment.

3.2.3   Land Use within the Suir Catchment
The Suir catchment area comprises areas of counties Cork, Limerick, Laois, Kilkenny, Tipperary and Waterford. The CORINE (Co-ordinate of Information on the Environment) 2000 land use database supplied by the EPA was employed to define the land use types within the catchment. The shapefiles from Cork, Limerick, Laois, Kilkenny and Waterford were loaded and merged using the merge command from data management in ArcToolBox. In the accompanying shapefile databases the land use codes were recorded under "CODE 3". The six counties were merged under this code, in order to aggregate the land use codes for the different shapefiles.

The Suir catchment is characterised by a mainly rural agricultural hinterland. Pasture is by far the dominant land use type in the catchment, accounting for 70% of the catchment area (see Figure 3.4). Coniferous forests account for a further 7% each of the catchment. Non-irrigated arable land and peat bogs are the next most dominant land use types, accounting for a further 5% of the catchment. Major urban areas form a very small part of the catchment, with 80% of the population of the SERBD living in small villages. However, the SERBD is the most densely populated RBD after the Eastern RBD. Despite the rural nature of the catchment, population pressure is putting demands on the natural resources of the area.
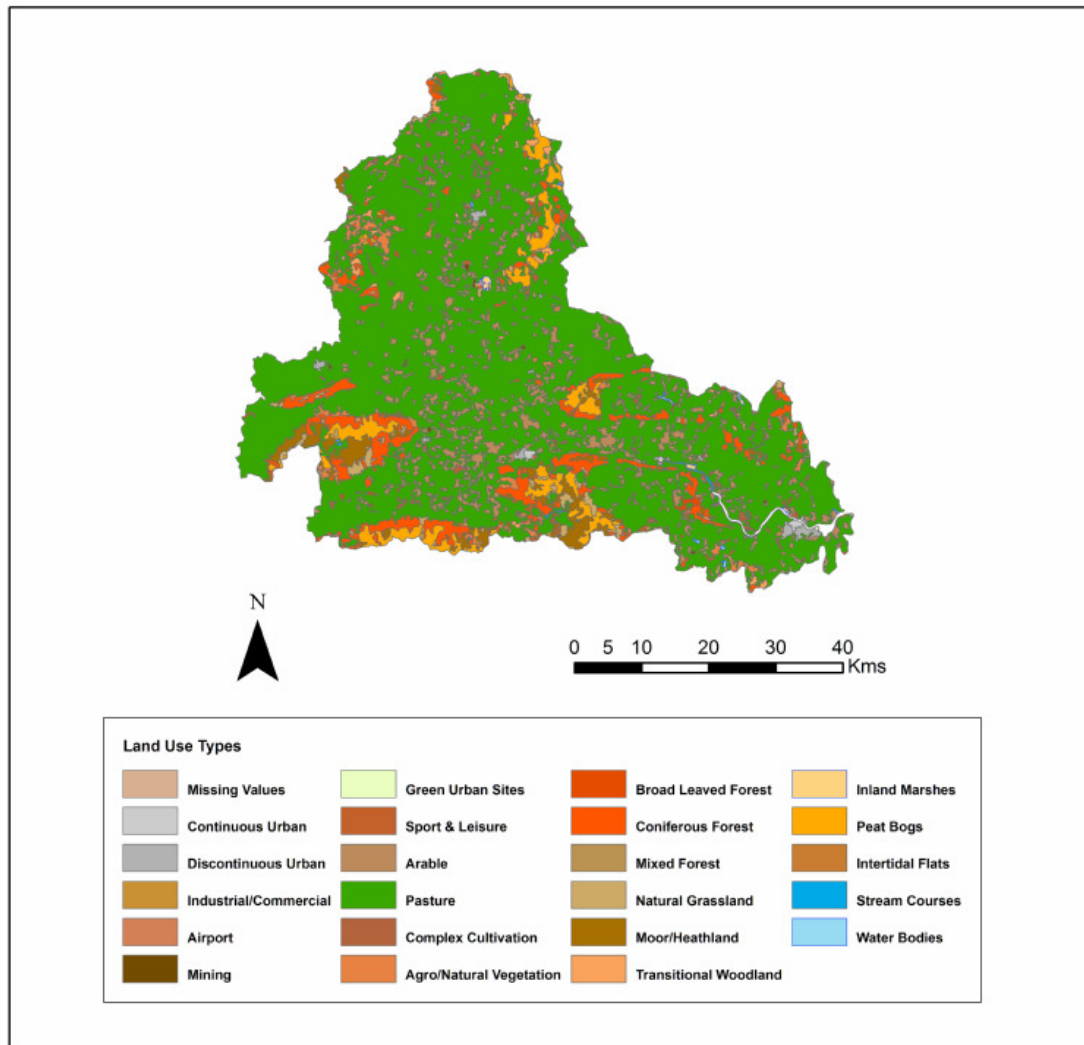
Figure 3.4 Land use types within the Suir catchment

3.2.4 Suir Catchment Aquifer Potential

In most Irish aquifers, groundwater flow is through fissures and fractures due to the karstic nature of the bedrock (largely limestone). Within the Suir catchment there are a number of regionally and locally important aquifers. Figure 3.5 below was delineated from the aquifer map of the Geological Survey of Ireland (GSI). Moderately productive, locally important aquifers underlie almost half the catchment. Regionally important aquifers account for a further 35% approximately of aquifer types within the catchment and of these diffuse karst aquifers are the most common type. In the land above these aquifers there is a strong connection between groundwater and surface water. The principle aquifer types in the catchment are shown below:

Rf : Regionally important aquifer – fissured bedrock

Rkd : Regionally important aquifer – karsified (diffuse)

Lm : Locally important aquifer – bedrock moderately productive

LI : Locally important aquifer – bedrock moderately productive only in local zones

Lk :   Locally important aquifer – karsified

PI :   Poor aquifer – bedrock unproductive except for local zones

Pu :   Poor aquifer – bed generally unproductive
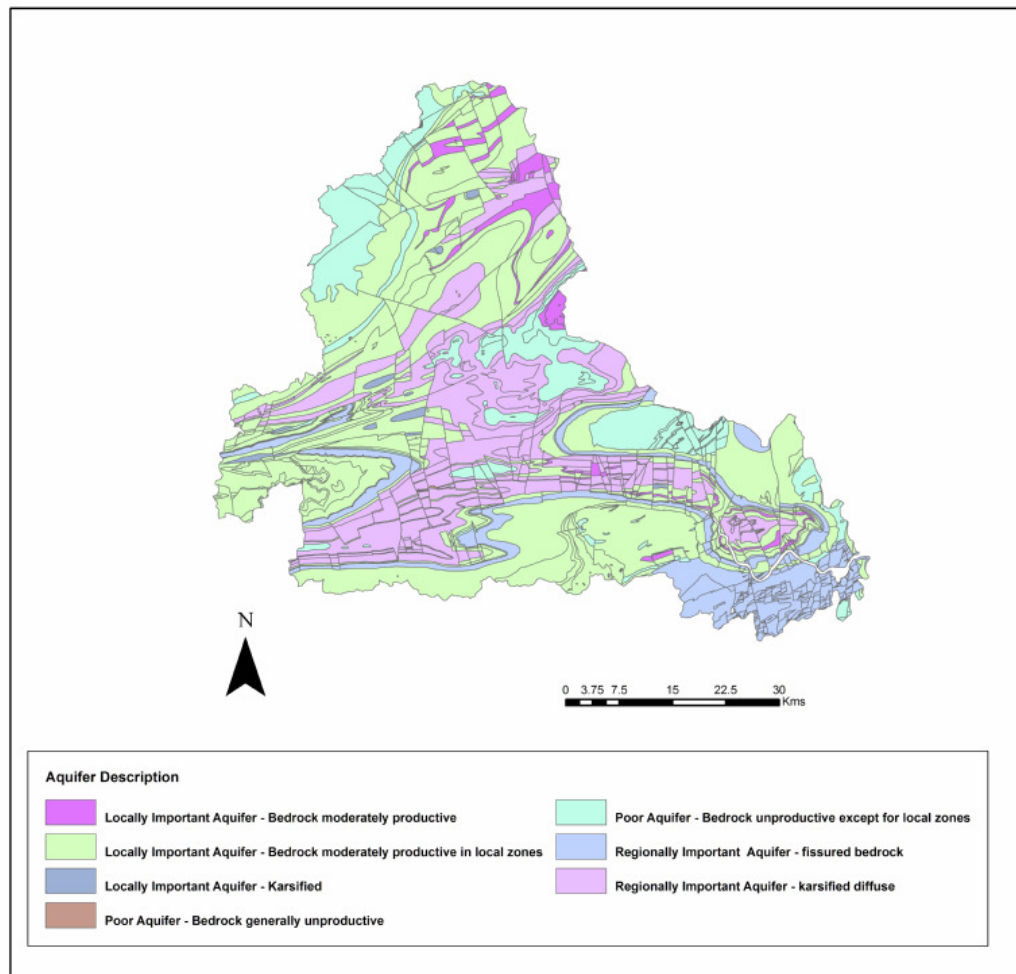
Figure 3.5 Suir catchment aquifer potential

3.3   The Climate of Ireland

Ireland lies in the mid latitudes off the north-western European landmass between 51.43°N and 55.38°N and 5.38°W and 10.51°W. The climate of Ireland is dominated by its proximity to the Atlantic Ocean and by the accompanying thermohaline circulation which

ensures that north-western Europe has a milder climate than other regions at the same latitude. Average annual temperature within Ireland is approximately 9ºC. Ireland's proximity to the Atlantic means that there is great year to year variability in rainfall. Based on thirty year averages (1961 – 1990) precipitation receipts in lowland areas range from 750 mm in eastern and north-eastern parts to more than 1200 mm in the west, north-west and south-west (Keane and Sheridan, 2004). However, there is a lot of spatial variation around the island with mountainous areas having much higher precipitation receipts. For example, on Corrán Tuathail annual precipitation can reach a maximum of 3200 mm (Keane and Sheridan, 2004).

There are also prominent rain shadows in the lee of mountain ranges, for example the Wicklow mountains. April is generally the driest month of the year, however in southern areas June is the driest month while December and January are the wettest months (Met Eireann, 2010). In general, the dry period in Ireland extends from April to July while the wettest period is from October to January. In terms of seasons, winter is the wettest season followed by autumn. The average number of wet days (days with more than 1 mm of rain) ranges from 150 days in the east and southeast coasts to approximately 225 days per year in parts of the west (Met Eireann, 2010). At present there are 15 synoptic stations where air pressure, wind air and soil temperatures, humidity and precipitation are measured hourly and a number of climatological stations where precipitation and air temperature are measured daily (Figure 3.6).

Mean annual temperature exhibits a north-northeast to southwest gradient with average values varying from 9ºC in parts of the northeast to 10.6ºC in the extreme southwestern part of the country (Keane and Sheridan, 2004 p.34). Lowest air temperatures in Ireland occur in mid-winter with mean daily maximum temperatures during the summer reaching 16ºC to 17ºC in coastal areas and 19ºC or 20ºC inland (Keane and Sheridan, 2004). A warming trend has been observed in Ireland during the twentieth century with a temperature increase of 0.7ºC between 1890 and 2004 and six of the ten warmest years on record occurring since 1995 (McElwain and Sweeney, 2007).
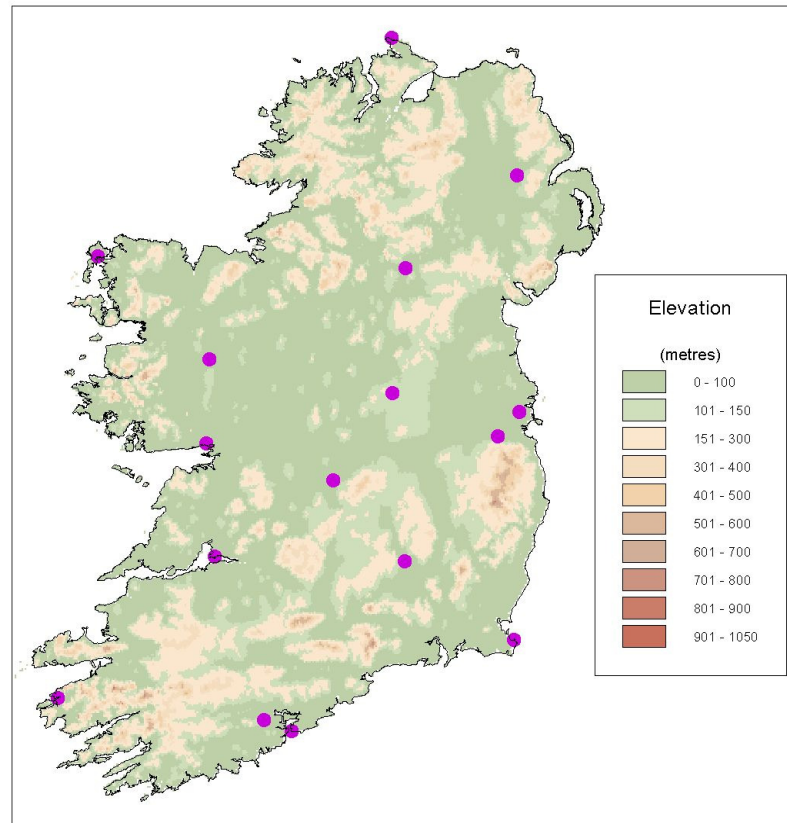
Figure 3.6 The Irish synoptic weather stations

The amount of solar radiation received in Ireland is strongly correlated to the seasons. Because of Ireland's northerly position, the length of day varies between 7.5 hours in mid-winter to 16.5 hours in mid summer.   There is a west to east gradient in annual sunshine hours from under 1200 hours in parts of the north-west, west and south-west, to approximately 1600 hours in the south-east. Based on mean monthly totals of sunshine from a sample of nine synoptic stations from 1971 to 2000, May tends to be the sunniest month of the year in most of the synoptic stations, followed by June (Keane and Sheridan, 2004).

Evapotranspiration (ET) is the sum of evaporation and transpiration (water flux through plant stomata) from land surfaces into the atmosphere. In Ireland, The energy for ET is supplied principally by solar radiation but also depends on humidity and wind speed. Potential evapotranspiration (PE) is the same flux under saturated soil conditions. It can be difficult to measure accurately. In Ireland, PE is calculated from data recorded at the synoptic stations using the Penman-Monteith equation.

3.3.1 Climate Variability within Ireland

Several authors have examined changes in the synoptic pattern of precipitation in Ireland (Houghton and O'Cinneide, 1976; Sweeney, 1985; Sweeney and O'Hare, 1992; Kiely, 1999; McElwain and Sweeney, 2007). Sweeney (1985) studied the influence of Lamb circulation categories over Ireland. He observed that while cyclonic and westerly circulation categories accounted for 66% of annual rainfall, the influence of the westerly circulation type had noticeably diminished between 1961 and 1984 compared to the previous 100 year averages. There was a substantial reduction in days with westerly circulation patterns from 80 per year in the 1940s to approximately 50 per year in the 1970s, which has been linked to changes in the global circulation. However, in terms of total precipitation, decreasing contributions from westerly airflows had been balanced by increases in precipitation from other sources, principally cyclonic and hybrid. (Sweeney, 1985 p.478). Furthermore, days with westerly circulation increased once again in the 1970s (Mayes, 1991).

Kiely (1999) studied changes in precipitation patterns in Ireland arising in the mid 1970s which were strongly correlated to a positive phase of the North Atlantic Oscillation Index (NAOI). The resulting enhanced flow of westerly winds increased precipitation depths and streamflow especially in the west of the island. Kiely (1999) observed that there was a significant increase in precipitation on the west coast after the change point year of 1975, however there was little increase in post-1975 annual precipitation on the east coast. Discharge series (1958 to 1995) for the rivers Boyne, Erne, Blackwater and Brosna were also examined to detect any changes in streamflow. Three rivers (the Erne, Blackwater and Boyne) showed increases in annual mean daily flow after the mid 1970s. Kiely (1999) notes that Ireland is experiencing an enhanced hydrological cycle (beginning in the mid-1970s) which will have critical implications for flood management, particularly in the west.

3.4 Trends in the Climate of Ireland

3.4.1 Temperature

Trends in the observed temperature of Ireland are largely consistent with the global temperature increase. McElwain and Sweeney (2007) used data from 11 synoptic stations in Ireland to evaluate key meteorological indicators of climate change. From 1890 to

2004, mean annual temperatures in Ireland have risen by 0.7°C at a rate of 0.06°C per decade. Nonetheless this trend is not linear, with particular increases in two periods: 1910 to 1949 and 1980 to 2004 (McElwain and Sweeney, 2007). During the first period the rate of warming was 0.23°C, while during the latter period the rate of warming increased to 0.42°C. McElwain and Sweeney (2007) also identified fewer frost days from 1961 to 2005 due to a marked increase in the maximum and minimum observed temperatures.
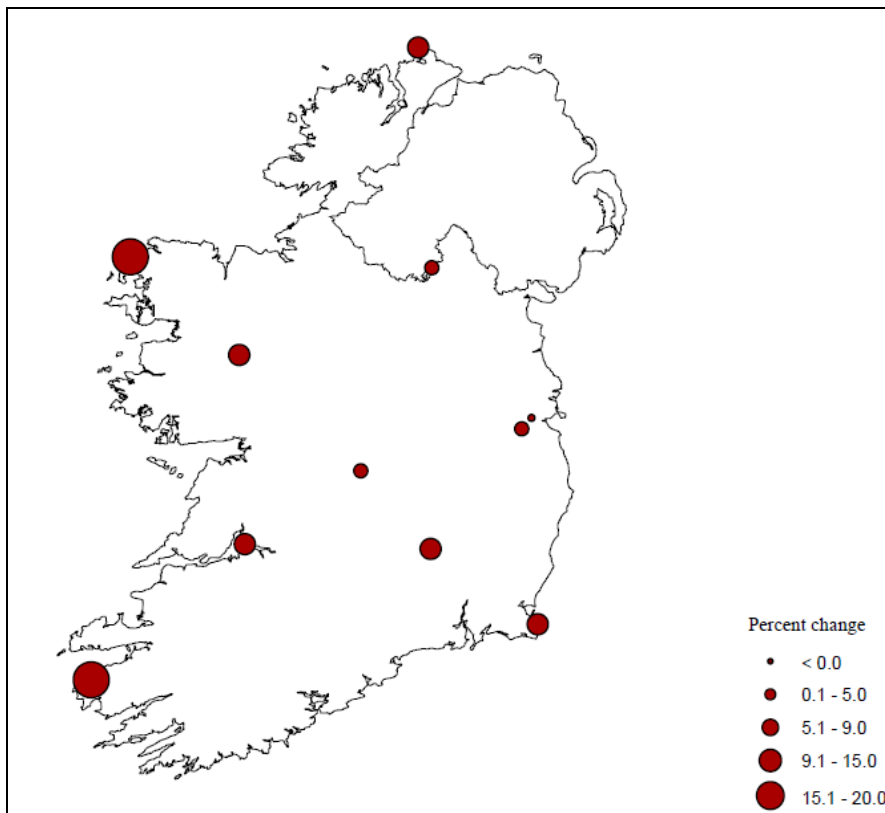
Figure 3.7 Percentage change in annual precipitation, 1960 – 2005 (McElwain & Sweeney, 2007)

3.4.2 Precipitation

McElwain and Sweeney (2007) also noted changes to precipitation patterns with increases in precipitation in the northern and western Ireland. Westerly synoptic station records showed the greatest increases in the maximum number of consecutive wet days. The authors also noted increases in the number of wet days greater or equal to 10 mm in the west coast synoptic stations (Claremorris, Valentia and Belmullet) across all seasons (McElwain and Sweeney, 2007). The general trend was for an increase in the number of wet days on the west coast while decreases were observed at east coast synoptic stations

(see Figure 3.7). These findings support those of Kiely (1999) who noted the enhancement of the hydrological cycle particularly in the west of Ireland and the significance of this development regarding fluvial flood management.

3.5   Generation of the Future Climatic Data

The data used in this project were obtained from the Irish Climate Analysis and Research Units (ICARUS) in N.U.I. Maynooth. An in-depth discussion of the techniques employed in generating the downscaled data is beyond the scope of this project. Full details are presented in Fealy and Sweeney (2007). A brief description methodology employed for generating the statistically downscaled data is provided here followed by an outline of the results.

The data used for the downscaling were obtained from Met Eireann. It comprised daily precipitation, sunshine hours and temperature from 14 synoptic stations for the period 1961 to 2000. Only observed values were used in the downscaling. The UK Statistical DownScaling Model (SDSM) data archive was used as the source of the surface and atmospheric data. After these data were re-gridded to conform to the output of the Hadley Centre GCM, transfer functions were then calibrated to link large-scale atmospheric and surface variables to each of the 14 synoptic station daily precipitation data series (Fealy and Sweeney, 2007).

GCM data from three models (the UK Hadley Centre Model HadCM3; the Commonwealth Scientific and Industrial Research Model CSIRO Mark2; and the Canadian Centre for Climate Modelling and Analysis CCCM2) and 2 emissions scenarios (A2 and B2) were obtained in order to derive the future climate series from the transfer functions. This ensemble of models overcomes the danger of deriving a climate series from just one model and one emissions scenario, thus repressing much uncertainty. An ensemble of models and emissions scenarios allows for a more comprehensive representation of the uncertainty ranges.

3.5.1 Temperature

Temperature, being a relatively homogenous variable with a normal distribution was modelled using multiple linear regressions. The calibration period chosen for both temperature and precipitation was 1961 to1978 and 1994 to 2000 with the independent verification period 1979 to 1993. Seasonal variation accounted for a large portion of the variance in the regression models of the maximum and minimum temperature data series.

3.5.2 Precipitation

Precipitation is far more variable within Ireland than temperature and it is more challenging to produce plausible daily future precipitation output using empirical statistical downscaling as it varies both spatially and temporally throughout the island.

Precipitation occurrence: Logistic regression, one of the family of Generalised Linear Models (GLM) was used to model wet and dry day sequences of precipitation.

Precipitation amounts: A gamma distribution was employed to model precipitation amounts.

Radiation: The Angstrom formula together with sun hours was employed to convert sun hours to radiation, as only sun hours are recorded in all synoptic stations. Local climate variables as well as large scale predictors were used in the regression model as local predictors can provide additional useful information at a small spatial scale.

Potential Evaporation (PE): Precipitation occurrence, precipitation amounts, and radiation were used as predictors for the regression model for PE. Wind was excluded as a predictor variable as it has a strong seasonal dependence, being more common during the winter months than in other seasons of the year. Potential evaporation is also at its minimum values during the winter months.

3.6 Statistical Downscaling Results

3.6.1 Temperature

Results for three distinct time periods during the present century were modelled for temperature and precipitation. These are the 2020s (2010 to 2039), the 2050s (2040 to 2069) and the 2080s (2070 to 2099). Results for the 2050s and 2080s will be presented

here as analysis of data from the 2020s has been emitted from this project due to the predominance of natural climate variability. The seasons follow those used by Met Eireann i.e.. Winter is December, January and February (DJF); Spring is March, April, and May (MAM); Summer is June, July and August (JJA); and Autumn is September, October and November (SON).

2050s: The HADCM3 shows the smallest temperature range between the 14 synoptic stations by the 2050s while the CCCM shows the greatest between-station temperature range. While all the models simulate a warming during all the seasons by this period, the temperature difference is greatest in the winter with a difference of almost 2^oC between the warmest station according to the CCCM GCM and the coolest station according to HADCM3.
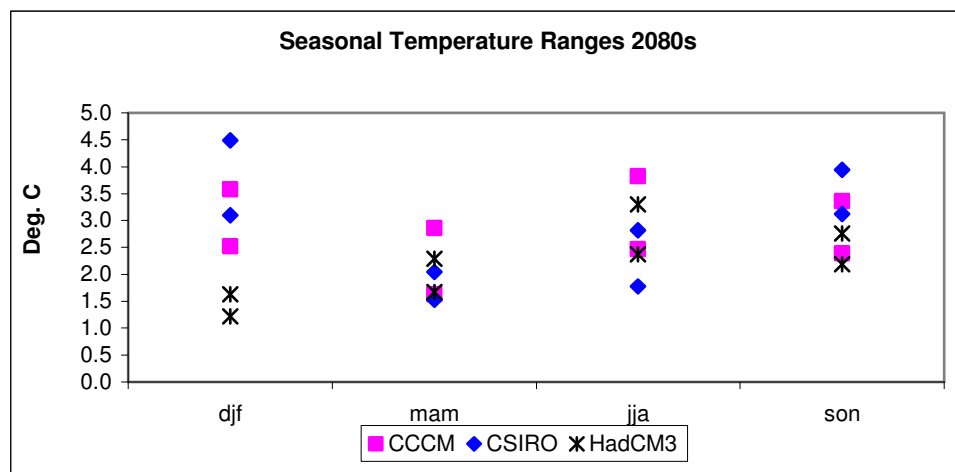
Figure 3.8 Seasonal temperature ranges in the 2080s for stations showing the smallest and greatest changes for the A2 emissions scenario (Fealy & Sweeney, 2008)

2080s: The temperature increase across all seasons is greatest by the 2080s. The temperature range between seasons is also greatest by this period. The range is again greatest in the winter season with a difference between the warmest and coolest synoptic station and model of almost 3^oC, while in the summer season the range is approximately 2^oC (see Figure 3.8).

3.6.2 Precipitation
The only season in all the future time periods in which all the GCMs agree on the direction of change is the summer season where all the models show a decrease in precipitation

receipts, in particular the CSIRO model which shows the greatest decrease during each time period.   However the ranges differ between time periods.

2050s: By the 2050s both the winter and summer seasons show a definite trend with all models simulating increases in winter precipitation receipts. Decreases in summer receipts more marked than those in the 2020s.

2080s: Winter ranges in this period widen from a slight decrease to an increase in precipitation of approximately 40%. The only season in which all models agree during this period is again in the summer period. All the results indicate that large spatial and seasonal ranges in precipitation occur even on a small island like Ireland. This further illustrates the importance of taking account of local topographical and climate variables when downscaling (see Figure 3.9).
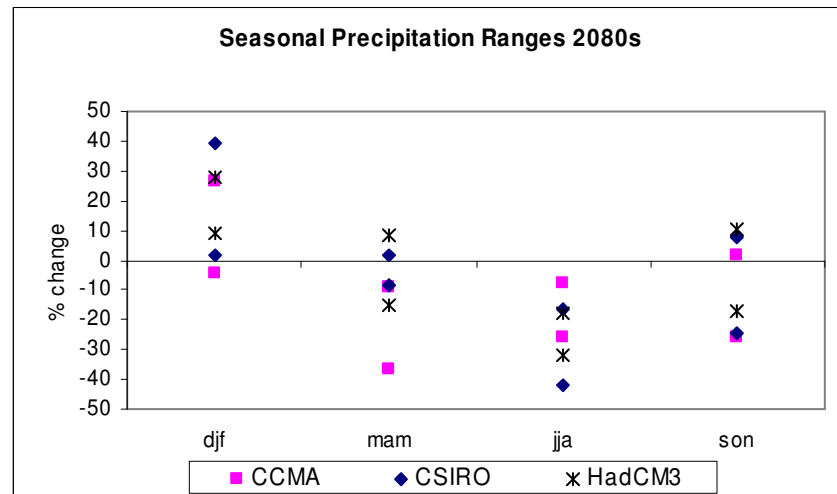
Figure 3.9 Seasonal precipitation ranges for stations showing the smallest and greatest changes for the A2 emissions scenario (Fealy & Sweeney, 2008)

3.6.3   Changes in Extremes of Temperature and Precipitation

Changes in the projected extremes of temperature and precipitation are important in a project such as this, which is investigating possible changes to magnitude and frequency of fluvial flooding for the present century due to climate change. The proximity of Ireland to the Atlantic Ocean and its small size buffers the island from extremes of precipitation and temperature in comparison to the climate of mainland Europe where there is a marked continental effect. However, variability is an intrinsic aspect of all climates and the severe

flooding in the western and southern areas of Ireland in November 2009 may become more frequent throughout the course of the present century.

The period of unsettled weather started in October 2009 and the amount of precipitation falling on already saturated ground exacerbated the flood conditions. November 2009 rainfall totals were the highest November totals on record in most synoptic stations, including the long-term stations at Valencia and Malin Head, where records extend back over 100 years. Indeed, Valencia station recorded its highest total (360 mm) of any month since records began in 1866 (McGrath *et al.,* 2010). Parts of the Shannon, Suck and Lee catchments saw their greatest floods in living memory as river levels rose to unprecedented heights. While it is not possible to infer trends from such extreme events or indeed from a series of events, flooding of this magnitude may become more common in the future.

TEMPERATURE INDICES OF EXTREMES	
T_{max} 90th Percentile	Hot day threshold
T_{min} 90th Percentile	Cold day threshold
Number of frost days	Frost days
Heatwave duration	Longest heatwave
PRECIPITATION INDICES OF EXTREMES	
90th percentile of rain-day amounts	Heavy rainfall threshold
Greatest 5-day total	Greatest 5-day accumulation
Daily intensity (rain per rain-day)	Average wet-day rainfall
Number of consecutive dry-days	Longest dry period
% total rainfall from events >90th percentile	Heavy rainfall proportion
No. of events >90th percentile of rain days	Heavy rainfall days

Table 3.1 Indices of extreme temperature and precipitation used in the analysis (Fealy and Sweeney, 2008)

As noted above, downscaling may simulate temperature and precipitation extremes that are too moderate compared with observations (Kyselỳ, 2002). Fealy and Sweeney (2007, p.2083) state that "difficulties still exist with predicting extreme precipitation events, which tend to be underestimated by the methodology employed". The authors also observe that as the downscaling focused primarily on producing mean climate projections for the present century, changes in the extremes of precipitation and temperature are likely to be

underestimated (Fealy and Sweeney, 2008). Nevertheless, ten core indices of extremes were selected, based on those in the STARDEX (2006) project (see Table 3.1).

3.6.4 Changes in Extreme Temperature

Significant trends (1% significance level) were observed at all stations for all temperature indices selected. A significant decrease in the number of frost days per decade was associated with a marked increase in cold night temperatures. Heat wave durations were found to increase by 3 to 4 days per decade according to the data. Warming at all stations was also suggested according to the hot day threshold and was particularly marked in inland synoptic stations away from the coast.

3.6.5 Changes in Extreme Precipitation

An increasing trend was suggested in the greatest 5-day precipitation totals for eight of the synoptic stations studied (5% significance level) which are located in the midlands and the east coasts. Conversely, a positive trend was also suggested in the maximum number of consecutive dry days. An increasing trend was evident for this from the west to the east coasts. Trends in the indices of heavy rainfall days, heavy rainfall threshold and average wet-day amount were found to be small but significant. Fealy and Sweeney (2007) highlight the fact that the methodology employed tends to underestimate extreme precipitation events. Consequently, the results should be interpreted as indices of likely changes based on the climate projections employed (Fealy and Sweeney, 2008 p.32).

3.7   Analysis of the Downscaled Climatic Data for the Kilkenny Synoptic Station

This section focuses on an analysis of the statistically downscaled climatic data for the Kilkenny synoptic station, as this station is located closest to the Suir catchment and is the source of the future climatic data employed in the project. The main climatic parameters of temperature, precipitation and potential evaporation were analysed in order to detect percentage changes in precipitation and potential evaporation, and degree changes in temperature for the 2050s and the 2080s due to climate change. Nonetheless, while one GCM output may be more extreme, it is important to note that the structure of hydrological models is highly non-linear and therefore this influences greatly the data output from such models.

3.7.1 Projected Changes in Seasonal Temperature
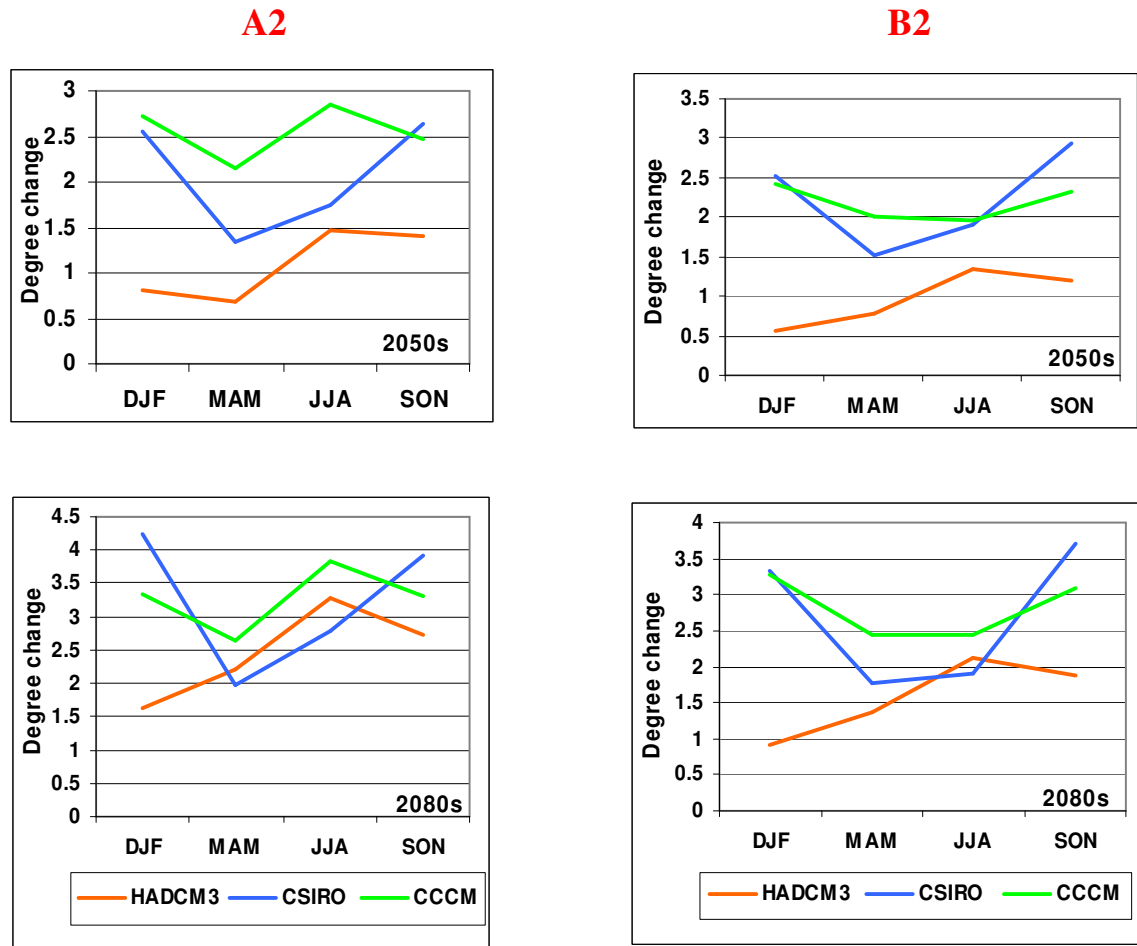
Figure 3.10 Degree changes in seasonal temperature for all GCMs and scenarios for the 2050s and the 2080s (Fealy and Sweeney, 2007)

Figure 3.10 above details the projected seasonal changes in temperature for the 2050s and the 2080s for both emissions scenarios. All GCMs model temperature increases across all seasons in the 2050s and the 2080s. In the 2050s under the A2 scenario, both CSIRO and CCCM show a marked temperature increase in winter temperature (over 2.5°C), however HADCM3 models a more conservative increase and the uncertainty range is particularly marked. Indeed, the uncertainty range is marked for all seasons in the 2050s. By the 2080s the uncertainty range is again high for winter with CSIRO modelling a dramatic increase in temperature of ~4.2°C. Apart from the A2 scenario in the 2050s, the temperature ranges are marked by higher increases and a greater uncertainty range in winter (all models and scenarios) and autumn (all models and scenarios apart from the A2 scenario in the 2080s).

Another notable point is that CCCM models the highest increases in summer and autumn temperatures across all scenarios and time slices and CSIRO models the greatest increases in autumn and winter temperature. Notably, too, HADCM3 models the lowest increases in temperature across all time slices and scenarios, apart from the spring and summer in the 2080s under the A2 scenario. Greater increases in temperature are also projected for the A2 than the B2 scenarios for both time periods. The dramatic increases in seasonal temperatures suggested by the GCMs for both time slices could have very negative effects on a host of natural and anthropogenic systems.

3.7.2   Projected Changes in Seasonal Precipitation

All GCMs model increases to precipitation during the winter season for all scenarios and time slices, however unlike the temperature projections, there is more agreement among the models for the percentage change in precipitation during the winter season for both scenarios and time slices apart from the A2 scenario in the 2050s (see Figure 3.11). By the 2050s under the A2 scenario, CSIRO and CCCM model an increase of 20% in winter precipitation. There is no change in precipitation according to HADCM3 in the 2050s. However under the B2 scenario HADCM3 models a winter increase of 10% while CSIRO again models a 20% increase in precipitation. The summer season shows the greatest range of uncertainty in the 2050s (under the A2 scenario). CCCM and HADCM3 show a decrease in precipitation of ~10%.   Conversely, CSIRO A2 models a decrease of almost 30% in precipitation. The models show much more agreement in the 2050s for the B2 scenario, with a notable agreement in the spring, and an uncertainty range of ~10% for both the summer and the autumn.

In the 2080s, CSIRO A2 again models the greatest increase in winter precipitation. However, it is only slightly greater than the 2050s, at 23%. The uncertainty range is smaller than the 2050s with HADCM3 again modelling the smallest increase of 8% in winter precipitation. The range of uncertainty is greater for spring and by summer HADCM3 models the greatest decrease in precipitation of -30%, while CCCM models a more modest decrease of ~12%. In the B2 scenario there is general agreement among the models as to the percentage increase in precipitation during the winter time. Nonetheless, the range of uncertainty in the spring is much greater, with disagreement between the GCMs as to the direction of change. CCCM models a decrease of -15%, while CSIRO and HADCM3

41

model a slight increase of 2% and 5% respectively. The percentage decrease in summer precipitation is not as extreme as the A2 scenario with HADCM3 again modelling the greatest decrease in precipitation of ~18%; however the uncertainty range is comparable to that of the A2 scenario. There is more agreement among the models in the autumn season.

A2   **B2**
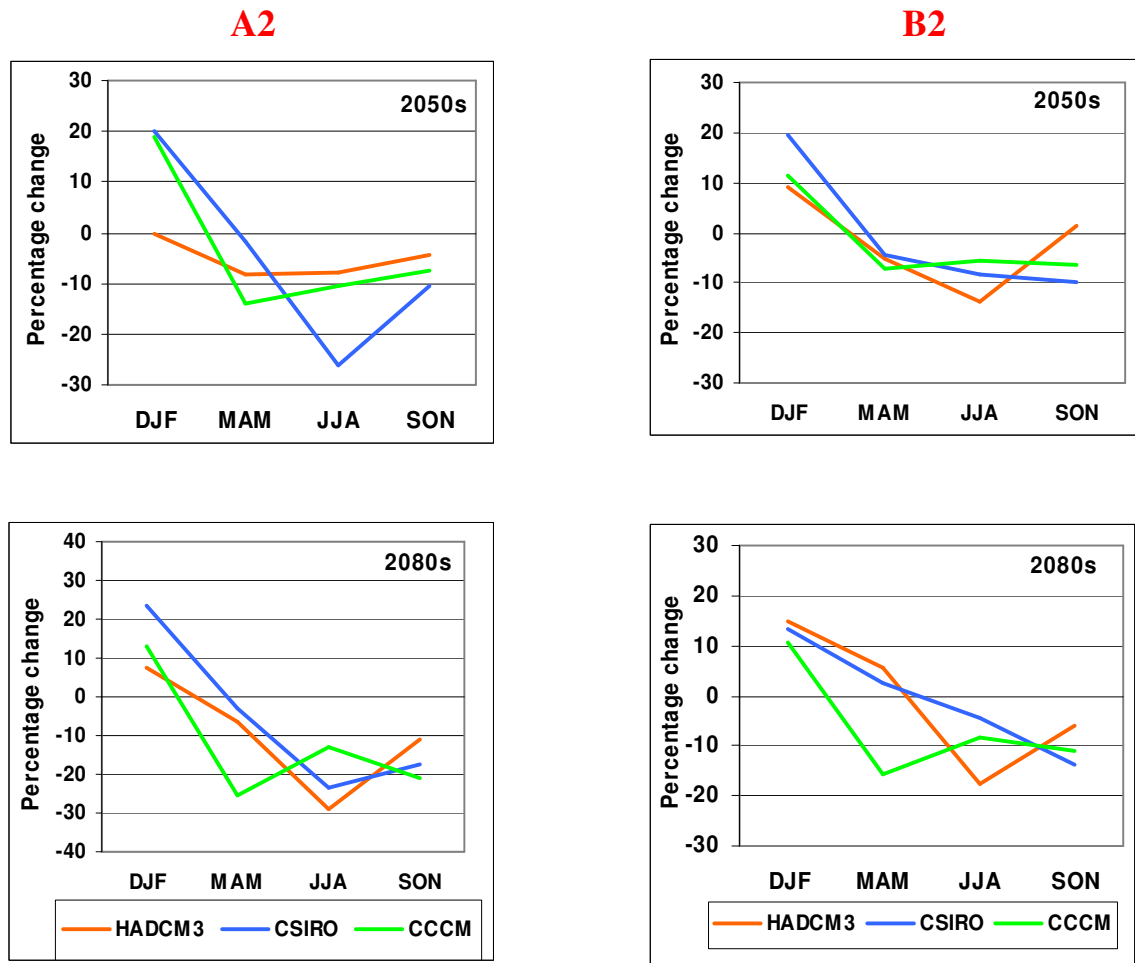
Figure 3.11 Percentage changes in seasonal precipitation for all GCMs and scenarios for the 2050s and the 2080s (Fealy and Sweeney, 2007)

3.7.3   Projected Changes in Potential Evaporation

All the GCMs show agreement in the direction of change in potential evaporation (PE) for both scenarios and time slices, especially for the autumn and winter seasons (Figure 3.12). What is also notable is that HADCM3 models the lowest reductions during the winter and autumn periods, and the greatest increases during the summer months for both time slices and scenarios, apart from the B2 scenario in the 2080s when CCCM models a slightly higher increase. Moreover, CSIRO consistently models the greatest decreases in PE for the

42

winter period for both scenarios and time slices. In the 2050s during the winter season CSIRO and CCCM A2 model a decrease in PE of -15%, while HADCM3 models a more modest decrease of -8%. By summer, the models agree on a slight increase of ~4%.
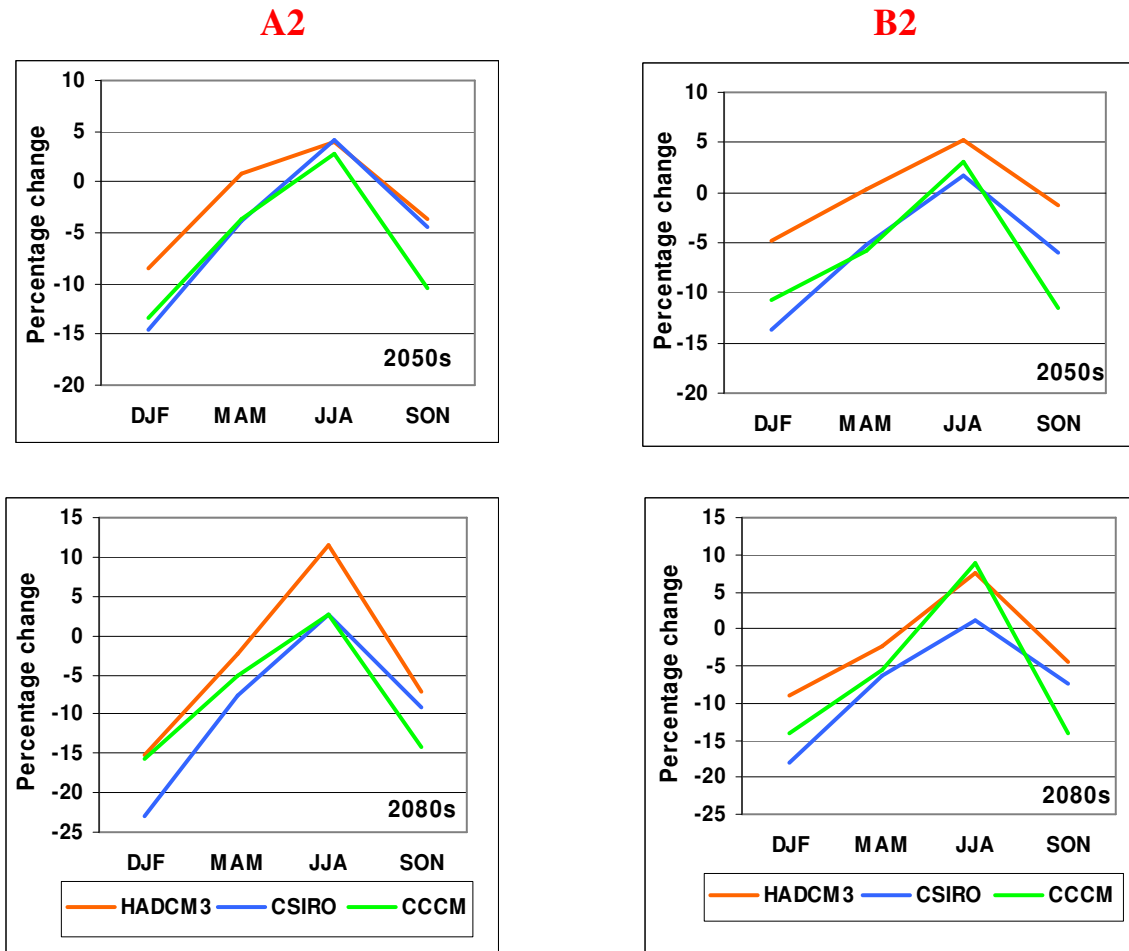
Figure 3.12 Percentage changes in seasonal PE for all GCMs and scenarios for the 2050s and the 2080s (Fealy and Sweeney, 2007)

The uncertainty ranges are higher for the B2 scenario across all seasons in the 2050s, however the maximum and minimum values of percentage change are comparable to those of the A2 scenario. In the 2080s, HADCM3 A2 models an increase in PE of over 10% during the summer period, while the other two models output values close to those of the control period. Decreases in PE in the winter are greater than the 2050s with CSIRO modelling a decrease in PE of nearly -25%, while CCCM and HADCM3 show more agreement with -15%. Decreases in spring are closer to control period value at ~-5% for all models, while decreases in the autumn are more pronounced (between -7% and -15%).

Percentage changes according to the B2 scenario are not as extreme for any season apart from autumn.

3.8   Conclusion

This chapter began with a description of physical characteristics of the Suir catchment. These will be revisited in the Chapter 5, which focuses on the parameterisation of the rainfall-runoff models. Recent trends in the climate of Ireland (largely consistent with global scale ones and include an average temperature increase of 0.7°C from 1890 to 2004) and changes to precipitation patterns with increases in precipitation, particularly in northern and western Ireland were then outlined (McElwain and Sweeney, 2007). This was followed by a brief description of the methodology employed for generating the future climatic data being used in this project. Regarding the statistical downscaling of extreme precipitation, Fealy and Sweeney (2007) caution that statistical downscaling tends to underestimate such extremes.

In the concluding section of the chapter an analysis was made of the downscaled future climatic data for the Kilkenny synoptic station, from where the future data employed in this project originates. The increases that are projected for temperature, precipitation and PE for the 2050s and the 2080s may have a marked effect on catchment hydrology and extreme events. This is particularly relevant as the highest percentage increase to precipitation is projected for the winter, which is main flood season in Ireland. Notably too are projected rises in temperature and evaporation (during the summer) which could have a marked effect on soil moisture storage in a highly permeable, baseflow dominated river like the Suir. These data will be used as input to HYSIM and HBV-Light in order to generate future time series data for analysis. The next chapter will outline the differences in the structures of the rainfall-runoff models.

Chapter 4: Choice and Structure of the Rainfall-Runoff Models

4.1   Introduction

This chapter begins by giving reasons for the choice of the hydrological models employed in the project, followed by a discussion of hydrological model development. Different classes of hydrological models will be presented and the procedure for building hydrological models will be outlined. The rationale for the choice of lumped conceptual rainfall-runoff models will be given.   The structure of the two lumped conceptual models employed in this project, HYSIM and HBV-Light, will then be outlined. Although both models are conceptual and lumped, there are also many differences in structure and in the philosophy behind the development of the models.   The chapter will conclude with a comparison of the soil moisture accounting routine and the routine for the generation of runoff in both models.

4.1.1   Reasons for the Choice of Hydrological Models

Both HYSIM and HBV-Light were chosen for this project as they have been employed successfully in recent research on the effects of climate change on catchment hydrology in Ireland and both models have proved plausible representations of the hydrological behaviour of Irish rivers (Charlton *et al.,* 2006; Murphy and Charlton, 2008; Semmler *et al.,* 2006; Steele-Dunne *et al.,* 2008; Wang *et al.,* 2006). However, to date they have not been employed together in an analysis of the effects of climate change on an Irish catchment.

One of the ways in which hydrological models are defined is by the degree of parsimony i.e. that a model should only be as complex as is necessary to simulate observations precisely enough to be useful (Beven, 2000). This is another reason for choosing the two models. Although both models are lumped, HYSIM has a more complex, physically realistic structure than HBV-Light, whose structure is based on parsimony.

4.2 Hydrological Model Development

4.2.1 Classes of Hydrological Models

A model is a conceptual representation of a real-world complex system. In hydrology, models have been applied to a range of issues in both surface and sub-surface water systems such as surface and groundwater flow, water quality, geo-chemical properties of water and sediment transport. Refsgaard and Knudsen (1996) distinguished between three classes of hydrological models:

- empirical black box models
- lumped conceptual models
- physically based distributed models

The unit hydrograph is a simple example of an empirical black box model. Black box models are based on the analysis of inputs and outputs with little explanation of the physical principles of the underlying processes. Physically based distributed models such as MIKE-SHE have parameters that have a physical counterpart within the catchment (soil, land use, groundwater, vegetation etc.). They also divide the catchment into distinct spatial units to take account of the spatial heterogeneity within a given catchment. However, distributed models require much computing power and have large data requirements. For this reason lumped conceptual models have been the models of choice for climate impact assessment studies. Moreover, all hydrological models, no matter how sophisticated, are lumped at some scale, because "their equations (and therefore their parameters) are aggregate descriptions…of real world processes" (Wagener *et al.,* 2003, p.398). In this thesis one particular class of hydrological model, the lumped conceptual rainfall-runoff model, will be employed.

Like all hydrological models, lumped conceptual models are a gross simplification of the processes operating within a unique open flow system such as the catchment system. These models are based on the developer's concepts of the main processes governing runoff within a catchment and do not necessarily have their basis in rigorous physical laws (Bergström, 1976). Furthermore, these models do not allow for spatial descretisation; they treat the catchment as a single spatial unit without allowing for heterogeneity in soils,

topography, vegetation or land-use. However, their low data requirements (precipitation, ET, temperature and flow) mean that lumped conceptual models have been the models of choice in many catchment studies (e.g., Charlton *et al.,* 2006; Driessen *et al.,* 2009; Perrin *et al.,* 2001; Refsgaard and Knudsen, 1996; Steele-Dunne *et al.,* 2008; Uhlenbrook *et al.,* 1999; Wilby, 2005; Wilby and Harris, 2006). In this project two lumped conceptual rainfall-runoff models, HYSIM (Hydrological Simulation Model) and HBV-light (Hydrologiska Byråns Vattenbalansavdelning), have been chosen to simulate future flow in the Suir catchment. While structurally there are similarities (e.g. in both models the catchment system is represented by a series of stores) each model structure is also defined in a subjective way.

Both HBV and HYSIM were developed during the 1970s, shortly after digital computers become more widely available. Other models which developed at this time and are still in use include the HSPF and Sacramento models from the USA and the Tank model which was developed in Japan. As the digital age progressed and hydrological model structures became more complex, Dawdy and O'Donnell (1965 cited in Beven, 2000) were among the first researchers to attempt to define a generic model structure with just a few parameters (see Figure 4.1). The structure that they proposed is based on a series of stores (reservoirs). The model structure consists of soil moisture and groundwater stores which are common to many conceptual rainfall runoff models. Both HYSIM and HBV have similarities with this generic type model in that their structures are a series of different stores, and they are both soil moisture storage type models (Perrin *et al.,* 2001). However, there are also differences in the degree of complexity in the two model structures. HBV has a relatively simple structure with 9 free parameters, whilst HYSIM is a more complex model with 22 hydrology parameters and 8 hydraulics parameters (albeit that all but four of these parameters can be estimated from a knowledge of catchment characteristics). This reflects the subjectivity of the model developer's ideas and perceptions about the most important processes which lead to runoff in a catchment.
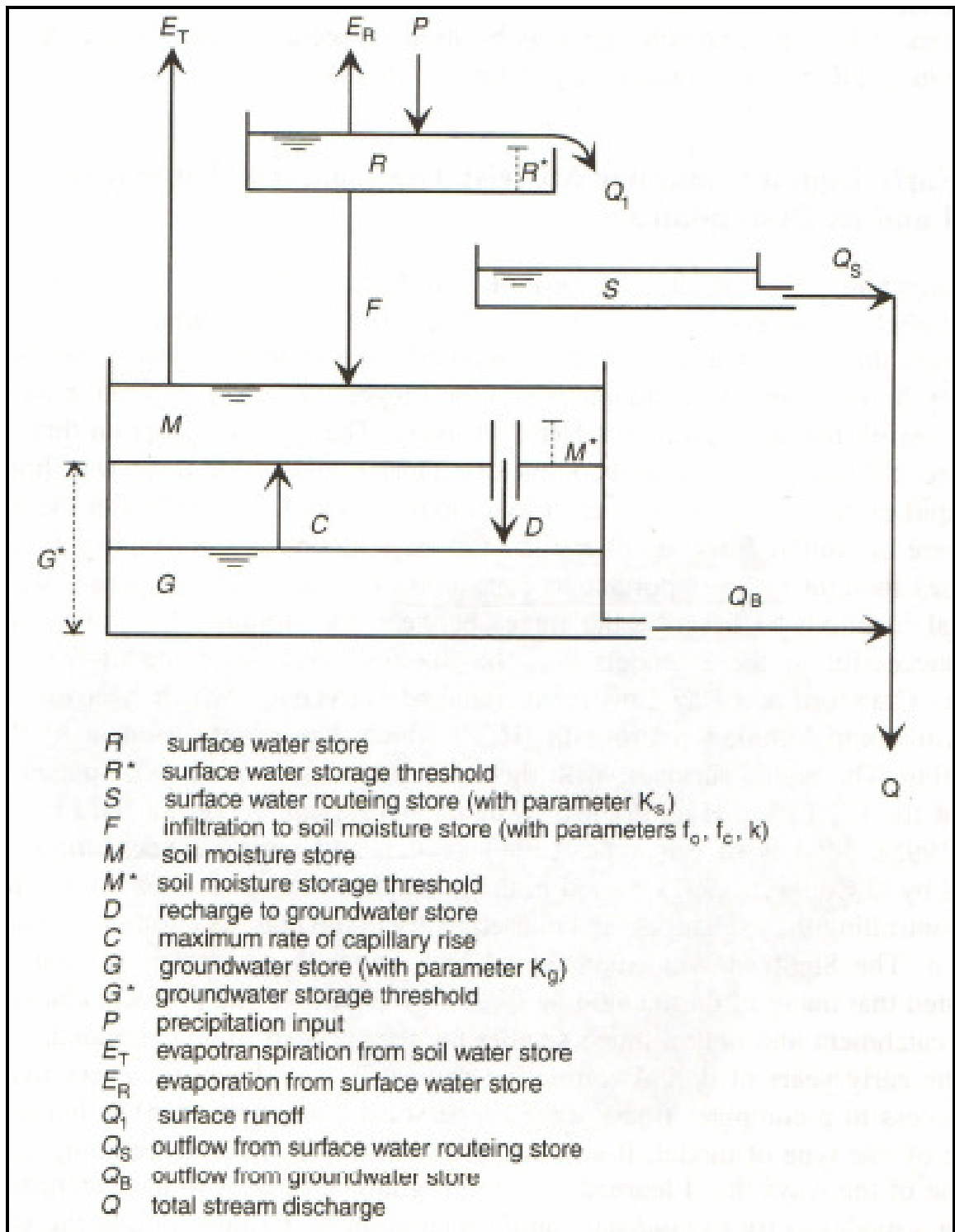
Figure 4.1 Schematic diagram of the conceptual rainfall-runoff model in Dawdy and O'Donnell (1965) (taken from Beven, 2000)
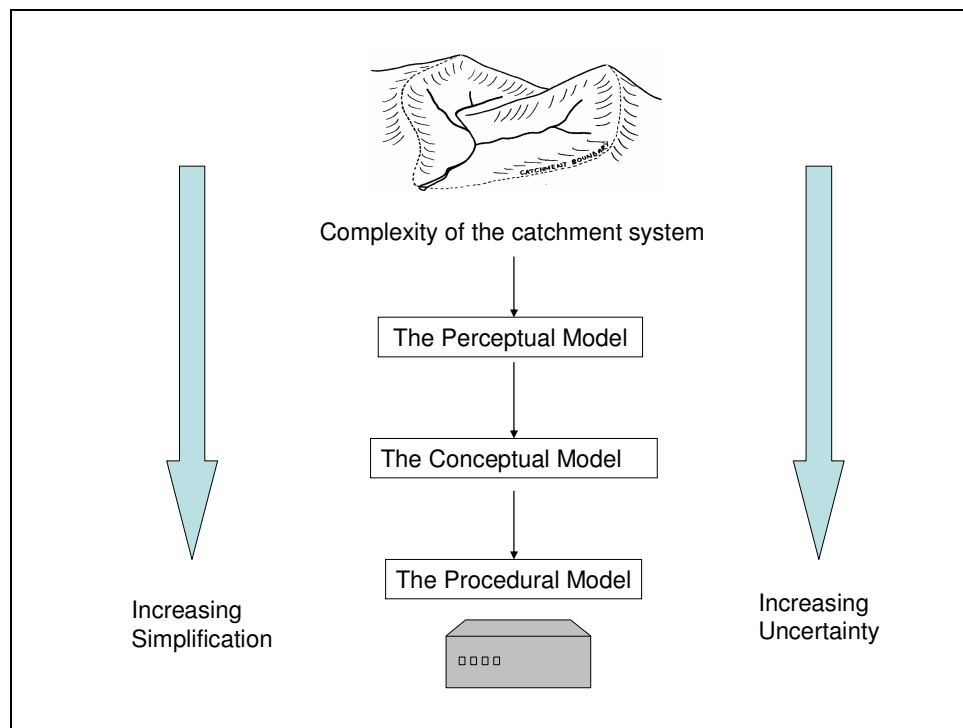
Figure 4.2 Procedure for building hydrological models. After Beven (2000)

4.2.2   Building Hydrological Models

The subjectivity in the model developer's beliefs is evident from the beginning of the model development procedure. The process of building hydrological models starts with the perceptual model (see Figure 4.2). This is a set of personal beliefs about the different processes which control the hydrological response of a catchment and is not limited by mathematical theory. In effect, it is the model developer's hypothesis about the main processes leading to runoff (Beven, 2000). Also contained within the perceptual model are the developer's views about the type of hydrological model to be built, e.g., whether the model should be parsimonious or physically realistic. Such decisions take place at the level of the perceptual model.

 The conceptual model is based on the perceptual model and is defined in the form of mathematical equations (Beven, 2000).   At each stage of this model building process there is increasing simplification and increasing uncertainty. The equations of the conceptual model are a gross simplification of the qualitative descriptions within the perceptual model. Beven (2002, p.2467 italics given) notes that "The perceptual model may only be as realistic as current understanding allows. The conceptual model will, however, be wrong

49

and *will be known to be wrong*…but will still have the possibility of being *approximately realistic*". This process results in the procedural model which takes the form of computer code (Beven, 2000). In order to obtain output from a hydrological model, its system must also be closed. This presents further uncertainty, i.e. attempting to model a unique open flow system such as a river catchment within the closed system of the hydrological model (Beven, 2002). Indeed, Beven (2002, 2009) has identified the central problem of environmental modelling as the uncertain mapping of the landscape space (in this case, the river catchment) into the model space.

At the perceptual model level within HYSIM and HBV-Light there are notable differences in the philosophy of model development. In Bergström (1976, p.7) the author notes that only the most important parts of the runoff-generating process were included in the HBV model as a detailed description of all components of the hydrological would lead to a model of excessive complexity. The HBV model was developed based on the hypothesis in Nash and Sutcliffe (1970) of building a simple model and only adding further complexity insofar as the model efficiency improved and the parameters remained stable. Thus, a guiding principle in the development of the HBV model was parsimony. Furthermore, soon after building in more complexity the point was reached at which model performance did not improve (Bergström, 1991).

A different philosophy underpins the perceptual model on which HYSIM is based. One of the major objectives in the development of the model was that it should be physically realistic "and in particular use relationships whose validity has been demonstrated experimentally" (Manley 1978, p.190). Manley (1978) contrasts the approach of Nash and Sutcliffe (1970) with that of Dawdy and O'Donnell (1965) who argue that a model should be as physically realistic as possible, with physical parameters reflecting the properties of a catchment and processes within it which lead to runoff. Manley (1978) adds that the HYSIM model fulfils many of the requirements of such a physically based model. Wagener *et al.* (2004) note that such models (e.g. the Stanford Watershed Model, the Sacramento Model and HYSIM) show a high level of complexity, especially within the soil moisture routine. HYSIM exhibits this complexity with 13 basic hydrology parameters, 9 advanced hydrology parameters and 8 hydraulic parameters. However, these models can suffer from over-parameterisation, whereby there are enough degrees of freedom within the

model to give a good fit to observed data after optimisation. Conversely, the degrees of freedom mean that many other parameter combinations may give equally good fits to the observed data (Wagener *et al.,* 2004).

Wagener *et al.,* (2004, p.42) identify four sources of uncertainty within the modelling process:

Data uncertainty: errors introduced by the input data.

Model structural uncertainty: simplifications and errors within the model in the description or real-world processes, errors in the model code.

Model specification uncertainty: arises from data and model structural uncertainty and is the inability to identify the globally optimal model (parameter set) from the information provided by the data.

Uncertainty due to unknown initial conditions: the internal states of the model are usually unknown at the beginning of a calibration or modelling exercise. However, this can be minimised by using a warming-up period.

Wagener *et al.* (2004) further emphasise that even if the above uncertainties could be minimised, there is still irreducible uncertainty due to the random nature of processes within the river catchment. Input data uncertainty (e.g. precipitation) is an important external source of uncertainty at the local stage of a climate impact analysis and can arise from instrument and measurement error, inadequate spatial or temporal resolution and the chaotic nature of weather systems (e.g., Melching, 1995; Georgakakos *et al.,* 2004; Butts *et al.,* 2004). However, it will not be evaluated within this thesis. Model parameter uncertainty will be examined through the GLUE methodology and model structural uncertainty will be evaluated through analysing differences in the output of future streamflow from both HBV-Light and HYSIM.

4.3 Structures of the Rainfall Runoff Models

4.3.1 Description of HYSIM

In Manley (1976, p.341) the author states that "a catchment may be defined as a series of natural reservoirs of moisture and the calculation of the transfers between these reservoirs represents the central problem of catchment modelling". HYSIM is a lumped conceptual rainfall runoff model which can be run on a daily time-step (Manley, 2003). Parameters are calculated both through estimation of physical properties of a catchment and through automatic calibration. Unlike other conceptual models where parameters do not necessarily have a physical interpretation within the river catchment, in HYSIM every effort has been made to give the parameters a physically realistic interpretation (Manley, 2003). For example, physically identifiable parameters such as soil rooting depth, impermeable proportion and bubbling pressure are included in the model.

HYSIM parameters are divided into hydrological and hydraulic parameters. There are also a precipitation correction factor and a potential evaporation correction factor. The hydrological parameters can be further subdivided into soil, groundwater, and land use parameters. Of these parameters, most are estimated from knowledge of catchment characteristics. There are, however, four process parameters (saturated permeability-horizon boundary; saturated permeability – base lower horizon; interflow runoff from upper horizon at saturation; interflow runoff from lower horizon at saturation) that are adjusted with reference to the flow record, during calibration (Manley, 1978). HYSIM can use five types of input data: precipitation, potential evaporation (PET), potential snowmelt, discharges to and abstractions from the river system, abstractions from and augmentation of groundwater. The model can also be run in a semi-distributed basis to simulate the natural heterogeneity of a river catchment. However, in this project the Suir catchment is treated as a single unit and both HYSIM and HBV-Light are run in lumped mode in order to achieve standardisation in the output of both models. HYSIM has been successfully applied in several studies (Charlton *et al.,* 2006; Murphy and Charlton, 2008; Pilling and Jones, 2002).
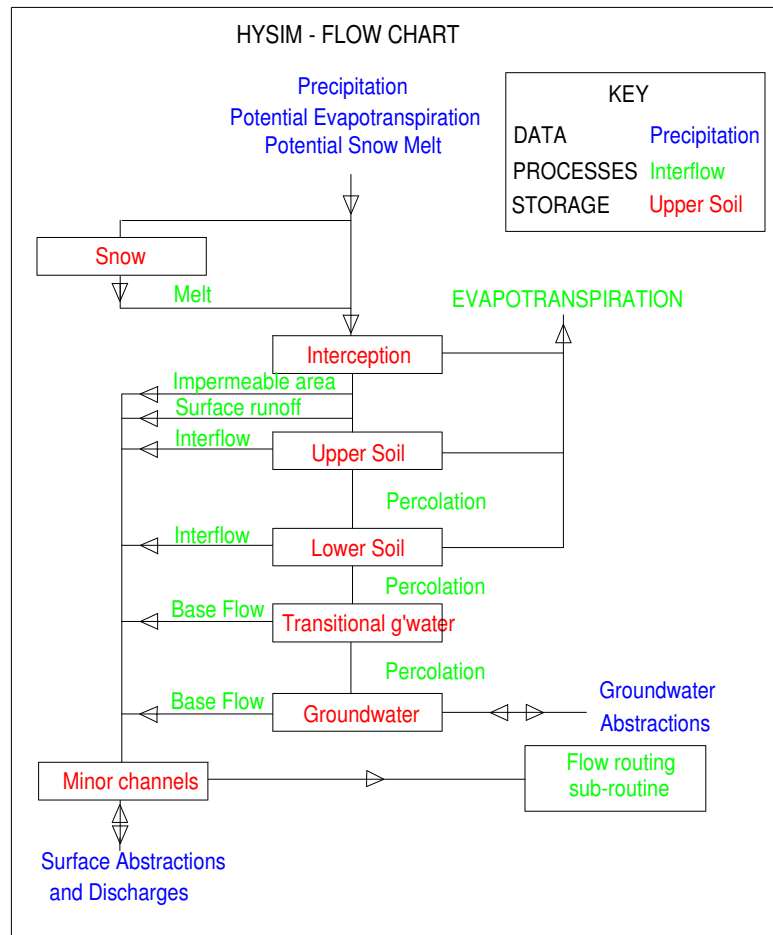
Figure 4.3 Hysim model structure

This store is often reduced through potential evaporation, which is allowed for in HYSIM. Any moisture in excess of the storage limit is transferred onto the next store. In the model the impermeable proportion of the catchment is also taken into account as a percentage of the excess moisture from the interception storage is diverted to minor channel storage. The next store is the upper soil horizon reservoir. This represents moisture held in the A horizon of the soil profile. This reservoir has a finite capacity. At more than 15 atmospheres pressure evaporation takes place at a rate lower in proportion to the remaining storage.

Interflow is the next moisture loss from the model. The equation for interflow in Manley (2003) is given as:

$$\text{Interflow} = \text{Rfac}_1(S_e)^{(2+3\gamma)/\gamma}$$

Where Rfac$_1$ is interflow runoff from the upper soil horizon at saturation, S$_e$ is the effective saturation in the upper and γ is the pore size distribution index parameter. The final moisture transfer from the upper to the lower soil horizon is percolation, which is given by the equation:

Percolation = $K_b(S_e)^{(2+3\gamma)/\gamma}$

Where K$_b$ is the saturated permeability at the horizon boundary and S$_e$ is the effective saturation in the upper horizon.

The next store in HYSIM is the lower soil horizon reservoir (still in the rooting zone), which represents the B and C horizons of the soil profile. Excess evaporation is subtracted from this store at the potential rate, subject to capillary suction of less than 15 atmospheres. Interflow runoff and percolation to groundwater are simulated with similar equations to the upper soil reservoir. Three parameters define the rate of the movement of moisture in the soil layers: the pore size distribution index, saturated permeability and bubbling pressure.

There are two stages of percolation represented in HYSIM: percolation for the upper soil horizon to the lower soil horizon and percolation from the lower soil horizon to groundwater. Within the model, inter-horizon percolation is effected by capillary suction while the percolation to groundwater is assumed to be due to gravity only. Transitional groundwater is the next store in the model. This is an infinite reservoir and is the first stage of groundwater storage in HYSIM. In karstic limestone or chalk catchments many fissures holding water may lead to a stream rather than to deeper groundwater and this effect is represented in the transitional groundwater reservoir. The last store is the groundwater reservoir, another infinite reservoir that is assumed in HYSIM to have a constant discharge coefficient. Minor channel storage is also represented in HYSIM to simulate the routing of flows in minor streams and ephemeral channels if the catchment is saturated.

4.4   The HBV Model

The HBV model was first developed at the Swedish Meteorological and Hydrological Institute (SMHI) to be used for hydrological forecasting (Bergström, 1976; 1992). It has now become the standard model for runoff simulations in Nordic countries. The HBV model is a semi-distributed conceptual model which is usually run in daily time-steps. The

model simulates daily streamflow using daily rainfall, temperature and potential evapo-transpiration (PET) as inputs. Each river catchment can be divided into a number of sub-catchments and a contributing area approach used in the soil routing routine when the model is run in semi-distributed mode.

The structure of the HBV model is based on parsimony. In the model there are three reservoirs: oil moisture, upper groundwater and lower groundwater. Within HBV are process parameters which do not necessarily have a physical correspondence within a catchment. Reasonable ranges for the parameter values are first estimated and then calculated through calibration. The only physical features to be specified within the model are mean catchment elevation and elevation of precipitation and temperature gauges.

4.5   HBV-Light Model

HBV-Light (Seibert, 2005) is a more recent version of the HBV model. HBV-Light Version 2 employed in this project corresponds to the SMHI version 6 (Bergstrom, 1992). There are two modifications to the original version of the model. A "warming up" period has been included in HBV-Light and the routing parameter MAXBAS can now incorporate non-integer values (Seibert, 2005). A further advantage of the HBV-Light model is that Monte-Carlo simulations can be performed to take account of parameter uncertainty and equifinality of model output using random numbers from a uniform distribution within the set ranges for each parameter. This model has also been successfully employed in several Irish studies evaluating the effects of climate change on river catchments (e.g., Wang *et al.,* 2006: Steele-Dunne *et al.,* 2008).

In this project the HBV-Light model is run in lumped mode. The structure of the model is shown below (see Figure 4.4). The HBV-light model consists of routines for snow accumulation and melt, soil moisture accounting, runoff response and river routing. In the snow routine, precipitation falls as snow when the temperature falls below a threshold value (TT). The snow routine consists of three parameters (TT, SFCF, and CWH) and can be distributed depending on whether different elevation and vegetation zones are specified within the model.
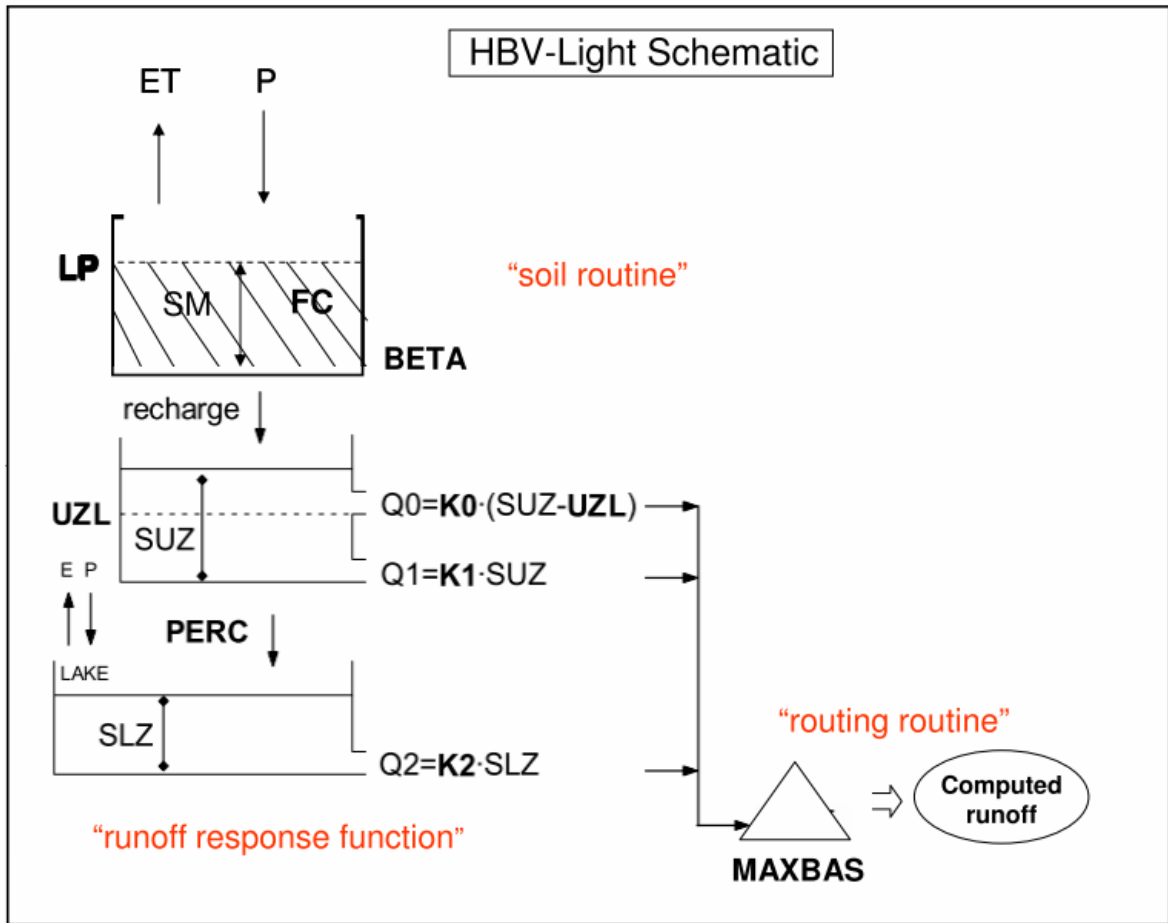
Figure 4.4 Simplified schematic of the HBV-Light model structure. After Seibert (2005)

The schematic is shown without the snow routine as this component of the model is rarely activated in Ireland where air and soil temperatures seldom fall below the threshold where snow is common. Furthermore, snowfalls in winter rarely amount to more than 20 to 30 mm and do not last long except in upland areas (Keane and Sheridan, 2004). The three sub-routines in the HBV-Light model are described below.

4.5.1   Soil Moisture Routine

Parameters: The soil moisture accounting routine consists of a soil box (SM) and is controlled by three free parameters: FC, LP and BETA.

Soil Moisture Routine Parameters

FC: maximum soil moisture storage

LP: threshold value of soil moisture above which actual ET equals potential ET

BETA: determines relative contribution to runoff from rain or snowmelt

Rainfall and snowmelt (P) are divided into water filling the soil box and groundwater recharge depending on the relation between the water content of the soil box (SM [mm]) and its maximum value (FC [mm]) (see Figure 4.5). It should be noted here that FC is a model parameter and is not necessarily equal to "field capacity" values. Actual evaporation from the soil box equals potential evaporation if SM/FC is above a threshold LP. BETA determines the relative contribution to runoff from rainfall or snowmelt. Bergström (1976) acknowledges that the simplicity of this simple linear reservoir means that it is incapable of representing the great heterogeneity in the soils of most catchments and that the response will be very abrupt if the soil moisture exceeds the parameter FC. Therefore, in most applications of HBV the catchment is divided into a number of soil zones in the model, and a distribution of FC is assumed. However, both Braun and Renner 1992) and Uhlenbrook *et al.* (1999) tested the HBV model with the soil routine and response function fully lumped (although the snow routine was distributed into different elevation zones) and got satisfactory results comparing model output to observed data. Nonetheless, Uhlenbrook *et al.* (1999) achieved better model simulation results with increased distribution of the sub-routines. In this project each model is employed fully lumped, in order to compare like with like.

$$\frac{recharge}{P} = \left(\frac{S_{sm}}{FC}\right)^{BETA}$$
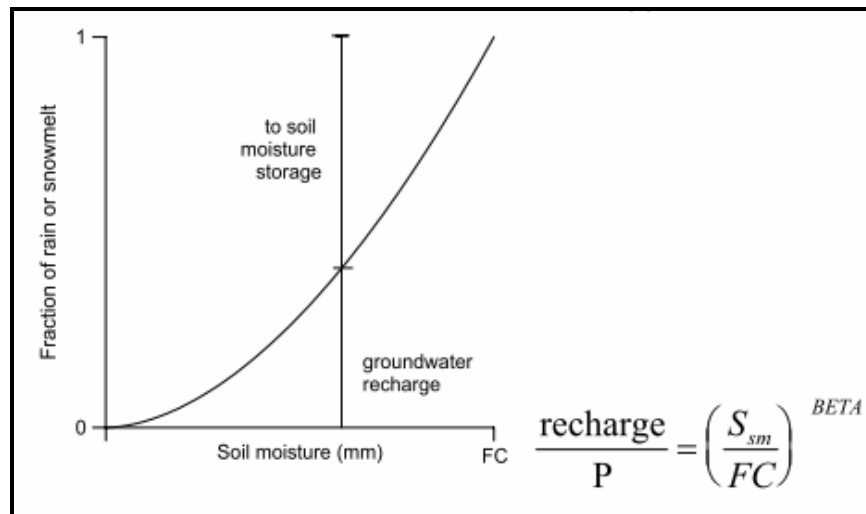
Figure 4.5 Contributions from precipitation to soil moisture storage and to upper groundwater store (Seibert, 2005)

4.5.2   Runoff Response Function

This function transforms excess water from the soil moisture routine into runoff for the catchment. It distributes generated runoff in time, so that quick and slow components of

the recession are obtained (Harlin, 1991). The runoff response routine consists of two stores: an upper groundwater reservoir (SUZ) and a lower one (SLZ). Groundwater recharge is added to the upper groundwater reservoir (SUZ [mm]). PERC [mm d^{-1}] defines the maximum percolation rate from the upper to the lower groundwater tank (SLZ [mm]). The lower groundwater reservoir is a simple linear reservoir representing contributions to baseflow. This reservoir is filled by percolation (PERC) from the upper box and K_2 is the recession coefficient. The reservoir also includes the effects of precipitation and evaporation over lakes in the catchment.

Runoff Response Function Parameters

UZL: threshold separating Q0 and Q1 flow

PERC: percolation from upper (SUZ) to lower (SLZ) groundwater box.

K_0: recession coefficient upper groundwater storage (SUZ)

K_1: recession coefficient upper groundwater storage (SUZ)

K_2: recession coefficient lower groundwater storage (SLZ)

The upper reservoir starts to fill if soil moisture exceeds percolation capacity (PERC). Storage in the upper reservoir (SUZ) is depleted by two recession coefficients K_0 and K_1, depending on whether SUZ is above a threshold value, UZL [mm], or not. This reservoir models the response to flood periods. Peak flow (Q0) activates the three recession coefficients (K_0, K_1 and K_2) if the threshold parameters PERC and UZL are exceeded. Intermediate flow (Q1) activates K_1 and K_2 if PERC is exceeded. Baseflow (Q2) activates only the K_2 recession coefficient.

4.5.3   Routing routine

The contributions from the upper and lower reservoir are added together to compute runoff. The latter is then transformed by a triangular weighting function defined by the parameter MAXBAS to give simulated runoff [mm d-1]. This parameter is employed to account for the dampening of the flood pulse in the river before reaching the catchment outlet (Harlin, 1991).

Routing Routine Parameter

MAXBAS: determines the base in an equilateral triangular weighting function

4.6   Comparison of HYSIM and HBV-Light Model Structures

The structures of HBV-Light and HYSIM will be compared under:

1. Soil moisture accounting routine
2. Generation of runoff and transformation of the hydrograph (Bergström, 1976).

4.6.1   Soil Moisture Routine of the HBV-Light Model

In both HBV-Light and HYSIM the soil moisture accounting routine is the part of the model which determines the main contribution to runoff from precipitation. However, each model simulates the movement of moisture through the soil layers very differently. As the philosophy underlying the HBV-Light model is parsimony, the soil moisture accounting procedure was developed from greatly simplified assumptions. Bergström (1976, p.58) adds that factors governing the retention and transport of moisture in heterogeneous soil columns are so complex that "striving for a physically correct representation of the processes in the soil moisture zone would lead to a very complex model".
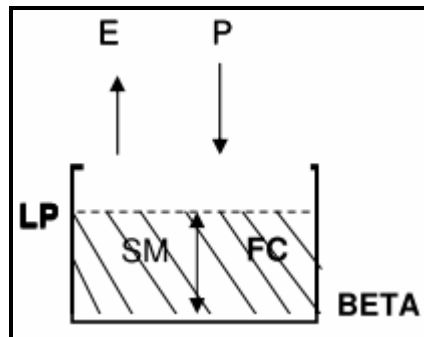
Figure 4.6 Soil moisture accounting routine in HBV-Light

In HBV-Light the soil moisture routine includes all losses, including interception. Consequently, it is more an index of catchment wetness than a detailed description of the soil environment (Bergström, 1976). Surface runoff is not explicitly simulated within the model, as the water is controlled by conditions in the soil moisture zone before any runoff can be generated (Bergström, 1976). The soil moisture routine consists of just one linear reservoir (SM) and three free parameters (see Figure 4.6). The soil reservoir has to be filled to a certain level (FC) before any moisture can permeate through to the groundwater zone. The parameter FC therefore represents the maximum available moisture in the soil zone. LP is a parameter representing the fraction of FC above which actual evapo-transpiration

(AET) equals potential evapo-transpiration (PET). BETA is a parameter that determines relative contribution to runoff from rain or snowmelt. Inter-flow runoff is not simulated within the soil moisture routine. With just one reservoir and three free parameters, the soil moisture routine in HBV-Light is thus extremely simplified.

4.6.2   Soil moisture routine in HYSIM

In contrast to the philosophy of parsimony underlying the HBV model, the development philosophy of HYSIM is based on a physically realistic interpretation of the catchment. Consequently, its structure is more complex than that of HBV-Light with six reservoirs (interception; upper soil; lower soil; transitional groundwater; groundwater) in comparison to three in HBV-Light (see Figure 4.7). Before precipitation can reach the soil moisture reservoirs the interception store is first filled, then any excess is diverted to minor channel storage, representing runoff from the impermeable proportion of the catchment. There are fixed parameters controlling interception storage and the impermeable proportion of the catchment.
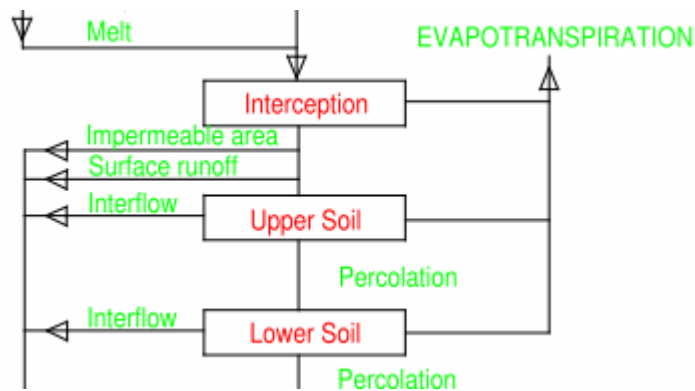
Figure 4.7 Soil moisture routine in HYSIM

The soil moisture routine is an extremely important component of HYSIM. It consists of two finite reservoirs: the upper soil reservoir and the lower soil reservoirs which correspond to the A and B soil horizons respectively.   That every effort is made to give HYSIM a physically realistic basis is also reflected in the choice of soil parameters and the means of their estimation (see Table 4.1). Three parameters determine the rate of moisture movement through these layers: pore size distribution index (PSDI), bubbling pressure and saturated permeability. PSDI is one of the most important parameters in the model and controls the way a soil responds to moisture by virtue of its effective permeability and capillary suction

(Manley, 1978). The value of PSDI is dependent on predominant soil texture of the catchment. PSDI also determines the values for bubbling pressure and porosity. Bubbling pressure is analogous to the negative pressure at which bubbles first appear in a porous medium during the dewatering process and is related mathematically to capillary suction. Its value was derived from field experiments (Manley, 1976). Thus, every effort is made to give these soil parameters a value which is physically relevant in the catchment being modelled. The methodology for estimating parameter values will be explained in depth in the next chapter.

The next four parameters control the rate of moisture movement between the soil horizons and from the soil layers to groundwater. Saturated permeability at the top of the upper horizon controls the rate of infiltration and overland flow, its value being estimated from knowledge of soil type. Saturated permeability - horizon boundary and saturated permeability - base lower horizon are two important parameters which control the rate of moisture movement between the two soil reservoirs and percolation to groundwater from

Parameter	Function
Pore Size distribution Index	General
Bubbling pressure	General
Saturated permeability – top upper horizon	Infiltration and overland flow
Saturated permeability – horizon boundary	Inter-horizon percolation
Saturated permeability base lower horizon	Percolation to groundwater
Interflow runoff from upper horizon at saturation	Interflow from upper horizon
Interflow runoff from lower horizon at saturation	Interflow from lower horizon
Soil Rooting Depth	Determines capacity of the upper and lower soil storages

Table 4.1 Principle soil parameters and their function within HYSIM

the lower soil reservoir. The last two parameters (interflow-upper horizon; interflow-lower horizon) control the lateral runoff from the two soil horizons. Estimation of the soil parameters requires knowledge of catchment soil type, texture and land-use. In contrast, in HBV-Light surface runoff and interflow are not explicitly modelled within the soil moisture routine. Furthermore, there no attempt at either defining specific soil horizons or modelling moisture transfers between horizons or to groundwater in terms of parameters.

61

4.7   Runoff Generation in HBV-Light

In both HBV-Light and HYSIM there are two groundwater reservoirs. In HBV-Light the runoff response function is the model routine which transforms excess water from the soil moisture zone to runoff, whereas in HYSIM runoff is simulated from all reservoirs in the model.   It also includes the effect of direct precipitation and evaporation from lakes, wetlands and tributaries within the catchment, unlike HYSIM where evapo-transpiration depletes only the interception and the soil moisture reservoirs.   Excess water enters the upper groundwater reservoir. It either leaves as runoff (through two outlets controlled by two parameters K_0 and K_1 which represent the quick runoff component of the hydrograph) or percolates down at a constant rate (PERC) to the lower groundwater reservoir where moisture depletion represents the slow, baseflow component of the hydrograph (K_2). The majority of parameters in HBV-Light are contained within this sub-routine. The generated runoff is then distributed on the following days with the parameter MAXBAS.

4.7.1   Runoff Generation in HYSIM

In HYSIM both groundwater reservoirs (transitional groundwater and groundwater) are infinite linear reservoirs. The parameters (groundwater recession; ratio groundwater to surface catchment; proportion of catchment with no groundwater; transitional recession; proportion – transitional) that control movement of groundwater are either estimated from aquifer maps or from studying precipitation time-series from within the catchment. Before total runoff is calculated it passes through the last reservoir in the model which represents minor channel storage. Runoff is then routed through the flow routing sub-routine which is described in the HYSIM through a simplified form of the St. Venant equations known as the kinematic method. Although this is more an approximation of a fully dynamic wave description than the St. Venant equations the sub-routine endeavours to describe channel flow realistically (Butts *et al.,* 2004). Thus, the groundwater and flow routing sub-routine in HYSIM also adheres to a physically realistic philosophy.

4.8   Conclusion

In this chapter the two rainfall-runoff models being employed in the project have been introduced. The structure of both HYSIM and HBV-Light has been outlined and a comparison has been made of two sub-routines of the models (soil moisture routine and the routine for runoff generation). Although both models have similarities in that they are both

lumped and both consist of a series of stores, it is obvious that structure of HYSIM is a reflection of the physically realistic philosophy which underlies the development of the model. This is in contrast to the structure of HBV-Light which is based on parsimony. This contrast in the philosophy of model development and model structure becomes more apparent when the methodology for the parameterisation of each model is described. This will be the focus of chapter 5.

Chapter 5: Parameterisation of the Rainfall-Runoff Models

5.1 Introduction

This chapter will focus on the parameterisation of the both HYSIM and HBV-Light. In the previous chapter the differences in the philosophy and structure of both models was explored. These differences will be highlighted again when the different methodologies involved in parameterising the models are described. The methodology for parameterising HYSIM will be outlined in the first section of the chapter. As HYSIM is a physically based model, most of its parameters are evaluated from physical characteristics of the Suir catchment. The final section of this chapter will describe the parameterisation of the HBV-Light model. HBV-Light is a simpler model whose parameters cannot be obtained from point measurements within the Suir catchment. Rather, the same parameter ranges can be applied to different catchments, and unique values for each parameter (relevant to the catchment) obtained during calibration.

5.2 Calculation of the HYSIM Parameters

HYSIM is a lumped rainfall-runoff model with 8 hydraulics parameters and 22 hydrology parameters. Of these, 4 are process parameters which are estimated during calibration. The other parameters must be calculated from the physical characteristics of the catchment. This section describes the methodology employed in calculating the hydraulic and hydrological parameters of HYSIM. In Manley (2003) parameters are divided into hydraulic, basic hydrology parameters and advanced hydrology parameters (see Table 5.1 and Table 5.2). In this thesis parameters are divided into soil parameters, land use and vegetation parameters, groundwater parameters and hydraulic parameters. In order to calculate the physical parameters for HYSIM, the EPA's 20m resolution Digital Elevation Model (DEM) was employed. This is supplied in sheet format with each DEM raster file representing one hydrometric area designated by the EPA. The Suir Catchment is represented in Sheet number 16 from the South Eastern River Basin District (SERBD). In order to calculate the hydrological and hydraulic parameters for the HYSIM model, this DEM was employed in conjunction with a Geographical Information System (GIS),

ArcMap version 9.2 which is a component of the Environmental Systems Research Institute's (ESRI) ArcGIS system. The advantage of GIS is that the map and its associated database are separated in a windows environment and are available in a variety of spatial resolutions making local area mapping of different aspects (e.g. land use, aquifer potential, soil classes, bedrock geology) of a specific location extremely versatile. The database and map can also be updated by the user thus permitting visualisation of user defined layers and shapefiles.

5.2.1   Delineation of the Suir Catchment and Hydraulic Parameters

The Suir catchment was delineated as far as Clonmel, using the ArcMap 9.2 Hydrology extension in the Spatial Analyst tool within ArcToolbox (ESRI). The grid projection for all raster files and shapefiles employed in this project is the Irish National Grid TM65 co-ordinate system (see Figure 5.1).   Please see Appendix 2 for the steps involved in delineating the Suir Catchment.
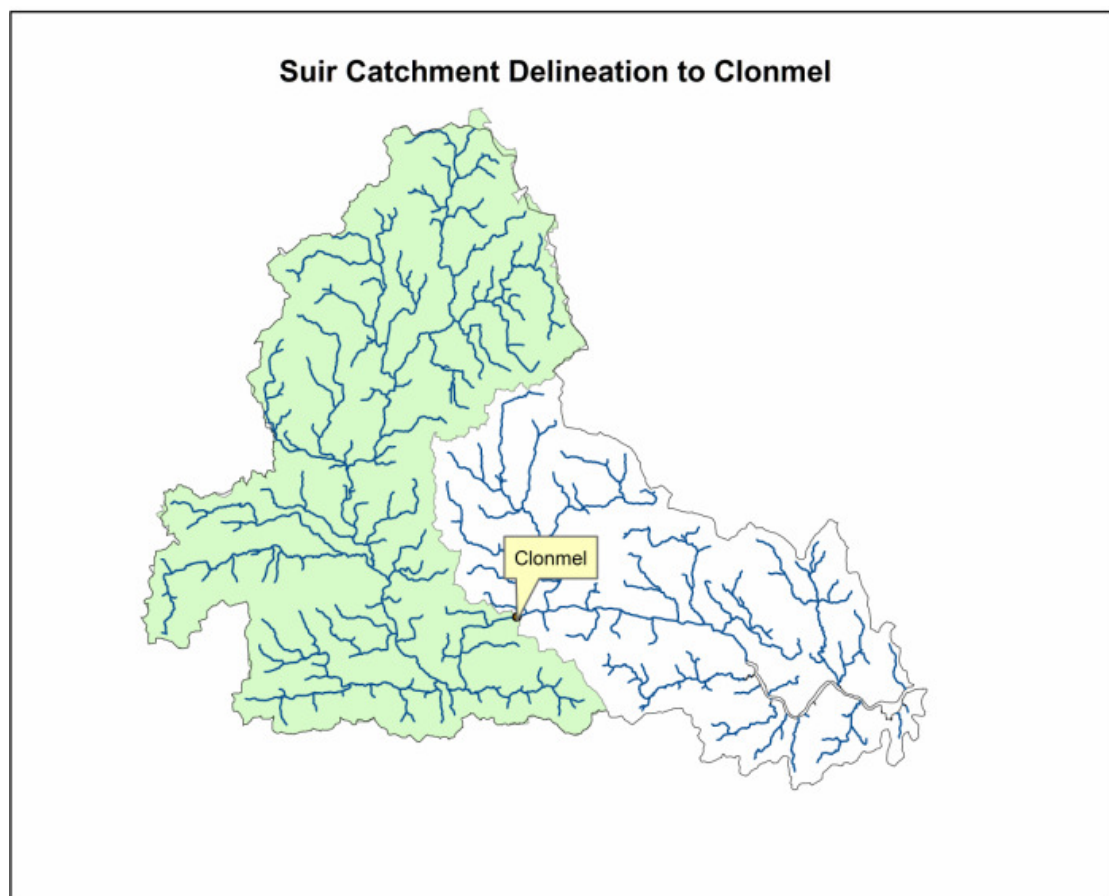
Figure 5.1 Delineation of the Suir catchment to Clonmel

65

In the sensitivity analysis of the HYSIM parameters undertaken by Murphy (2006) the hydraulic parameters (channel top width; channel base width; channel depth; channel roughness; reach gradient; floodplain width; flood plain roughness; reach length) were found to be insensitive when long term daily time-step modelling was undertaken. Manley (2003) also highlights the fact that the role of hydraulics in small catchments with daily data is negligible and the significance of the parameters is small. However, catchment area was found to be sensitive. The hydraulic parameters were estimated using the catchment characteristics calculated from the DEM and the Hydrology extension in ArcMap 9.2.

5.3   HYSIM Hydrology Parameters

5.3.1   Soil Parameters

Of the hydrology parameters, the soil parameters are some of the most sensitive and important in the model. Following after the methodology of Murphy (2006) the General Soil Map of Ireland was employed to estimate the soil parameters (Gardiner and Radford, 1980). The main soil types within the Suir catchment have already been described in Section 3.2.2. The next task was to assess the different soil associations within the catchment. Gardiner and Radford (1980) provide a detailed description of 44 soil associations present in Ireland, formed from the great soil groups such as brown podzolics, acid brown earths, gleys and blanket peats. Soil associations are cartographic units consisting of two or more soils (usually from the same parent material) that are related to a specific landscape type (Gardiner and Radford, 1980). The important component of soil for parameterisation purposes in HYSIM is texture. Soil texture refers to the proportion of various sized particles such as sand, silt and clay which make up the upper layers of the soil. Texture influences such soil properties as infiltration, water holding capacity, and soil porosity.

In ArcMap 9.2, a map of the Suir catchment soil associations was created in order to calculate the percentage occurrence of the different soil associations, from which soil texture can be derived. The soil associations with highest percentage occurrence were association 34 with 34.39% coverage, association 31 with 12.36% coverage, association 21 with 9.73% and association 1 with 8.06%. Together these associations comprise 65.54% of the catchment area (see Figure 5.2).

HYSIM Basic Hydrology Parameters		
Name	**Description**	**Method of Calculation**
Interception Storage	First store to be filled by incoming rain and depleted by PET	*Standard value for vegetation type*
Impermeable Proportion	Proportion of catchment considered impermeable	*Standard values: predominantly rural 0,02; predominantly urban 0.2*
Time to Peak (hours)	Controls simulation of minor channels within catchment	*Equation given by: $Tp=2.8(L/\sqrt{S})^{0.47}$ (Manley, 2003)*
Rooting Depth (mm)	Rooting depth of vegetation	*500 - 1000mm for arable land/crops up to 5000mm for woodland*
Pore Size Distribution Index	Controls way in which soils respond to moisture	*Values vary depending on soil texture class*
Saturated permeability at the horizon boundary (mm/hour)	Controls rate at which moisture moves between A and B horizons	*Calibrated*
Saturated permeability at base of lower horizon (mm/hour)	Controls rate at which moisture leaves the soil layers	*Calibrated*
Interflow runoff from upper horizon at saturation (mm/hour)	Controls lateral run-off from upper soil horizon	*Calibrated*
Interflow runoff from lower horizon at saturation (mm/hour)	Controls direct run-off from lower soil horizon	*Calibrated*
Groundwater Recession (per month)	Assessed by studying periods in a dry summer when little rain has fallen	*Equation given by $(q_2/q_1)^{(1/m)}$ (Manley, 2003)*

HYSIM Basic Hydrology Parameters (Continued)		
Precipitation Correction Factor	Allows for fact that catchment rain gauges may over or under-estimate precipitation	*Standard value 1.04* *Can be calibrated to achieve water balance*
PET correction factor	Allows for the fact that PET values may notbe accurate	*Can be calibrated to achieve water balance*
Catchment Area (km^2)	Area of catchment in Km^2	*Calculated using Catchment maps*

Table 5.1 HYSIM basic hydrology parameters

HYSIM Advanced Hydrology Parameters		
Name	**Description**	**Method of Calculation**
Saturated permeability at the top of the upper horizon	Rate at which water enters top of upper soil horizon	*Standard value 1000mm/hr*
Proportion of moisture storage in upper horizon	Proportion of available soil moisture in upper horizon	*Standard value 0.3*
Ratio of groundwater to surface catchment	Ratio of groundwater to surface catchment	*Estimated from aquifer maps*
Proportion of catchment with no groundwater	Proportion of catchment without groundwater	*Estimated form aquifer maps*
Riparian Proportion	Allows for fact that ET occurs in marshy riparian area adjacent to river channels at the potential rate	*Standard value 0.02*
Porosity	Value for porosity of soil - calculated from soil texture class	*Calculated from soil texture class*
Bubbling pressure	Represents capillary suction as soil is drying	*Calculated from soil texture class*
Transitional Recession (per month)	Represents recession constant for transitional groundwater	*Value taken from Murphy (2006)*
Proportional Transitional	Represents delayed response of groundwater entering channels	*Value taken from Murphy (2006)*
Interception Factor	Weighting for ET from interception storage	*Values 1.1 for grassland up to 1.5 for woodland*

Table 5.2 HYSIM advanced hydrology parameters
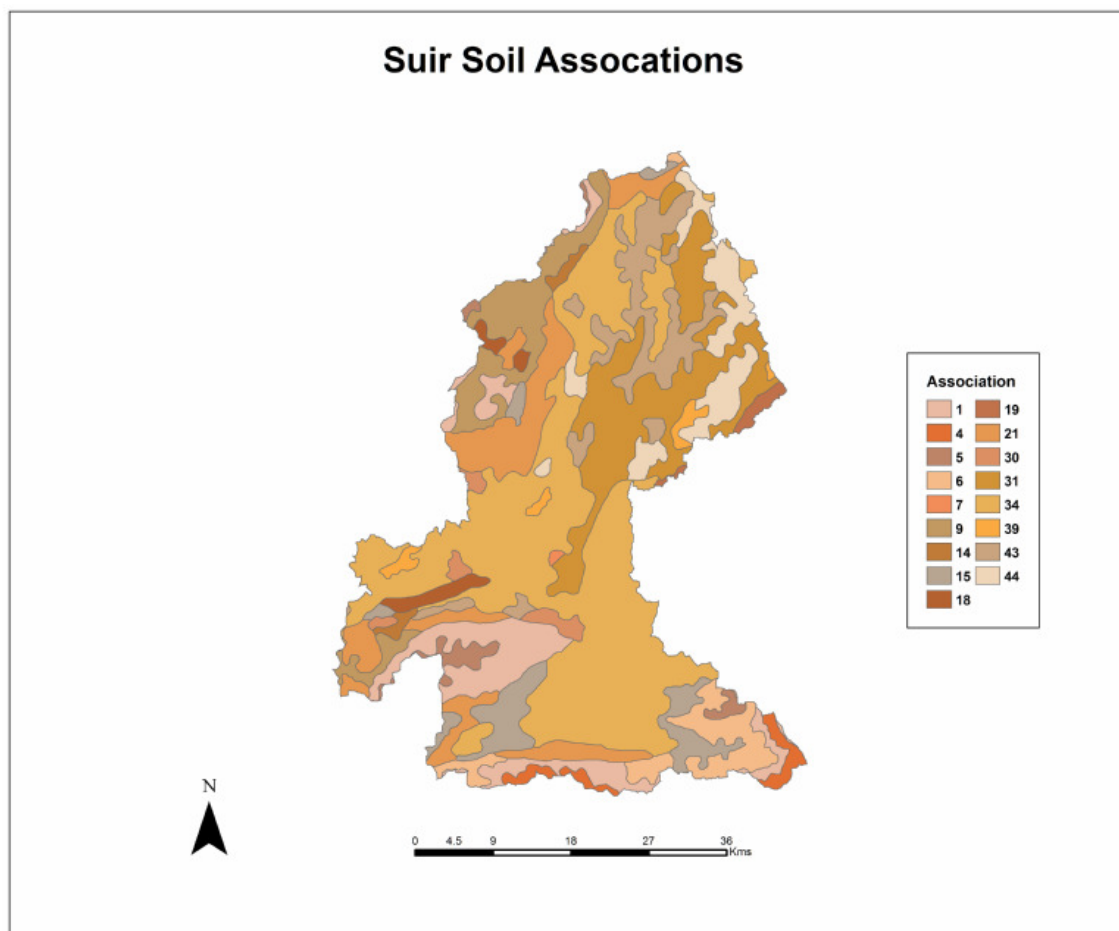
Figure 5.2 Soil associations in the Suir catchment

5.3.2 Soil Association Descriptions

Association 34 - Minimal Grey Brown Podzolics 70%, Gleys 20%, Brown Earths 10%

Association 34	Depth(cm)	% Sand	% Silt	% Clay	% Coverage
Horizon A	0 - 37	46.5	34	19.5	34.39
Horizon B	37 - 100	40	33	27	

Association 31 - Minimal Grey Brown Polzolics 80%, Gleys 10%, Brown Earths 5%, Basin Peats 5%

Association 31	Depth(cm)	% Sand	% Silt	% Clay	% Coverage
Horizon A	0 - 20	42.5	39.5	18	12.36
Horizon B	20 - 40	43	32	25	

Association 21 - Gleys 75%, Peaty Gleys 25%

Association 21	Depth(cm)	% Sand	% Silt	% Clay	% Coverage
Horizon A	0 - 35	43	33	24	9.73
Horzon B	35 - 81	44.5	33	22.5	

70

Association 1 – Peaty Podzols 75%, Lithosols 15%, Blanket Peats 10%

Association 1	Depth(cm)	% Sand	% Silt	% Clay	% Coverage
Horizon O	25 - 0	60	38	2	8.06
Horzon A	0 - 10	67	24	9	

Figure 5.3 Predominant soil associations of the Suir catchment (Gardiner and Radford, 1980)

The predominant soil associations of the Suir catchment are detailed in Figure 5.3 above. The next step in identifying the predominant soil texture of the catchment was to relate the different percentages of sand, silt and clay in each association with the main soil texture classes. Ternary diagrams have been developed that specify the main soil texture classes in graphic form. The United States Department of Agriculture (USDA) ternary diagram was employed to calculate the dominant soil texture by plotting the percentages of sand, silt and clay to obtain the soil texture class, as Gardiner and Radford (1980) used the same system in determining soil textures (Figure 5.4). The diagram is triangular with percentages of clay, silt and sand ranging from 0 to 100%. Once the percentage of each is known, the overall texture of the soil can be read off the ternary diagram.
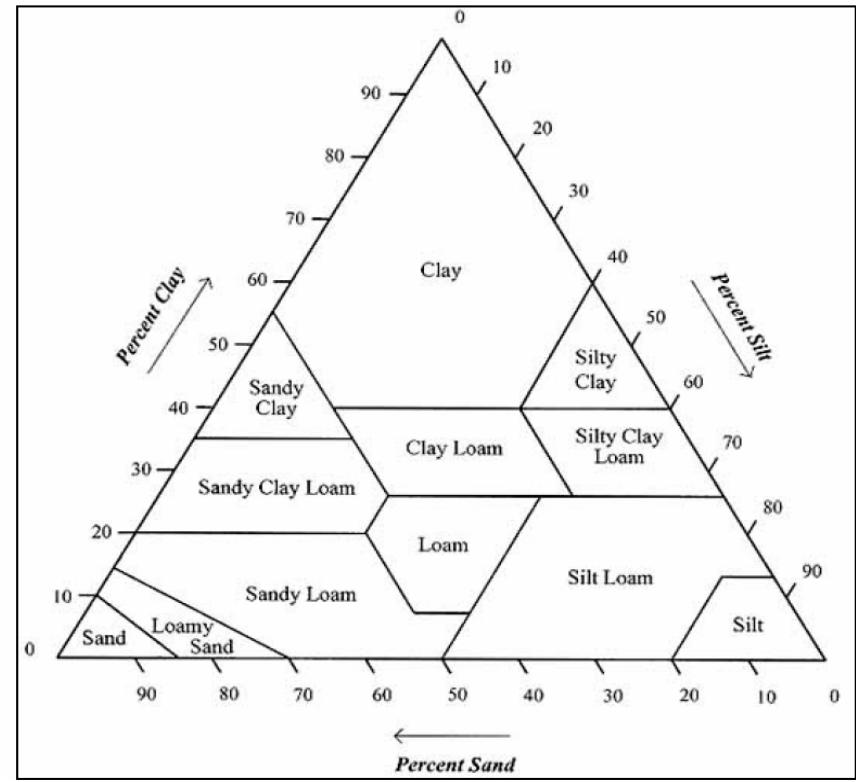
Figure 5.4 U.S.D.A. Ternary Diagram showing the percentages of sand, silt and clay in the basic soil texture classes

71

Soil textures can be estimated for the different soil associations in the Suir catchment by using the different percentages of sand, silt and clay present to define the basic soil texture of each association. The dominant soil texture class of the Suir catchment is loam comprising approximately 74% of the area total (see Table 5.3). A further 9% is comprised of sandy loam. Table 5.4 provides values for three soil parameters once soil texture class has been established namely Pore Size Distribution Index (PSDI), Bubbling Pressure, and Porosity (Manley, 2003). Pore Size Distribution Index is one of the most important parameters as it controls the way soils respond to moisture and to dewatering (Manley, 1978). Its value also determines the values for Bubbling Pressure and Porosity. Bubbling Pressure is another important soil parameter which represents capillary suction at the point that bubbles appear in the soil when it is being de-watered under increasingly negative pressure (Manley, 1978).

Association	Texture	Area Km^2	% Total
19	Clay Loam	12.86	0.60
39	Clay Loam	22.92	1.07
6	Loam	88.29	4.12
9	Loam	138.13	6.44
14	Loam	14.40	0.67
15	Loam	102.14	4.77
18	Loam	28.18	1.31
21	Loam	208.59	9.73
31	Loam	265.00	12.36
34	Loam	737.13	34.39
5	Peat	30.21	1.41
44	Peat	115.23	5.38
4	Peaty Clay	29.37	1.37
7	Peaty Clay Loam	1.97	0.09
1	Sandy Loam	172.79	8.06
30	Sandy Loam	27.40	1.28
43	Silty Clay Loam	148.93	6.95
Total		**2143.54**	**100.00**

Table 5.3 Soil associations of the Suir catchment, their associated texture and percentage of the total catchment area occupied by each

Soil Texture	PSDI	Bubbling Pressure (mm)	Permeability mm/hr	Porosity
Peat	.50	100	500	.70
Sand	.25	120	630	.40
Loamy Sand	.23	90	560	.41
Sandy Loam	.20	220	125	.44
Silt Loam	.19	80	26	.49
Loam	**.18**	**500**	**25**	**.45**
Sandy Clay Loam	.14	300	23	.42
Silty Clay Loam	.13	360	6	.48
Clay Loam	.12	630	9	.48
Sandy Clay	.10	150	8	.43
Silty Clay	.10	490	4	.49
Clay	.09	410	4	.48

Table 5.4 Values of PSDI, Bubbling Pressure and Porosity (Manley 2003)

5.3.3 Land Use Parameters

Section 3.2.3 has already described the methodology for deriving land use types for the Suir catchment using the CORINE database. As was already noted, pasture is by far the most common land use type in the Suir catchment accounting for 70% approximately of the total land area delineated as far as Clonmel. Please note that the values for land use in Section 3.2.3 may be slightly different to those in the table below as the values in that section were calculated for the catchment as a whole, not the catchment delineated to the outlet in Clonmel.

Table 5.5 shows the percentage of different land use types in the Suir catchment. As HYSIM is a lumped conceptual model which treats the catchment as a single unit, pasture was used to calculate the soil rooting depth. The HYSIM manual gives a typical value for grass/pasture of 700 mm – 800 mm in contrast to woodland which can have a value up to 5000 mm. As forestry and transitional woodland comprises approximately 9% of the catchment area the rooting depths were weighted accordingly to give an average rooting depth for the catchment of 1200mm. Soil Rooting Depth is an important parameter as it controls the amount of moisture in the upper and lower soil stores.

CODE3	Description	Area Km2	Percentage
121	Industrial/Commercial	0.36	0.02
512	Water bodies	0.61	0.03
124	Airports	0.81	0.04
511	Stream courses	0.90	0.04
111	Continuous Urban	1.23	0.06
142	Sport and Leisure	1.75	0.08
411	Inland Marshes	2.05	0.10
131	Mining	2.26	0.11
311	Broad Leafed Forest	4.79	0.22
112	Discontinuous Urban	8.10	0.38
242	Complex Cultivation	21.53	1.00
321	Natural Grassland	25.57	1.19
324	Transitional woodland	35.49	1.66
243	Agri/Natural Vegetation	48.53	2.26
322	Moors/heathland	91.45	4.27
412	Peat Bogs	116.28	5.42
211	Non-irrigated arable land	122.41	5.71
312	Coniferous Forest	151.23	7.06
231	Pasture	1508.23	70.36
	TOTAL	2143.56	100.00

Table 5.5 Land use types and percentage area in the Suir catchment

5.3.4   Groundwater Parameters

The Groundwater Recession rate is calculated by studying periods during a dry summer when little or no rain has fallen. The formula for calculating the value is supplied by Manley (2003):

$$(q2/q1)^{(1/m)}$$

where *q1* is the discharge at the start of the dry spell, *q2* is the discharge at the end of the dry spell and *m* is the time period in months. Precipitation data from several raingauges within the Suir catchment were obtained from Met Eireann. The data from Knockderry Reservoir was used to calculate the groundwater recession rate as this raingauge has the highest quality data within the catchment at 99% satisfactory rating. The summer of 1976 was chosen to calculate the rate as this was the driest summer during the baseline climate period (1961 to 1990) (see Figure 5.5).
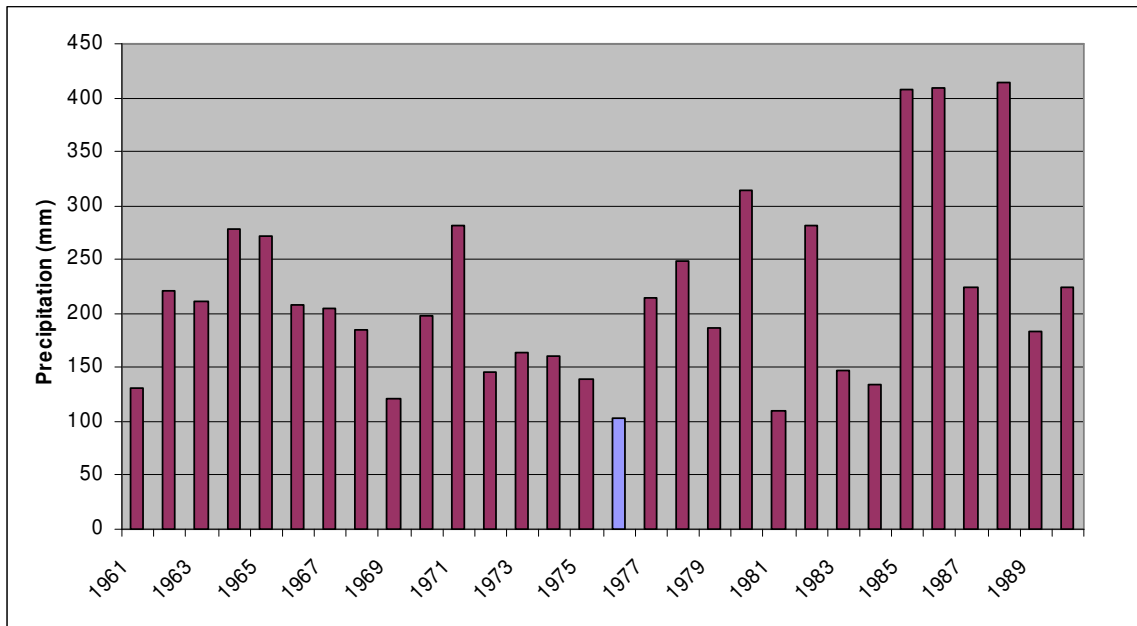
Figure 5.5 Knockaderry Reservoir summer precipitation 1961 – 1990

Flow amounts in the Suir catchment on 31st May 1976 (29.54m^3/sec) (beginning of dry period) and 1st September 1976 (6.41m^3/sec) (end of dry period) were applied to the formula giving the following result:

$(6.41/29.54)^0.33 = .61$

The aquifer potential of the Suir catchment has already been described in Section 3.2.4. There are many locally and regionally important aquifers in the Suir catchment, owing to highly permeable subsoils and the percentage of land underlain by karstic bedrock formations. The GSI aquifer map was used to calculate the Ratio of Groundwater to Surface Catchment parameter. As HYSIM is a lumped model areas with good aquifer potential were assigned groundwater and areas with poor aquifer potential were assigned no groundwater. Regionally important aquifers account for 27.21% of aquifer types in the catchment, locally important aquifers comprise 62.44% of the catchment area and poor aquifers comprise 10.35% of the catchment area (see Figure 5.6). The Ratio of Groundwater to Surface Catchment was given the value 0.9 and the proportion of the catchment with no groundwater was assigned a value of 0.1. The values of the Transitional Recession parameter and the proportion of moisture leaving transitional groundwater that enters channels parameter (Proportion Transitional) were taken from Murphy (2006).
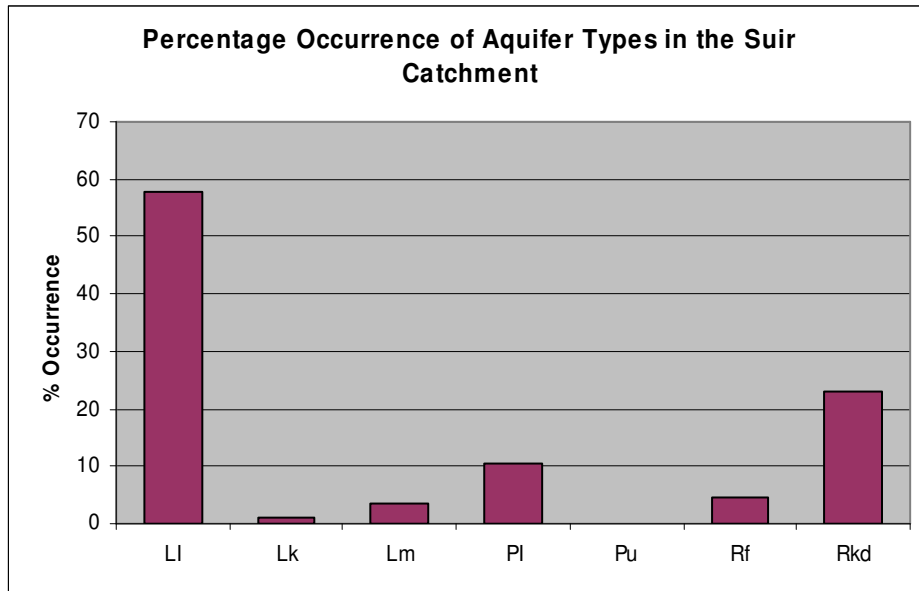
Figure 5.6 Percentage occurrence of aquifer types in the Suir catchment

5.3.5 Time to Peak – Minor Channels

Time to Peak – Minor Channels controls the response of minor channels within the catchment. The equation which has been used in Manley (2003) to determine this parameter is from the UK flood Studies Report, as follows:

$$T_p = 2.8(L/\sqrt{S})^{0.47}$$

Where L is stream length in km, S is the stream slope in m/km and T_p is time to peak in hours. The value of this parameter should be the average value obtained from 4 or 5 small contributing streams. Four tributaries of the Suir upstream from the outlet at Clonmel (the Aherlow, Multeen, Neir and Tar) were chosen to calculate this parameter (see Figure 5.7).

The lengths of the tributaries were calculated using the attribute table in ArcMap 9.2. The stream gradient from its headwaters to the confluence with the Suir was estimated using the Ordinance Survey Ireland (OSI) Discovery series 1:50,000 maps number 74 and 75. Each time to peak was the calculated using the above formula. The average Time to Peak value was 11.4 hours which was the value assigned to this parameter (Table 5.6).
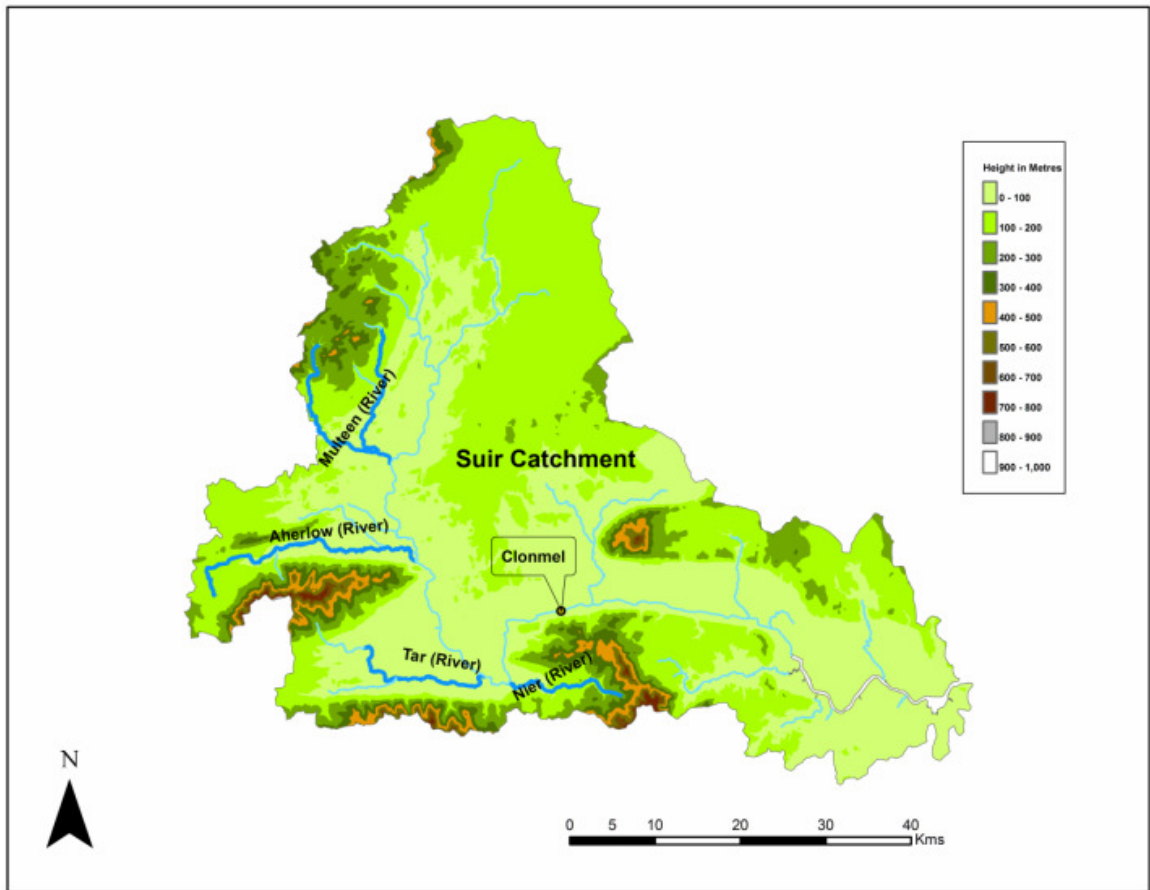
Figure 5.7 Tributaries of the Suir used in calculating Time to Peak

Name	Length (km)	Gradient (m)	Slope (m/km)	Time to Peak
Aherlow	38.13	125	3.27	11.73
Multeen	21.43	180	8.38	7.17
Neir	16.84	120	7.12	16.74
Tar	21.70	45	2.07	10.02

Table 5.6 Values of the Time to Peak for each tributary

Parameter	Suir Values
Channel top width (m)	40
Channel base width (m)	37
Channel depth (m)	1.5
Channel roughness	.015
Reach gradient	.001
Flood plain width	140
Flood plain roughness	.035
Reach length (m)	98000
Interception storage* (mm)	2
Impermeable proportion*	.02
Time-to-peak	11.4
Pore size distribution Index	.18
Rooting depth	1200
Groundwater recession (per month)	.61
Precipitation factor	1.4
PET factor	1
Catchment Area (km^2)	2173
Permeability – top upper horizon* (mm/hour)	1000
Proportion upper horizon	.3
Ratio groundwater to surface catchment	.9
Proportion of catchment no groundwater	.1
Riparian proportion*	.02
Porosity	.45
Bubbling Pressure	500
Transitional recession (per month)	.9
Proportional transitional	.7

Table 5.7 Values of physical parameters calculated for the Suir catchment. Parameters highlighted with asterisk were given default values recommended by Manley (2003)

The final values for the physical parameters of the HYSIM model of the Suir catchment are above. Four parameters were given the default values recommended by Manley (2003).

5.4 Parameterisation of HBV-Light

Unlike HYSIM which has physically based parameters, the parameters in HBV-Light are process parameters which must be calibrated. Indeed, Bergstrom (1991, p.126) cautions that "physical interpretation of the parameters of a conceptual model are...normally very vague and should be regarded with sound scepticism". There is no "best" method for estimating parameter values in HBV-Light. Indeed, previous research used a variety of different methods to estimate parameter values for HBV and HBV-Light. Mein and Brown (1978) performed a sensitivity analysis to calculate parameter values. Harlin and Kung (1992) estimated reasonable ranges of parameter values by selecting the minimum and maximum values of each parameter from eight autonomous calibrations of two study catchments. Seibert (1999) used 300,000 Monte Carlo runs to estimate parameter values based on three different objective function scores. Booij (2005) used the experience of previous researchers to identify reasonable ranges for the parameters. A literature review was also undertaken in this project to estimate the parameter ranges (Booij, 2005; Harlin and Kung, 1992; Seibert, 1997, 1999; Steele-Dunne *et al.,* 2008; Uhlenbrook *et al.,* 1999) (see Table 5.8). After consideration, the parameter ranges in Seibert (1999) were adopted as the same ranges were employed successfully in Steele-Dunne *et al.* (2008) to calibrate HBV-Light (see Table 5.9).

Reference	FC mm	LP -	BETA -	K0 d^{-1}	UZL mm	K1 d^{-1}	K2 d^{-1}	PERC mm d^{-1}	MAXBAS d
Harlin & Kung 1992	50-274	0.73-1.0	1.0-5.9	0.197-0.450	12 - 44	0.093-0.180	0.0008-0.05	0.90-2.10	1 - 2
Siebert 1997	50-500	0.3-1.0	1 - 6	0.05-0.5	0 - 100	0.01-0.3	0.001-0.1	0 - 6	1 - 5
Siebert 1999	50-500	0.3-1.0	1 - 6	-	-	0.01-0.4	0.001-0.15	0 - 3	1 - 7
Steele-Dunne *et al.* 2008	50-500	0.3-1.0	1 – 6	0.05-0.5	0 – 100	0.01-0.4	0.001-0.15	0 – 3	1 - 7
Uhlenbrook et. al. 1999	100-550	0.3-1.0	1 -5	0.1-0.5	0 - 70	0.01 – 0.2	0.00005-0.1	0-4	1 - 2.5

Table 5.8 Parameter ranges used by other researchers for calibrating HBV and HBV-Light

Parameter	Definition	Units	Max	Min
Soil and ET Routine				
FC	Maximum Soil Moisture	mm	50	500
LP	Fraction of LP above which Et_{act} equals PET	-	0.3	1
BETA	Shape co-efficient	-	1	6
Groundwater and response routine				
K_0	Recession co-efficient (upper reservoir)	d^{-1}	0.05	0.5
K_1	Recession co-efficient (upper reservoir)	d^{-1}	0.01	0.3
K_2	Recession co-efficient (lower reservoir)	d^{-1}	0.001	0.1
UZL	Threshold for K_0 outflow	mm	0.0	100
PERC	Maximum flow from upper to lower groundwater box	$mm\ d^{-1}$	0	6
MAXBAS	Length of triangular weighting function in routing routine	d	1	5

Table 5.9 Reasonable ranges employed for calibration of the parameters in HBV-Light

5.5 Conclusion

Although HYSIM and HBV-Light are both lumped rainfall-runoff models, the methodology for parameterising each model differs significantly. HYSIM is a more complex model and most of its parameters are estimated from physical catchment characteristics. All but four of the parameters in HYSIM are fixed values. The parameterisation of HYSIM also takes account of the unique characteristics of the catchment being modelled, albeit on a lumped scale. HBV-Light is a simpler model with process parameters. Reasonable ranges for parameter values were estimated based on the experience of other researchers. The method for parameterising HBV-Light also reflects the generic nature of conceptual rainfall-runoff models, which can be applied successfully to streamflow simulations in many catchments with unique characteristics. Although HBV-Light has fewer dimensions on its response surface than HYSIM, the parameter ranges allow for great interaction during calibration. The next chapter will focus on calibration and validation of both models.

Chapter 6: Calibration and Validation of the Rainfall-Runoff Models

6.1 Introduction

This chapter focuses on the methodology for calibrating and validating both HYSIM and HBV-Light, using a split sample procedure. A description of a traditional calibration follows, as historically modellers have focused on finding an optimal parameter set through calibration. However, in order to take account of model structural uncertainty and equifinality of parameter sets the Generalised Likelihood Uncertainty Estimation (GLUE) method will be employed for calibration (Beven and Binley, 1992). The methodology for calibrating and validating both models will then be outlined.

6.2 Model Calibration

Calibration is the process of adjusting model parameters to obtain as good a fit as possible between observed and modelled flow. Calibration can be undertaken manually or with the aid of an optimisation algorithm. Manual calibration is a trial and error process whereby the hydrologist continually adjusts the parameters to fit observed flow data, taking account of the fact that the adjusted parameters should realistically reflect the main processes affecting runoff in the catchment. The limitations of manual calibration include the large amount of subjectivity involved, the length of the process and the fact that it is not possible to objectively analyse parameter uncertainty (Wagener, 2003). Furthermore, there may be few people highly experienced in manual calibration (Sorooshian and Gupta, 1995). Therefore, automatic calibration schemes have been developed.

The traditional purpose of calibration is to find the parameter combination that optimises the value of a particular objective function (e.g., Duan *et al.,* 1992; Lindström, 1997). Sorooshian and Gupta (1995, p.27) outline the procedure of parameter optimisation during calibration. Key decisions required for automatic calibration include choice of:

1. Objective function
2. Optimisation algorithm
3. Termination criteria
4. Calibration data

6.2.1 Objective Function

An objective function is an equation used to measure the performance a hydrological model in simulating catchment behaviour. In the case of rainfall-runoff models, it provides a quantitative indicator of the success of the model at simulating observed flow. There are many such measures such as absolute error, relative error and regression techniques. Evaluation measurements also provide a means of distinguishing between the performances of different models (Wagener, 2003). However, a universal measurement metric has yet to be found, as all such evaluation equations are biased towards one part of the hydrograph (Dawson *et al.,* 2007). This means that parameter sets deemed acceptable by one performance measurement cannot represent both the high and low flow behaviour of the catchment system (Wagener, 2003 p.3376). For this reason, it is better to quantify a model's success at simulating flow using several evaluation measures (Dawson *et al.,* 2007).

6.2.2 Optimisation Algorithm

An optimisation algorithm is a mathematical procedure which searches the model space (response surface) for the parameter combination which optimises the value of the objective function (Sorooshian and Gupta, 1995). There are a plethora of optimisation algorithms now available for calibration from local search algorithms (e.g. the Rosenbrock method used in HYSIM) to global and multi-start search methods such as the genetic algorithm used for calibration in HBV-Light. In local search methods the starting place of the algorithm within the response surface influences where the search ends. Genetic algorithms are based on the concept of biological evolution and involve creating a population (different parameter sets) and evolving that population over several iterations until the performance is optimised according to the evaluation measure (Beven, 2000).

There is no guarantee that an optimisation algorithm, however sophisticated, will find the global optimal parameter set. Conceptual rainfall-runoff models tend to be highly non-linear with parameter interactions complicating the search for the optimal set. The optimal parameter set is also contingent on the calibration period, and different calibration periods may lead to multiple optimal parameter sets (e.g., Beven, 1993; Wilby, 2005). The optimal set is also contingent on the objective function employed in calibration (Wagener, 2003). Over-parameterisation is also an issue the response surface of the model may be extremely

complex, further complicating the search for the optimal set. It is obvious that HBV-Light with 9 parameters has a much simpler parameter response surface than HYSIM with 30 parameters. Duan *et al.* (1992) identified multiple optimal sets within a conceptual rainfall-runoff model response surface. Even if the global optimal set is found, there is a high possibility that this optimal parameter combination is contingent on the calibration data, the model structure, the objective function and the optimisation algorithm employed (Beven, 2009). Indeed, there may be many parameter combinations within the response surface which simulate observed flow equally well (Sorooshian an Gupta, 1995; Beven, 2000; 2009). In this project, parameter uncertainty will be accounted for by applying the GLUE methodology (which allows for equifinality of parameter sets and models) in calibrating and validating the models.

6.2.3 Termination Criteria

One means by which the search algorithm ceases the search is when changing the parameter combination does not improve the value of the objective function (parameter convergence). However, this does not mean that the search algorithm has found the global optimal set. There are several other methods of determining when a search should be terminated, however Sorooshian and Gupta (1995) note that parameter convergence is the technique most suitable for calibration of hydrological models.

6.2.4 Calibration Data

Sorooshian and Gupta (1995) stress the importance of variability within calibration data in training the hydrological model (otherwise, certain processes within the model may not be activated). For example, if calibration data are employed from a relatively dry period, parameters controlling overland flow processes and percolation to groundwater may not be activated, leading to insensitive parameters and poor model response (Sorooshian and Gupta, 1995). Choosing data from calibration periods with hydrological variability will lead to more informed responses.

The above methodology has traditionally been employed to search for the optimal parameter set within a single hydrological model. However, in this project the concept of equifinality is accepted as a viable hypothesis for the calibration and validation of the rainfall-runoff models (e.g. Cameron *et al.,* 2000; Duan *et al.,* 1992; Murphy and Charlton, 2008; Wilby and Harris, 2006) (see Section 2.7.4).

6.3   The GLUE Procedure

Section 2.7.6 outlines the decisions to be taken in the GLUE methodology which explicitly takes equifinality of parameter sets into account in model calibration. Beven and Binley (1992) outline the GLUE procedure in a number of steps. They are:

1. The definition of a likelihood measure selected to determine model performance.
2. A definition of a suitable range of values for each parameter.
3. The use of Monte Carlo Random Sampling to sample a large number of parameter sets from a given distribution.
4. The selection of a pre-defined threshold to determine behavioural or non-behavioural parameter sets.
5. The generation of results for all behavioural sets and employment of these to determine weighted mean discharge and simulation probability bounds if using the model for prediction purposes (Melching, 1995).

In this project logical reasons have already been given for the choice of rainfall-runoff models. HYSIM is a physically based model while the structure of HBV-Light is based on parsimony. Furthermore, the methodology involved in selecting relevant parameter values (HYSIM physical parameters) and parameter ranges (HBV-Light) has been outlined in the previous chapter. The sampling strategy used is the Monte Carlo method. The Nash-Sutcliffe dimensionless efficiency criterion (NS) is employed as the likelihood measurement as it is the only evaluation metric common to both models (Nash and Sutcliffe, 1970). However, other likelihood measures will also be employed to evaluate further the performance of the models during calibration and validation. These are: Mean Actual Error (MAE); Root Mean Square Error (RMSE); Percent Bias (PBIAS) and the Coefficient of Determination (R^2).

6.4   Calibration of the Rainfall-Runoff Models

6.4.1   Calibration data employed in the project

Records of daily mean flow at Clonmel (Station No.16011) on the River Suir from 1961 to 2000 were obtained from the Office of Public Works Hydro-Data website (www.opw.ie/hydro). Daily records of precipitation and potential evapo-transpiration

(PET) were obtained from Met Eireann for the Kilkenny Synoptic station from 1961 to 2000 and employed as input to the models for the calibration period (1963 to 1990) and the validation period (1991 to 2000). Kilkenny is the nearest synoptic station to the Suir catchment. Additionally, the statistically downscaled future data was generated only for the Irish synoptic stations.   Therefore, the empirical temperature, precipitation and PET recorded at this station were also used as input to the models for calibration and validation. Although this introduces input data uncertainty (i.e., all input data employed was recorded outside the Suir catchment) it will not be evaluated in this project as the focus is on evaluating model structural uncertainty and parameter uncertainty.

An initial spin-up period of 1961 to 1963 was employed to allow adjustment to initial and boundary conditions, then the models were calibrated from 1963 to 1990. This time period was chosen by the World Meteorological Organisation as the baseline period in comparing future climate change as it includes both dry periods (the 1970s), wet periods (the 1980s) and natural climate variability which dominates any climate change signal. The records of this period are also of a high quantity and quality compared to other historical periods (Prudhomme *et al.,* 2003).

6.4.2   The Nash-Sutcliffe Criterion of Efficiency

The Nash Sutcliffe dimensionless efficiency criteria (NS) was employed as the likelihood measurement for calibration of the parameter sets in both HYSIM and HBV-light, as it is the only evaluation measurement common to both models. NS is given by the equation:

$$E = 1 - \frac{\sum_{t=1}^{T}(Q_o^t - Q_m^t)^2}{\sum_{t=1}^{T}(Q_o^t - \overline{Q_o})^2}$$

where Qo is the observed discharge, Qm is the modelled discharge and Q_o^t is the discharge at time *t*.   The score for a perfect fit between observed and modelled flow according to the NS criterion is 1. As NS is sensitive to differences between observed modelled means and variances it is an improvement over the coefficient of determination (Legates and McCabe, 1999). Nevertheless, it is biased towards higher flows because the largest residuals tend to be found near the hydrograph peaks, and as the errors are squared greater weight is given to

prediction of the peaks of the hydrograph rather than low flows (Legates and McCabe, 1999; Krause *et al.,* 2005).

6.4.3   Calibration of the HYSIM Process Parameters

Within HYSIM there are four process parameters (saturated permeability horizon boundary; saturated permeability base lower horizon; interflow runoff upper horizon; interflow runoff from lower horizon). Initial value ranges for each process parameter were based on the ranges given in Manley (2003) and are contained in Table 6.1.

Process Parameter	Value Range
Saturated permeability – base lower horizon	1.00 mm/hr – 100.0 mm/hr
Saturated permeability – horizon boundary	5.00 mm/hr – 200.0 mm/hr
Interflow runoff – upper horizon	1.00 mm/hr – 100.0 mm/hr
Interflow runoff – lower horizon	1.00 mm/hr – 100.0 mm.hr

Table 6.1 Initial value ranges for the four process parameters in HYSIM

HYSIM was calibrated using Monte Carlo sampling to generate 10,000 random parameter combinations. Only parameter sets with a score of 0.7 or higher were deemed behavioural. The run yielded 2452 parameter sets of 0.7 or higher. Of these, the top 500 sets were retained (NS values 0.75 - 0.769) and employed to validate the model. Scatter plots of each parameter were produced to evaluate parameter definition (Figure 6.1). A parameter may vary in definition according to the calibration period and the characteristics of the catchment being modelled (Wilby, 2005; Uhlenbrook *et al.,* 1999).   The only poorly defined parameter was permeability – horizon boundary. The other parameters were **more or less** well defined. However, all the parameters had good NS values scattered through the parameter space.   The mean, median, maximum and minimum values of the four process parameters in the calibration parameter sets are presented in Table 6.2.

	SP BHL	SP HB	I U	I L
Mean	60.13	131.51	23.55	43.58
Median	61.91	139.44	22.27	43.19
Min	3.59	8.74	2.31	1.934
Max	100.44	204.93	52.42	87.81

Table 6.2 Mean, median, maximum and minimum values for the behavioural parameters
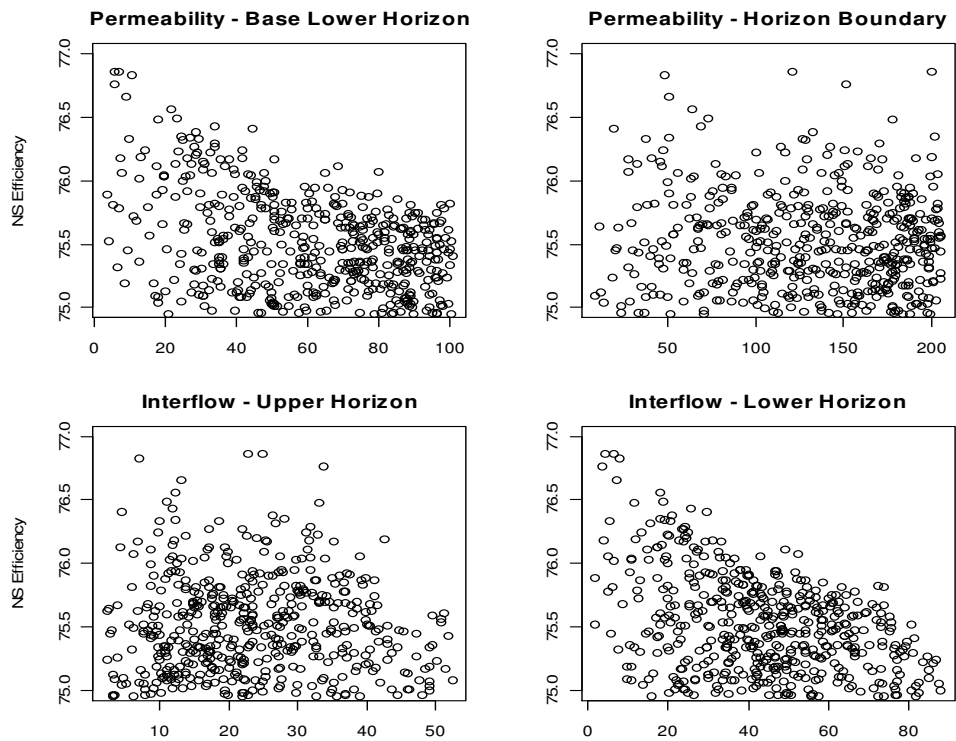
Figure 6.1 Scatter plots of the four process parameters in HYSIM showing parameter identifiability

What is notable in the above values is that interflow - upper horizon (IU) has particularly low mean and median values, given the initial value range (1 – 100mm/hour) and its highest value within the behavioural parameter sets is slightly higher than the median of the initial value range. Conversely, the mean and median values of interflow – lower horizon (IL) lie towards the middle of the value range. This may be reflective of the permeable nature of the Suir catchment, which is baseflow dominated. This observation is reinforced by higher values for the two other process parameters (saturated permeability - base lower horizon and saturated permeability - horizon boundary). Indeed, the maximum values of these two parameters within the calibration parameter sets are at the highest end of the initial value range. Furthermore, for each of these parameters the mean and median values within the behavioural sets are within the top 40% of the initial parameter value ranges.

6.4.4 Calibrating HBV Light

In the HBV-Light model the parameter space was preliminarily sampled by 10,000 Monte-Carlo runs specifying the threshold NS efficiency value of 0.7. Each of the parameters was sampled from within reasonable ranges (defined from the literature review) using a uniform distribution. However, no parameter sets with an NS value of 0.7 or over were generated.

The threshold for NS was then lowered to 0.6, and a further 10,000 Monte Carlo runs were generated, which resulted in 683 parameter sets of value 0.6 or over. Individual parameters were then plotted against NS values and a visual inspection of the spread of each parameter was made (see Appendix 3).

After the visual inspection, value ranges for the well defined parameters were constrained in order to generate more parameter sets with a high NS value (see Table 6.3). Based on the visual inspection, the value ranges of FC, LP, BETA, MAXBAS, K_1 and K_2 were constrained, whilst the values of the poorly defined parameters UZL, PERC and K_0 (with acceptable values spread throughout the parameter space) were left unchanged.

Parameter	Original Value Range	Constrained Value Range
FC	50 – 500	50 - 175
LP	0.3 – 1.0	0.7 -1.0
BETA	1.0 – 6.0	1.0 – 3.0
K₁	0.01 – 0.4	0.1 – 0.25
K₂	0.001 – 0.15	0.02 – 0.10
MAXBAS	1 – 7	2 - 4

Table 6.3 Constrained value ranges for well-identified parameters in HBV-Light

A further 500,000 Monte Carlo samples were generated. What is notable is the much higher amount of Monte Carlo runs required to generate behavioural parameter sets compared to HYSIM. The run yielded 530 sets with an acceptable NS score, which ranged from 0.7 to 0.7112. The top 500 parameters were used to calibrate and validate HBV-Light. Figure 6.2 shows the scatter plots of the individual parameters. Well defined parameters include FC, LP, BETA, K2 and MAXBAS. Identifiability of specific parameters depends on factors such as catchment characteristics and calibration period and it is difficult to know beforehand if a specific parameter will be well or badly defined (e.g., Siebert, 1997a; Uhlenbrook *et al.,* 1999)   In this project, the three soil routine parameters (FC, LP and BETA) are particularly well defined (Figure 6.2).
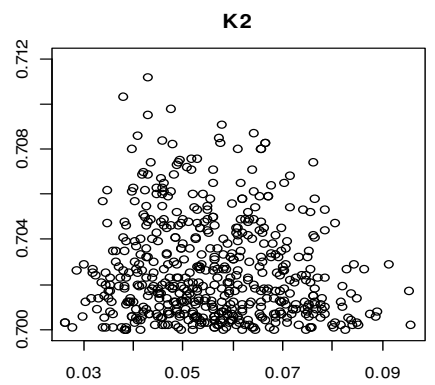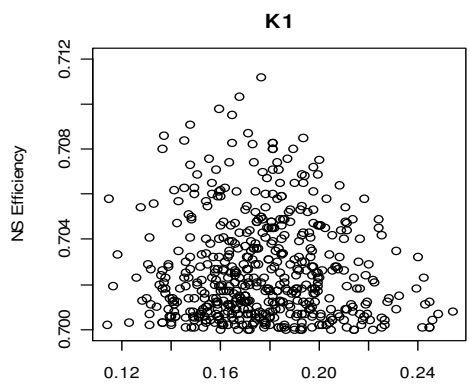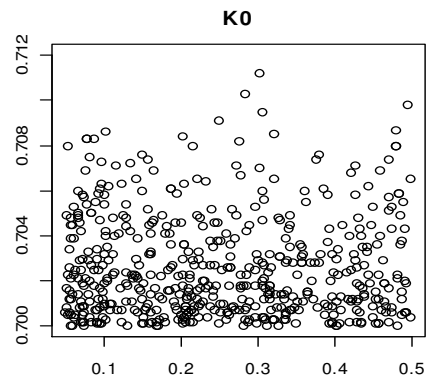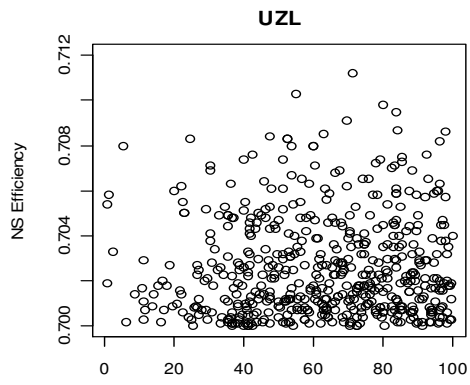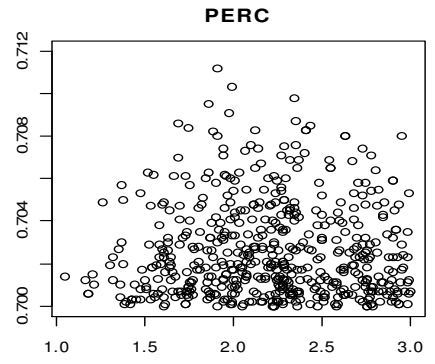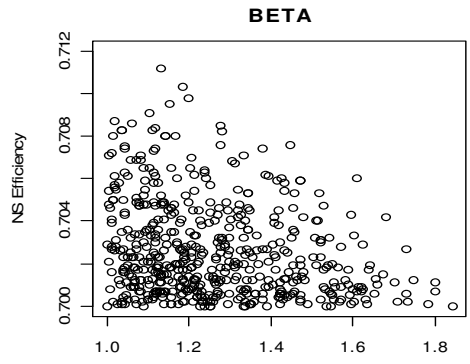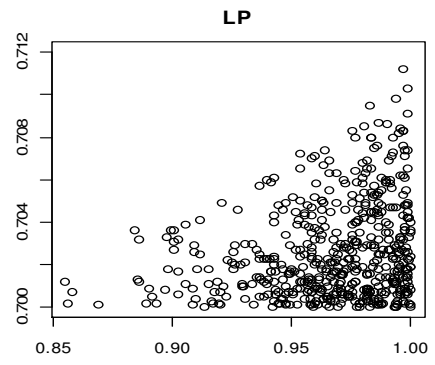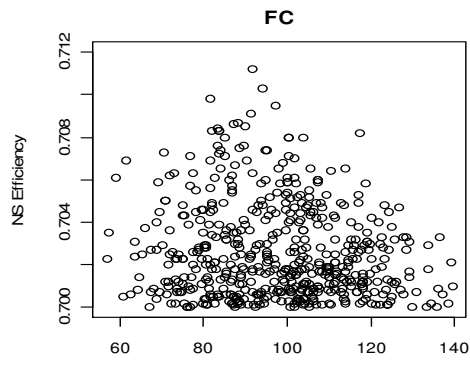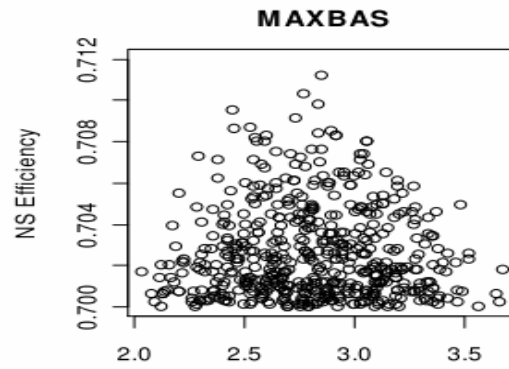
Figure 6.2 Scatter plots for each HBV-Light parameter

Steele-Dunne *et al.* (2008) calibrated and validated the HBV-Light model for 10 catchments within Ireland, including the Suir catchment. In that study lower values of the recession coefficients (K_0, K_1 and K_2) are associated with larger catchments (such as the Suir) with more damped hydrographs (Steele-Dunne *et al.,* 2008). A similar observation can be made in this project (see Table 6.4). It is also notable that the mean and median values of PERC are towards the higher end of the parameter range (0 – 3). High values of this parameter imply that there is more flow to the lower groundwater box (Steele-Dunne *et al.,* 2008).

	FC	LP	BETA	PERC	UZL	K0	K1	K2	MAXBAS
Mean	97.532	0.967	1.256	2.201	63.049	0.251	0.176	0.0561	2.81
Median	98.456	0.973	1.217	2.22	64.65	0.238	0.174	0.0549	2.807
Max	139.38	0.999	1.801	2.996	99.969	0.498	0.253	0.096	3.674
Min	56.878	0.854	1.002	1.054	0.752	0.05	0.114	0.026	2.034

Table 6.4 Mean, median, maximum and minimum values for the process parameters

6.5   Comparison of the models during calibration

 shows the maximum, mean and minimum NS values of the behavioural calibration parameter sets of HYSIM and HBV-Light. HYSIM performs better than HBV-Light during calibration. However, the NS values of both models are within a comparable range.

Calibration NS Values			
	Maximum	Mean	Minimum
HYSIM	0.769	0.755	0.750
HBV-Light	0.711	0.702	0.700

Table 6.5 Maximum, mean and minimum NS values for both models during calibration

6.5.1   Other evaluation metrics used in calibration

Measuring the performance of a model against one evaluation metric can give misleading results about the ability of the model to simulate observed flow (Dawson *et al.,* 2007). Therefore, other evaluation metrics were chosen in order to test the robustness of model skill during calibration. Firstly, two time series were created which consisted of the median daily values from the 500 behavioural parameter iterations derived from the calibration of both HYSIM and HBV-Light. The Hydrotest website (www.hydrotest.org.uk) has 20 different evaluation metrics for measuring model performance against observed flow. Evaluation metrics of absolute error and relative error were included as absolute error metrics do not necessarily give an indication of the importance of a model error (Dawson *et al.,* 2007). The metrics chosen were Mean Actual Error (MAE), Root Mean Square Error (RMSE), Percent Bias (PBIAS) and the Coefficient of Determination (R^2).   A brief description of each evaluation measurement follows.

$$\left(\frac{\sum_{i=1}^{n}(O_i - \overline{O})(P_i - \overline{P})}{\sqrt{\sum_{i=1}^{n}(O - \overline{O})^2}\sqrt{\sum_{i=1}^{n}(P - \overline{P})^2}} \right)^2$$

The coefficient of determination (R^2) is given by the above equation, where *O* are observed and *P* are predicted values. This coefficient describes the proportion of the variance in the observed time series that can be explained by the model. R^2 is limited as an evaluation measurement as only linear relationships between the variables of the modelled and observed flow are evaluated.   Furthermore, correlation measures are more sensitive to outliers than to observed variations which lie near the mean (Legates and Davis, 1997; Dawson *et al.,* 2007).

$$\text{MAE} = \frac{1}{n}\sum_{n=1}^{n} |Q_i - \hat{Q}_i|$$

Mean actual error (MAE) records in real units the overall level of agreement between observed (Q_i) and simulated $(\hat{Q}_i)$ flow. It is a non-negative metric which is unbounded and a perfect simulation would be zero. All deviations from the observed values are evaluated equally, so this metric is not biased towards high or low flows. The MAE score is dependent on the length of the time series.

$$\text{RMSE} = \sqrt{\frac{\sum_{i=1}^{n} (Q_i - \hat{Q}_i)^2}{n}}$$

Root mean square error (RMSE) is a non-negative evaluation measurement which has no upper bounds and a perfect score is zero. In RMSE, Q_i is the observed value and $\hat{Q}_i$ is the simulated value. Because it is computed using squared differences it is biased towards higher flows, like the NS criterion of efficiency. The RMSE score is also dependent on the length of the time series.

$$\text{PBIAS} = \frac{\sum_{n=1}^{n} (Q_i - \hat{Q}_i)}{\sum_{n=1}^{n} Q_i}$$

Percent bias (PBIAS) records the level of overall agreement between observed and simulated flow as a ratio. This evaluation measure is unbounded and a perfect score is zero. Like RMSE the score is dependent on the length of the data series. Studies using PBIAS as an evaluation measurement include Yu and Yang (2000) and Murphy (2006). PBIAS is a relative measure of the overall water balance of a model. However, a low score does not necessarily indicate a behavioural model, as positive and negative errors can cancel each other out (Dawson *et al.,* 2007). Table 6.6 shows the value of the different metrics for the median value time series from the behavioural iterations of both models.

Calibration 1963/01/01 - 1990/12/31				
	MAE	RMSE	PBIAS	R^2
HYSIM	12.672	19.481	-0.006	0.752
HBV-Light	14.106	21.091	0.1984	0.776

Table 6.6 Scores for the different evaluation metrics for HYSIM and HBV-Light

While noting that the median time series values are biased towards NS as it was the only evaluation measurement employed for calibration, the evaluation metric values in Table 6.6 nevertheless gives an indication of the performance of both models with regard to other evaluation measures. Again, HYSIM scores better. Nonetheless, both models' scores are within a small range.

6.5.2 Comparison of the Models' Simulations in a single Year

The year with the highest flow volume within the calibration time series (1982) was selected in order to examine the performance of each model against the observed flow record (see Figure 6.3).
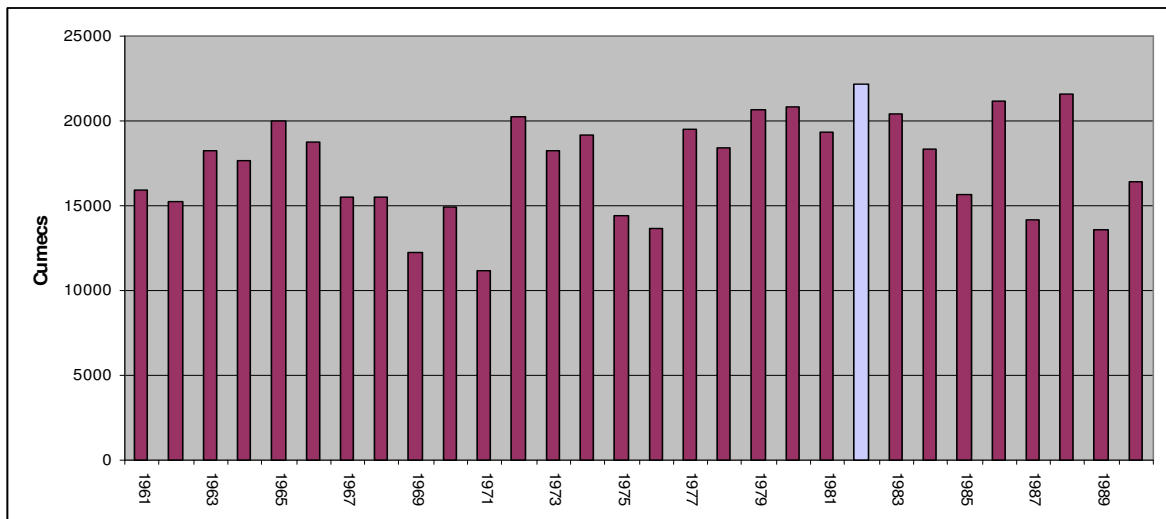
Figure 6.3 Yearly flow volume during the calibration period

The NS values were computed for each model's behavioural iterations for 1982. HYSIM had a NS range over the 500 parameter sets from 0.683 – 0.705. This is considerably lower than the range for the calibration time series (0.75 – 0.769). HBV-Light had lower NS values over its parameter sets of 0.588 - 0.627. These values would not have been

acceptable as calibration NS scores. Thus, behavioural parameter sets are not always transferable within sub-periods of the calibration time series (Wilby, 2005).

The behavioural parameter sets for both models were then analysed along with observed flow (see Figure 6.4 and Figure 6.5). A visual inspection shows that HYSIM tends to over-predict low flows while HBV-Light tends to under-predict. It is notable too that HYSIM displays a narrower range of uncertainty for autumn and winter flows compared to HBV-Light. Furthermore, HYSIM over-predicts the highest yearly flow compared to HBV-Light.
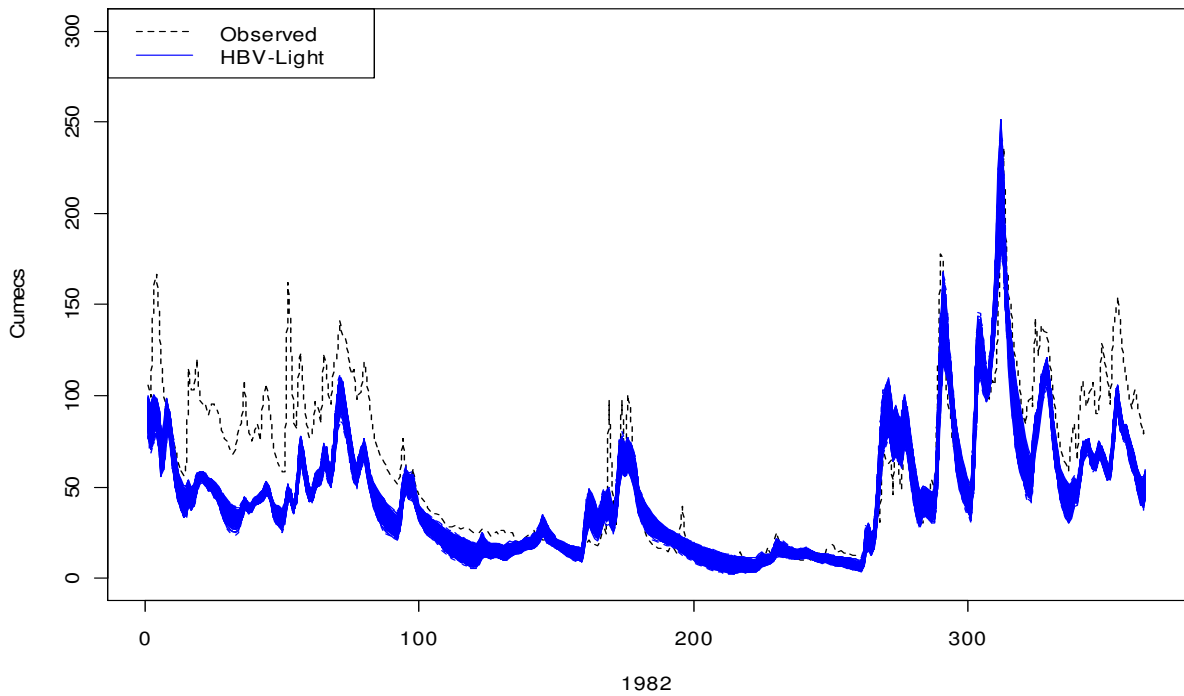
Figure 6.4 HBV-Light behavioural iterations for 1982 plotted against observed flow
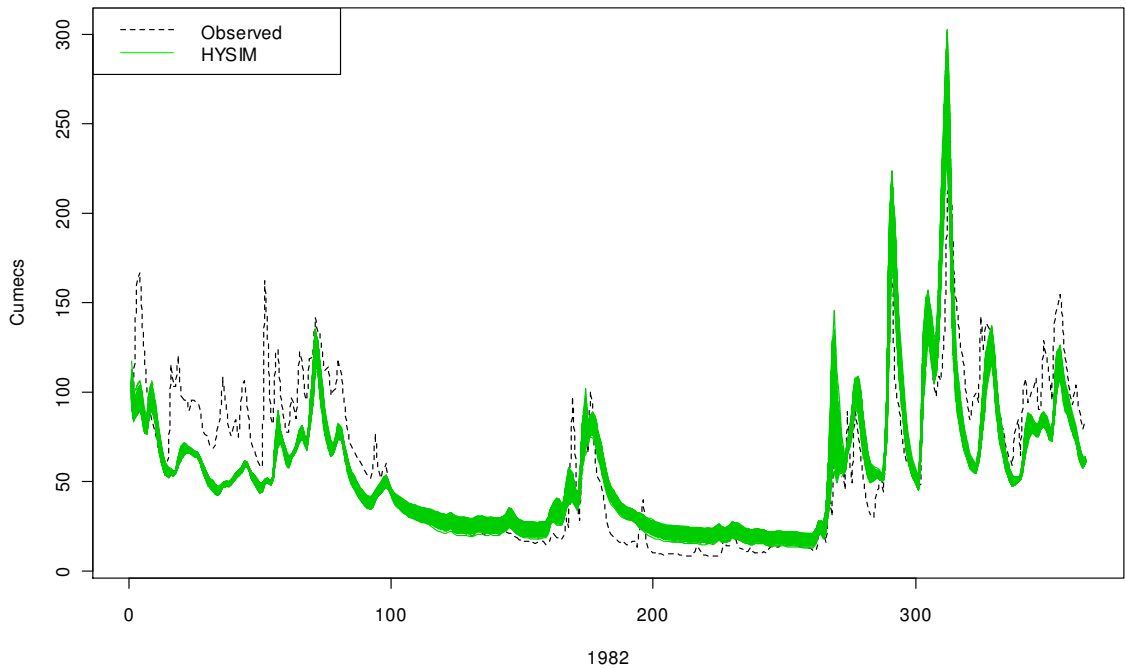
Figure 6.5 HYSIM behavioural iterations for 1982 plotted against observed flow

6.6   Validation of the Rainfall-Runoff Models

It is good modelling practice to evaluate the chosen parameter sets as good representations of catchment behaviour using an independent validation time period. The period from 1st January 1991 to 31st May 1991 was chosen as a spin-up period and then the 500 behavioural parameter iterations from both models were evaluated against observed flow from 1st June 1991 until 31st December 2000 using NS. The robustness of the models can also be measured by the increase or decrease in average performance over the validation period (Perrin *et al.,* 2001).

Validation NS Values			
	Maximum	Mean	Minimum
HYSIM	0.785	0.767	0.760
HBV-Light	0.750	0.742	0.734

Table 6.7 Maximum, mean and minimum NS values for the validation period

Table 6.7 shows the maximum, mean and minimum NS values for the validation period. Both models display higher NS values during this time period in contrast to the calibration

period, which may be due to the shorter time period employed. However, it is also an indication of the robustness of both models as reliable simulators of catchment behaviour (Perrin *et al,* 2001). The other evaluation metrics employed for the calibration period were also computed for the validation period, using the modelled time series from the parameter sets with the median NS score (see Table 6.8).

Validation 1991/06/01 - 2000/12/31				
	MAE	RMSE	PBIAS	R^2
HYSIM	12.371	20.278	-0.016	0.78
HBV-Light	14.377	21.7	0.185	0.805

Table 6.8 Values for MAE, RMSE, PBIAS and R2 for the validation period

Again, as the parameter sets were chosen as behavioural using only NS, this will bias the scores of the other evaluation metrics. What is notable here is that although HYSIM has better scores over MAE, RMSE and PBIAS, HBV-Light scores higher on R^2. Thus, although HYSIM's evaluation scores are generally better for the evaluation metrics chosen, both models' scores are again within a comparable range.

6.6.1 Comparison of model skill in three different years of the validation period

The three years with the highest flow volume in the validation period (1993, 1994, and 1996) were chosen in order to test the skill of both models in simulating observed flow (see Figure 6.6). Each of the behavioural parameter sets were plotted against the observed flow series (Figure 6.7, Figure 6.8 and Figure 6.9). HYSIM exhibits similar behaviour to its performance in the wettest year of the calibration time period (1982). It over-predicts both low flow and the hydrograph peaks in comparison to HBV-Light.

The uncertainty range of the behavioural parameter sets is also narrower in the autumn/winter period in HYSIM. The NS values were also computed for each of the behavioural parameter sets for three years. Although NS is biased towards higher flows, there is considerable flow variability even within wet years. Wider difference in skill measures in 1993 (0.757 -0.808 for HYSIM; 0.642 – 0.707 for HBV-Light) may be reflective of the fact that HYSIM simulates the winter flood peaks better than HBV-Light (Figure 6.7).
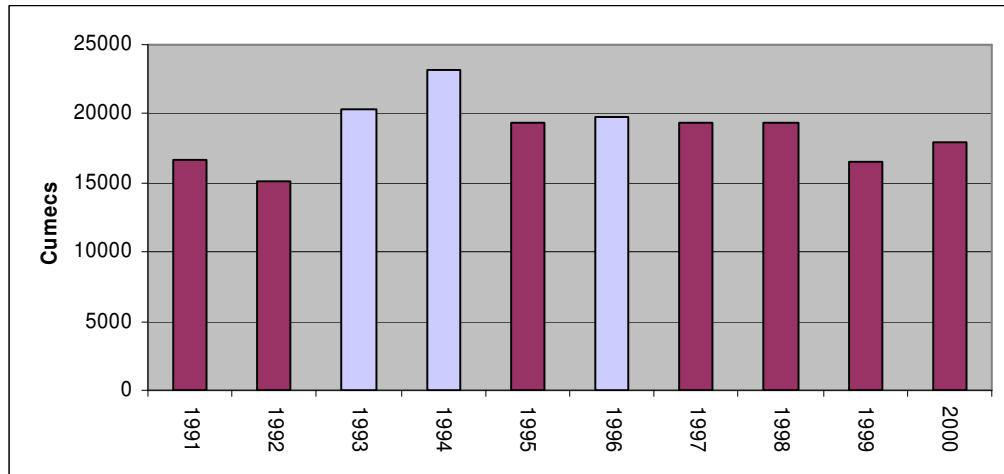
Figure 6.6 Yearly flow volume during the validation period. Years with highest flow volume (1993, 1994 and 1996) are highlighted

Both models have lower scores in 1994, possibly because the flood peaks in the first three months of the year are not well simulated by either model (although again HYSIM scores better than HBV-Light) (Table 6.10). However, the highest NS scores are exhibited in 1996, with HBV-Light showing higher skill than HYSIM. Visual inspections of the diagrams show that both models simulate the flood peaks particularly well (Figure 6.9). These different ranges for NS again show that the behavioural parameter sets from the calibration period are not necessarily transferable within shorter periods of either the calibration or validation time series (Wilby, 2005).

NS Value Range		Maximum	Minimum
1993	HYSIM	0.808	0.757
	HBV-Light	0.707	0.642
1994	HYSIM	0.701	0.643
	HBV-Light	0.679	0.62
1996	HYSIM	0.831	0.797
	HBV-Light	0.846	0.828

Table 6.9 NS Values for the three highest flow years in the validation period
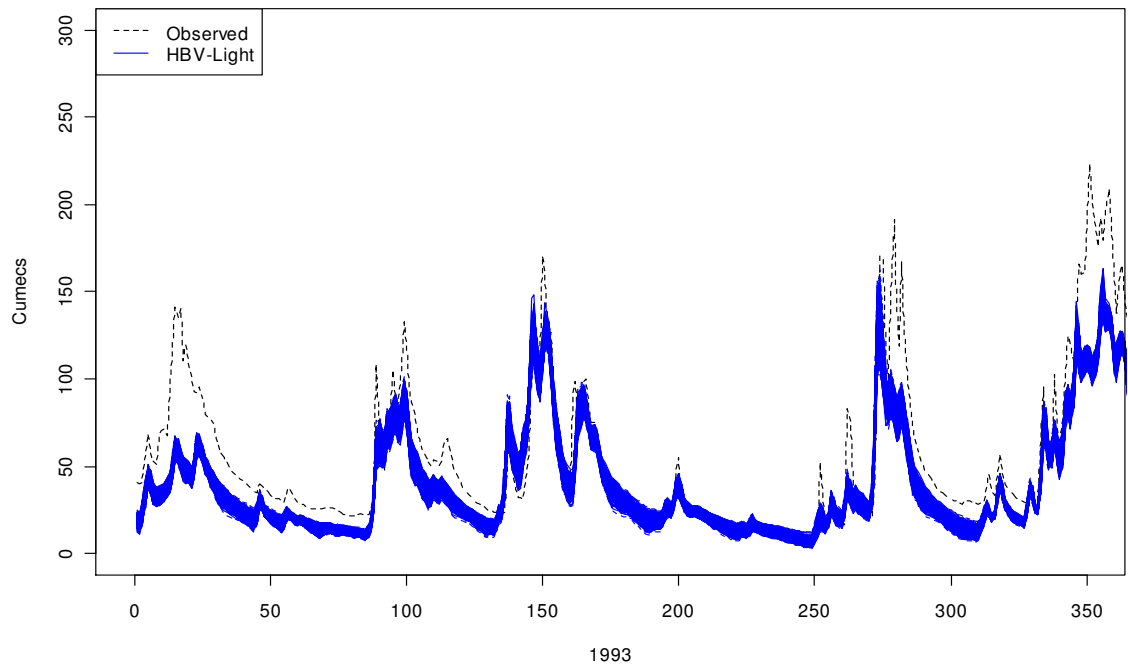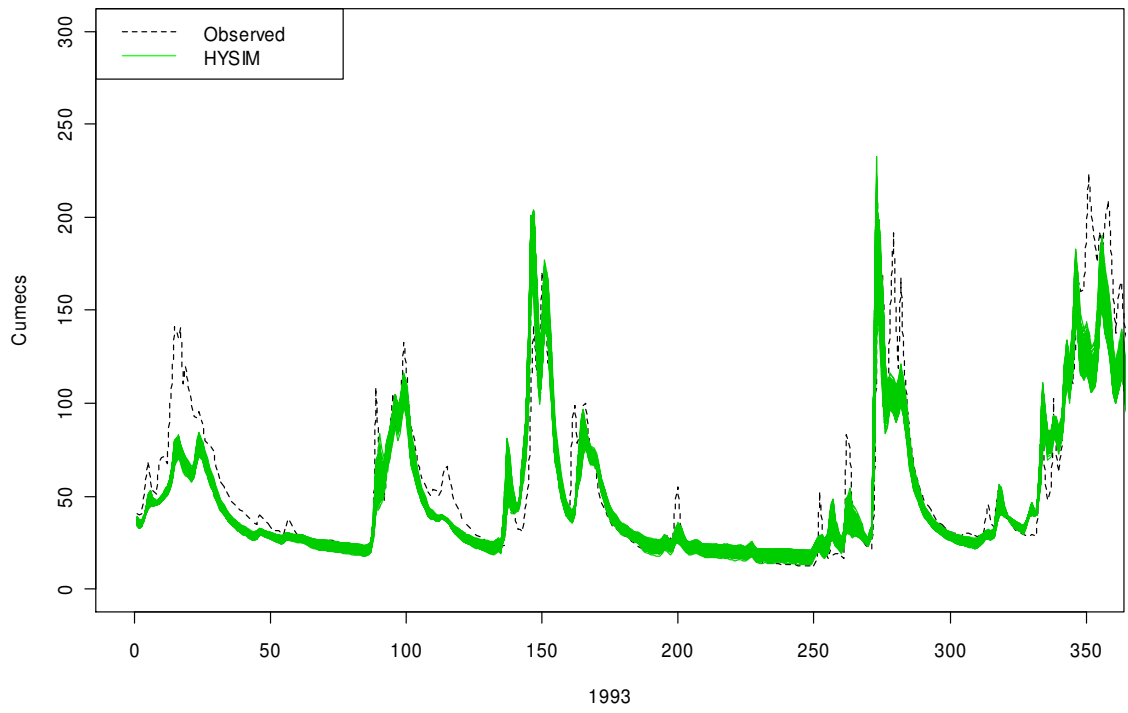
Figure 6.7 500 behavioural parameter iterations for HYSIM and HBV-Light for 1993 plotted against observed flow

98
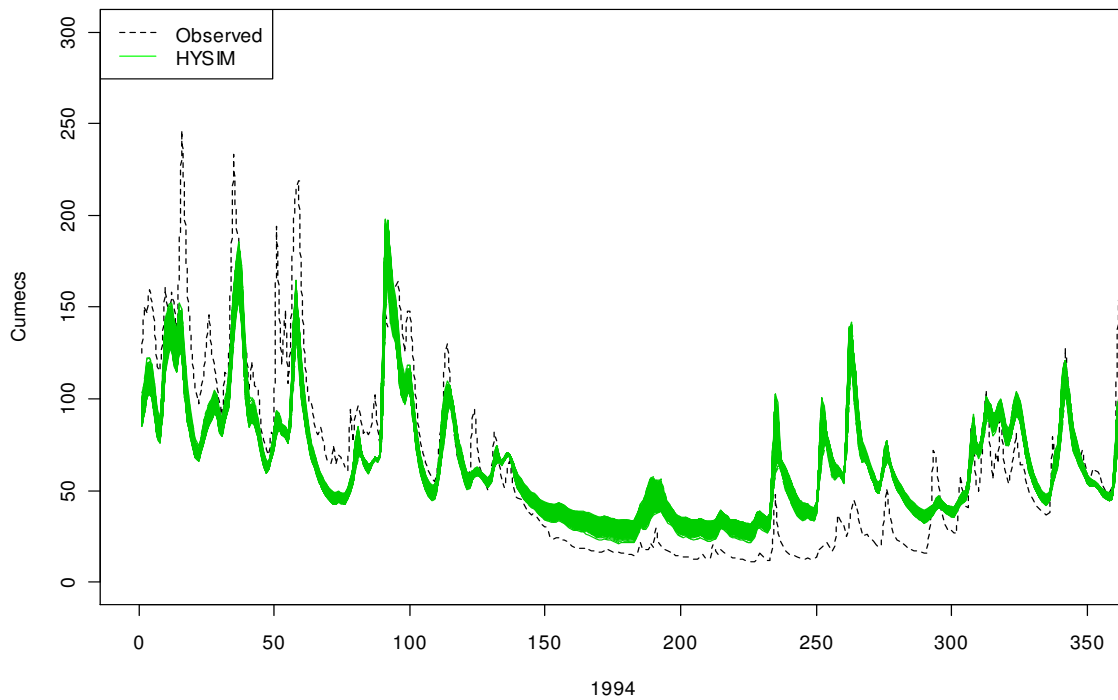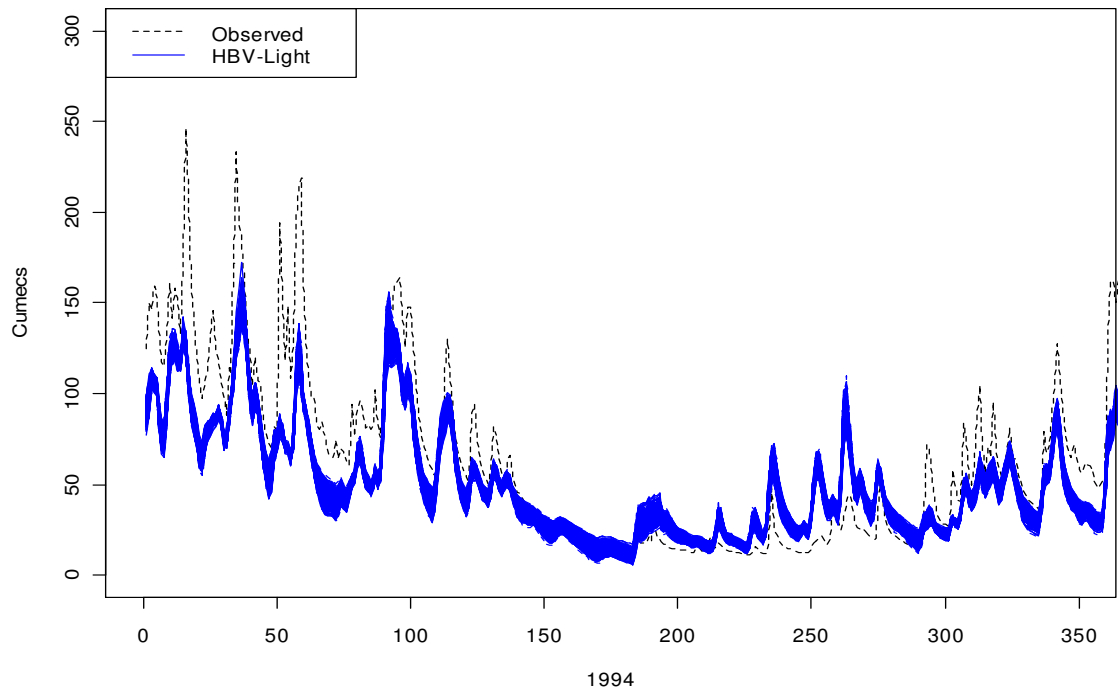
Figure 6.8 500 behavioural parameter iterations for HYSIM and HBV-Light for 1994 plotted against observed flow
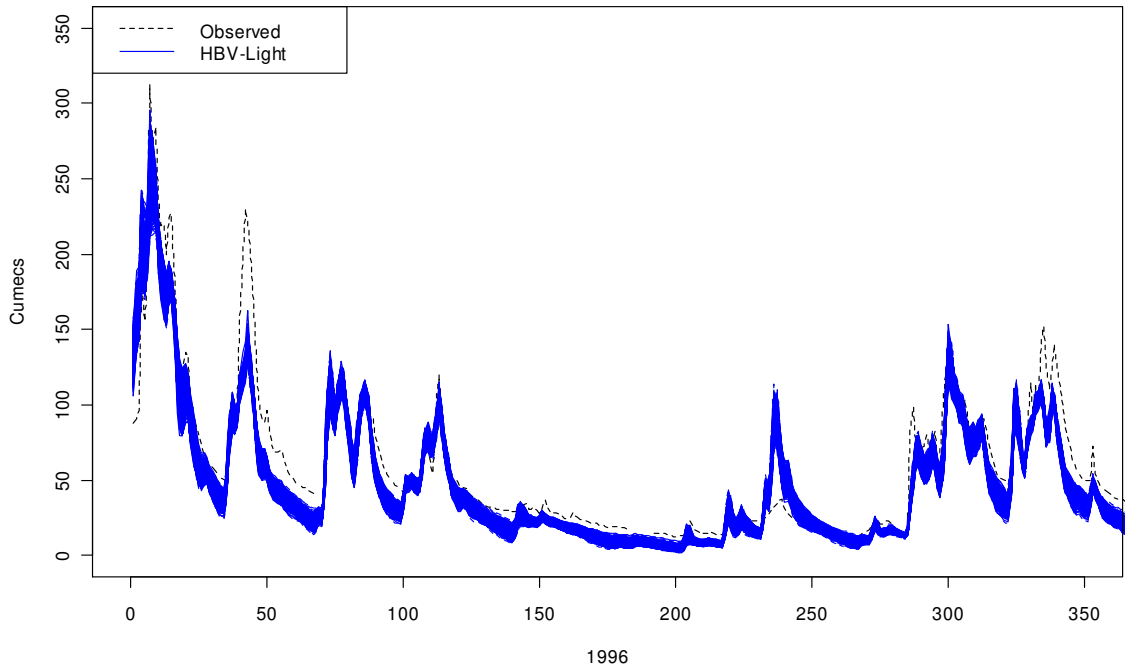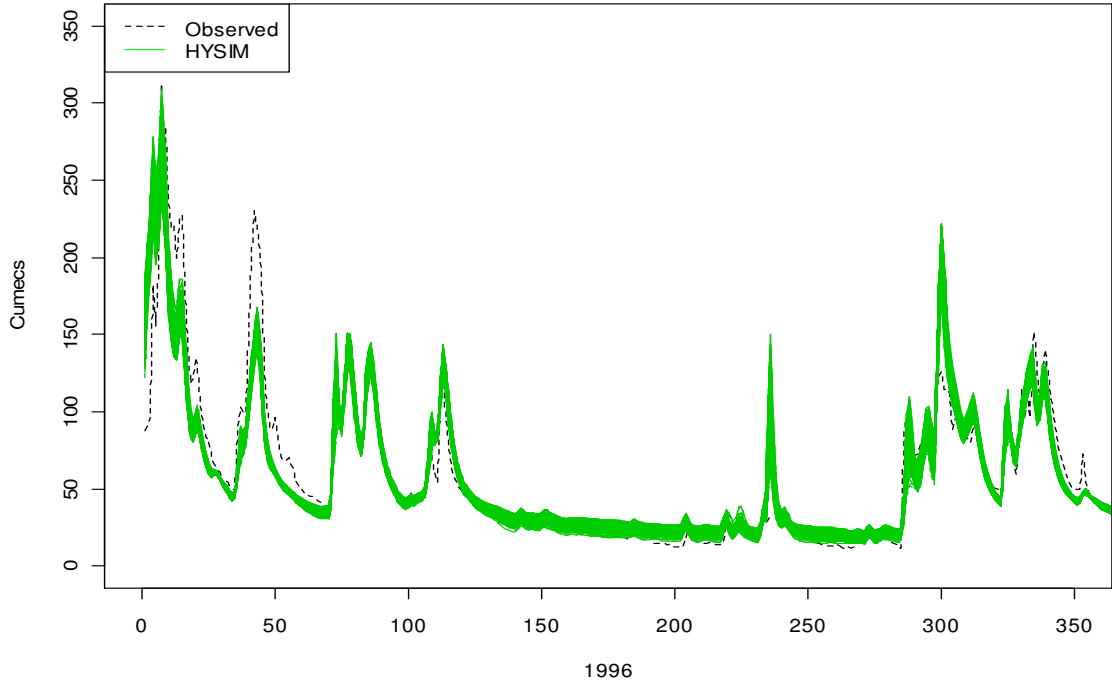
Figure 6.9 500 behavioural parameter iterations for HYSIM and HBV-Light for 1996 plotted against observed flow

6.7   Simulation of annual maximum flow for the validation period
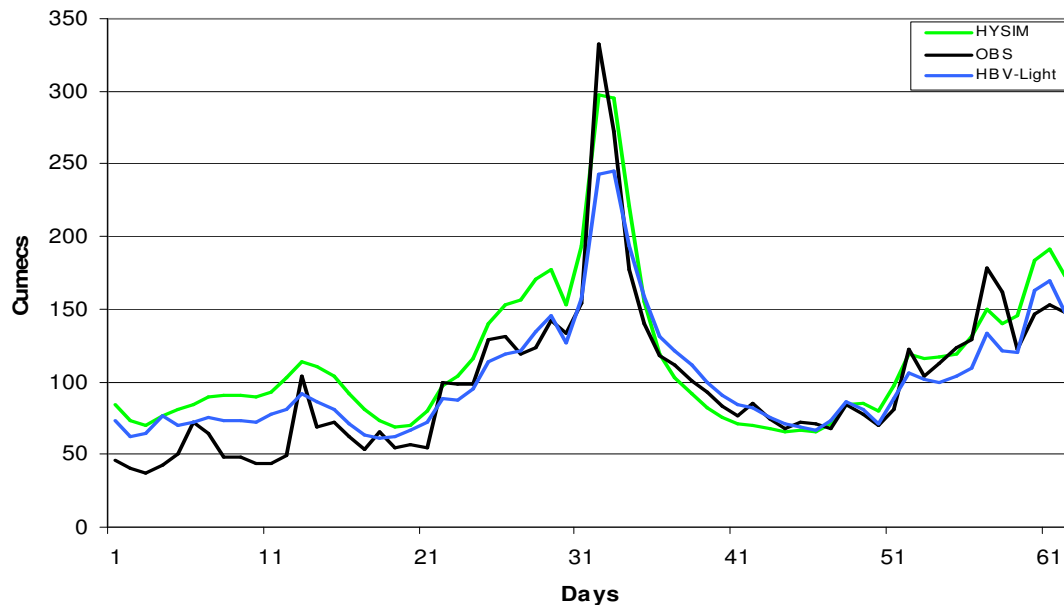
Figure 6.10 Models' simulations of the highest flow event in 2000

This project will analyse changes to flood magnitude/frequency relationships within the Suir catchment due to climate change. Therefore, the maximum observed flow from each year in the validation time period was selected and the models' skill at simulating the yearly highest flow event was measured using different evaluation metrics. NS and RMSE were omitted from this exercise as these metrics are more suitable for the evaluation of continuous hydrographs. Another metric, peak difference (PDIFF) was included.

$$\textbf{PDIFF} = \textbf{max}\,(Q_i)\; \textbf{-}\; \textbf{max}\,(\hat{Q}_i)$$

This is a signed metric with no upper limit and for a perfect model the score would be zero. It records in actual units how the highest simulated value in the modelled data set matches the recorded value in the observed set. As a signed metric it is positive if the model under-estimates observed flow and negative if the model over-estimates observed flow. PDIFF is particularly suitable for single flow events (Dawson *et al.,* 2007).

The observed daily flow data from the two months on either side of the flow event was selected in order to generate reasonable values for the different metrics. This was compared to the corresponding time series of median parameter values for both HYSIM

and HBV-Light. Scatter plots were created of the year 2000 flow event using the observed flow as the independent variable (x) and the modelled flow as the dependent variable (y) with the intersect line shown on each graph (see Figure 6.11). The maximum flow event for the year 2000 was also the highest flow event for the 40 year time period from 1961 to 2000.
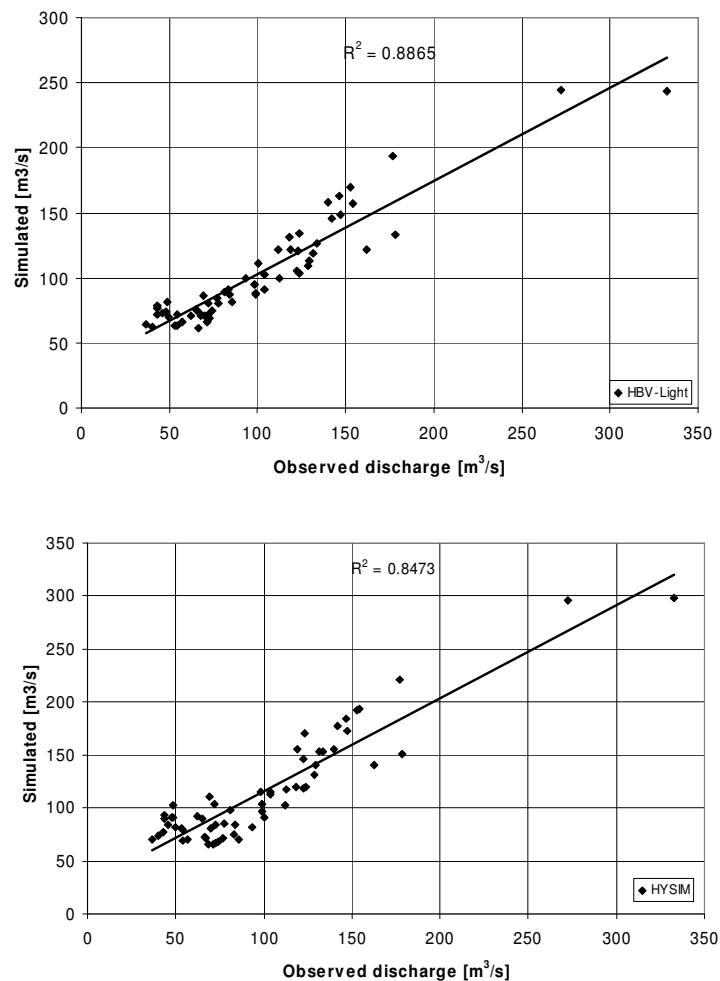
Figure 6.11 Scatter plots showing R2 values for the highest flow event in 2000

Table 6.10 below details the results for the different metrics chosen to evaluate the annual maximum flood events for each year of the validation period. The figures highlighted in grey are the best scores for the given metric in a particular year. There are only two years when one model consistently scores better than the other; 1994 (HYSIM) and 1998 (HBV-Light). The models' scores for PDIFF and MAE vary more than for PBIAS and R^2, where they are within comparable ranges. Otherwise it is difficult to evaluate from the scores

102

which model is better at simulating these events, as there is no discernable pattern in the performance of the models.   HYSIM has 70% of the top scores for PDIFF, and 60% of the top scores in MAE. However, both models have an equal amount of highest scores for PBIAS and HBV-Light has 60% of the top scores according to the R^2 metric.   Although HYSIM does score higher according to two of the evaluation measurements no model is a clear "winner" in terms of the metrics chosen and both models' scores are again within comparable ranges.

Year	Date Max Flow	Model	Evaluation Metric			
			PDIFF	MAE	PBIAS	R2
1991	25/11/1991	HYSIM	43.22	16.29	-0.118	0.56
		HBV-Light	52.12	17.14	-0.101	0.544
1992	13/09/1992	HYSIM	-30.88	6.6	-0.041	0.8974
		HBV-Light	7.01	7.12	-0.105	0.888
1993	17/12/1993	HYSIM	56.73	24.10	0.089	0.781
		HBV-Light	83.14	29.67	0.219	0.841
1994	16/01/1994	HYSIM	56.73	26.68	0.173	0.651
		HBV-Light	74.01	34.88	0.238	0.612
1995	03/11/1995	HYSIM	157.5	25.77	0.221	0.819
		HBV-Light	170.4	33.31	0.303	0.826
1996	07/01/1996	HYSIM	4.54	25.27	-0.092	0.742
		HBV-Light	17.3	16.70	-0.089	0.858
1997	06/08/1997	HYSIM	-3.52	11.15	-0.219	0.863
		HBV-Light	41.44	10.39	-0.117	0.9
1998	30/12/1998	HYSIM	-83.4	22.33	-0.219	0.863
		HBV-Light	-28.46	16.66	-0.117	0.9
1999	26/12/1999	HYSIM	-71.13	12.55	-0.075	0.893
		HBV-Light	-25.84	13.07	0.105	0.851
2000	06/11/2000	HYSIM	34.74	-15.62	-0.157	0.847
		HBV-Light	87.72	-2.759	-0.028	0.886

Table 6.10 The values of the different evaluation metrics for single-event analysis in the validation period

6.8   Conclusion

Both HYSIM and HBV-Light were calibrated and validated taking into account equifinality of parameter sets and models by employing the GLUE methodology. Monte Carlo random sampling was used to generate random parameter sets and the NS dimensionless criterion of efficiency was used as the likelihood measure in GLUE. However, while 10,000 Monte

Carlo runs produced over 500 behavioural parameter sets in HYSIM, 500,000 Monte Carlo runs were required to produce a similar amount of behavioural sets in HBV-Light. Both models proved robust simulators of catchment behaviour through their improved performance during the validation period (Perrin *et al.,* 2001). While HYSIM had higher NS scores for both the calibration and validation periods, the scores of both models were within a comparative range. This finding was strengthened when the models' skill was tested against other evaluation metrics. HBV-light had slightly lower NS scores than HYSIM when the model simulations were compared to observed flow for one year of the calibration period and also had lower scores for two of the three years selected in the validation period. However, in the simulation of single peak flow events in the validation period, neither model consistently scored higher than the other on the evaluation metrics employed. Both models had comparable scores. Thus, both models simulated observed flow robustly and with in a comparable range (according to the evaluation metrics chosen) in both the calibration and validation periods. This finding will be taken into consideration in chapter 7, when the models' performances will be compared when evaluating how much uncertainty is due to model structural error, in comparison to GCM uncertainty and scenario uncertainty.

Chapter 7 – Future Simulations of Catchment Hydrology

7.1   Introduction

In chapter 3 there was an overview of the statistically downscaled data employed in this project. After successfully calibrating and validating HYSIM and HBV in chapter 6, this chapter will focus on future simulations of catchment hydrology. The results presented are based on the output of three GCMs (HadCM3, CCCM and CSIRO) and two emissions scenarios (A2 and B2). The model output will also be evaluated over two future time slices; 2040 to 2069 (2050s) and 2070 to 2099 (2080s). The impact of GCM uncertainty and scenario uncertainty will be analysed by employing the highest-scoring behavioural parameter set from the validation period. Model structural uncertainty will be evaluated by employing 500 iterations arising from the behavioural parameter sets identified in validation and the six combinations of GCMs and emissions scenarios. The amount of uncertainty derived from GCM, emission scenario and model structure will be compared over the two future time periods for both models so that the contribution of each to impact uncertainty can be analysed.

7.2   Modelling of the Future Flow Simulations

Both HYSIM and HBV-Light were forced with the statistically downscaled future data. PE and precipitation from the control period (1961 to 1990) and the six future scenarios (HADCM3 A2; HADCM3 B2; CCCM A2; CCCM B2; CSIRO A2 and CSIRO B2) together with the 500 behavioural parameter sets from validation were used as input to HYSIM. This resulted in 500 one hundred and thirty year time series of streamflow for each different scenario which were then split into the control time period time slice and two different 30-year future time slices; 2040 to 2069 (2050s) and 2070 to 2099 (2080s). Thus, for each future time slice a total of 3,000 different model runs were produced (500 runs x 6 scenarios). The same methodology was used to force HBV-Light with the future data using temperature, PE and precipitation from the statistically downscaled data as input to the model. All data output from HBV-Light is produced in runoff (mm/km^2 of the catchment area). This was converted to cumecs (m^3/sec) using the R Statistical Programme (2010) in

order to standardise the values with the simulations from HYSIM. The formula used was $n*2173000000/86400/1000$ (n*Catchment area in metres/number of seconds per day/1000). The daily mean flow regime for the Suir catchment was calculated using the observed streamflow data for the baseline period. This was compared to the daily mean flows for the control simulations in order to detect biases in the flow regime due to the GCM and hydrological model employed. The graphs below (Figure 7.1) compare the observed daily mean flow to the control daily mean flow for HADCM3, CCCM and CSIRO using the validation parameter set with the highest NS value in both models.
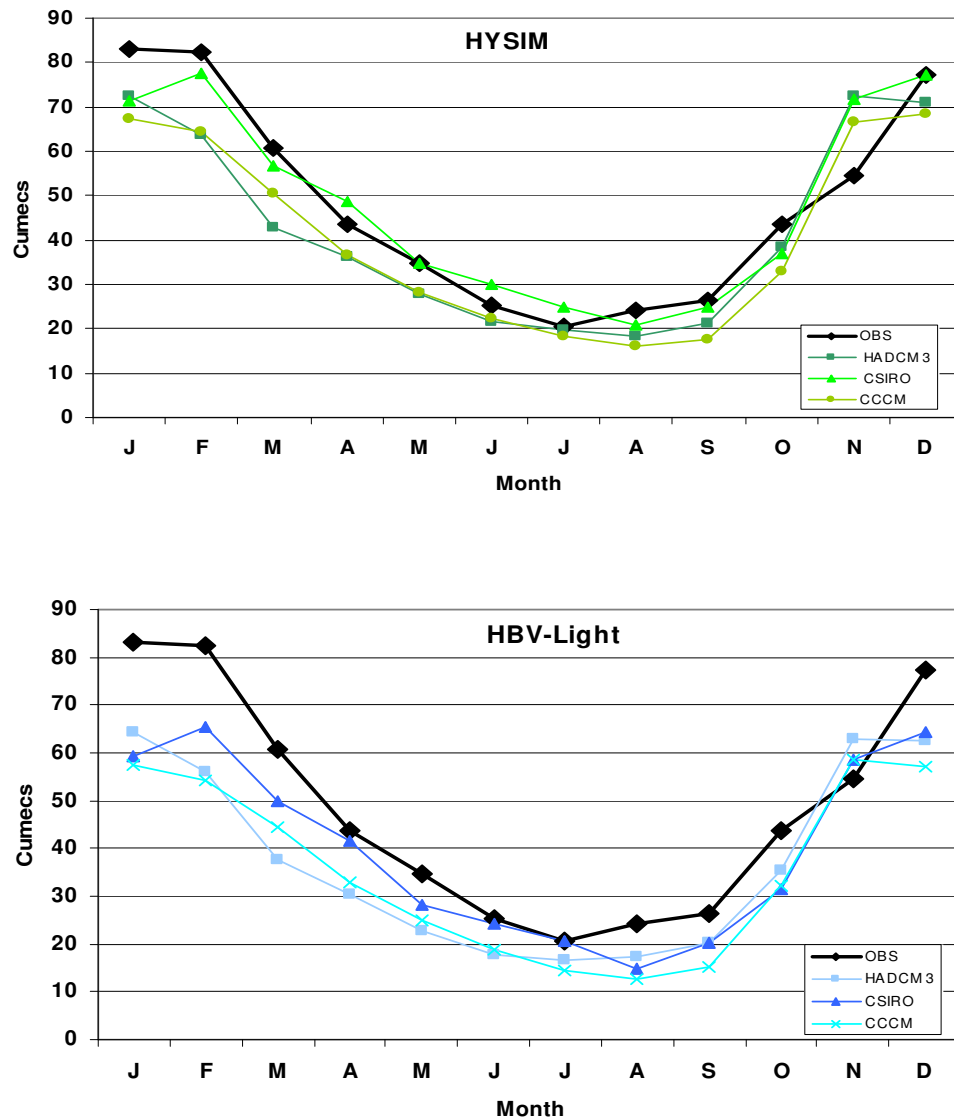
Figure 7.1 Observed daily mean flow compared with control values for the three GCMs

In the HYSIM simulations, CSIRO has the wettest flow regime, and there are slightly higher values for April, June and July than in the observed flow regime. Particularly noteworthy are the simulated values for November, where all GCMs record higher flows than the observed, up to 133% of observed flow in the case of HADCM3. The reverse is the case regarding January values, where all GCMs record lower flow than the observed mean flow value, with CCCM recording 80% of observed flow values. CCCM has the driest flow regime of the control GCM simulations in HYSIM.

Overall, HBV-Light underestimates winter flow and simulates a drier yearly flow regime for all GCMs. Particularly low values are simulated in winter (DJF) compared to the observed monthly mean flow. Simulated values for December range from 73 – 83% of observed daily mean flow, compared with 68% - 77% in January and 66% to 78% in February. Only in November do simulated values exceed observed ones. The highest November value (HADCM3) is 115% of observed flow, which is significantly lower than corresponding value simulated by HYSIM. Both models simulate a greater inter-GCM value range in February, March and April with smaller ranges for the rest of the year. Furthermore, in both models, CCCM has the driest flow regime and CSIRO the wettest.

7.3   Uncertainty in Future Streamflow due to different GCMs

Uncertainty in future simulations of streamflow derived from the different GCMs employed in the project was evaluated by using the highest scoring validation parameter sets (according to NS) in both HYSIM and HBV-Light and analysing the output of the A2 scenario for each GCM for the 2050s and 2080s.

7.3.1   Uncertainty in Streamflow in the 2050s

What is most notable on a visual inspection of the graphs is that the percentage change in monthly streamflow is more extreme for HBV-Light than for HYSIM with a more pronounced direction of change (see Figure 7.2). The ranges of uncertainty for each month are also greater in HBV-Light. For the 2050s in January, HBV-Light models an increase of up to 40% in monthly streamflow with CSIRO A2. This compares to a 20% increase for CSIRO A2 in HYSIM. This may be due to the more complex soil moisture routine in HYSIM and the fact that the model includes a parameter for capillary suction (bubbling pressure), thus preserving more moisture in the soil layers even during dewatering of the

soil. The soil moisture routine in HBV-Light is much simpler when it is run in fully-lumped mode, and the response of the routine may be
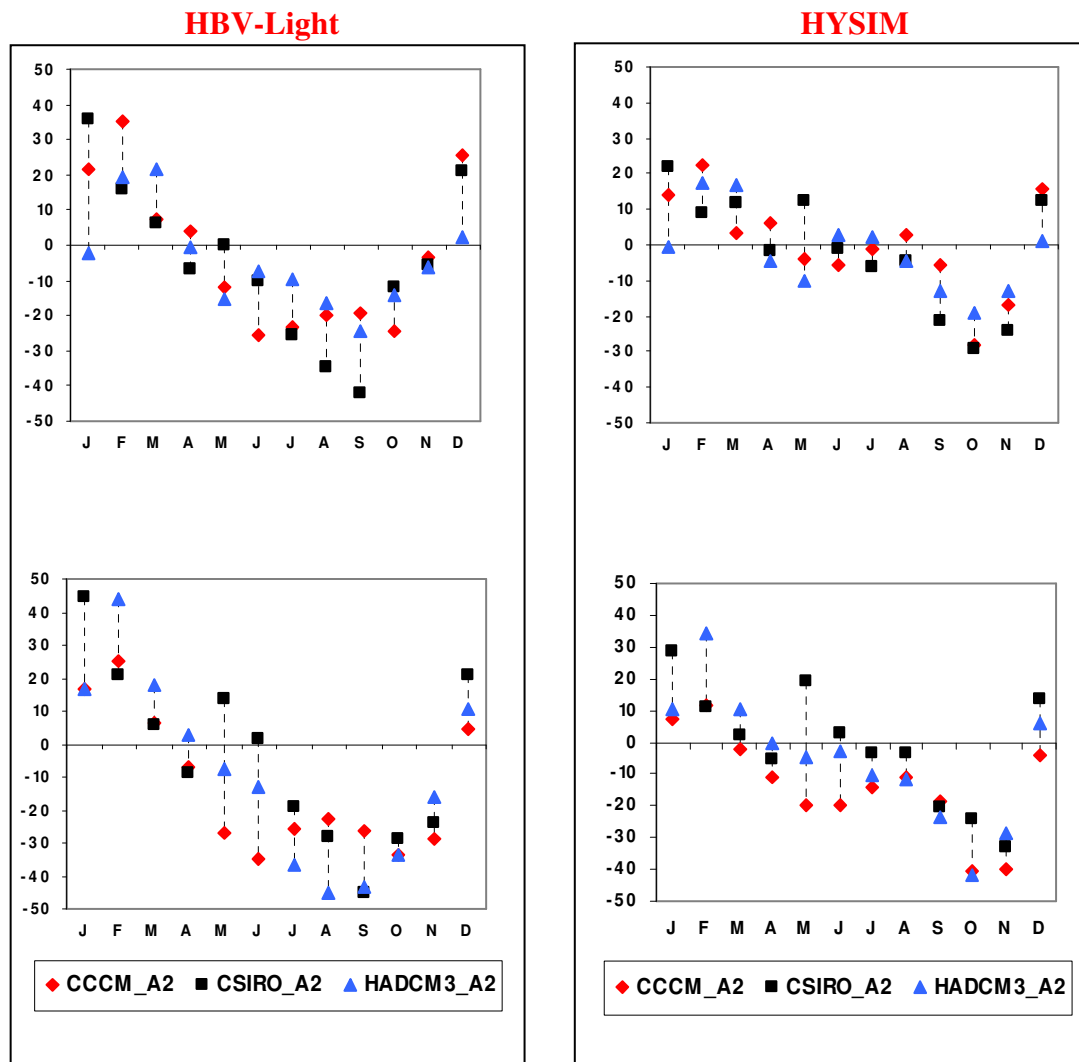
Figure 7.2 Uncertainty in streamflow due to choice of GCM for the 2050s (top) and the 2080s (bottom) using the best validation parameter set in both models

too abrupt once storage is filled to FC, as any excess moisture will be routed to the runoff response routine to become simulated streamflow (Bergström, 1976). In contrast, HYSIM has three stores in its soil moisture routine with the soil parameters being some of the most important in the model. Bubbling pressure, in particular, simulates capillary suction as the soil is being dewatered and more moisture will be held in the soil layers. Nevertheless, both models proved robust simulators of observed flow during validation and both

therefore are equally plausible for employment as impact models in modelling future streamflow.

In both models in the 2050s, the direction of the uncertainty is not clear in January, where HADCM3 simulates very little change in streamflow. The output of both models shows an increase in streamflow in both February and March, however the change is more conservative in HYSIM (up to 22% (Feb) and 16% (Mar)) in contrast to a 35% and 21% maximum difference for the same months in HYB-Light. In HYSIM the direction of GCM uncertainty is unclear for the rest of the spring months (April, May) and for the summer months. Indeed, for the summer months in the 2050s, GCM uncertainty is very small and does not vary much from the control period values ranging from -5% to 2.7% (June), minus 6% to 2% (Jull) and -4% to 2.7% in August. In contrast, the range of uncertainty for the summer months is greater in HBV-Light and the direction of change is more definite with considerable reduction in daily streamflow compared to the control period. The ranges are -7% to -25% (June); -9 to -25% (July); -16% to -35% difference in streamflow by August.

HBV-Light records the biggest percentage change in monthly streamflow in September of the 2050s, where streamflow is only 58% of the control period value according to CSIRO A2. Notably, CSIRO A2 modelled the largest percentage decrease in summer and autumn precipitation in the 2050s (Figure 7.2). HADCM3 A2 and CCCM A2 have more conservative figures modelling 76% and 81% of control period values. Such a difference in streamflow could potentially have large consequences for water abstraction activities in the Suir and for fluvial ecology, if realised. Conversely, the largest reduction in streamflow in HYSIM occurs in October and November, with a 28% reduction in October (CSIRO A2) and a slight recovery in streamflow in November to -24% of control values. HBV-Light has November streamflow values much nearer the control ones (-6% to -3%). As A2 has medium-high emissions and is therefore a dry scenario, this is reflected in the output of the models. Under such a scenario, more precipitation will be required by the autumn wetting-up period in order to replenish drier soils and hence groundwater and streamflow (Wilby, 2005). However, there is a lack of agreement in the models as to which month has the greatest reduction in streamflow. Reasons for this may be the different soil moisture routines of the models. The key point is that is the structure of the rainfall-runoff models that determines the range of uncertainty.

7.3.2   Uncertainty in Streamflow in the 2080s

By the 2080s, the output of both models shows more pronounced trends in autumn and winter streamflow with greater increases and reductions than in the 2050s. The output of HBV-Light is again more extreme than that of HYSIM.   In December, HBV-Light models an increase in streamflow ranging from 4% to 20%. In HYSIM the direction of change is less certain, with streamflow changes between -3% and 13%.   The largest increase in December flow in both models is from CSIRO A2. There are increases in streamflow in January ranging from 16% to 44% in HBV-Light where CSIRO records the greatest increase and a similar increase in February, although inter-GCM uncertainty is smaller with 20% - 44% difference and CCCM A2 showing the greatest increase in this month.   There is a similar pattern in HYSIM although increases are on a more conservative scale of 7% to 28% increase in January.   In HYSIM the largest increase in monthly streamflow in the 2080s is in February, with a range between 11% and 34%.

The direction of change in streamflow is more uncertain in the spring months in both models. March streamflow in HYSIM ranges from -2% to 10% increase (HADCM3 A2). April streamflow levels show a reduction across all GCMs in contrast to the 2050s. However, the change is relatively modest in comparison to the control period values and ranges from 0% to 10% (CCCM A2). However, in HYSIM in the 2080s May shows the greatest inter-GCM uncertainty with streamflow change ranging from -19% according to CCCM A2 to 19% increase in streamflow (CSIRO A2) with HADCM3 A2 showing little change in comparison to the control period value. In HBV-Light, percentage change in streamflow in March ranges from 6% to 18% and in April the changes are similar to those in HYSIM varying between -6% and 2%. Like HYSIM, inter-GCM uncertainty is large in May and the direction is also uncertain, ranging between 13% (CSIRO A2) and -26% (CCCM A2).

There is a marked difference between the models in streamflow change for the summer months.   Streamflow changes in HYSIM are closer to the control period values, with differences ranging from -20% to 3% in June, -14% to -3% in July and -12% to -3% in August.   CCCM A2 is the driest GCM and CSIRO A2 the wettest.   In contrast, the reductions in summer streamflow are much greater in HBV-Light. Inter-GCM uncertainty is greatest in June (1% to -34%) with greatest reductions from CCCM A2.   However,

reductions in streamflow are particularly marked in July and August with ranges from -19% to -36% (July) while in August, streamflow is between 55% and 78% (-22% to -45%) of the control period values. It is also notable that the greatest reductions in streamflow in July and August are from HADCM3 A2, reflecting GCM output. Reductions such as these could have serious implications for fluvial ecology.

In HBV-Light, reductions in streamflow are not as great for the remainder of the autumn period as September. October shows a recovery in streamflow with a small inter-GCM range between -33% and -28%. The inter-GCM range in November is greater (-28% to -15%) with CCCM showing the greatest reduction in streamflow. There is a marked reduction in autumn streamflow in HYSIM compared to the 2050s, with a notable agreement between GCMs in September (-18% to -23%). The biggest reductions in monthly streamflow are again recorded in October (similarly to the 2050s) although inter-GCM uncertainty is more marked with reductions ranging from -24% (CSIRO A2) to -42% (HADCM3 A2). This finding concurs with that of Murphy and Charlton (2008) where reductions in monthly streamflow were greatest in October. The reduction in streamflow compared to the control values is almost as great in November, however there is more agreement between GCMs with a range between -40% (CCCM A2) and -28% (HADCM3 A2). In both models December shows a distinct recovery in streamflow.

While there are similarities in the changing patterns of streamflow in the 2080s, HBV-light models more extreme changes in winter and summer streamflow. However, autumn changes in streamflow are more pronounced in HYSIM, as can be seen from Figure 7.3. The reduction in streamflow between August and November is more pronounced than in HBV-Light. This may be due to HYSIM retaining more moisture in the soil stores (i.e., more soil rewetting) before excess moisture can replenish either groundwater or streamflow. Conversely, in the summer months the retention of moisture in the soil stores may keep replenishing groundwater (and streamflow) thus enabling differences in streamflow values to be more conservative than HBV-Light. However, by autumn soil moisture may reach critically low values. The parameter "bubbling pressure" may become more influential in the model and conserve more moisture in the soil stores rather than release moisture to replenish the groundwater store and thus streamflow.
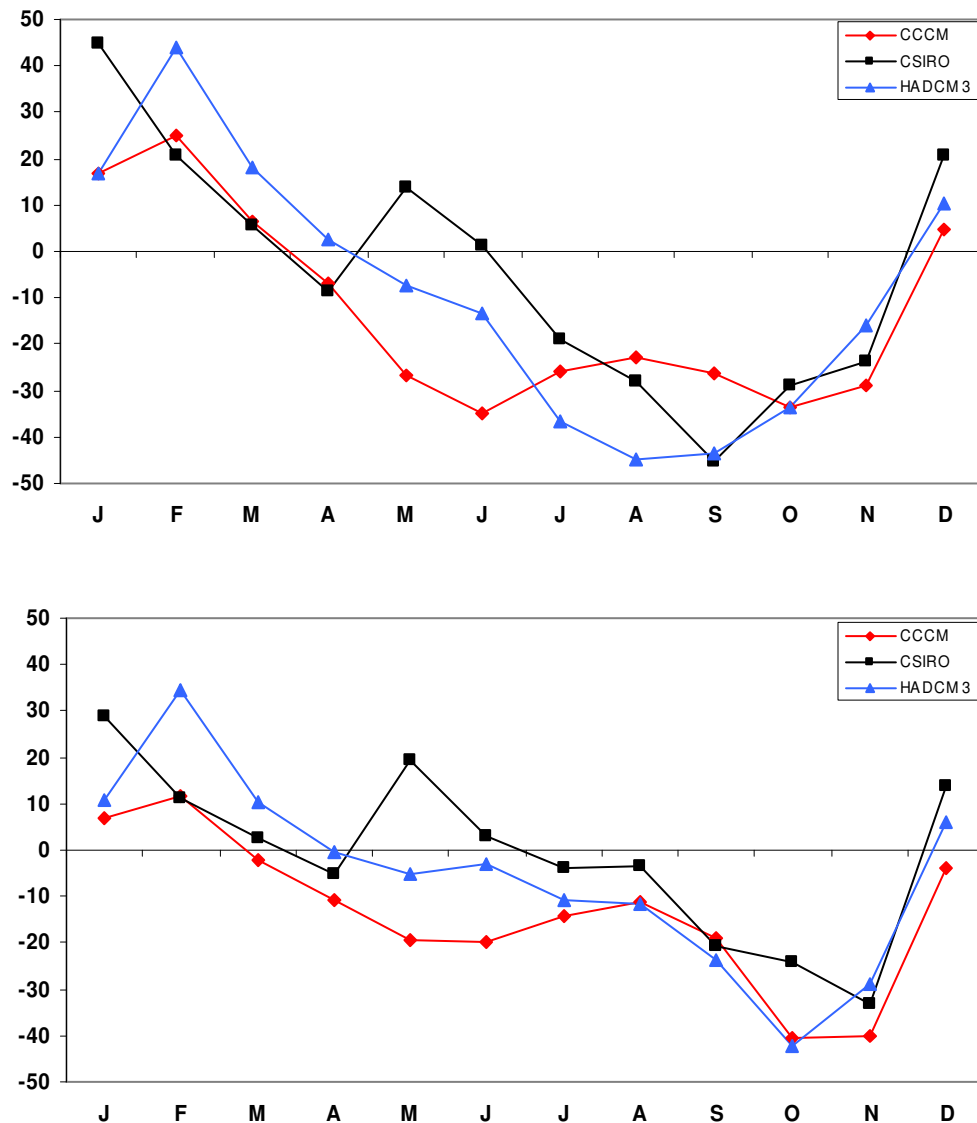
Figure 7.3 Percentage change in streamflow by the 2080s for HBV-Light (top) and HYSIM (bottom) using the A2 emissions scenario and the best validation parameter sets in both models

Conversely, the simpler structure of HBV-Light may be the reason why the model responds quicker to increases or decreases in precipitation. This highlights the importance of taking model structural uncertainty into account and to understand the reasons for differences in model output.

7.4   Uncertainty in Future Streamflow due to different Emissions scenarios

Like GCM uncertainty, uncertainty due to emissions scenarios was evaluated by employing the best validation parameter sets in both HYSIM and HBV-Light and the HADCM3 A2

and B2 scenario. One limitation of this project is that only 2 emissions scenarios are employed; A2 (medium-high) and B2 (medium-low). More extreme scenarios are omitted. However, these scenarios were the ones recommended for use in the IPCC TAR (Nakicenovic *et al.,* 2000). The HADCM3 GCM has been employed for this experiment and the next one because it originates from the Hadley Centre in the UK, where climatological conditions are closer to Irish ones than those of either Australia or Canada (where CSIRO and CCCM GCMs originate). A somewhat counter-intuitive observation is that in the 2050s greater decreases in streamflow are suggested by the B2 scenario (with medium-low emissions and a decreased rise in temperature compared to the A2 scenario with medium-high emissions) for the summer months (JJA) in both models (see Figure 7.4).

Figure 7.4 Uncertainty due to emission scenario for the 2050s (top) and the 2080s (bottom) using the HADCM3 A2 and B2 scenarios and the best validation parameter set in both models

113

This trend continues into the autumn (September, October) however by November the highest increase in streamflow is suggested by the B2 scenario, as would be expected.

For both models in January of the 2050s, the B2 scenario suggests the largest increase in streamflow with very similar ranges between emissions scenarios (1% to 7% in HYSIM; 2% to 8% in HBV-Light). The inter-emission scenario unce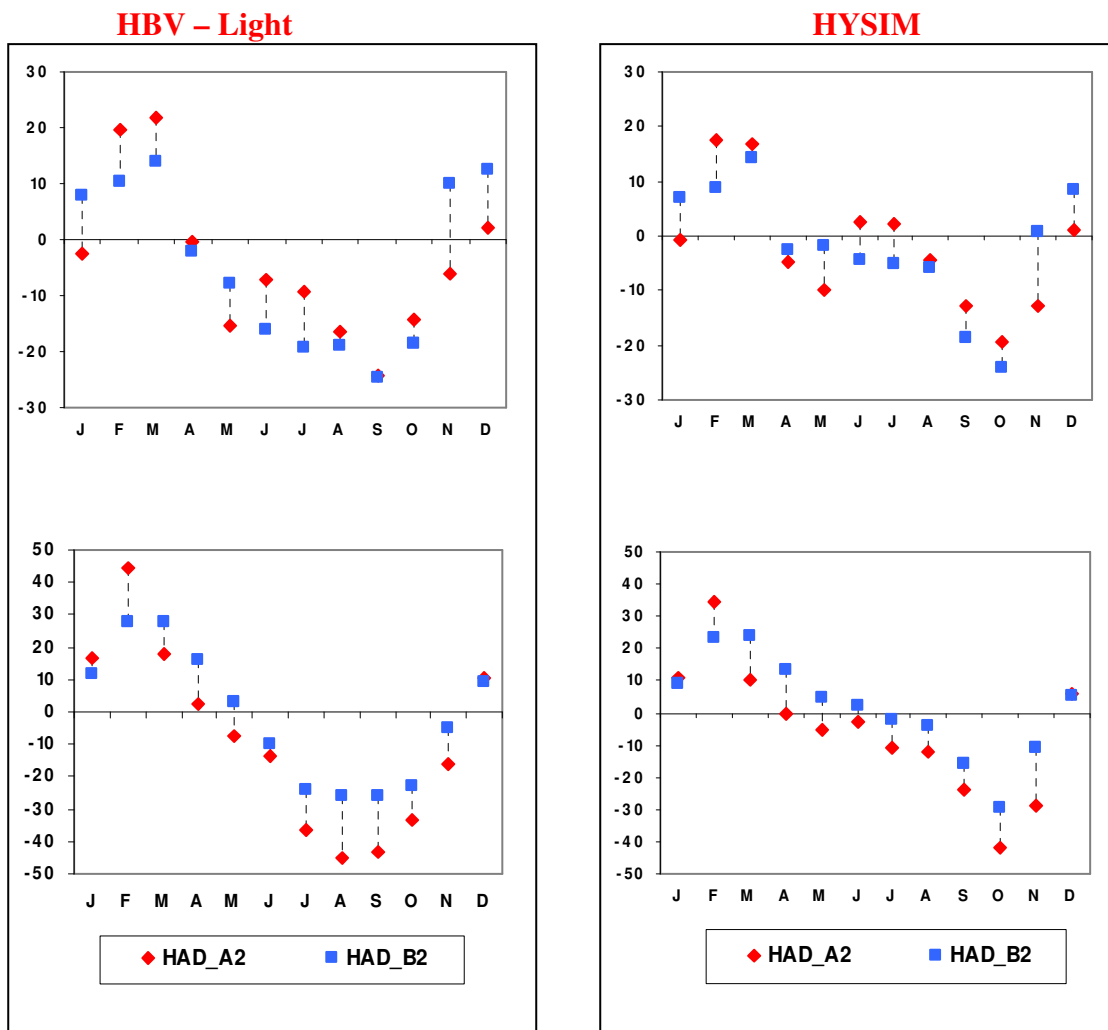rtainty range is greater in HBV-Light than in HYSIM across most months in the 2050s. Decreases in streamflow follow similar patterns to those highlighted in Section 7.3 (uncertainties in streamflow due to choice of GCMs) with HBV-Light streamflow decreasing markedly in the summer season in contrast to HYSIM, where small inter-emission scenario ranges are very close to control period values. In August, there is very little inter-emission scenario uncertainty. However, model structural differences assert themselves with HYSIM suggesting a small reduction in streamflow (-4% to -5%) while there is a reduction in streamflow between -16% and -18% suggested in HBV-Light. Model structural uncertainty also accounts for the large reduction in monthly streamflow (-24%) in September in HBV-Light (where there is notable inter-emission scenario agreement in reductions). In contrast, October is the month with the largest reduction in streamflow in HYSIM. In November, both models show the largest amount of inter-emission scenario uncertainty, however, ranges are different (-12% to 1% in HYSIM; -6% to 10% in HBV-Light).

By the 2080s the emission scenario pattern in both models is more intuitive, with A2 being the driest scenario for most months, apart from January and February. This is again reflective of GCM output. The direction of change is also more extreme than in the 2050s with HBV-Light modelling the largest increase in streamflow in February according to A2 (44% increase). Percentage changes in streamflow in HYSIM are more constrained. Again model structural uncertainty asserts its presence as the output of HBV-Light shows notable reductions in streamflow throughout the summer months and early autumn before a slight recovery by October. These reductions are more extreme than in the 2050s with inter-emission scenario uncertainty also being larger (-24% to 36% in July; -26% to -44% in August; -26% to -43% in September). In contrast, in HYSIM summer streamflow differences are close to control period values until autumn when there is a marked streamflow reduction in September, with the biggest reduction in streamflow again happening in October. However, the inter-emission scenario uncertainty range is not as

great as in HBV-Light with reductions between -15% and -23% in September and -29% and -42% in October.

The reductions in November show similar patterns to the 2050s with HBV-Light suggesting a lower reduction in streamflow compared to control period values (-5% to -16%) than HYSIM (-11% to -29%). There is inter-emission scenario agreement in streamflow changes in December with HBV-Light modelling a 9% to 10% increase in streamflow over control period values compared to 5% to 6% increase in streamflow in HYSIM. In these experiments it is difficult to separate GCM and emission scenario uncertainty from the uncertainty due to model structure and equifinality of parameter sets, as the latter two influence both GCM uncertainty and emission scenario uncertainty, with output of each model showing a distinct pattern that is unique (Butts *et al.,* 2004). For example, in general HBV-Light models more extreme increases and reductions in streamflow over the year than HYSIM. This is a function of the structure and parameters of the model, which interact in a unique way with GCM and emission scenario data input.

7.5   Uncertainty in future streamflow due to Equifinality of Parameter Sets

Uncertainty in future streamflow due equifinality of parameter sets was evaluated by employing the HADCM3 A2 output for the 2050s and 2080s and calculating the maximum, mean and minimum values of the 500 behavioural parameter iterations for each month of the respective time slices. This methodology was used for each model (see Figure 7.5). Model output shows similar patterns to uncertainty due to emission scenario, with some distinct patterns. Once again, HBV-Light models more extreme percentage changes in streamflow over both time slices than does HYSIM. However, generally there are smaller ranges of uncertainty each month due to equifinality of parameter sets than either GCM or emission scenario uncertainty. Indeed, the month with the greatest range of uncertainty in the 2050s according to HBV-Light is May with a difference of 12% (-12% to -24%). In the same time slice, September has the greatest range of inter-parameter uncertainty according to HYSIM (-10% to -19%). This contrasts with the total percentage change in streamflow for some months, (notably February and August in HBV-Light) which by the 2080s is comparable with, or greater than, GCM uncertainty.
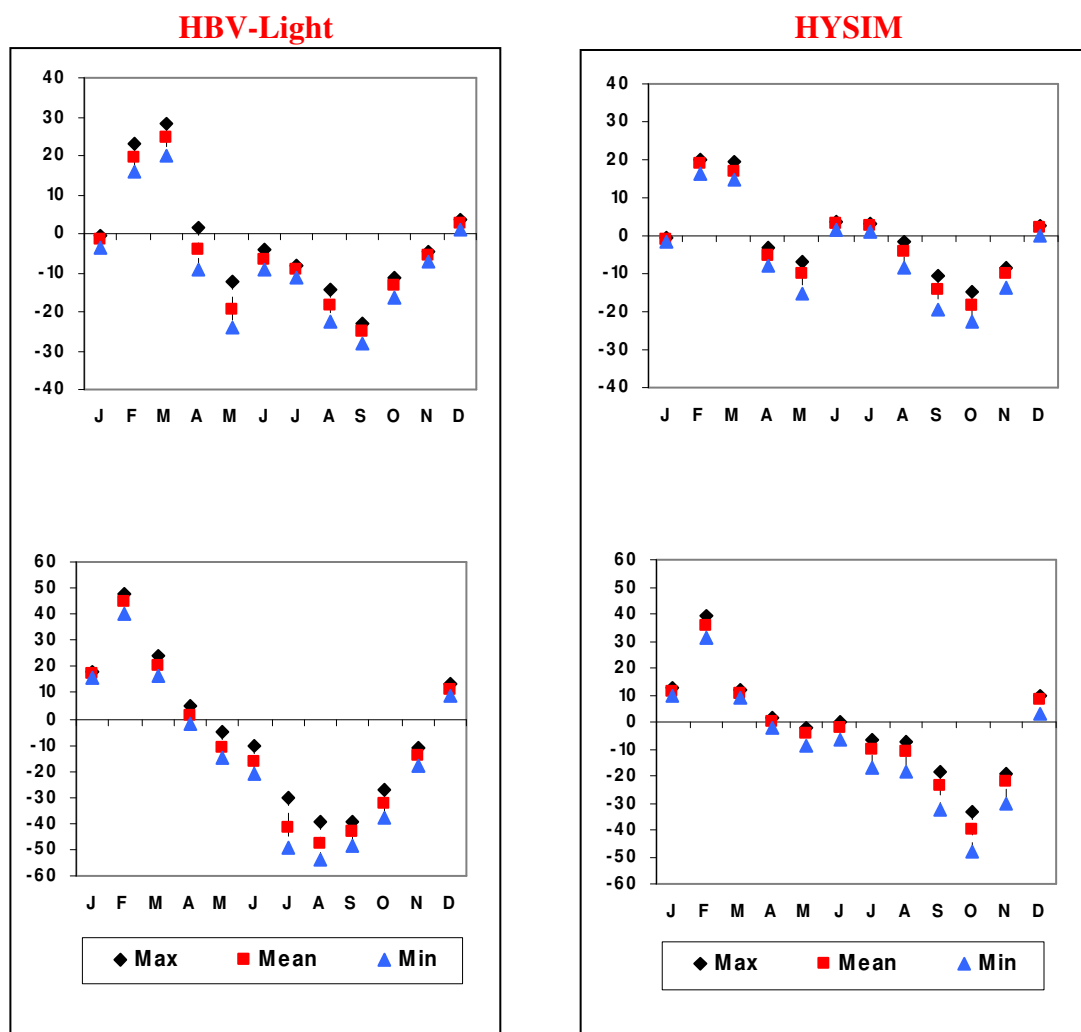
Figure 7.5 Uncertainty due to equifinality of parameter sets for the 2050s (top) and the 2080s (bottom) using the HADCM3 A2 scenario

Both models display similar patterns of change in the 2050s with very little percentage change in streamflow modelled in either January or December. By February and March increases in streamflow are displayed by both models with HBV-Light modelling a greater increase (28% in March) than HYSIM, which displays similar increases for both February and March (20% and 19% respectively). In both models, there is a reduction in streamflow in May, which is more marked in HBV-Light than in HYSIM (a maximum of -24% in HBV-Light; -15% in HYSIM). Model structural uncertainty asserts itself again as reductions in streamflow in June and July are not as marked in HYSIM as in HBV-Light and differ very little from control values. Furthermore, the greatest reductions in streamflow occur in September in HBV-Light (-28%) and October in HYSIM (-22%). Streamflow amounts recover to near control values by December in both models.

116

In the 2080s increases and decreases in streamflow are more marked with the greatest range of uncertainty occurring in the summer in HBV-Light and in the autumn in HYSIM. In both models streamflow increases are greatest in February (maximum of 48% in HBV-Light and 39% in HYSIM). This compares with the increase in February streamflow due to GCM uncertainty (44% for HBV-Light; 35% for HYSIM). This makes the equifinality of parameter sets the source of the most extreme percentage change in monthly streamflow by the 2080s. Once again model structural uncertainty adds a familiar pattern to the monthly differences in mean flow as there are significant reductions in streamflow in July, August and September in HBV-Light (-49%, -54% and -48% respectively). Indeed, the total reduction in August streamflow in the 2080s due to equifinality of parameter sets is greater than the reduction due to GCM uncertainty (-44%) or emission scenario uncertainty (-44%). In contrast, the reduction in streamflow becomes significant in September in HYSIM (-32%) and again the greatest reduction in streamflow happens in October (-48%).

7.6 Uncertainty in future streamflow from GCMs, Emissions scenarios and Equifinality of Parameter Sets and Model Structure

Figure 7.6 below shows the combined uncertainty in future streamflow from all sources (GCMs, emissions scenarios, model structure and equifinality of parameter sets) and both models for the 2050s and 2080s. What is noticeable about the plots is that although the direction of the percentage change increases in the 2080s compared with the 2050s, the median of each box plot lies close to 0% change relative to the control data. In the 2050s only in the winter months does the median percentage difference lie above 10% increase in streamflow. By late summer (August) and the autumn season (September, October) median percentage difference lies between 10% and 20% for streamflow reductions. Although October has the lowest median value of the data, the range of uncertainty is much less than September where the outliers (representing the 5th and 95th percentiles) suggest much greater range in percentage change in streamflow (from 5% to -45% approx.). For the rest of the year namely spring, early summer and late autumn (April, May; June, July and November) median values for percentage change in streamflow lie between 0% and 10%. It can be argued that HBV-Light contributes more to the extremes of the box plots while HYSIM has a constraining effect on the spread of the data in each box plot. It can be also argued that this range is within that of natural climate variability. However, if streamflow in February of a given year in the future time slices was 20% higher than normal (due to

climate variability) and climate change added another 20% increase in streamflow to that total, the consequences in terms of flooding could be very serious.

By the 2080s the value of the median percentage difference has generally become more extreme than the 2050s, although for three months (January, March, May and December) the median has decreased relative to the 2050s, which may reflect the drying projected to occur in the 2080s relative to the 2050s. Only in February and October do the median values exceed the 20% difference in streamflow. The month with the greatest range of uncertainty is May, although its median lies very close to control values. The direction of change is also uncertain for May and June. However, the outliers (representing the 5th and 95th percentile) suggest large ranges of uncertainty (3% to -50% approximately) for August and September. Once again the data is more tightly constrained for October, the month with the greatest median reduction in streamflow, with 90% of the data suggesting reductions between -20% and -40%.
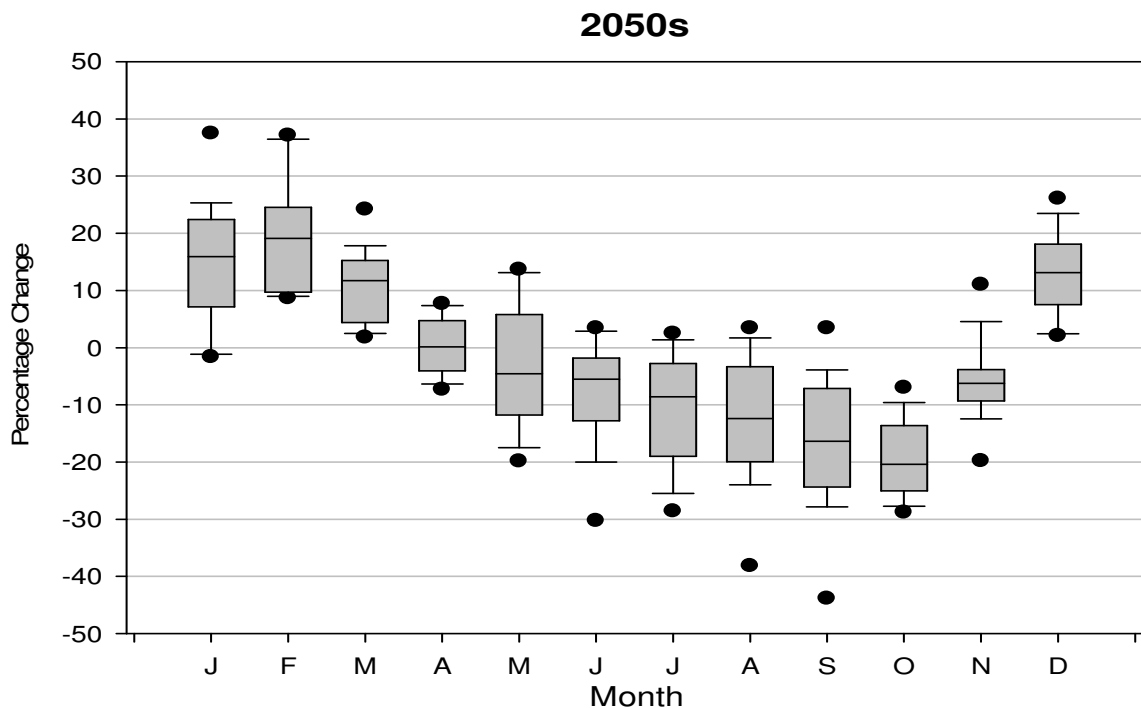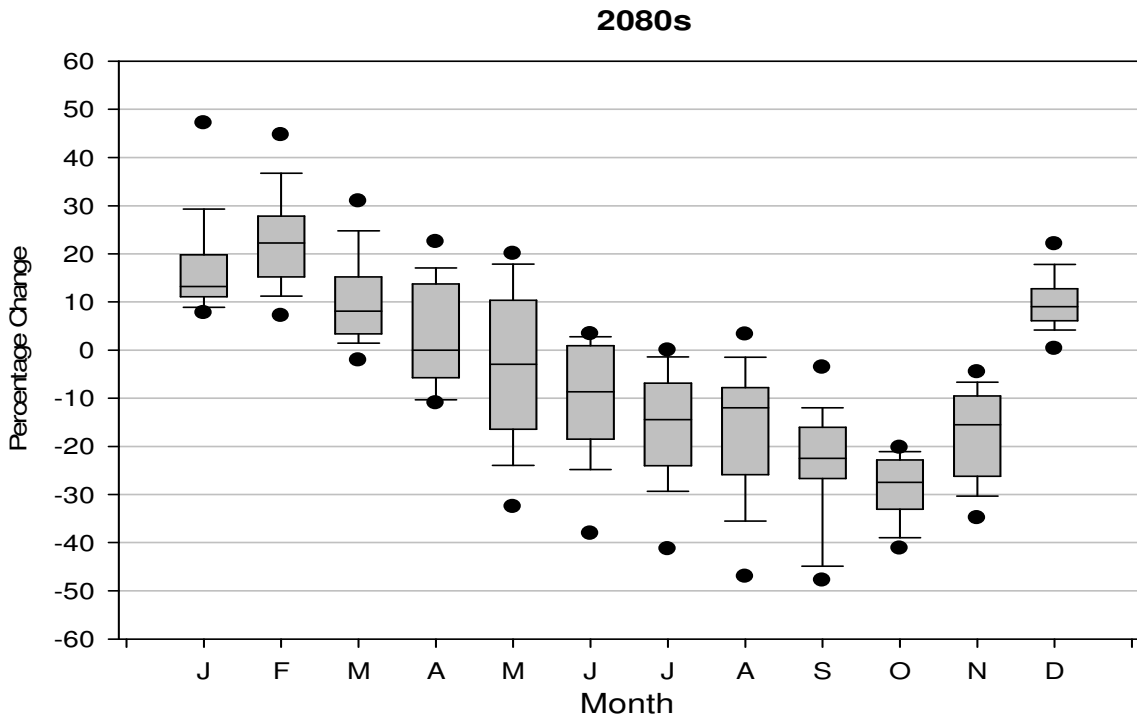
2050s

2080s

Figure 7.6 Combined output of both models, GCMs, emissions scenarios and behavioural parameter sets for the 2050s and 2080s. The outliers represent the 5th and 95th percentiles of the data

Although the main theme of this thesis is an analysis of uncertainty at the local stage of a climate impact assessment, it is pertinent to discuss the possible impact of changes to streamflow detailed in the diagrams above. The outliers representing the extremes of the percentage changes in monthly streamflow suggest a major intensification in streamflow patterns in both time slices. Increases to January and February streamflow range up to ~40% in the 2050s and up to ~50% in the 2080s. Increases this large have worrying implications for Clonmel, a town already prone to flooding. The new flood defences planned for the town will be built withstand a 100-year flood event of 500m^3/sec with an option of protecting against a flood event 20% larger (600m^3/sec) (O'Domhnaill, 2010 personal communication). The data contained above suggest that this is a prudent adaptation decision. Furthermore, it highlights the importance of data measurement and analysis which will be vital to inform adjustments to flood adaptation options in a rapidly changing climate. Modelling may be a useful adjunct to data measurement, but cannot replace it (Silberstein, 2006). The above diagrams also highlight the importance of including all sources of uncertainty in a future analysis of climate change. While it is necessary to perform a sensitivity analysis on individual uncertainty sources, only by

combining all output does one gain a comprehensive understanding of the total uncertainty range, which is important if such analyses inform climate impact adaptation plans or policy frameworks.

7.7 Absolute Changes in Streamflow Discharge

This chapter has focused on percentage changes to monthly streamflow due to different future climate scenarios. However, it is important to reiterate that during the control period HYSIM simulated a wetter flow regime than HBV-Light (see Figure 7.1).
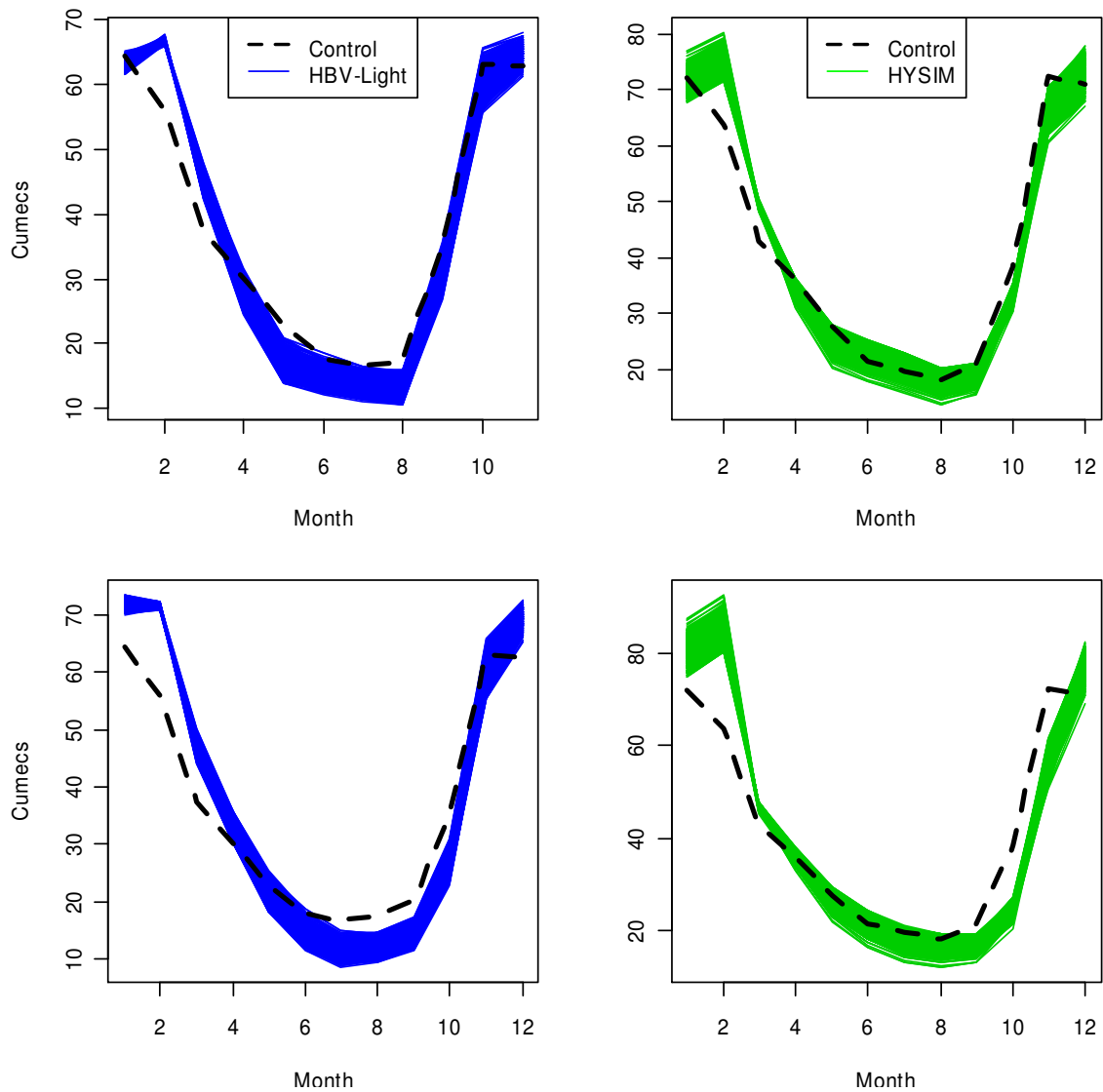

Figure 7.7 Absolute changes in streamflow for the 2050s (top) and the 2080s (bottom) using the HADCM3 A2 scenario

120

This fact is reinforced by the diagram above (Figure 7.7), which details *absolute* changes to streamflow (in m^3/Sec) in the monthly flow regime for 2050s and 2080s for the HADCM3 A2 scenario, employing the 500 validation parameter sets for both models (in the X axis, 2, 4, 6 represent February, April, June etc.). The black dotted line represents the mean value of the control period simulations for HADCM3 A2. By the 2080s, (for HADCM3 A2) HYSIM models a significantly wetter monthly flow regime than HBV-Light, particularly for January and February, which is the main season for flooding in Ireland. This change in streamflow will be further explored in Chapter 8, which will evaluate changes to flood magnitude and frequency due to climate change.

7.8   Conclusions

This chapter has evaluated changes to catchment hydrology due to climate change for two future climate scenarios using the output from three GCMs. Uncertainty due to choice of GCM, emission scenario and equifinality of parameter sets were evaluated separately, with GCM uncertainty being the greatest source of uncertainty in the 2050s and the 2080s, followed by equifinality of parameter sets and finally emission scenario uncertainty. Model structural differences asserted themselves through the distinct pattern of percentage change in monthly streamflow, which is evident in both the 2050s and the 2080s. However, by the 2080s in HBV-Light, uncertainty due to equifinality of parameter sets was responsible for the largest percentage difference in streamflow for February and August (although the range of uncertainty on a monthly basis was greatest due to inter-GCM differences).

The output of HBV-Light shows more extreme percentage changes than HYSIM, which models more conservative percentage differences in streamflow until the autumn period, when there are marked reductions in flow. The differing soil moisture routines in the models (HBV-Light's more simple routine; HYSIM's more complex routine) may account for this distinct pattern. Indeed, some of the reductions in streamflow during the summer and autumn seasons may have major implications for fluvial ecology, if realised. However, when all sources of uncertainty and the output of both models are combined it can be argued that the median percentage changes each month do not differ much from natural climate variability.   In terms of *absolute* changes to the streamflow regime, HYSIM models a wetter regime than HBV-Light (at least for the HADCM3 A2 scenario).

This change to absolute streamflow volume will be the focus of Chapter 8, when possible changes to flood magnitude and frequency will be evaluated.

To date, little research has been conducted in Ireland which examines the effect of local impact model uncertainty in climate impact assessments. Most recent studies have employed either HYSIM (Charlton *et al.,* 2006; Murphy and Charlton, 2008) or the HBV model (e.g., Semmler *et al.*, 2006; Wang *et al.,* 2006; Steele-Dunne *et al.,* 2008) to evaluate possible future changes to both average catchment runoff and extreme flow. Vrugt and Robinson (2007, p.1, italics mine) observe that "…predictive uncertainty analyses are typically carried out using a single conceptual mathematical model of the hydrologic system, *rejecting a priori valid alternative plausible models* and possibly underestimating uncertainty in the model itself". Moreover, in two important reports recently published (Ireland in a Warmer World, Scientific Predictions of the Irish Climate in the 21st Century (C4I) and Climate Change in Ireland; Refining the Impacts for Ireland (EPA)) only one impact model was employed in each report to evaluate changes to hydrology in Ireland due to climate change (HBV-Light in the former; HYSIM in the latter). The output of both models indicated that an increase in seasonality of streamflow will occur under climate change in Ireland.

In the aforementioned studies both HYSIM and the HBV model have proved to be plausible representations of the hydrological behaviour of several important Irish catchments. In these studies equifinality of parameter sets was evaluated and an ensemble of GCMs and emissions scenarios were also included, in order to represent uncertainty stemming for these sources in a more comprehensive way. It can be argued that equifinality of model *structures* is as important a source of uncertainty in a climate impact assessment as equifinality of parameter sets, GCMs or emissions scenarios (e.g., Perrin *et al.,* 2001; Højberg and Refsgaard, 2005; Wilby, 2005). It therefore stands to reason that this source of uncertainty should be included in further climate impact assessment research by employing an ensemble of impact models (e.g., Ajami *et al.,* 2007; Georgakakos *et al.,* 2004; Vrugt and Robinson, 2007).

Chapter 8 – Impact of Climate Change on Flood Magnitude/Frequency

8.1 Introduction

Chapter 7 focused on possible changes to the flow regime of the Suir catchment due to climate change and the uncertainty that arises due to different impact models. In this chapter the focus will shift to the analysis of possible changes to one extreme event in a fluvial regime: flooding. Specifically, possible changes to flood magnitude and frequency will be evaluated in terms of the uncertainty arising from GCMs, emissions scenarios and the impact models. A trend analysis will also be carried out in order to test the data record for trends in the annual maximum series (AMS). One of the underlying assumptions in evaluating possible changes to flood magnitude and frequency is that land use remains constant for the period of analysis and there are no changes to the fluvial system due to human intervention, as these changes may effect flood magnitude and frequency. Changes to fluvial flood magnitude and frequency can have important consequences for human welfare, structural integrity and economic activities around rivers.

There is growing evidence that, due to climate change, the global hydrological cycle is intensifying leading to an increase in extreme hydrological events (Huntington, 2006) and flooding (Milly *et al.,* 2002). Robson (2002) noted that although there were trends in high flows in the last 30 to 50 years in the UK, this could reasonably be attributed to climate variability. Furthermore, there were no appreciable trends detected in longer series of flood data (80 to 120 years). Nevertheless, Kiely (1999), in a study of streamflow in four rivers in Ireland (Boyne, Brosna, Blackwater, Erne) noted that an enhanced cycle of both precipitation and streamflow had occurred from the mid-1970s which was correlated to an increase in the NAOI. Climate variability can have a major influence on streamflow. Moreover, because there is large inter-annual variability of streamflow in Ireland, climate change trends may not be detectable for a number of years. Harrigan (2010) has demonstrated that detection of climate change within Irish streamflow records may not be possible in the first half of the present century. However, a trend that is not yet statistically significant may still have important effects on water resources (Ziegler *et al.,* 2006).

8.2 Trend analysis

8.2.1 Data used in the Trend Analysis

Daily mean flow data from the gauging station at Clonmel (station no.16011) from 1 November 1953 to 27 August 2008 were obtained from the OPW Hydro-Data website. An exploratory data analysis showed that the data from 1954 to 2004 was of acceptable quality for use in constructing the Suir AMS. The importance of good quality data in any modelling exercise cannot be overemphasised. No matter how good a model, it cannot compensate for poor quality input data (Beven, 2000, 2007, 2008; Kundzewicz and Robson, 2004). Indeed, although no dataset is perfect (there may be measurement errors, instrument malfunction, errors in data conversion, typographical errors etc.), it is fair to assume that the errors lie mostly with the model and not with the data (Beven, 2000). In the forthcoming Flood Studies Update report (OPW, 20l0) the gauging station at Clonmel is one of 45 hydrometric stations to be given an A1 (high quality) rating.

8.2.2 Testing for Trends in the Suir Annual Maximum Series

Testing for trend is difficult and often depends on the time series over which the tests are conducted. Furthermore, what appears to be a trend or step jump in a data series may be part of climate variability in a longer record (Robson, 2002). It is important to consider the role of climate variability in causing apparent trend and fluctuations in precipitation and streamflow. Indeed, Kundzewicz and Robson (2004) emphasise that climate variability may cause apparent trend where none exists and therefore a record of at least 50 years is necessary for climate change detection. It is also important to assess any man-made changes within the catchment that may cause fluctuations in streamflow such as arterial drainage, construction of dams, land use change and urbanisation.

In order to derive the AMS the data from 1953 to 2005 were divided into hydrometric years (1 October – 30 September). The AMS was then calculated from the hydrometric years (Figure 8.1). The Peaks-over-threshold (POT) method is another means of evaluating trend. The reasoning behind use of POT is that parameters for extreme value distributions be estimated more accurately and it also gives additional information about the upper tails of the distribution (Katz *et al.,* 2002). However, it is vital to choose a suitable threshold for

estimation of POT. Too low a threshold may include unnecessary data and too high a threshold may omit important values from the calculation. Moreover, autocorrelation and seasonal dependence is often demonstrated between different flood peaks (violating the rule of independence) and techniques such as declustering must be applied (Katz *et al.,* 2002). This project followed the methodology employed in the Flood Estimation Handbook (1999) and used the AMS for trend analysis (Robson and Reed, 1999). A visual inspection of the 50 year AMS time series shows that the 1950s and 1980s were wet decades while the decade from 1970 to 1980 was a drier one.
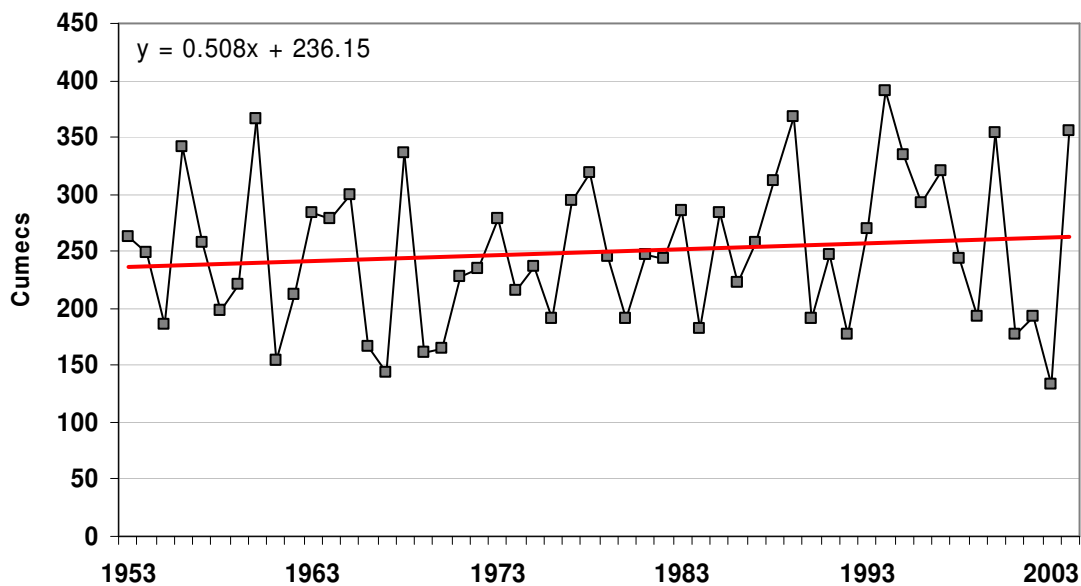
Figure 8.1 Suir AMS from 1953 to 2004

It is important to choose the relevant tests for trend in a hydrological data series and to carry out more than one test (Kundzewicz and Robson, 2004). Hydrological data display non-normality; they tend to be strongly skewed and show dependence. Although linear regression is often used to test for a trend in AMS, it is not a robust test for hydrological data as the underlying assumption is that the data are normally distributed. Parametric tests are generally more powerful than non-parametric tests but they also make an assumption about the characteristics of the underlying distribution such as normality. In distribution free (non-parametric) tests no assumption is made about the shape of the underlying statistical distribution. These tests are more suitable for use with hydrological data.

Resampling methods such as permutation and bootstrapping are also suitable for use with hydrological data, as they make minimal assumptions and are relatively robust (Robson, 2002). These methods involve re-ordering the original time series many times without replacement (permutation) or with replacement (bootstrapping) and testing for trend at each new combination. After many combinations (in this project 1000) the original test statistic is compared to the regenerated test statistic values. If the original test statistic is different to the newly generated values, it is reasonable to assume that the order of the original values was significant and that a trend exists. Permutation is a more powerful test than bootstrapping, but it is also a less flexible test so bootstrapping is often the preferred resampling method.

In testing for trend, it is important to be aware of two confounding errors: either falsely detecting a trend where none exists (Type I), or not detecting a real trend because of stochastic variations (Type II). Type I errors are addressed by pre-defining the confidence level α. In this project α is set at the 0.1, 0.05 and 0.01 levels. The power of the statistical tests, the length of the record and the trend magnitude are some factors that influence Type II errors. In order to carry out the analysis, the Trend software package from the University of Melbourne was employed (Chiew *et al.,* 2005). It provides several tests for use with AMS and includes resampling analysis (bootstrapping) for estimating the significance level. The TREND user manual recommends 1000 resamples for robust significance level testing (Chiew *et al.,* 2005). In this project only tests suitable for detecting a monotonic trend were employed. The Mann-Kendall and Spearman's Rho non-parametric tests from trend have been widely used in hydrological studies (e.g., Wilby, 2006: Yue *et al.,* 2002; Ziegler *et al.,* 2006). Although Linear Regression is not always a suitable test for trend, using 1000 resamples adds to the robustness of the test statistic. The Rank Difference non-parametric test was also included in the trend analysis in order to test for randomness in the AMS data series.

Tests for Trend

Mann-Kendall (non-parametric test for trend)

Spearman's Rho (non-parametric test for trend)

Linear Regression (parametric test for trend)

Tests for Randomness

Rank Difference (non-parametric test for randomness)

The null hypothesis in the trend analysis (H_0) is that there is no trend or change in the mean of the AMS over time. Each test produces results at the 0.1, 0.05 and 0.01 significance levels. Test equations are available in the TREND manual (Chiew *et al.,* 2005). Table 8.1 gives the trend test results. No significant trends were detected in the tests undertaken. However, while there is *no statistically significant* trend, nonetheless a trend is detectable from a visual inspection of the time series and from the test results (e.g., Mann-Kendall positive test value means that there is an increasing trend). Wilby (2006, p.4, italics given) emphasises that "a distinction should be made between *practical* and *statistical* significance of changes". Statistically unimportant trends may still have a major effect on streamflow and, by taking an anticipatory approach to adaptation decisions (rather than waiting for definite proof of the effects of climate change), vulnerable populations can be protected (Ziegler *et al.,* 2006).

Description	Test statistic	Critical values (Statistical table)			Critical values (Resampling)			Result
		$\alpha=0.1$	$\alpha=0.05$	$\alpha=0.01$	$\alpha=0.1$	$\alpha=0.05$	$\alpha=0.01$	
Mann-Kendall	0.892	1.645	1.96	2.576	1.712	2.028	2.683	NS
Spearman's Rho	0.781	1.645	1.96	2.576	1.652	1.964	2.49	NS
Linear regression	0.889	1.68	2.01	2.68	1.755	2.231	2.822	NS
Rank Difference	-0.234	1.645	1.96	2.576	1.677	1.989	2.769	NS

Table 8.1 Trend tests and results

8.3   Changes in the 95th flow percentile

The future data series were analysed in order to evaluate changes in the 95th flow percentile (Q5). The 95th percentile of annual flow is an important statistic in an annual flow series; it represents the flow that is exceeded 5% of the time. Other important percentiles are the 50th (Q50, flow that is exceeded 50% of the time) and the 5th percentile (Q95, the flow that is exceeded 95% of the time). Firstly the data were analysed to detect percentage difference in Q5 flow using flow data from the best validation parameter set for both HBV-Light and HYSIM. The output of all the GCMs and emissions scenarios for the 2050s and the 2080s were compared with the control period using the best validation parameter sets in both

models (see Figure 8.2). What is most notable in Figure 8.2 is the large uncertainty range in percentage change in Q5 flow in HBV-Light (1% to 31.23%) in contrast to HYSIM (-0.32 to 9.23%), where the range is much more constrained.
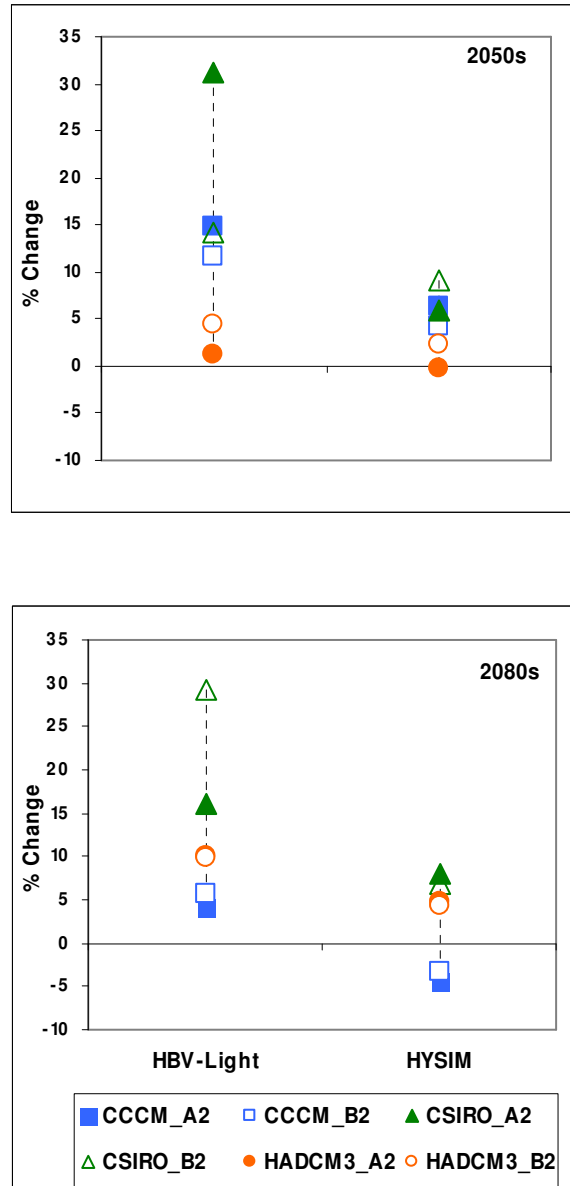

Figure 8.2 Percentage change to Q5 for the 2050s and 2080s for all GCMs and Emissions scenarios using the output of the best validation parameter sets in both HBV-Light and HYSIM

In the 2050s the direction of change in Q5 ranges from 1.23% (HADCM3 A2) to 31.23% (CSIRO A2).   In contrast, percentage change in HYSIM ranges from -0.32% in HADCM3 A2 to 9.23% in CSIRO B2. Furthermore, while there is very little difference in the output of the HADCM3 and CCCM A2 and B2 scenarios in the 2050s (for both models) in HBV-

128

Light the range of difference between output of the CSIRO A2 and B2 scenarios is especially marked, with a 17% difference between the scenarios. In HYSIM the uncertainty range for all GCMs and scenarios is much smaller. This highlights again the unique way in which each model structure interacts with similar input data.

In the 2080s, there is a similar range of uncertainty in percentage changes to Q5 in HYSIM. Nonetheless, the direction of change is more uncertain, with values ranging from -4.41% in CCCM A2 to 6.92% in CSIRO B2. This contrasts markedly with the output of HBV-Light, where the direction of change is more certain with a slightly lower range of uncertainty compared to the 2050s (25.13% difference between CCCM A2 (4.15% change) and CSIRO B2(29.28% change)). Once again, in HBV-Light there is a marked range of uncertainty between the CSIRO A2 and B2 scenarios, although the range is such smaller for the other GCMs. Also in contrast to the 2050s output where HADCM3 A2 and B2 scenarios showed the smallest change in Q5 values (in both models, very similar to control period values) in the 2080s CCCM A2 and B2 scenarios provide the smallest difference in Q5 values.

8.3.1 Changes in the 95th percentile values due to equifinality of parameter sets

In order to evaluate changes to Q5 due to equifinality of parameter sets, the minimum, maximum and mean values of Q5 for the 500 behavioural parameter sets in both models were calculated and analysed by employing each GCM A2 scenario. The diagrams below (Figure 8.3 and Figure 8.4) show Q5 values from the control period through the 2050s and the 2080s.

As can be seen in the diagram below, in the control period, HYSIM models the highest values in Q5 for all GCMs. Indeed, there is very little overlap in the values simulated by the two models. What is also notable is that the range of values is greater in HYSIM than in HBV-Light, possibly reflecting the greater spread of NS values in the calibration behavioural parameter sets (0.769 – 0.750) compared with HBV-Light (0.711-0.700).
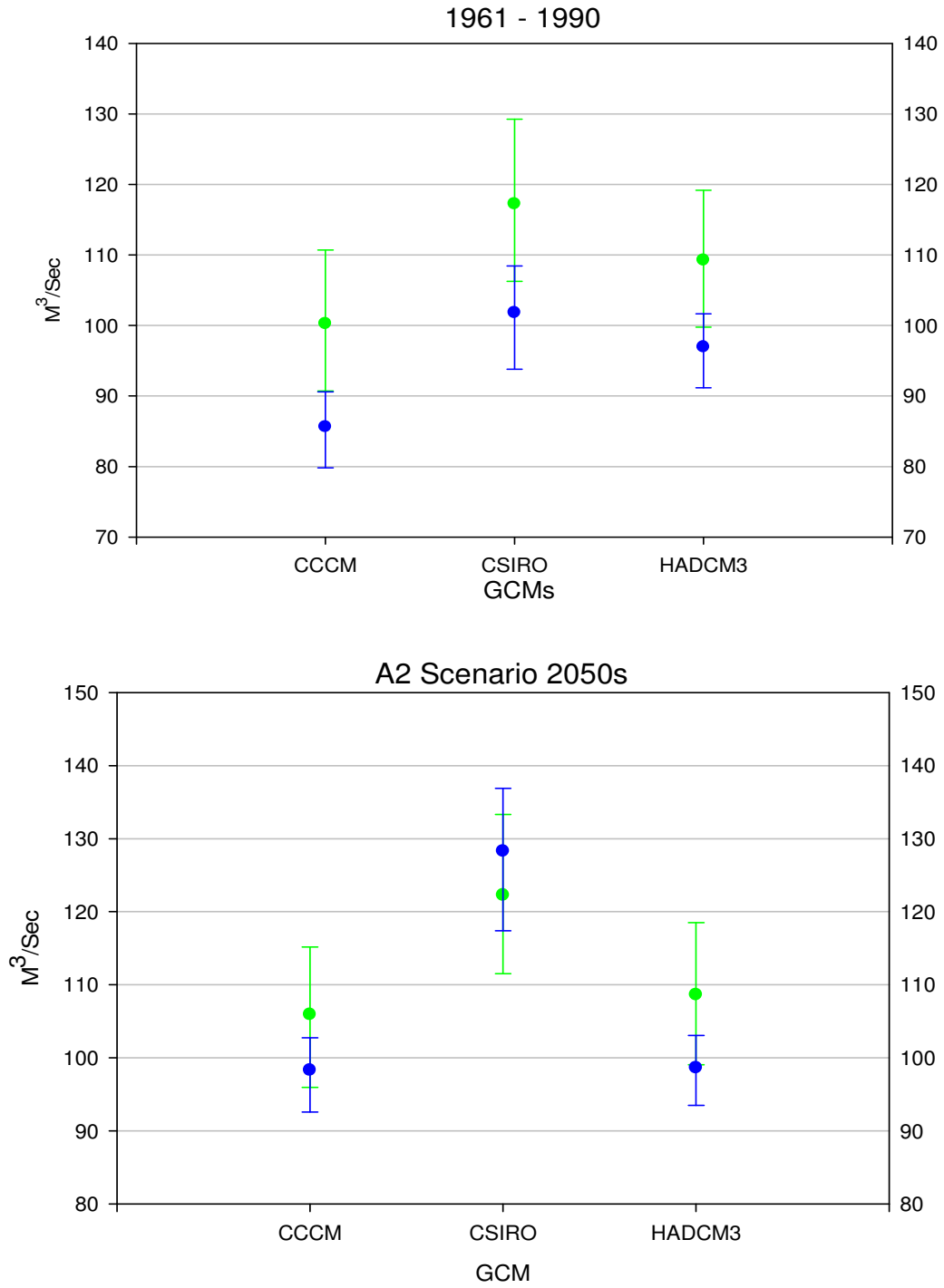
Figure 8.3 Q5 flow values taking into account equifinality of parameter sets for the control period (top) and the 2050s (bottom). HYSIM is represented by the green bars and HBV-Light by the blue bars. The symbols represent the mean of the Q5 values and the error bars represent the maximum and minimum values

However, by the 2050s HBV-light models higher values for Q5 for the CSIRO A2 scenario and the spread of the values is greater than for either CCCM or HADCM3 where the values are more constrained (-0.7% t0 6.76%). Another notable feature is how much the absolute minimum value of the CCCM A2 and CSIRO A2 scenarios have increased with respect to the control period values (from 80m^3/sec to 92m^3/sec for CCCM and from approx. 93m^3/sec to 111m^3/sec for CSIRO). In contrast, GCM output in HYSIM varies relatively little compared with the control period.
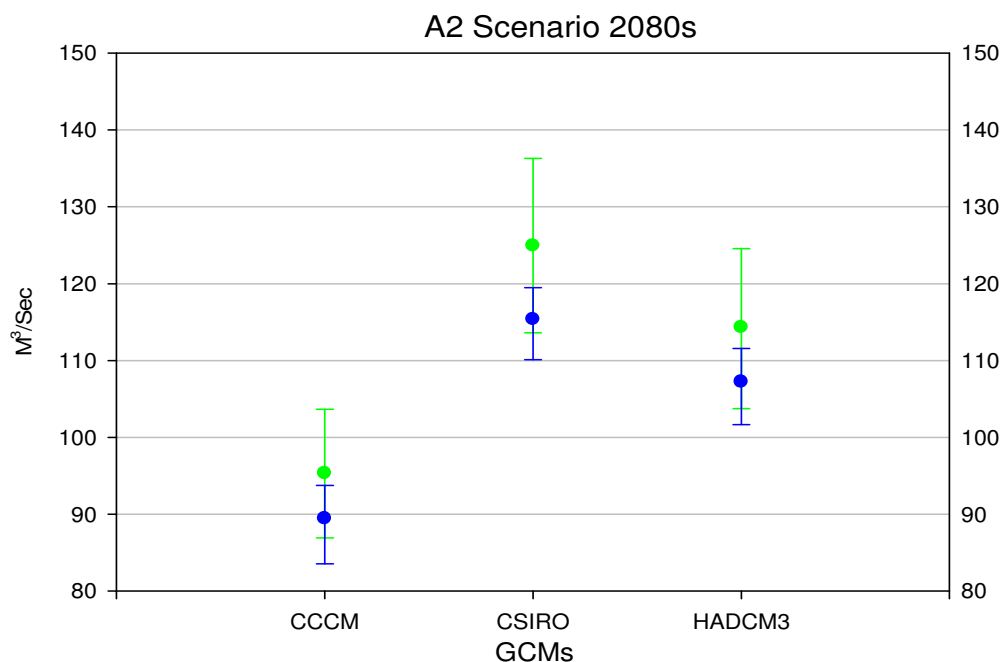

Figure 8.4 Q5 flow values for the 2080s taking into account equifinality of parameter sets

By the 2080s, HYSIM models higher mean and maximum values for all the GCMs than HBV-light, similarly to the control period. What is most notable about the Q5 values in the 2080s is how much CCCM A2 values have decreased in both models compared with the 2050s, while HADCM3 values have risen. CSIRO values are quite similar to those of the control period and in HYSIM they have decreased slightly compared to the control period values. Although CSIRO values have risen for both HBV-Light and HYSIM compared to the control period they too have decreased compared with the 2050s. Only HADCM3 A2 absolute values have risen compared to the control period and the 2050s with the minimum value (102 m^3/sec in HBV-Light) rising more than the maximum one (124 m^3/sec in HYSIM). In all this analysis the minimum values of Q5 have risen more than the maximum values.

Figure 8.5 shows the total uncertainty of Q5 flow for the 2050s and 2080s using the combined output of all GCMs, emissions scenarios and behavioural parameter sets for both HYSIM and HBV-Light. The decrease in minimum values of Q5 in the 2080s relative to the 2050s is possibly due to the drier GCM output, particularly CCCM. The range of uncertainty is quite large (though differences in the uncertainty range for both time periods are small) from approx $90m^3$/sec to $140m^3$/sec in the 2050s and from approx. $83m^3$/sec to $142m^3$/sec in the 2080s. A difference of $50m^3$/sec in Q5 flow could effect the fluvial flow regime and present problems for water managers and engineers planning flood defences.

It is difficult to identify a model that consistently models higher Q5 values, because all model output is a combination of model structure and parameter sets interacting in a distinct manner with the different GCMs and emissions scenarios. Table 8.2 shows the percentage difference in Q5 values for each model compared with the control period. HBV-Light models much greater changes to Q5 values than HYSIM, which has more constrained values. Nonetheless, HYSIM modelled greater absolute values for all scenarios analysed during the control period and also modelled consistently higher values for the scenarios analysed during the two future periods, apart from CSIRO A2 in the 2050s. This highlights how important it is to include local impact model uncertainty analysis in a climate impact assessment (Pappenberger and Beven, 2006). It also highlights that because these different components of uncertainty are so interlinked, a global analysis of uncertainty should be undertaken in addition to individual sensitivity analyses of uncertainty due to GCMs, emissions scenarios, equifinality of parameter sets and model structure.
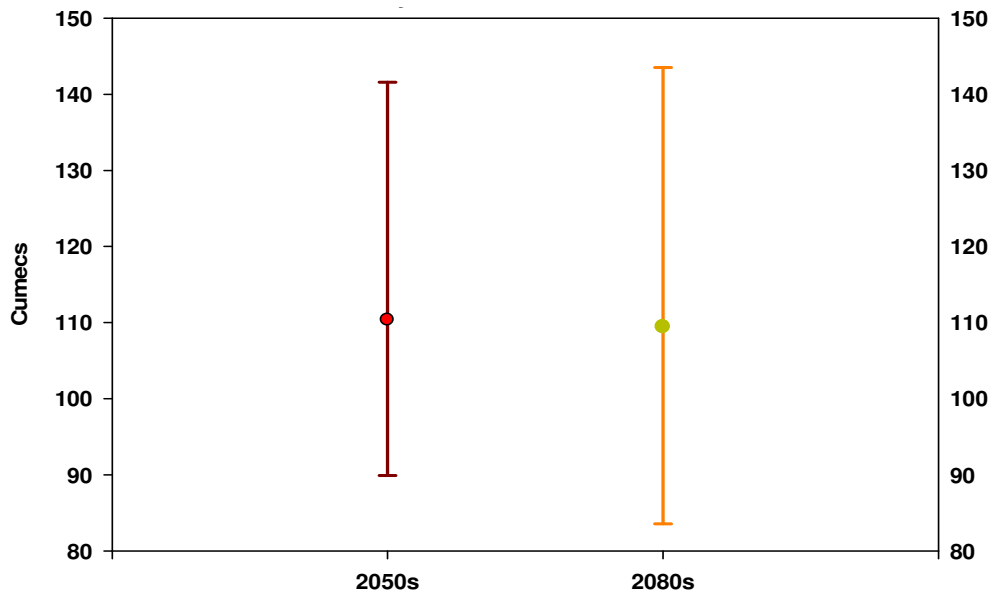
Figure 8.5 Total uncertainty in Q5 flow for the 2050s and 2080s using the combined output of both models

	GCM	Value	HBV-Light	HYSIM
2050s	**CCCM**	Min Mean Max	13.91 14.74 16.04	5.81 6.76 6.40
	CSIRO	Min Mean Max	25.16 28.98 31.33	4.97 5.68 5.84
	HADCM3	Min Mean Max	1.34 1.40 2.03	-0.38 -0.50 -0.70
2080s	**CCCM**	Min Mean Max	3.94 4.40 4.72	-3.92 -4.19 -4.23
	CSIRO	Min Mean Max	14.63 16.00 17.36	6.92 8.01 8.21
	HADCM3	Min Mean Max	9.76 10.16 10.92	3.99 4.70 4.71

Table 8.2 Percentage change in Q5 values due to equifinality of parameter sets for the 2050s and 2080s

8.4　Extreme Value Analysis

Extreme value analysis is a branch of statistical analysis which focuses of the behaviour of data in the tails of a distribution. In the case of floods, it is the data contained in the upper tails that are of interest. These data are much rarer (and therefore more uncertain) than other data in the distribution and a specific class of statistical model has been developed for analysis of extreme data and by which extrapolation is possible. There are a number of such models (extreme value distributions), for example the Gumbel distribution, the Generalised Extreme Value (GEV) distribution and the Generalised Logistic distribution. Each of these models allows for distinct behaviour in the tails of the distribution. In this project, the extreme value distribution selected for estimation of changes in flood magnitude and frequency is the Generalised Logistic distribution (GL) which is recommended in the Flood Estimation Handbook (Robson and Reed, 1999). The reason for this is that the GL distribution is unbounded above.

Before proceeding further, it is pertinent to consider one caveat in the methodology of evaluating flood magnitude/frequency relationships. Underlying all such analyses is the assumption of stationarity within a flood series data set i.e. that the sample of values is reflective of an underlying population with a stable mean and variance. However, an intrinsic characteristic of all natural systems is *variability,* both spatially and temporally (e.g., Clarke, 2007; Milly *et al.,* 2008). The influence of climate change will add yet more variability to the behaviour of natural systems. The assumption of stationarity is at odds with the behaviour of natural systems, where variability is an inherent feature. This will pose challenges for the discipline of statistics. Indeed, Milly *et al.* (2008, p574) recommend that "hydrologists, engineers and managers (both current and future) will require extensive training in non-stationarity and uncertainty".

8.4.1　The Generalised Logistic Distribution
The GL distribution is being employed in this project to evaluate flood magnitude/frequency relationship as it is the one recommended in the Flood Estimation Handbook (Robson and Reed, 1999). Although the GEV distribution is another plausible distribution to use for flood frequency estimation, the GL distribution results in fewer growth curves that are bounded above. The formula for the GL distribution is given as:

$$Q(F) = \xi + \frac{\alpha}{\kappa}\left[1 - \left(\frac{1-F}{F}\right)^{\kappa}\right]$$

where ξ is the location parameter, α is the scale parameter and κ is the shape parameter. F is the non-exceedence probability. The range of values for the GL distribution is:

$$-\infty < Q \le \xi + \frac{\alpha}{\kappa} \text{ if } \kappa > 0$$

$$\xi + \frac{\alpha}{\kappa} \le Q < \infty \text{ if } \kappa < 0$$

The GL is bounded above for $\kappa > 0$, and bounded below for $\kappa < 0$. QMED (the median annual maximum flood or index flood) is the flood which occurs once every two years at a given site and is the value of a distribution for which F = 0.5 (i.e. the median value, there is equal chance of observing a value above or below the median). If F = 0.5 is substituted into the GL distribution equation then, QMED = ξ (Robson and Reed, 1999). The GL growth curve is obtained from the flood frequency curve by substituting $x = Q/QMED = Q/\xi$ into the GL equation:

$$x(F) = 1 + \frac{\beta}{\kappa}\left[1 - \left(\frac{1-F}{F}\right)^{\kappa}\right]$$

where $\beta = \alpha/\xi$. The growth curve can also be written in terms of the return period T:

$$x_T = 1 + \frac{\beta}{\kappa}\left[1 - (T-1)^{-\kappa}\right]$$

8.4.2   L-Moments for Flood frequency Analysis

A theoretical distribution (population) is defined in terms of its moments (mean, variance, skewness and kurtosis). The moments of a sample can then be derived and a distribution fitted so that the sample moments are equated to those of the underlying population. The method of moments uses the above technique but works best for normally distributed data. Since flood data are not normally distributed, ordinary moments are not a robust method of

describing the parameters of the sample distribution. L-moments are a more robust method (Hosking and Wallace, 1997).

L-moments developed from probability weighted moments (Greenwood *et al.,* 1979). Another statistical model used for flood frequency analysis is based on maximum likelihood estimation (MLE) which can incorporate the presence of covariates such as the NAO cycle. However, the computational simplicity of L-moments and their robustness of use with small samples make them particularly suitable for flood frequency estimation (Katz *et al.,* 2002). L-moments are derived from linear combinations of the data. The L-moment ratios used for obtaining flood growth curves are L-CV, L-skewness and L-kurtosis. They are derived by scaling the L-moments by either L-mean or L-scale. Sample L-moments are calculated for use in flood growth curves and are then equated to the population L-moments. The probability weighted moment estimator equations are as follows:

$$b_0 = n^{-1} \sum_{j=1}^{n} x_{(j)}$$

$$b_1 = n^{-1} \sum_{j=2}^{n} \frac{(j-1)}{(n-1)} x_{(j)}$$

$$b_2 = n^{-1} \sum_{j=3}^{n} \frac{(j-1)(j-2)}{(n-1)(n-2)} x_{(j)}$$

$$b_3 = n^{-1} \sum_{j=4}^{n} \frac{(j-1)(j-2)(j-3)}{(n-1)(n-2)(n-3)} x_{(j)}$$

where *n* is the sample size and $x_{(j)}$ is the jth element of a sample of size n sorted into ascending order. The sample L-moments are then calculated by:

$$l_1 = b_0$$

$$l_2 = 2b_1 - b_0$$

$$l_3 = 6b_2 - 6b_1 + b_0$$

$$l_4 = 20b_3 - 30b_2 + 12b_1 - b_0$$

From these the L-moment ratios are obtained. The L-moment ratios are dimensionless and scale-independent and are employed in the construction of a flood growth curve (Robson and Reed, 1999):

$$\text{L-CV } (t_2 = l_2/l_1)$$

$$\text{L-skewness } (t_3 = l_3/l_2)$$

$$\text{L-kurtosis } (t_4 = l_4/l_2)$$

8.4.3 Growth curve estimation

The parameters κ and β are calculated from the sample L-moments ratios, t_2 amd t_3 as

$$\kappa = -t_3;$$

$$\beta = \frac{t_2 \kappa \sin \pi\kappa}{\kappa\pi(\kappa + t_s) - t_2 \sin \pi\kappa}$$

Once the growth curve parameters are calculated, the growth curve and flood frequency curves can then be produced. Figure 8.6 and Figure 8.7 below show the flood frequency curves and growth curves for the Suir catchment calculated using the AMS from 1953 to 2004. The flood frequency curve is QMED times the growth curve (Robson and Reed, 1999).
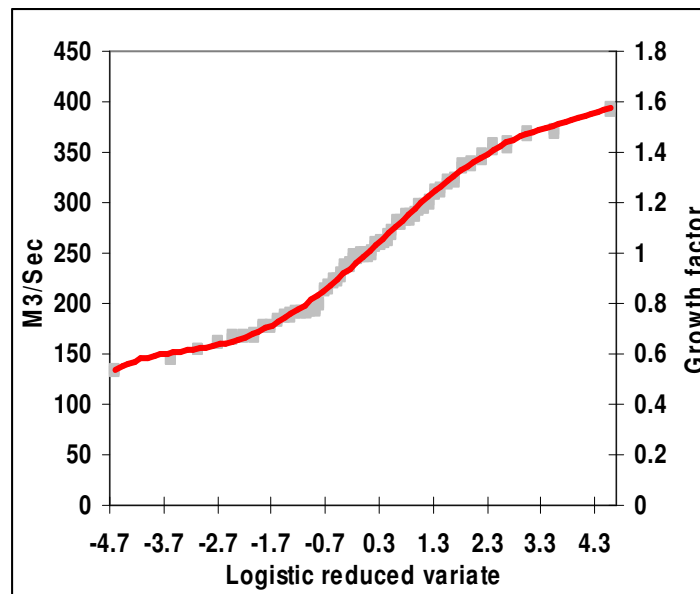

Figure 8.6 Growth curve for the Suir catchment estimated from AMS 1961 to 1990
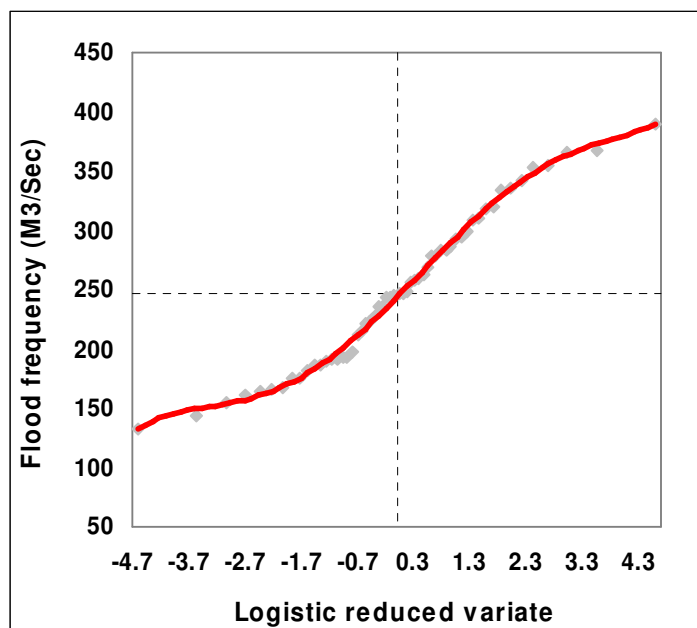
Figure 8.7 Flood frequency curve for Suir catchment estimated using AMS from 1961 to 1990

8.5 Results of the Extreme Value Analysis

8.5.1 Changes in Flood Magnitudes

In this project, four different magnitudes of floods (in m^3/sec) have been selected for analysis; Q2, Q10, Q25 and Q50. Q2 is the flood event which occurs *on average* every two years and Q50 the flood event which occurs *on average* once every 50 years. Analysis of extreme events such as floods is subject to very large uncertainties (even in a stable climate). Indeed, statistical experiments suggest that 1,000 years of data would be necessary to estimate the magnitude of the 1 in 100 year flood event with small uncertainty (Beven, 2009). In this project analysis of flood magnitudes will be limited to no more than the 1 in 50 year event (Reynard *et al.,* 2004).

Another issue that must be addressed is the assumption of stationarity. Climate change will introduce non-stationarity into an AMS for the future time slices being employed in this project (2050s and 2080s). However, Prudhomme *et al.,* (2003, p.5), suggest that "it is possible to assume stationarity around the time horizon of interest, for example the 2050s, i.e. to assume that the samples of data used to assess the flood regime…were measured in a stationary climate (current or changed)". This assumption will also be employed in this project.

The results of the extreme value analysis were analysed similarly to the changes in catchment hydrology. However, the different sources of uncertainty were also analysed in a cumulative fashion. In order to evaluate the uncertainty due to the GCMs, the output of the best validation parameter set in both models was employed together with the A2 scenario. In order to evaluate the ranges of uncertainty due to the emissions scenarios, the best validation parameter sets were employed with both the A2 and B2 scenarios for each single GCM. Finally, a combination of all sources of uncertainty was evaluated by calculating the minimum, maximum and median values for all the 500 behavioural validation parameter sets, GCMs and emissions scenarios for both HYSIM and HBV-Light. Appendix 5 contains an analysis of single sources of uncertainty (GCMs, emissions scenarios and equifinality of parameter sets) in influencing changes to flood magnitude volumes.

With regard to GCM uncertainty, HYSIM models greater absolute values for each flow magnitude during the control period (Figure 8.8). The uncertainty ranges are also very small for both models. However, there is a difference of approximately $100m^3$/sec in flows, particularly for the larger magnitude events. Q50 values for HBV-Light range from $176m^3$/sec to $200m^3$/sec whereas in HYSIM the Q50 values range from $249m^3$/sec to $200m^3$/sec. When all the output data is combined, HYSIM also models greater absolute minimum, median and maximum values for all the selected flood magnitude and a greater range of uncertainty. Furthermore, the uncertainty ranges for both models are also greater particularly for the higher flood magnitudes (Q25 and Q50) (see Table 8.3).

Control		Q2	Q10	Q25	Q50
HBV-Light	min	115.2	141.6	152.9	161
	median	135.4	167.6	183.4	195.6
	max	157	204.8	234.2	263.5
HYSIM	min	146.5	193.4	212.5	227
	median	172.3	229.6	261.8	288.6
	max	190.7	270	327.8	382.8

Table 8.3 Minimum, median and maximum values from the combination of all modelled output for HBV-Light and HYSIM for the control period.

By the 2050s (Figure 8.9) the range of uncertainty due to choice of GCM for each magnitude of flood is greater in HBV-Light with the CSIRO A2 scenario showing the highest values in each of the selected floods. Conversely, in HYSIM CSIRO A2 has the lowest values of the three GCMs, with HADCM3 having the highest values. This again highlights the uncertainties due to model structure and how difficult it can be to completely separate model structural uncertainty from parameter, emission scenario and GCM uncertainty. When the uncertainties due to emissions scenarios are analysed, again HBV-Light has greater ranges of uncertainty for each magnitude of flood and also greater absolute values than HYSIM.
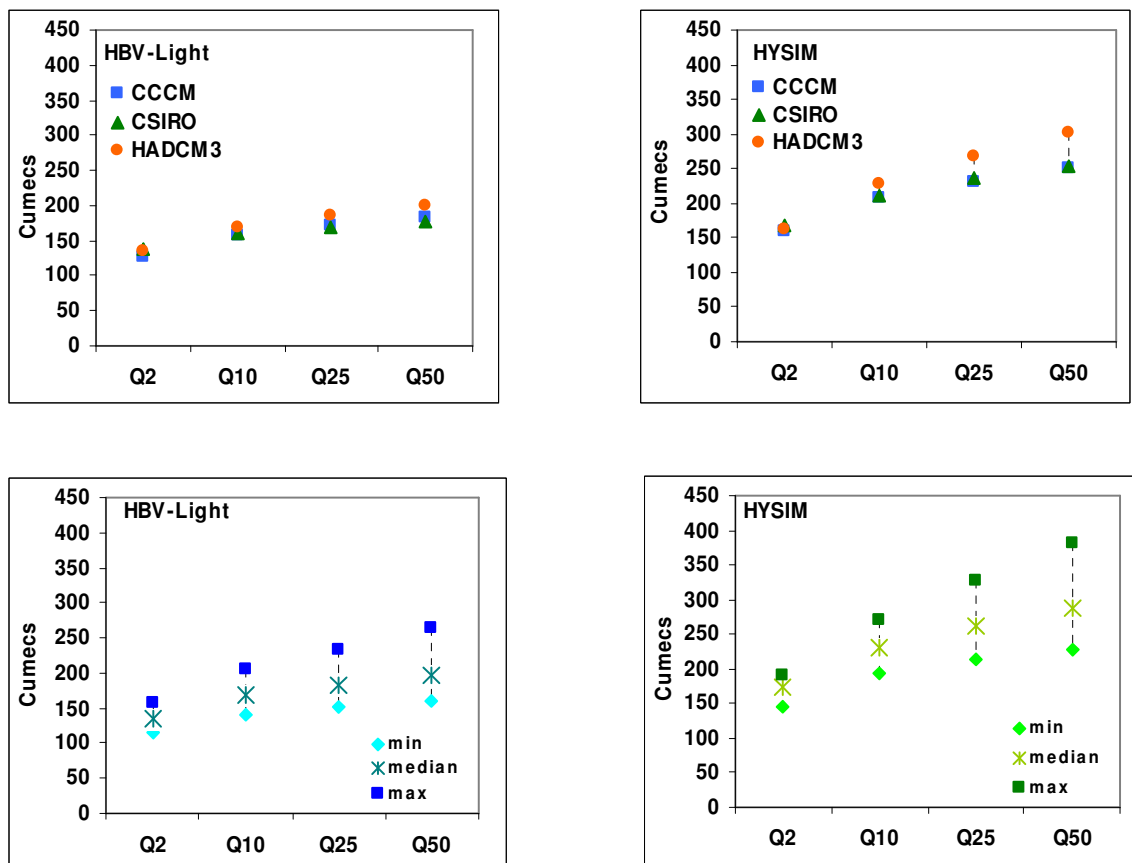
Control

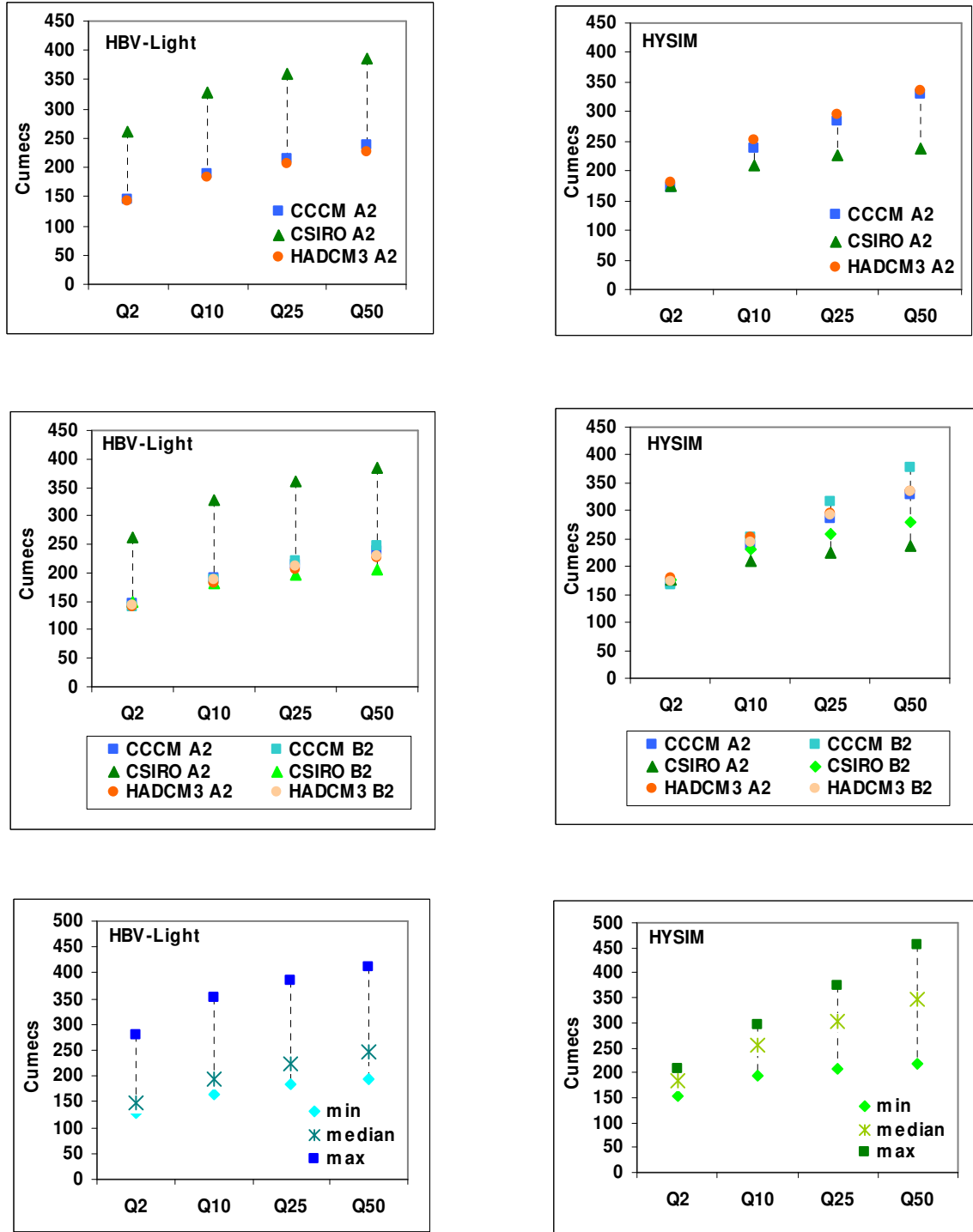Figure 8.8 Uncertainty due to GCMs (top row) and all sources of uncertainty combined (bottom row) for the control period

Figure 8.9 Uncertainty due to GCMs, (top row) emission scenario (middle row) and all sources of uncertainty combined (bottom row) for the 2050s
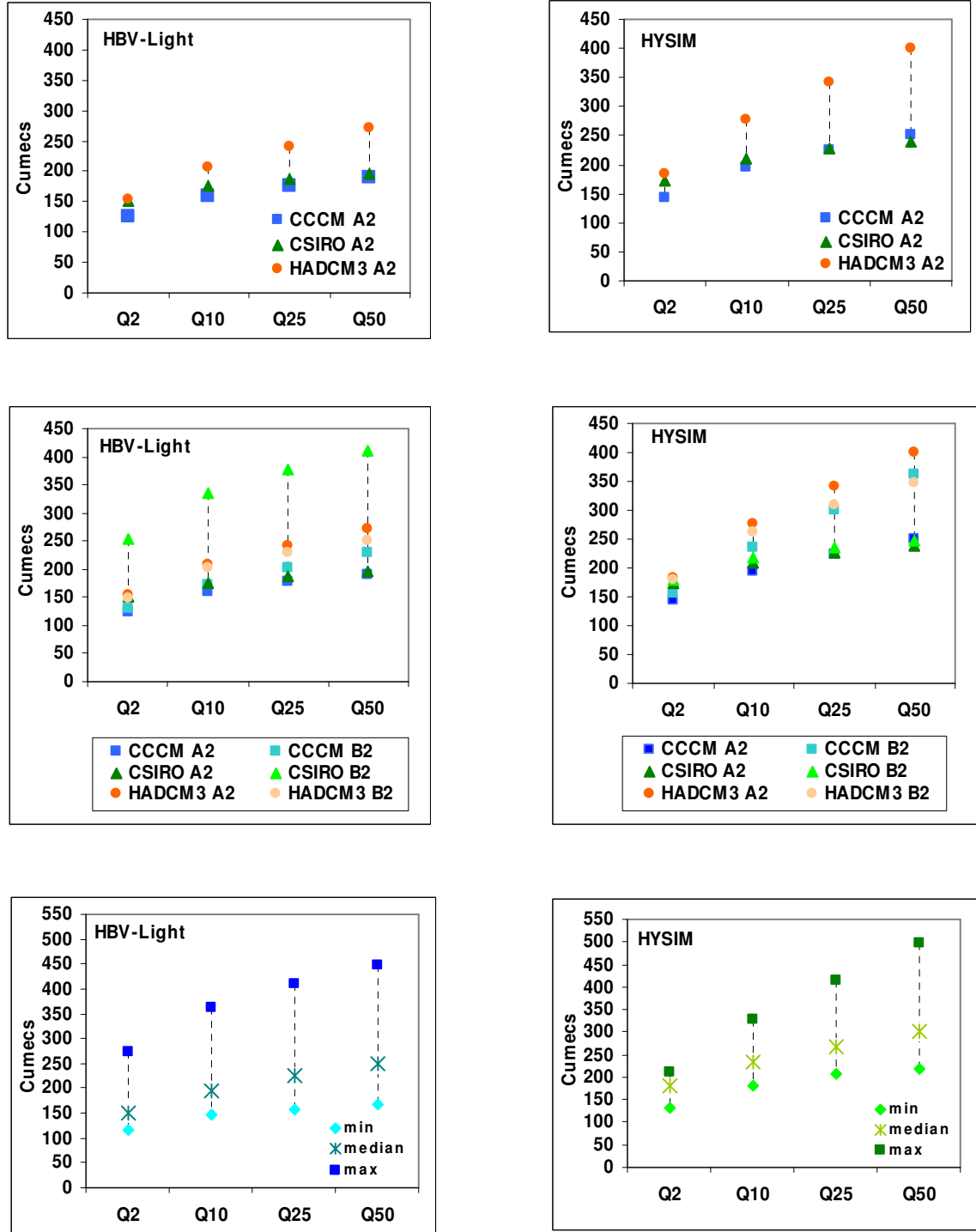
2080s

Figure 8.10 Uncertainty due to GCMs, (top row) emission scenario (middle row) and all sources of uncertainty combined (bottom row) for the 2080s

Also in HBV-Light, there is very little uncertainty between all the scenarios apart from CSIRO A2, which has the maximum value for all flood magnitudes with a significant range between its value and the values for the other scenarios (Q25, 219m^3/sec for CCCM B2 to 360m^3/sec for CSIRO A2).

In the 2080s, (in HBV-Light) the CSIRO B2 scenario has much higher values than the rest of the scenarios. This anomaly highlights the importance of model structural uncertainty in a climate impact assessment (Figure 8.10). The structure of HBV-Light may interact with the CSIRO data in this way because of the very quick flow of moisture through the soil moisture routine. In contrast, in HYSIM there is a more even spread between the values of the different emissions scenarios, even though the uncertainty range is smaller than in HBV-Light.   When all sources of uncertainty are combined (GCM, emission scenario, model structural uncertainty and parameter uncertainty) HBV-Light has both greater ranges of uncertainty for each magnitude of flood and also higher absolute values than HYSIM, until the largest flood (Q50) when HYSIM records a greater absolute value (Table 8.4). Furthermore, in HYSIM the minimum and median values for each flood are greater than in HBV-Light. Only the maximum values are greater in HBV-Light, until Q50, when HYSIM records a greater value. Thus, depending on the severity of the flood, the contribution of different sources of uncertainty is also different.

2050s		Q2	Q10	Q25	Q50
HBV-Light	min	129.4	164.1	184.0	195.0
	median	149.1	194.7	223.4	248.1
	max	280.9	350.7	385.4	411.8
HYSIM	min	154.7	193.2	207.4	217.9
	median	183.1	254.2	303.3	348.2
	max	206.9	296.7	373.9	457.0

Table 8.4 Minimum, median and maximum values from the combination of all modelled output for the 2050s

By the 2080s uncertainty due to GCMs is greater than the 2050s in HYSIM, but less than the 2050s in HBV-Light (e.g., Q25: 177m^3/sec to 241m^3/sec (HBV-Light) 225m^3/sec to 341m3/sec (HYSIM)). The HADCM3 A2 scenario has the highest values for all the floods in both models. Indeed, in HYSIM, the output of HADCM3 A2 has consistently shown the highest values for all the flood magnitudes for each period in the analysis. Conversely,

while HADCM3 A2 has also output the highest values for the control period and the 2080s in HBV-Light, CSIRO A2 has the highest values in the 2050s. When scenario uncertainty is analysed, HBV-Light has great ranges of uncertainty for all flood magnitudes. Moreover, like the 2050s, one GCM (CSIRO B2) has much greater values than the other scenarios. The value range for the other scenarios is much smaller. For example, the Q25 values range from 177m^3/sec (CCCM A2) to 228m^3/sec (HADCM3 A2) and up to 376m^3/sec for CSIRO B2. In HYSIM, HADCM3 A2 values are the highest for all flood magnitudes analysed, while CSIRO B2 values are the lowest, together with CCCM A2). Similarly to the 2050s, there is a more even spread in the uncertainty range of the different scenarios in HYSIM than in HBV-Light.

2080s		Q2	Q10	Q25	Q50
HBV-Light	min	116.8	145.3	158.2	167.8
	median	151.0	194.1	224.2	249.9
	max	272.6	360.5	408.9	448.1
HYSIM	min	132.3	179.6	206.7	217.2
	median	179.1	234.4	269.1	301.4
	max	211.5	329.5	415.7	498.1

Table 8.5 Minimum, median and maximum values of the different magnitude flood events from the combination of all modelled output for the 2080s

When all sources of uncertainty are taken into account, HYSIM again has higher minimum and median values for all flood magnitudes analysed than HBV-Light (see Table 8.5). HBV-Light has higher maximum values for Q2 andQ10 however, HYSIM models higher maximum values for both Q25 and Q50. Minimum and median values for all flood magnitudes are also higher in HYSIM than in HBV-Light. What is also notable when analysing the figures from the three periods is that for HYSIM the minimum values for all flood magnitudes are lower than the control period minimum values, while in HBV-Light the minimum values for the 2080s are only slightly higher than the control period values. This is reflective of the drying that some of the GCMs project to occur by the 2080s, particularly the CCCM A2 scenario. The median values for all flood magnitudes analysed (in HYSIM) are higher than those of the control period but lower than those in the 2050s. In HBV-Light the median values are higher than the control period ones, and very similar to those of the 2050s.
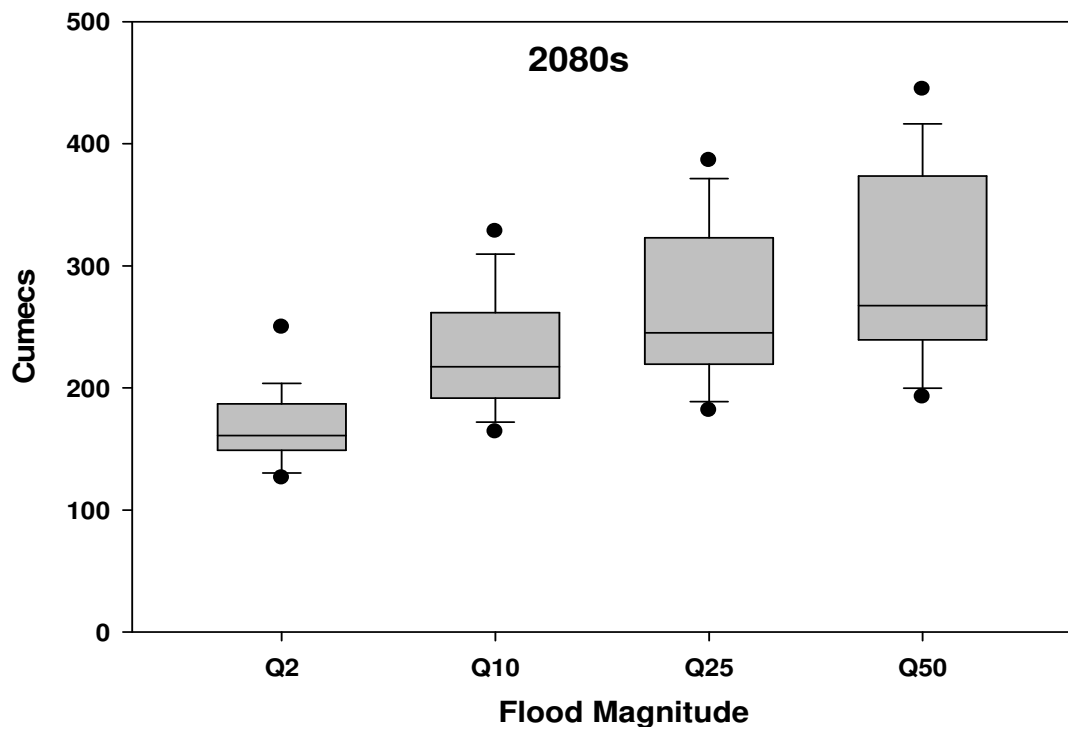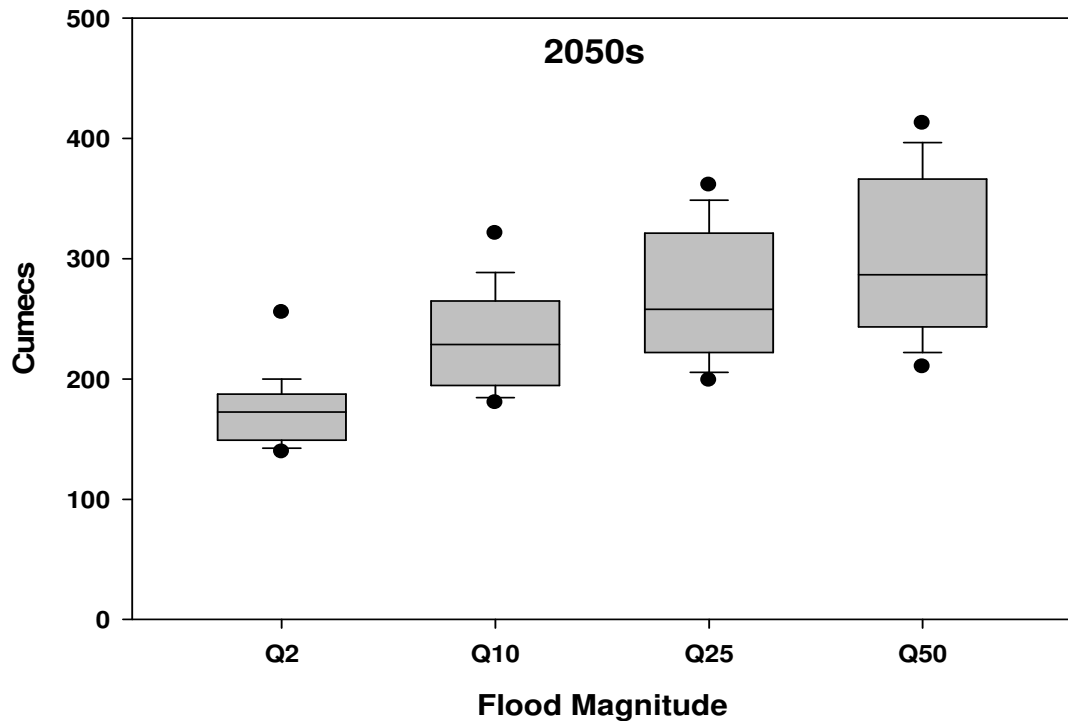
Figure 8.11 Combined output of both models including all sources of uncertainty (GCMs, emissions scenarios, and all behavioural parameter sets) showing the uncertainty ranges in flood magnitude volumes. The outliers represent the 5th and 95th percentile values.

Figure 8.11 shows the combination of all data for both models. The ranges of uncertainty have increased between the two future time slices, with the minimum and median values from all flood magnitudes analysed decreasing between the 2050s and the 2080s, which may be a reflection of the drying expected by that time period. However, maximum values of all flood magnitudes have increased, apart from Q2 (the index flood). The ranges of uncertainty are also greater for the higher magnitude events (Q25 and Q50), as is the increase in flow volume compared to the control period values. In view of these results, the new flood defences that are being built in Clonmel to withstand a 100-year flood event of 500m3/sec, with the possibility of increasing the defences to cope with a flood event 20% greater, are prudent adaptation decisions.

8.5.2   Changes to Flood Frequencies

This analysis also includes analysing changes to flood frequencies compared with the control period. The change in return period was analysed as the *average* value of the combined output of all GCMs, ES and behavioural parameter sets in both models. Table 8.6 illustrates the changes in return periods for the 2050s and the 2080s. Both models record very similar new return period values, particularly for the 2080s. The 50-year return period in the 2050s is the only return value where the output of both models diverges significantly, with the new return period in HYSIM being larger than that of HBV-Light. Both models' output shows decrease in return period values, with the 10-year event becoming a 5.5 year event (HBV-Light) or a 6.2 year event (HYSIM). However, by the 2080s the new return period values are very similar with the 10 year flood event becoming a 3.2 year event, the 25 year event becoming a 5.4 year event and the 50 year flood event becoming a 9 year event. This is a robust finding. Thus, the output of both models suggests intensification in flood magnitude/frequency relationships within the Suir catchment under climate change, with flood magnitudes increasing relative to the control period and the relevant frequencies decreasing.

		T2	T10	T25	T50
2050s	HBV-Light	1.6	5.5	12	20.4
	HYSIM	1.5	6.2	14.4	30
2080s	HBV-Light	1.3	3	5.4	9
	HYSIM	1.3	3.2	5.4	8.5

Table 8.6 Average changes in return periods for the 2050s and the 2080s

8.6   Conclusion

This chapter has focussed on the analysis of changes to extreme flow (Q5) and flood magnitude and frequency under climate change scenarios for the 2050s and the 2080s. In the analysis of changes to the 95th flow percentile, HBV-Light models much greater percentage changes than HYSIM for the 2080s. Nevertheless, HYSIM models greater absolute changes in Q5 flow for both periods, apart from the CSIRO A2 scenario in the 2050s when HBV-Light models greater values. Increasing magnitudes of flood events analysed are evident in the two future time slices with the greatest increases in flow volume occurring in the higher magnitude events. The output of both models also suggests that flood magnitude and frequency relationships will intensify under climate change, with the 25 year flood event becoming a 5.4 year event by the 2080s and the 50 year flood event a 9 year one during the same period. HYSIM also models greater absolute values for the highest magnitude event analysed (Q50).

It is important to reiterate that natural climate variability was not analysed in this project. If flow volumes modelled in this project for the 50-year event were added to high streamflow due to natural variability, the resulting flood would be even larger than those modelled above. Even though the new flood defences in Clonmel have the capability of protecting against a one in 100 flood event of 600 m^3/sec, careful consideration may have to be given to revising that figure higher still.

Chapter 9 – Conclusions

9.1   Introduction

This research sought to build on previous Irish studies by employing two lumped conceptual rainfall-runoff models (HYSIM and HBV-Light) and analysing uncertainty in future changes to catchment hydrology and flood magnitude/frequency relationships due to model structural error and equifinality of parameter sets *in addition to* uncertainty due to GCMs and emissions scenarios. While uncertainty due to GCMs and emissions scenarios has been well documented, little research has been conducted into the uncertainty in climate change impact assessments derived from impact models. This thesis aimed at modelling changes to catchment hydrology that incorporate the uncertainty derived from three GCMs and two emissions scenarios as well as from the two impact models and compare ranges of uncertainty from the individual sources in order to evaluate which source contributed the greatest uncertainty to the total range. Furthermore, the thesis aimed to evaluate changes to flood magnitude and frequency derived from the same sources of uncertainty.

9.2   Project Assumptions and Limitations

There are a number of assumptions and limitations associated with this project:

- Only one type of downscaling was used in the project. Future climate impact assessments should include both statistically downscaled data and dynamically downscaled data in order to take into account uncertainty due to the downscaling methodology.

- The use of only two emissions scenarios represents another limitation to the project. The use of medium high (A2) and medium-low (B2) emissions scenarios omits two other families of emissions scenarios (A1 and B1). The A1 family represents more "extreme" emissions.   However, the A2 and B2 scenarios are the ones recommended for use by the IPCC and cover 90% of the total emission scenario range (Nakicenovic *et al.,* 2000).

- An important assumption of the project concerns the calibration of the two models. It is assumed that the calibration will be viable for the future time series. Both models performed better during validation than calibration, which was a test of the robustness of both models as plausible representations of the hydrological behaviour of the catchment. The 1990s were a warmer decade than the baseline climate period, which may indicate that the models will also perform well in a climate change situation.

- Both rainfall-runoff models were lumped ones, which treat the catchment as a single unit, thereby operating on a crude scale. Semi-distributed or distributed models may be more representative of the complex and unique nature of each catchment by including variability of relevant catchment characteristics such as topography, soils, groundwater resources, etc. However, all models are to some extent lumped (Wagener, 2003).

- As only one case study catchment was included in the project, the versatility of the models could not be tested. However, both models have proved plausible representations of the hydrologic behaviour of several important Irish catchments in previous research carried out in Ireland (e.g., Murphy and Charlton, 2008; Steele-Dunne *et al.,* 2008).

- This thesis did not include and analysis of climate variability, even though it is acknowledged to be an intrinsic source of uncertainty (Kundzewicz and Robson, 2004). Further research could include a more comprehensive uncertainty analysis taking into account climate variability (both of present and future climates) (e.g., Minville *et al.,* 2008; Prudhomme *et al.,* 2003).

9.3 Main Findings from the Project

There are several interesting findings from this project:

Although HYSIM is a physically realistic model and HBV-Light a parsimonious one, both models proved plausible representations of the hydrological regime of the Suir catchment during calibration and validation. During validation in particular, the NS score for both

149

models improved, which is an indication of the robustness of the models in simulating observed streamflow (Perrin *et al.,* 2001).

In the analysis of single sources of uncertainty (GCMs; emissions scenarios; equifinality of parameter sets) GCM uncertainty also proved the greatest source of uncertainty during the 2050s and the 2080s and showed the greatest range of uncertainty of all sources analysed. This supports the findings of other research (Bergström *et al.,* 2000; Minville *et al.,* 2008; Prudhomme *et al.,* 2003; Wang *et al.,* 2006; Wilby and Harris, 2006).

Equifinality of parameter sets and model structural uncertainty were also significant sources of uncertainty, especially in the 2080s. The months with the greatest percentage difference in streamflow were February (increase of 48% in HBV-Light/39% in HYSIM) and for HBV-Light August decreases in flow by the 2080s were -54% compared to control period values, while the month with the greatest decreases in flow according to HYSIM was October with a decrease of -48%. Although low flows were not analysed in this project, decreases such as these could have serious implications for fluvial ecology and for human activities such as water abstraction.

Model structural uncertainty added a distinctive pattern to the output especially during the late summer and autumn. In HBV-Light, September was generally the month with the largest decreases in flow, in contrast to HYSIM where the largest decreases in flow consistently occurred in October. HBV-Light also modelled more extreme increases and decreases, while HYSIM modelled conservative changes to the flow regime. This may occur because of the different soil moisture routines in the models. HBV-Light's simpler parsimonious routine may sensitise the model to increases in precipitation, in contrast to HYSIM, whose more physically realistic soil moisture routine allows a more conservative response.

It can be argued that the monthly median percentage changes in the combined output of both models do not differ much from natural climate variability. However, differences to streamflow suggested by the 95th percentile values are much more extreme. In the 2050s, increases in January and February are suggested of ~40%, while by the 2080s the increases for both months are 45% to 50%. This could have very serious consequences for Clonmel,

where flooding is a relatively common occurrence. If such percentage increases in streamflow were super-imposed on higher winter streamflow due to climate variability, the consequences could potentially be catastrophic.

In the analysis of changes to the 95th flow percentile, HBV-Light modelled much greater percentage changes than HYSIM for the 2050s and the 2080s with a higher uncertainty range. Nonetheless, HYSIM consistently modelled greater absolute changes in Q5 flow for both future time slices, apart from the CSIRO A2 scenario in the 2050s. Again the different soil moisture routines in the models could be responsible for the difference in responses.

The output of both models suggests that flood magnitude and frequency relationships will intensify due to climate change. A robust finding from the project is the notable agreement in new return period values in the 2080s with both models suggesting the 10 year flood event becoming a 3.2 year event; the 25 year event becoming a 5.4 year event and the 50 year flood event becoming a 9 year event. Based on these results, it is likely that the 1 in 100 year event may also become a more regular occurrence. This finding, if realised, could have major implications for adaptation decisions regarding flood defences in Clonmel. At present, all flood defences in Ireland are built to withstand the 1 in 100 year flood event. In the new OPW flood defences in Clonmel, the discharge volume of the 100-year event is set at $500m^3$/sec with the potential for adding a further 20% to the defences in response to climate change (O'Domhnaill, 2010 personal communication). In light of the results from this project (the maximum volume of the 50-year event in the 2050s is $457m^3$/sec increasing to a maximum value to $498m^3$/sec in the 2080s), such a precautionary, flexible approach is justified. It is worth noting too that engineers and planners may have to revise the magnitudes of these events in light of climate change.

Furthermore, as evidence comes to light of historical foods larger than any on current records, it becomes more important than ever to allow a degree of flexibility in flood adaptation decisions, as climate may be even more variable than previously thought. It highlights the need for anticipatory adaptation decisions that are flexible and can be updated in light of new information regarding flooding. It also highlights the fact that comprehensive uncertainty analyses for adaptation decisions (e.g., flood defences) should also include an analysis of the uncertainty in impact models.

It is also worth noting that, if climate change impact assessment continues to be a favoured method of translating future climate trends into local output for adaptation decisions, the envelope of quantifiable uncertainty is likely to grow larger for the foreseeable future. GCMs will grow more sophisticated to take account of new knowledge regarding the workings of the global climate system. This will have a trickle-down affect through all further stages of a climate change impact assessment and will lead to yet more uncertainty at the local stage (Wilby and Dessai, 2010). The scientific community should communicate the nature of such uncertainty to decision makers and be open to exploring other methods of adapting to climate change, for example exploratory modelling (Bankes, 1993).

Finally, the need for high quality data measurement and analysis becomes more vital during times such as these with rapid changes to socio-economic activity, population and the global climate system. As Silberstein (2006, p.1350) notes "modelling is an important accompaniment to measurement, but is no substitute for it; science requires observation, and without that we will cease to progress in understanding our environment, and therefore in managing it properly".

Appendix 1 – SRES Emissions scenarios
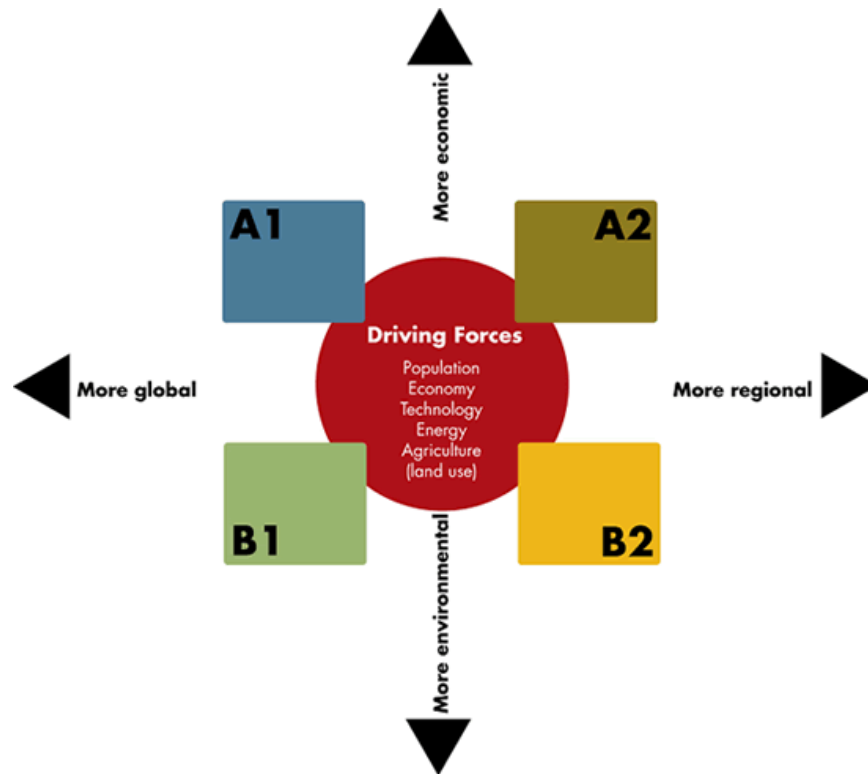
In simple terms, the four storylines combine two sets of divergent tendencies: one set varying between strong economic values and strong environmental values, the other set between increasing globalization and increasing regionalization . The storylines are summarized as follows (Nakicenovic et al., 2000):

- A1 storyline and scenario family: a future world of very rapid economic growth, global population that peaks in mid-century and declines thereafter, and rapid introduction of new and more efficient technologies.
- A2 storyline and scenario family: a very heterogeneous world with continuously increasing global population and regionally oriented economic growth that is more fragmented and slower than in other storylines.
- B1 storyline and scenario family: a convergent world with the same global population as in the A1 storyline but with rapid changes in economic structures toward a service and information economy, with reductions in material intensity, and the introduction of clean and resource-efficient technologies.
- B2 storyline and scenario family: a world in which the emphasis is on local solutions to economic, social, and environmental sustainability, with continuously increasing population (lower than A2) and intermediate economic development.

http://sedac.ciesin.columbia.edu/ddc/sres/

Appendix 2

The Suir catchment was delineated in ArcMap 9.2 using the Hydrology extension in the Spatial Analyst tool within ArcToolbox (ESRI). The grid projection used for all raster files and shapefiles employed in this project was the Irish National Grid TM65 co-ordinate system. There were a number of steps involved in delineating the Suir catchment.

1. The first task was to fill in sink cells within the spatial DEM, by employing the "Fill" command.   Sink cells are areas of internal drainage within a grid and must be elevated in order that ArcGIS can delineate a drainage network that flows off the edge of the grid, otherwise the cells will attempt to drain into each other.

2. After the sink cells had been filled, the BASIN extension tool was activated to delineate the Suir catchment outline.

3. The flow accumulation tool was used in order to create a raster map of accumulated flow to each grid cell to determine where the landscape drains.

4. The flow direction command was then executed in order to generate the drainage network by creating a raster of flow direction from each grid cell to its steepest downslope neighbouring cell.

5. The flow accumulation tool was then employed which identifies cells of high flow accumulation. These linked cells form the basis of a stream network but may not accurately represent the river network as they may be found in areas underlain by lakes or wetlands.

6. The raster calculator was then employed to create a stream network, formed from any cell with a flow accumulation grid value greater than 10,000.

7. Finally a stream shapefile was created from the stream network raster using the stream- to- feature tool.

8. The point shapefile representing the geographical location of Clonmel was then added to the other layers in the map project. This was chosen as the watershed outlet point (rather than the catchment outlet at Waterford) as Clonmel is the location of the gauging station where all the Suir river flow data used in this projected was recorded.
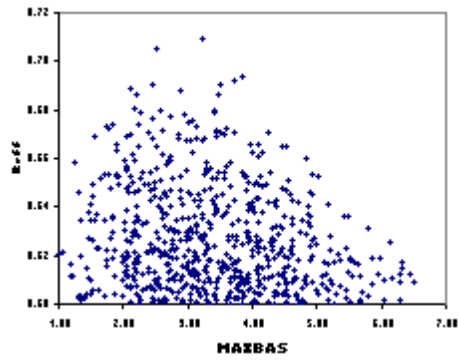
9. The watershed tool was then employed to create a catchment raster, which was then converted to a shapefile.
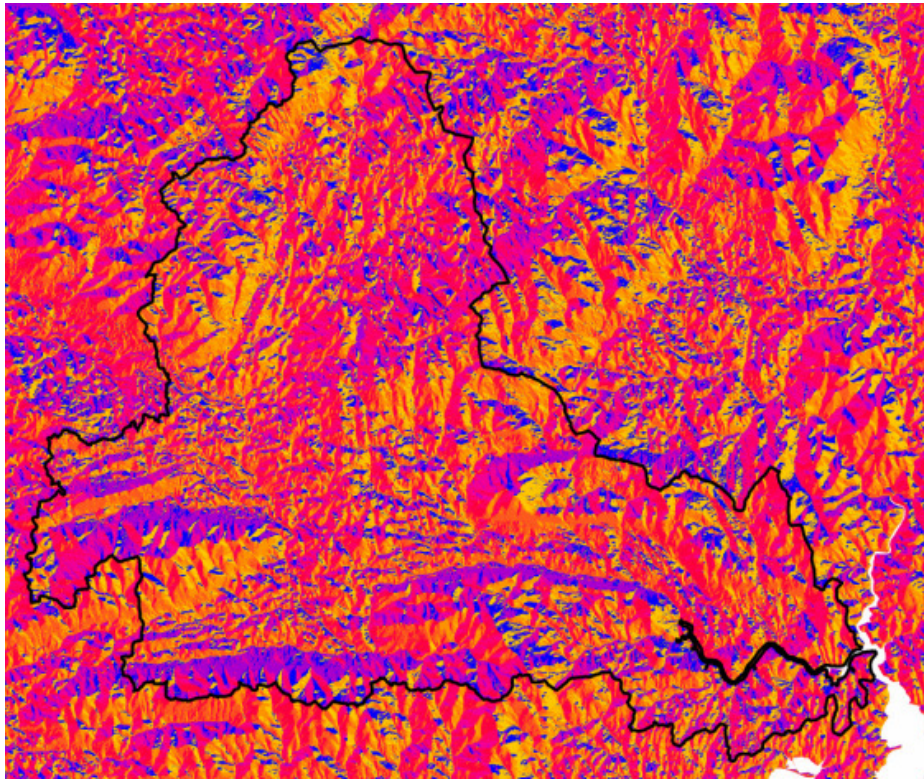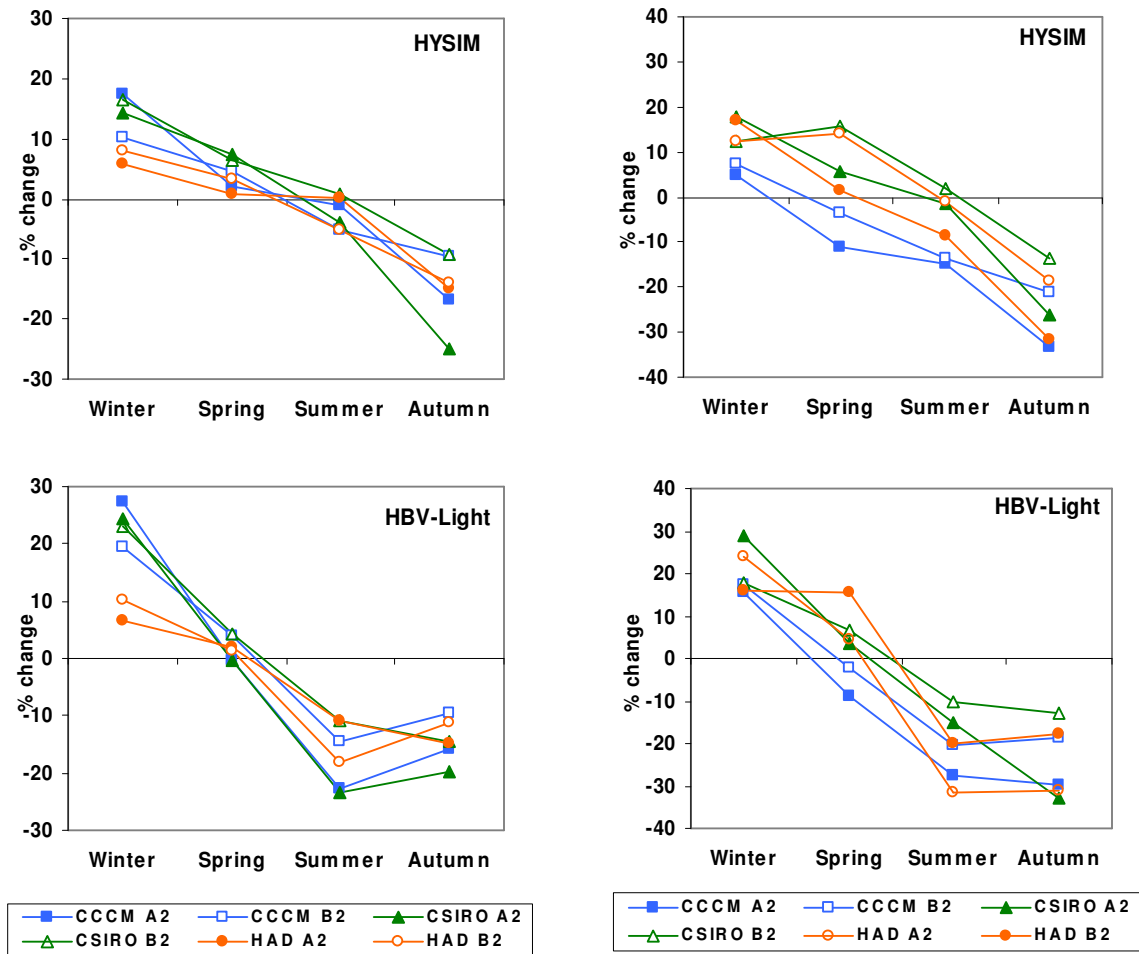

Flow direction Grid derived using ArcGIS 9.2
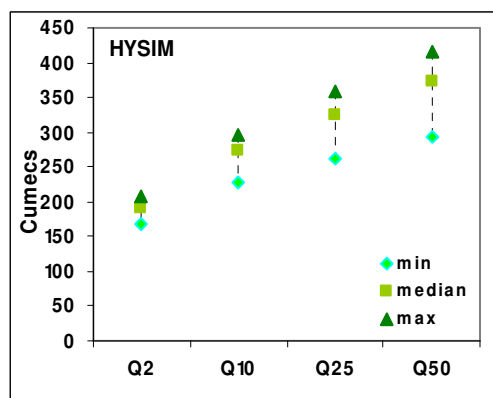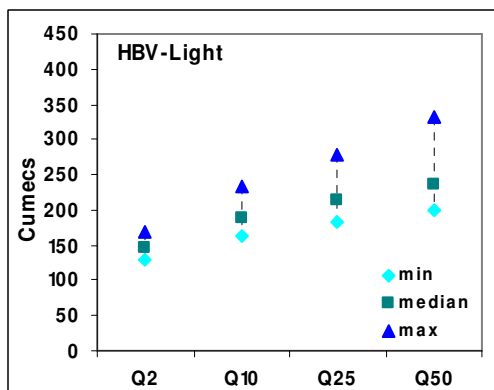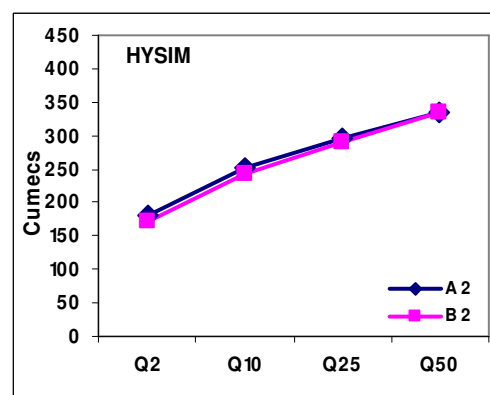
Appendix 3
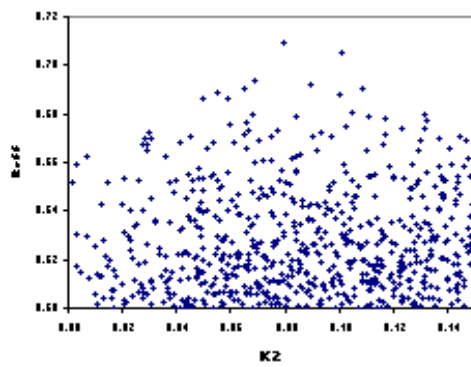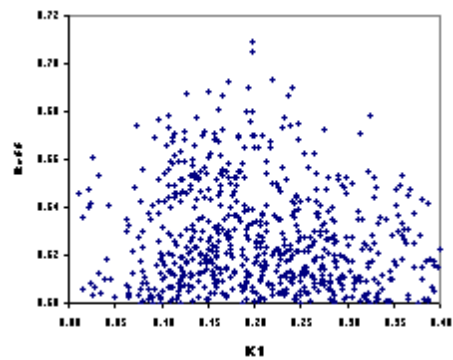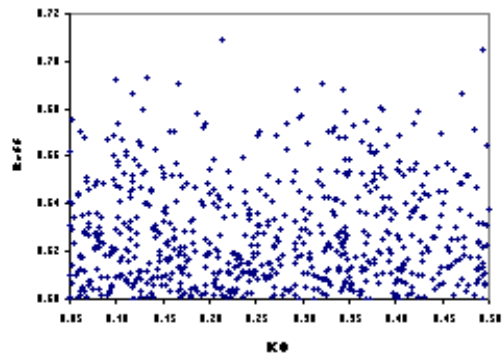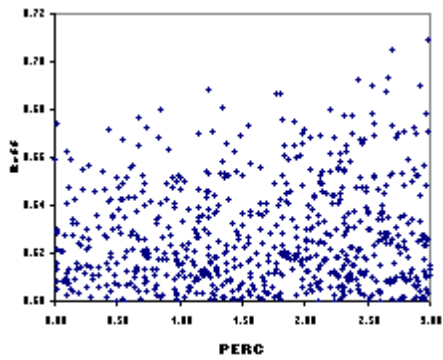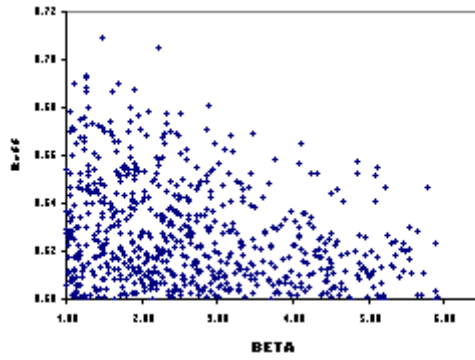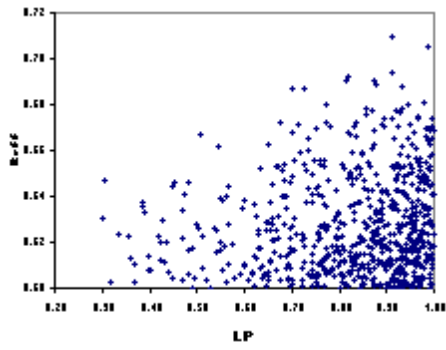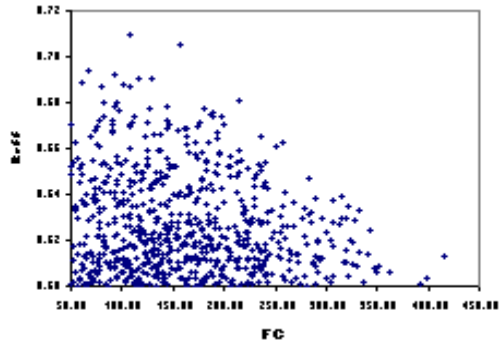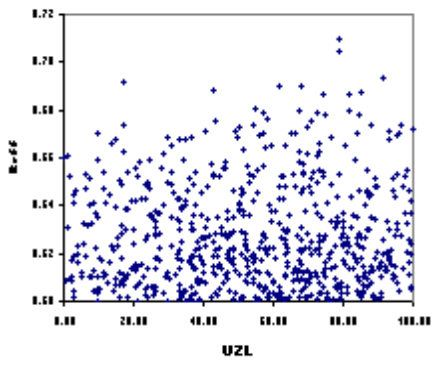
Individual ranges for parameters with NS values of 0.6 and above for 10,000 Monte Carlo runs

Appendix 4

Seasonal changes to flow for the 2050s (left) and the 2080s (right) from a combination of all GCMs and scenarios, using the best validation parameter sets in both models

Appendix 5
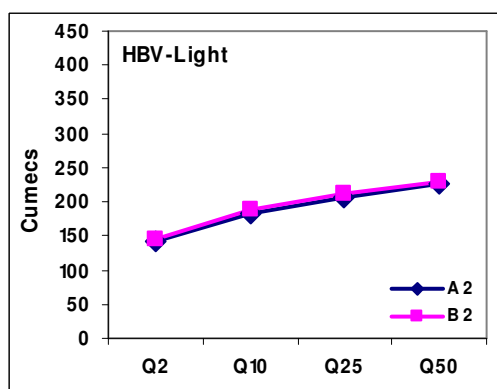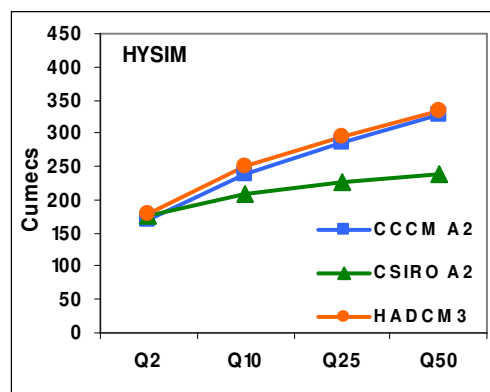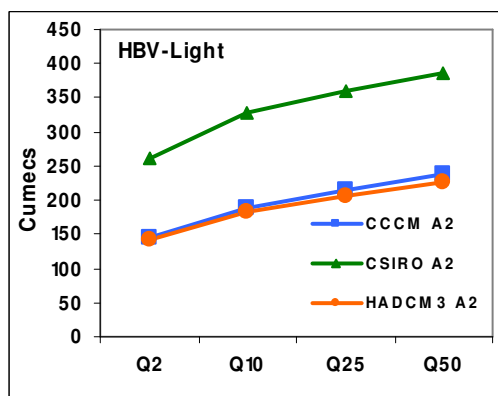
Analysis of changes to flood magnitude due to GCM uncertainty (top), emission scenario uncertainty (middle) and equifinality of parameter sets (bottom) for the 2050s.
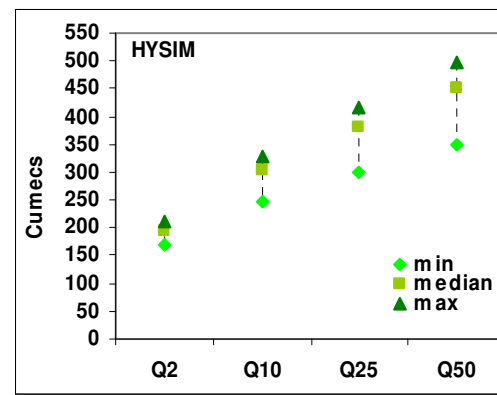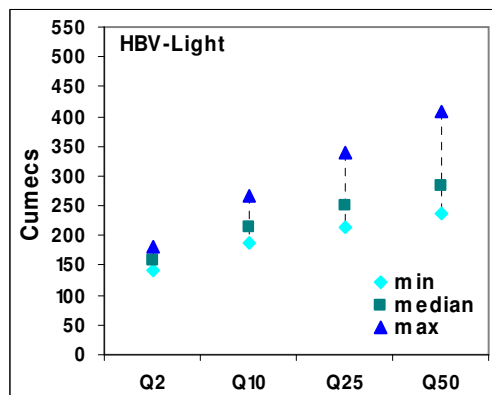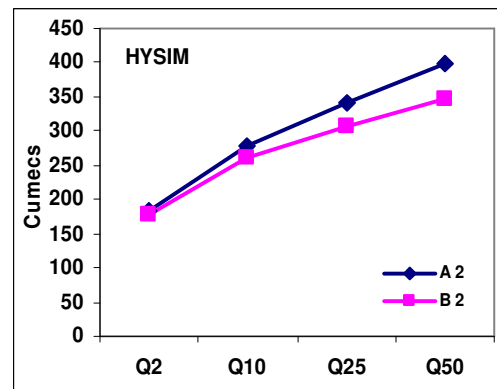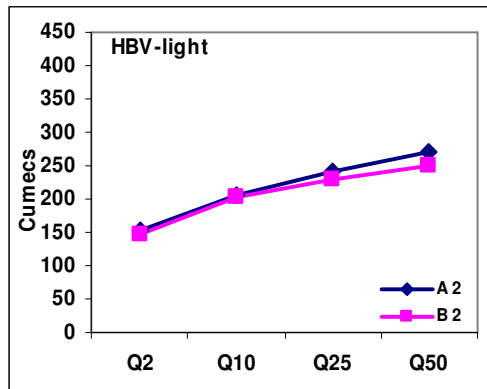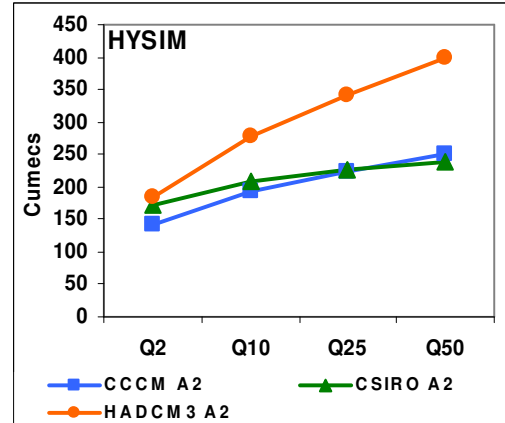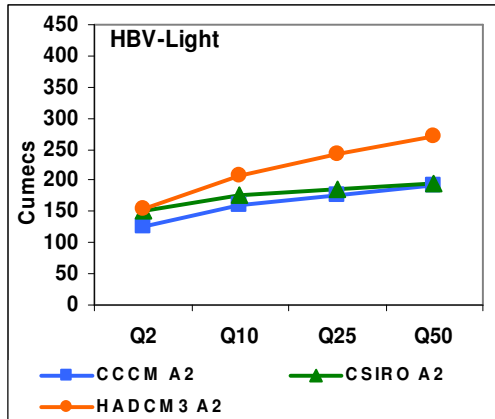
Analysis of changes to flood magnitude due to GCM uncertainty (top), emission scenario uncertainty (middle) and equifinality of parameter sets (bottom) for the 2080s.

Bibliography

Ajami, N.K., Duan, Q, and Sorooshian, S., 2007. An integrated hydrologic Bayesian multimodel combination framework: Confronting input, parameter, and model structural uncertainty. *Water Resources Research,* 43, W01413, doi:10.1029/2005WR004745.

Arnell, N.W., Livermore, M.J.L., Kovats, S., Levy, P.E. Nicholls, R., Parry, M.L., and Gaffin S.R., 2004. Climate and socio-economic scenarios for global-scale climate change impacts assessments: characterising the SRES storylines. *Global Environmental Change,* 14, pp. 3 – 20.

Australian Government Bureau of Meteorology, http://www.bom.gov.au/info/climate/change/gallery/images/74.gif [Accessed 20 August 2010]

Bankes, S.C., 1993. Exploratory Modelling for Policy Analysis. *Operations Research,* 41(3), pp.435-449.

Bergström, S. 1976. Development and application of a conceptual runoff model for Scandinavian catchments. *Swedish Meteorological and Hydrological Institute,* Report No.7.

Bergström, S., 1991. Principles and Confidence in Hydrological Modelling*, Nordic Hydrology,* 22, pp.123-136.

Bergström, S., 1992. The HBV Model – its structure and applications. *Swedish Meteorological and Hydrological Institute* Report. No. 4.

Bergström, S., Carlsson, B., Gardelin, M., Lindström, G., Pettersson, A and Rummukainen, M., 2000. Climate change impacts on runoff in Sweden – assessments by global climate models, dynamical downscaling and hydrological modeling. *Climate Research,* 16, pp.101-112.

Beven, K.J., 1993. Prophecy, reality and uncertainty in distributed hydrological modelling. *Advances in Water Resources,* 16, pp.41-51.

Beven, K.J., 2000. *Rainfall-Runoff Modelling: the Primer*. Wiley, Chichester.

161

Beven, K.J., 2002. Towards a coherent philosophy for modelling the environment. *Proceedings of the Royal Society of London,* 458, pp.2465 – 2484.

Beven, K.J., 2005. A manifesto for the equifinality thesis. Journal of Hydrology, 320, pp.18 – 36.

Beven, K.J., 2007. Towards integrated environmental models of everywhere: uncertainty, data and modelling as a learning process. *Hydrology and Earth System Sciences,* 11(1), pp.460-467.

Beven, K.J., 2008. Measures, model, management and uncertainty: the future of hydrological science. In: Tchiguirinskaia, I., Demuth, S. and Hubert, P. eds., 2008. *River Basins – from Hydrological Science to Water Management*, IAHS Publication 323, pp.139-149.

Beven, K.J., 2009. *Environmental Modelling: An Uncertain Future?* Routledge, Oxon., UK.

Beven, K.J. and Binley, A.M., 1992. The future of distributed models – model calibration and uncertainty prediction. *Hydrological Processes,* 6(3), pp.279 – 298.

Beven, K.J. and Freer, J., 2001. Equifinality, data assimulation, and uncertainty estimation in mechanistis modelling of complex environmental systems using the GLUE methodology. *Journal of Hydrology,* 249, pp.11-29.

Blasone, R-S., Vrugt, J.A., Madsen, H., Rosbjerg, D., Robinson, B.A. and Zyvoloski, G.A., 2008. Generalised Likelihood uncertainty estimation (GLUE) using adaptive Markov Chain Monte Carlo sampling. *Advances in Water Resources,* 31, pp.630-648.

Booij, M.J., 2005. Impact of climate change on river flooding assessed with different spatial model resolutions, *Journal of Hydrology,* 303, pp.176-198.

Braun, L.N. and Renner, C.B., 1992. Application of a conceptual runoff model in different physiographic regions of Switzerland. *Hydrological Science Journal,* 37(3), pp.217-233.

Butts, M.B., Payne, J.T., Kristensen, M. and Madsen, H., 2004. An evaluation of the impact of model structure on hydroogical modelling uncertainty for streamflow simulation. *Journal of Hydrology,* 298, pp.242 – 266.

Cameron, D., Beven, K. and Naden, P., 2000. Flood frequency estimation by continuous simulation under climate change (with uncertainty). *Hydrology and Earth System Sciences,* 43(3), pp.393-405.

Charlton, R., Fealy, R., Moore, S., Sweeney, J., and Murphy, C., 2006. Assessing the impact of climate change on water supply and flood hazard in Ireland using statistical downscaling and hydrological modeling techniques, *Climatic Change,* 74, pp.475-491.

Chiew, F.H.S., Stewardson, M.J. and McMahon, A., 1993. Comparison of six rainfall-runoff modelling approaches. *Journal of Hydrology,* 147 (1-4), pp.1 – 36.

Christiaens, K. and Feyen, J., 2002. Constraining soil hydraulic parameter and output uncertainty of the distributed hydrological MIKE SHE model using the GLUE framework. *Hydrological Processes,* 16(2), pp.373-391.

Clarke, R.T., 2007. Hydrological prediction in a non-stationary world. *Hydrology and Earth System Sciences,* 11(1), pp.408 – 414.

Dawson, C.W., 2010. Hydrotest Statistical Assessment of Hydrological Forecasts. Available at http://www.hydrotest.org.uk. [Accessed 10 May 2010].

Dawson, C.W., Abrahart, R.J. and See, L.M., 2007. HydroTest: a web-based toolbox of evaluation metrics for the standardised assessment of hydrological forecasts. *Environmental Modelling and Software,* 22, pp.1034-1052.

Dessai, S. and Hulme, M., 2003. *Does climate policy need probabilities?* Tyndall Centre Working Paper no. 34.

Dessai, S. and Hulme, M., 2007. Assessing the robustness of adaptation decisions to climate change uncertainties: A cases study on water resources management in the East of England, *Global Environmental Change,* 17, pp.59 – 72.

Dessai, S., Hulme, M., Lempert, R. and Pelke, R., 2009. Climate prediction: a limit to adaptation? In Adger, N., Lorenzoni, I. and O'Brien, K. (eds.) *Adapting to Climate Change: Thresholds, Values, Governance.* Cambridge University Press, UK.

Dessai, S., Hulme, M., Lempert, R., and Peilke, R,. 2009. Do we need better predications to adapt to a changing climate? *Eos Transactions AGU,* 90 (13), doi:10.1029/2009EO130003.

Driessen, T.L.A., Hurkmans, R., Terink, W., Hazenberg, P., Torfs, P.J. and Uijlenhoet, R., 2009. The hydrological response of the Ourthe catchment to climate change as modelled by the HBV model. *Hydrological and Earth System Sciences Discussions,* 6, pp.7143-7178.

Duan, Q., Sorooshian, S. and Gupta, V., 1992. Effective and efficient global optimisation for conceptual rainfall-runoff models, *Water Resources Research,* 28(4), pp.1015 – 1031.

Fealy, R. and Sweeney, J., 2007. Statistical downscaling of precipitation for a selection of sites in Ireland employing a generalised linear modeling approach. *International Journal of Climatology,* 27, pp.2083-2094.

Fealy, R. and Sweeney, J., 2008. Climate Scenarios for Ireland. In: Sweeney, J., Albanito, F., Brereton, A., Caffarra, A., Charlton, R., Donnelly, A., Fealy, R., Fitzgerald, J., Holden, N., Jones, M., and Murphy C., 2008. *Climate Change – Refining the Impacts for Ireland.* Environmental Protection Agency, Johnstown Castle Estate, Wexford, Ireland, pp. 5 – 37.

Fowler, H.J., Blenkinsop, S. and Tebaldi, C., 2007. Review: Linking climate change modelling to impacts studies: recent advance in downscaling techniques for hydrological modelling, *International Journal of Climatology,* 27, pp.1547-1578.

Fowler, H.J. and Ekström, M., 2009. Multi-model ensemble estimates of climate change impacts on UK seasonal precipitation extremes. *International Journal of Climatology,* 29, pp.385-416.

Franchini. M. and Pacciani, M., 1991. Comparative Analysis of Several conceptual Rainfall-Runoff Models. *Journal of Hydrology*, 122, pp.161-219.

Gardiner, M.J. and Radford, T., 1980. *Soil Associations of Ireland and their Land Use Potential.* An Foras Talúntais, Dublin.

Georgakakos, K.P., Seo, D.J., Gupta, H., Schaake, J., and Butts, M.B., 2004. Towards a characterization of streamflow simulation uncertainty through multi-model ensembles. *Journal of Hydrology,* 298, pp.222 – 241.

Greenwood, J.A., Landwher, J.M., Matalas, N.C. and Wallis, J.R., 1979. Probability Weighted Moments: Definition and relation to parameters of several distributions expressable in inverse form. *Water Resources Research,* 15(5), pp.1049 – 1054.

Hall, J., 2007. Probabilistic climate scenarios may misrepresent uncertainty and lead to bad adaptation decisions, *Hydrological Processes,* 21, pp.1127 – 1129.

Harlin, J., 1991. Development of a Process Oriented Calibration Scheme for the HBV Hydrological Model. *Nordic Hydrology,* 22, pp.15-36.

Harlin, J., and Kung, C., 1992. Parameter uncertainty and simulation of design floods in Sweden. *Journal of Hydrology,* 137, pp. 209-230.

Hallegatte, S., 2009. Strategies to adapt to an uncertain climate change. *Global Environmental Change,* 19, pp.240-247.

Harrigan, S., 2010. *Detection of climate change in Irish streamflow records.* M.Sc. Thesis (unpublished). Maynooth, National University of Ireland.

Haylock, M.R., Cawley, G.C., Harpham, C., Wilby, R.L. and Goodess, C.M., 2006. Downscaling heavy precipitation over the United Kingdom: a comparison of dynamical and statistical methods and their future scenarios, *International Journal of Climatology,* 26, pp.1397-1415.

Hewitson, B.C., and Crane, R.G., 2006. Consensus between GCM climate change projections with empirical downscaling: precipitation downscaling over South Africa. *International Journal of Climatology,* 26, pp.1315 – 1337.

Højberg, A.L. and Refsgaard, J.C., 2005. Model uncertainty – parameter uncertainty versus conceptual models. *Water Science and Technology,* 52(6), pp.177 – 186.

Hosking, J.R.M. and Wallis, J.R., 1997. *Regional frequency analysis: an approach based on L-moments.* Cambridge University Press, 224pp.

Houghton, J.G. an O'Cinneide, M., 1976. Distribution and synoptic origin of selected heavy precipitation events in Ireland. *Irish Geography,* 9, pp.1 – 8.

Hulme, M. and Carter, T., 1999. *Representing uncertainty in Climate Change Scenarios and Impact Studies.* ECLAT-2 Discussion Paper.

Huntington, T.G., 2006. Evidence for intensification of the global water cycle: Review and systhesis. *Journal of Hydrology,* 319, pp.83 – 95.

IPCC 2007: *Climate Change 2007: The Physical Science Basis. Contribution of working Group 1 to the Fourth Assessment Report of the Intergovernmental Panel on Climate Change* [Solomon, S., Qin, D., Manning, M., Marquis, M., Chen, Z., Averyt, K.B., Tignor, M., and Miller, H.L. (eds.)]. Cambridge University Press, Cambridge, UK and New York, USA. 996 pp.

IPCC, 2007: *Climate Change 2007: Impacts, Adaptation and Vulnerability: Contribution of Working Group II to the Fourth Assessment Report of the Intergovernmental Panel on Climate Change,* M.L. Parry, O.F. Canziani, J.P. Palutikof, P.J. van der Linden and C.E. Hanson, Eds., Cambridge University Press, Cambridge, UK, 976pp.

IPCC SRES Emissions scenarios. http://sedac.ciesin.columbia.edu/ddc/sres/ [Accessed on 26 August 2010]

Jakeman, A.J. and Hornberger, G.M., 1993. How much complexity is warranted in a rainfall-runoff model? *Water Resources Research,* 29 (8), pp.2637-2649.

Jones, R.N., 2000. Analysing the risk of climate change using an irrigation demand model. *Climate Research,* 14, pp.89-100.

Katz, R.W., Parlange, M.B. and Naveau, P., 2002. Statistics of extremes in hydrology, *Advances in Water Resources,* 25, pp.1287-1304.

Keane,T. and Sheridan, T., 2004. Climate of Ireland in Keane, T. and Collins, J.F., eds. *Climate, Weather and Irish Agriculture.* Joint Working Group on Agricultural Meteorology, Met Eireann, Dublin, Ireland. 395 pp.

Kiely, G., 1999. Climate change in Ireland from precipitation and streamflow observations. *Advances in Water Resources,* 34, pp.141 – 151.

Koutsoyiannis, D., 2010. HESS Opinions: A random walk on water. *Hydrology and Earth System Sciences,* 14, pp.585-601.

Krause, P., Boyle, D.P. and Bäse, F., 2005. Comparison of different efficiency criteria for hydrological model assessment. *Advances in Geosciences,* 5, pp.89-97.

Kundzewicz, Z. and Robson, A., 2004. Change detection in hydrological records – a review of the methodology. *Hydrological Sciences Journal,* 49 (1), pp.7 – 19.

Kysely, J., 2002. Comparison of extremes in GCM-simulated downscaled and observed central-European temperature series. *Climate Research,* 20, pp.211-222.

Legates, D.R. and Davis, R.E., 1997. The continuing search for an anthropogenic climate change signal: Limitations of correlation-based approaches. *Geophysical Research Letters,* 24, pp.2319-2322.

Legates, D.R. and McCabe, G.J., 1999. Evaluating the use of "goodness-of-fit" measures in hydrological hydroclimatic model validation, *Water Resources Research,* 35(1), pp.233-241.

Lindström, G., 1997. A simple calibration routine for the HBV Model. *Nordic Hydrology,* 28(3), pp.153-168.

Lorenz, E.N., 1993. *The essence of chaos.* University of Washington Press, Seattle.

Lowe, J.A., Hewitt, C.D., vanVuuren, D.P., Johns, T.C., Stehfest, E., Royer, F. and van der Linden, P.J., 2009. New Study for Climate Modelling, Analyses, and Scenarios, *Eos Transactions AGU,* 90(21), doi: 10.1029/2009EO210001.

Ludwig, R., May, I., Turcotte, R., Vescovi, L., Braun, M., Cyr, J.F., Fortin, L.G., Chaumont, D., Biner, S., Chartier, I., Caya D. and Mauser, W., 2009. The role of hydrological model complexity and uncertainty in climate change impact assessment. *Advances in Geosciences,* 21 pp.63-71.

McElwain, L. and Sweeney, J., 2007. *Key Meteorological Indicators of Climate Change in Ireland.* Environmental Protection Agency, Johnstown Castle Estate, Wexford, Ireland.

McGrath, R. and Lynch, P. eds., 2008. *Ireland in a Warmer World: Scientific Predictions of the Irish Climate in the Twenty-First Century.* Community Climate Change Consortium for Ireland, Dublin.

McGrath, R., Fealy, R. and Sheridan, T., 2010. *9th Scientific Statement: Recent Irish weather extremes and climate change.* RIA Climate change Sciences Committee, Dublin.

Manley, R.E., 1976. The soil moisture component of mathematical catchment simulation models. *Journal of Hydrology,* 35, pp.341 – 356.

Manley, R.E., 1978. Calibration of Model using Optimization. *Journal of the Hydraulics Division,* ASCE, 104 (2), pp.189-202

Manley, R.E., 2003. *A Guide to using HYSIM.* R.E. Manley and Water Resource Associates Ltd.

Mayes, J,. 1991. Regional airflow patterns in the British Isles. *International Journal of Climatology,* 11, pp. 473 – 491.

Mein, R.G. and Brown, B.M., 1978. Sensitivity of optimized parameters in watershed models. *Water Resources Research,* 14, pp.299-303.

Melching, C.S., 1995. Reliability Estimation. In P. Singh, ed. 1995. *Computer Models of Watershed Hydrology,* Water Resource Publications, Colorado.

Met Eireann, 2010. Monthly Weather Summary: The Weather of November 2009. Available at http://www.met.ie/climate/monthly-summarys/nov09.pdf. [Accessed 21 January 2010]

Met Eireann, 2010. Rainfall in Ireland. Available at: www.met.ie/climate/rainfall.asp [Accessed 08 January 2010]

Minville, M., Brissette, F. and Leconte, R., 2008. Uncertainty of the impact of climate change on the hydrology of a Nordic watershed. *Journal of Hydrology,* 358, pp.70-83.

Milly, P.C.D., Betancourt, J., Falkenmark, M., Hirsch, R.M., Kundzewicz, Z.W., Lettenmaier, D.P., and Stouffer, R.J., 2008. Stationarity is Dead: Whither Water Management? *Science,* 319, pp.573 – 574.

Milly, P.C.D., Wetherald., R.T., Dunne, K.A. and Delworth, T.L., 2002. Increasing risk of great floods in a changing climate. *Nature,* 415, pp.514-517.

Mitchell, D. and Hulme, M., 1999. Predicting regional climate change: living with uncertainty, *Progress in Physical Geography,* 23, (1) pp. 57 – 78.

Mitchell, F. and Ryan, M., 1998. *Reading the Irish Landscape.* Townhouse and Country House, Dublin.

Moss, R.H. and Schneider,S.H. (2000). Uncertainties in the IPCC TAR: Recommendations to lead authors for more consistent assessment and reporting, in Pachauri, R. Taniguchi, T. and Tanaka, K. (eds.). *Guidance Papers on the Cross Cutting Issues of the Third Assessment Report of the IPCC.* World Meteorological Organization, Geneva, Switzerland: , 33 – 51.

Murphy, C. and Charlton, R., 2008. Climate Change and Water Resources. *In: Climate Change – Refining the Impacts for Ireland.* EPA STRIVE Report No.12, Co. Wexford, Ireland, pp.39 – 81.

Murphy, C., 2006. *The impact of climate change on catchment hydrology and water resources for selected catchments in Ireland.* Ph.D. Thesis (unpublished). Maynooth: National University of Ireland.

Murphy, J.M., Sexton, D.M., Barnett, D.N., Jones, G.S., Webb, M.J., Collins, M. and Stainforth, D.A., 2004. Quantification of modelling uncertainties in a large ensemble of climate change simulations, *Nature,* 430, pp.768 – 772.

Nakicenovic, N., Alcamo, J., Davis, G., de Vries, B., Fenhann, J., Gaffin, S., Gregory, K., Grübler, A., Jung, T.Y., Kram, T., La Rovere, E.L., Michealis, L., Mori, S., Morita, T., Pepper, W., Pitcher, H., Price, L., Raihi, K., Roehrl, A., Rogner, H-H., Sankovski, A., Schlesinger, M., Shuykla, P., Smith, S., Swart. R., van Rooijen, S., Victor, S., Dadi, Z., (2000*). IPCC Special Report on Emissions Scenarios,* United Kingdom and New York, NY, USA, 599 pp.

Nash, J.E. and Sutcliffe, J.V., 1970. River flow forecasting through conceptual models 1. A discussion of principles. *Journal of hydrology,* 10, pp.282-290.

Oberkampf, W.L. DeLand, S.M. Rutherford, B.M Diegert, K.V. and Alvin, K.F., 2002. Error and uncertainty in modeling and simulation, *Reliability Engineering and System Safety,* 75, pp.333 – 357.

Office of Public Works, 2010. *Briefing note on the progress of the Flood Studies Update – Work Package 2.2: Flood frequency analysis.*

Pappenberger, F. and Beven, K.J., 2006. Ignorance is bliss: Or seven reasons not to use uncertainty analysis, *Water Resources Research,* 42, W05302, doi: 10.1029/2005WR004820.

Perrin, C., Michel, C. and Andréassian, V., 2001. Does a large number of parameters enhance model performance? Comparative assessment of common catchment model structures on 429 catchments. *Journal of Hydrology,* 242, pp.275 – 301.

Pilling, C.G. and Jones, J.A.A., 2002. The impact of future climate change of seasonal discharge, hydrological processes and extreme flows in the Upper Wye experimental catchment, mid-Wales. *Hydrological Processes,* 16, pp.1201-1213.

Pittock, A.B., and Jones, R.N., 2000. Adaptation to what and why? *Environmental Monitoring and Assessment,* 61, pp.9 – 35.

Prudhomme, C., Jakob, D. and Svensson, C., 2003. Uncertainty and climate change impacts on the flood regime of small UK catchments. *Journal of Hydrology,* 277, pp.1-23.

R Development Core Team 2009. *R: A language and environment for statistical computing.* R Foundation for Statistical Computing, Vienna, Austria. ISBN 3-900051-07-0, URL http://www.R-project.org.

Refsgaard, J.C. and Knudsen, J., 1996. Operational validation and intercomparison of different types of hydrological models. *Water Resources Research,* 32(7), pp.2189-2202.

Refsgaard, J.C., van der Sluijs, J.P., Brown, J. and van der Keur, P., 2006. A framework for dealing with uncertainty due to model srtructure error. *Advances in Water Resources,* 29, pp.1586-1597.

Reynard, N.S., Crooks, S.M. and Kay, A.L., 2004. *Impact of Climate Change on Flood Flows in River Catchments, Final Report for Defra/EA project W5B-01-050.* Department for Environment, Food and Rural Affairs, London, 80 pp.

Robson, A., 2002. Evidence for trends in UK flooding. *Philosophical Transactions of the Royal Society,* 360, pp.1327-1343.

Robson, A. and Reed, D., 1999. *Flood Estimation Handbook 3: Statistical Procedures for Flood Frequency Estimation.* Institute of Hydrology, Wallingford, UK.

Roe, G.H. and Baker, M.B., 2007. Why is Climate Sensitivity so Unpredictable? *Science,* 318, pp.629 – 632.

Schneider, S. H., 1983. 'CO$_2$, Climate and Society: A brief overview', in Chen, R. S., Boulding,E. M., and Schneider, S. H. (eds.), *Social Science Research and Climatic Change: An Interdisciplinary Appraisal.* D. Reidel Publishing, Dordrecht, pp.9–15.

Seibert, J., 1997a. Estimation of Parameter Uncertainty in the HBV Model. *Nordic Hydrology,* 28 (4/5), pp.247-262.

Seibert, J., 1999. Regionalisation of parameters for a conceptual rainfall-runoff model, *Agricultural and Forest Meteorology,* 98-99, pp.279-293.

Siebert, J., 2005. HBV Light Version 2 User's Manual. University of Stockholm.

Semmler, T., Wang, S., McGrath, R. and Nolan, P., 2006. Regional climate ensemble simulations for Ireland – impact of climate change on river flooding. *Proceedings of the National Hydrology Seminar*. Tullamore, Ireland, 2006.

Silberstein, R.P., 2006. Hydrological models are so good, do we still need data? *Environmental Modelling and Software,* 21, pp.1340-1352.

Sorooshian, S. and Gupta, V.K., 1995. Model Calibration. In P. Singh, ed. 1995. *Computer Models of Watershed Hydrology.* Water Resource Publications, Colorado.

STARDEX, 2006. *Downscaling Climate Extremes.* http://www.cru.uea.ac.uk/projects/stardex/

Steele-Dunne, S., Lynch, P., McGrath, R., Semmler, T., Wang, S., Hannifin, J and Nolan, P., 2008. The impacts of climate change on hydrology in Ireland. *Journal of Hydrology,* 356, pp.28-45.

Sweeney, J.C. and O'Hare, G.P., 1992. Geographical variations in precipitation yields and circulation types in Britain and Ireland. *Transactions of the Institute of British Geographers,* 17, pp.448 – 463.

Sweeney, J.C., 1985. The changing synoptic origins of Irish precipitation. *Transactions of the Institute of British Geographers,* 10, pp.467 – 480.

Tebaldi, C., and Knutti, R., 2007. Review: The use of multi-model ensemble in probabilistic climate projections. *Philosophical Transactions of the Royal Society,* 365, pp.2053- 2075.

Uhlenbrook, S., Seibert, J., Leibundgut, C., and Rodhe, A., 1999. Prediction uncertainty of conceptual rainfall-runoff models caused by problems in identifying model parameters and structure, *Hydrological Sciences,* 44 (5), pp.779-797.

UNEP (2002). *Global Environmental Outlook 3,* Earthscan, London.

UNFCCC, 2010. *Dynamical Downscaling*. Available at
http://unfccc.int/files/adaptation/methodologies_for/vulnerability_and_adaptation/applicati
on/pdf/dynamical_downscaling.pdf [Accessed 28 January 2010]

Vrugt, J.A. and Robinson, B.A., 2007. Treatment of uncertainty using ensemble methods:
Comparison of sequential data assimilation and Bayesian model averaging. *Water
Resources Research,* 43, W01411, doi:10.1029/2005WR004838.

Wagener, T., 2003. Evaluation of catchment models. *Hydrological Processes,* 17, pp.3375-
3378.

Wagener, T., Gupta, H.V. and Sorooshian, S., 2004. Stochastic formulation of a conceptual
hydrological model. In: *Hydrology: Science and Practice for the 21st Century.*
London, UK, 12-16 July 2004. British Hydrological Society, London.

Wagener, T., McIntyre, N., Lees, M.J., Wheater, H.S. and Gupta, H.V., 2003. Towards
reduced uncertainty in conceptual rainfall-runoff modelling: Dynamic identifiability
analysis. *Hydrological Processes,* 17, pp.455-476.

Wagener, T., Wheater, H.S. and Gupta, H., 2004. *Rainfall-Runoff Modelling in Gauged and
Ungauged Catchments.* Imperial College Press, London.

Walker, P., Harremoes, J., Rotmans, J.P., van der Sluijs, M.B. and van Asselt, P., 2003.
Defining uncertainty: A conceptual basis for uncertainty management in model-
based decision making. *Integrated Assessment,* 4(1), pp.5 – 17.

Wang, S., McGrath, R., Semmler, T., Sweeney, C. and Nolan, P., 2006. The impact of the
climate change on discharge of Suir River Catchment (Ireland) under different
climate scenarios. *Natural Hazards and Earth System Sciences,* 6, pp.387 - 395.

Webster, M., 2003. Communicating climate change uncertainty to policy-makers and the
public: An Editorial Comment. *Climatic Change,* 61, pp.1-8.

Wilby, R., 2005. Uncertainty in water resource model parameters used for climate change
impact assessment. *Hydrological Processes,* 19, pp.3201-3219.

Wilby, R.L., 2006. When and where might climate change be detectable in UK river flows?
Geophysical Research Letters, 22, L19407. doi: 10.1029/2006GL027552.

Wilby, R.L., Dawson, C.W. and Barrow, E.M., 2002. SDSM – a decision support tool for
the assessment of regional climate change impacts, Environmental Modelling and
Software, 17, pp.145-157.

Wilby, R.L. and Harris, I., 2006. A framework for assessing uncertainties in climate change impacts: Low-flow scenarios for the River Thames, UK. *Water Resources Research,* 42, WO2419.

Wilby, R.L., Troni, J., Biot, Y., Tedd, L., Hewitson, B.C., Smith, D.M. and Sutton, R.T., 2009. A review of climate risk information for adaptation and development planning. *International Journal of Climatology, 29,* pp.1193-1215.

Wilby, R.L. and Dessai, S., 2010. Robust adaptation to climate change. *Weather,* 65(7), pp.180-185.

Winkler, R.L., 1996. Uncertainty in probabilistic risk assessment. *Reliability Engineering & System Safety,* 54, pp.127 – 132.

Yu, P-S. and Yang, T-C., 2000. Fuzzy multi-objective function for rainfall-runoff model calibration. *Journal of Hydrology*, 238, pp.1-14.

Yue, S., Pilon, P. and Cavadias, G., 2002. Power of the Mann-Kendall and Spearman's rho tests for detecting monotonic trends in hydrological data. *Journal of Hydrology,* 259, pp.254-271.

Ziegler, A.D., Maurer, E.P., Sheffield, J., Nussen, B., Wood, E. And Lettenmaier, D.P., 2006. Detection time for plausible changes in annual precipitation, evapotranspiration and streamflow in three Mississippi River sub-basins. *Climatic Change,* 72, pp.17-36.